2013-01-21

Biogenic Methane Generation in Shallow Shale Gas Systems

Cokar, Marya

UNIVERSITY OF CALGARY

Biogenic Methane Generation in Shallow Shale Gas Systems

by

Marya Cokar

A THESIS

SUBMITTED TO THE FACULTY OF GRADUATE STUDIES

IN PARTIAL FULFILMENT OF THE REQUIREMENTS FOR THE

DEGREE OF DOCTOR OF PHILOSOPHY

DEPARTMENT OF CHEMICAL AND PETROLEUM ENGINEERING

CALGARY, ALBERTA

JANUARY, 2013

UNIVERSITY OF CALGARY

FACULTY OF GRADUATE STUDIES

The undersigned certify that they have read, and recommend to the Faculty of Graduate Studies for acceptance, a thesis entitled "Biogenic Methane Generation in Shallow Shale Gas Systems" submitted by Marya Cokar in partial fulfilment of the requirements of the degree of Doctorate of Philosophy in Chemical Engineering.

Supervisor, Dr. Michael S. Kallos, Chemical and Petroleum Engineering

Co-Supervisor, Dr. Ian D. Gates, Chemical and Petroleum Engineering

Dr. Ayodeji A. Jeje, Chemical and Petroleum Engineering

Dr. Jalel Azaiez, Chemical and Petroleum Engineering

Dr. Brij Maini, Chemical and Petroleum Engineering

Dr. Lisa M. Gieg, Biological Sciences

Dr. Ron C.K. Wong, Civil Engineering

Dr. Julia Foght, External, University of Alberta

Date

Abstract

Shale gas is an unconventional gas source now widely in production in the Appalachian and Michigan Basins in the United States. Shale gas production in the United States has increased tremendously over the past decade and many companies are now looking to Canada to expand gas production from shale gas sources in the Western Canadian Sedimentary Basin (WCSB). Natural gas is a favourable alternative fuel to other hydrocarbons because it results in lower greenhouse gas and carbon emissions. In North America there are several shale gas plays yet the potential for shale gas systems within Canada is still being evaluated. As conventional natural gas production in Canada declines shale gas may offset this decline in Canada. The WCSB contains over 1,000 Tcf of gas in its shale deposits thus the prize is significant. The research documented in this thesis focuses on understanding methane gas transport and generation mechanisms, identifying the microorganisms present in shale gas systems, determining how to quantify and model biogenic gas production rates, and determining how to enhance biogenic gas rates by substrate addition. In the near future as technology and research develops, methanogenesis may be a significant and sustainable source of natural gas production in shallow reservoirs. The key outcomes of the proposed research are to quantify the amount of biogenic gas produced in shallow shale reservoirs using a new gas material balance theory, reactive engineering modelling, and numerical reservoir simulation. Additionally, methane production rates were determined within the laboratory using produced water and core samples from shallow shale gas wells and the microorganisms that produce methane gas within the reservoir were identified at the family level.

Preface

The research work compiled in this thesis is novel and the first of its kind for a shallow biogenic shale gas reservoir in western Canada. It is the first time the amount of biogenic gas produced in a shale gas reservoir has been quantified by using a novel gas material balance theory, experimental methane production rates, reaction engineering modelling and numerical reservoir simulation using experimental methane generation kinetics. The following is a list of publications resulting from this Ph.D. research documented in this thesis.

1. Cokar M., Ford, B., Kallos, M.S., and Gates, I.D. "New Gas Material Balance to Quantify Biogenic Gas Generation Rates from Shallow Organic-Matter-Rich Shales," *FUEL*, vol. 104, pp. 443 - 451, 2012.
2. Cokar, M., Wilson, S., Ford, B., Gieg, L.M., Kallos, M.S., Gates, I.D. "Biogeochemical Analysis of Shale Gas Systems Reveals Links Between Geology, Biology and Reservoir Engineering," to be submitted, 2012.
3. Cokar, M., Kallos, M.S., Gates, I.D. "Biogenic Shale Gas Reservoirs: Kilometer Scale Biogeochemical Reactors," submitted to *American Institute of Chemical Engineering* ID: AIChe-12-14652, 2012.
4. Cokar M., Ford, B., Kallos, M.S., and Gates, I.D. "Reactive Reservoir Simulation of Biogenic Shallow Shale Gas Systems enabled by Experimentally Determined Methane Generation Rates," revisions submitted *to Energy and Fuels* ID: ef-2012-018223, 2012.

Acknowledgements

I would like to first and foremost thank Allah (swt) for helping and guiding me through this research. I would also sincerely like to thank my supervisors Dr. Michael Kallos and Dr. Ian Gates for their guidance, motivation and encouragement throughout my research with their great sense of imagination, enthusiasm, exceptional support, and trusting me with this project.

I would like to extend my sincere gratitude to a number of people whom without their support this research would not be possible. I would like to thank Brad Ford, who suddenly passed away during the writing of this thesis, from Husky Inc. for his support, great ideas, time, and most importantly with reservoir sample collection to complete the experimental portion of this research, without this the experiments would not be possible. I would also like to thank Dr. Lisa Gieg and Dr. Sandra Wilson who have helped me with the experiments, without their knowledge and expertise it would not have been possible. I would also like to thank Dr. Ayodeji Jeje, Dr. Jalel Azaiez, and Dr. Brij Maini for being on my supervisory and examination committee and providing constructive feedback for my thesis and research. And I would like to thank Dr. Ron Wong for being my internal/external examiner and Dr. Julia Foght for coming down from the University of Alberta as an external examiner.

I would also like to thank Dr. Patrick Hettiaratchi for the use of his gas chromatograph, and his technician Daniel Larson for training and lab support.

I would also like to acknowledge the Natural Sciences and Engineering Research Council (NSERC) and Alberta Innovates Technology Futures (AI-TF) for their financial support throughout the thesis. Also, the Department of Chemical and Petroleum Engineering in the Schulich School of Engineering at the University of Calgary, CMG for the use of their thermal reservoir simulator, STARS™. I would also like to thank colleagues that have helped me throughout this project Dr. Punitkumar Kapadia, Jingyi (Jacky) Wang, Yi Su, Christopher Istchenko, Dr. Ali Al-Turki and Holly Lee.

I would also like to extend my deep sense of gratitude to my parents, Mahmood and Nafees Cokar, without their unconditional love and support this research would not have been possible, and my brother Usman Cokar for helping me with Matlab™ and software support. I would also like to thank my husband Bilal Latif for always being there and supporting me throughout this research.

Dedication

I would like to dedicate this thesis to my parents, without their love and support this would not have been possible.

Table of Contents

List of Tables

List of Figures

List of Symbols, Abbreviations and Nomenclature

Symbol	Definition
A	Area (m^2)
C	Concentration (mol/m^3)
C_o	Initial concentration (mol/m^3)
C_E	Equilibrium isotherm (mol/m^3)
C_{Ei}	Initial equilibrium isotherm (mol/m^3)
c_ϕ	Porosity compressibility (1/Pa)
c_{*j}	Concentration
Day	Day
Da	Damköhler Number
d	Diameter (m)
G_p	Gas produced (m^3)
k	Permeability (m^2)
k_{abs}	Absolute Permeability
k_o	Zero order reaction rate constant (kg/m^3s)
k_r	Relative Permeability
L	Length of the reservoir (m)
M	Molar mass of gas (g/mol)
MW	Molar mass
n	Moles of gas
n_p	Moles of gas produced
n_{21}	Moles of gas initially in secondary porosity
n_{1i}	Moles of gas initially in primary porosity
n_2	Moles of gas in secondary porosity
n_1	Moles of gas in primary porosity
P_e	Pressure at model boundary (Pa)
P_{atm}	Atmospheric Pressure (Pa)
P	Pressure (Pa)
P_i	Initial Pressure (Pa)
P_{sc}	Pressure at standard conditions (Pa)
P_L	Langmuir pressure constant (Pa)
q	Flow rate (m^3/s)
R	Universal gas constant (J/mol·K)
Re_p	Particle Reynolds number
S_{gi}	Initial gas saturation
S_{wi}	Initial water saturation
S_{wavg}	Average water saturation
T	Temperature (K)
T_{sc}	Temperature at standard conditions (K)
TOC	Total organic carbon (vol%)
TOC_A	Amenable total organic carbon (vol%)
u	Velocity (m/s)
V	Volume (m^3)

Symbol	Definition
V_E	Volumetric adsorption isotherm (standard m^3/m^3)
V_L	Volume constant for Langmuir isotherm (standard m^3/m^3)
V_{b2}	Bulk volume of the secondary porosity (m^3)
x	Distance along a direction (m)
z	Gas compressibility
z_i	Initial gas compressibility
z_{sc}	Gas compressibility at standard conditions
ϕ_i	Initial Porosity
μ	Viscosity (Pa·s)
ρ	Density (kg/m^3)
γ	Moles of gas produced during production period by microbes

Chapter One: Introduction

1.1 Background

Natural gas demands have increased by about 30% within the last 15 years and are still on the rise as global populations increase (Martini, 2005). Further demand is forecast as natural gas evolves to become a major transportation fuel, potentially displacing liquid fuels such as gasoline and diesel as the environmentally-friendly fuel of choice. Furthermore, with the use of natural gas fired power plants (due to being cleaner than coal), demand for natural gas will grow. With this rise in demand, unconventional reservoirs such as coal beds and shale gas are being explored. Shale gas production in the United States since 2000 has increased from 1% to approximately 20% of total natural gas production and it is expected to increase to about 50% by 2025 (Davis et al. 2012). Shale gas systems consist of two major types: thermogenic – often deep systems that generate gas by thermal degradation of kerogen and biogenic – often shallow systems where gas is generated via microbial activity. In biogenic systems, gas is generated by microorganisms that consume organic matter in shale and convert it primarily to methane and carbon dioxide. The focus of the research documented in this thesis is biogenic shale gas reservoirs. Not only do shale gas systems have the potential to meet the world's growing energy demands, they are also a cleaner fossil fuel because of lower greenhouse gas and carbon emissions. Thus, biogenic shale gas production technologies appear to be effective yet little is known at a fundamental level about these systems e.g. basic understanding of gas generation rates and microbial activity, gas flow

and transport, and geological heterogeneity and its impact on production performance remains largely unknown.

1.1.1 Shale Gas Systems

Studies have been carried out for unconventional biogenic gas reservoirs in the United States but information is lacking in Canada. Biogenic shale gas reservoirs in Canada differ from those found in the United States because they generally have lower permeabilities (less than about 1 mD) and contain different isotopic compositions of oxygen, hydrogen, and carbon depending on their origins and how they were deposited (Cokar et al., 2012). Therefore, more work needs to be done to try to understand shallow shale gas reservoirs in the WCSB (Ross and Bustin, 2008).

Shale gas reservoirs are considered unconventional because of their low permeability and geochemical complexity. Natural gas generated from shale gas reservoirs has essentially never left its birthplace and is in essence trapped where it was generated due to very low shale permeabilities, small pore sizes, and poorly connected pore throats (Kerr, 2010). This adversely impacts productivity leading to low production rates and recovery factor unless well and reservoir stimulation is completed.

The main shale gas plays in Canada are the Horn River Basin and Montney shales in northeast British Columbia, Colorado group in Alberta and Saskatchewan, Utica Shale in Quebec, and Horton Bluff Shale in New Brunswick and Nova Scotia as shown in Figure 1.1.

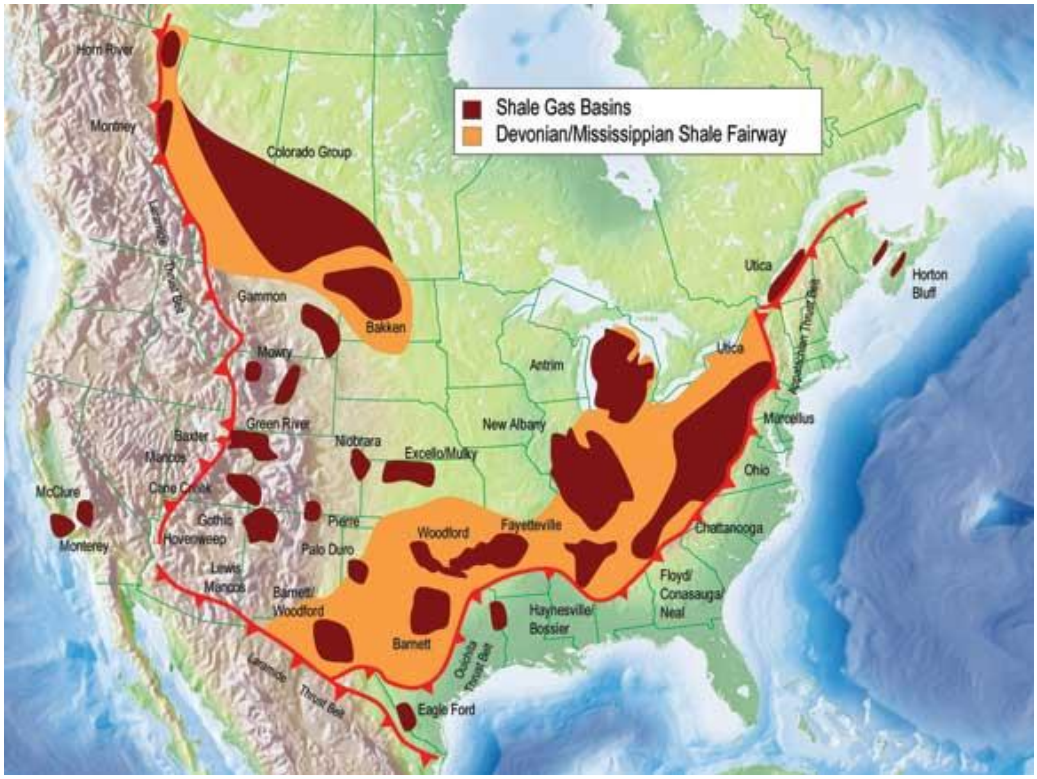

Figure 1.1. Shale gas plays in North America (NEB, 2009).

Shales in the Horn River basin are about 150 m thick and are found at depths between 250 and 3,000 m. The total organic content of this formation ranges from 1 to 6%. This formation is a mature formation, and the methane gas within this formation was generated thermogenically. The original gas in place for the Horn River basin is estimated to be equal to approximately 500 trillion cubic feet (Tcf) (NEB, 2009).

Natural gas in the Montney formation is produced from shallow water shoreface sandstones. The shales are found at depths between about 1,700 and 4,000 m below the surface. The thickness of this formation is estimated to be up to 300 m. The total organic content of the Montney shales is between 1 and 7%. Estimates for natural gas in place for this formation vary between 80 and 700 Tcf (NEB, 2009).

The Colorado group in southern Alberta and Saskatchewan have been producing natural gas from shale for more than 100 years. The top of the Colorado shales are found at depth equal to about 300 m, which is shallow enough that it is still being currently produced biogenically by microorganisms. The formation thickness ranges from 17 to 350 m. The total organic content of the reservoir varies between 0.5 and 12%. It is believed that the formation contains over several 100 Tcf of gas (NEB, 2009).

The Utica shales are found between Montreal and Quebec City and lie at a depth of between 500 and 3,300 m below the surface. Both biogenic gas and thermogenic gas can be found in the Utica shales. The thickness of these shales ranges from 90 to 300 m and it is estimated that they contain over 120 Tcf of natural gas (NEB, 2009).

All of the above described shale gas reservoirs are productive after well and reservoir stimulation (hydraulic fracturing) is done. For the biogenic shale gas reservoirs, Colorado and Utica, these are relatively shallow reservoirs and thus there are constraints on the pressure and volume of fracture fluid that can be placed within the reservoirs to stimulate production. To enhance productivity from these formations, there are essentially two primary drivers that can be completed. First, more extensive hydraulic fracturing to enhance mass transport and connection of the reservoir to the well to raise gas production rates can be carried out and second, enhancement of microbial activity so that the bioconversion rate of the kerogen to gas in the reservoir is raised.

The specific shale gas formation studied in the research and documented in this thesis is the Colorado group in southeast Alberta and southwest Saskatchewan. The main mechanism of gas generation in this relatively shallow reservoir is biogenic. It is not yet known, from published literature to the knowledge of the author, whether gas is generated actively during the operating lifetime of the well and it is not just stored gas biogenically generated in the ancient past. If a large fraction is generated during the operating life of the well, then this suggests that there is potential to stimulate not only the reservoir but also the microbes to enhance gas production rates.

1.2 Origin of Natural Gas

Methane gas is produced either thermogenically, biogenically or a mixture of both within a gas reservoir. Thermogenic gas is usually found in more mature deeper, and thus hotter reservoirs, and biogenic gas is found in shallower geologically younger reservoirs, and thus more moderate temperatures typically below 80°C. Chemical carbon isotopic compositions can be used to differentiate between gases of thermogenic, biogenic, or mixed origin (Stasiuk and Goodarzi, 1988; Rice and Claypool, 1981; Schoell, 1983; Rice, 1993; Whiticar, 1999).

For shale gas systems, natural gas production is divided into three distinct layers within the reservoir, as shown in Figure 1.2. The deepest level is known as the thermogenic kitchen. The thermogenic kitchen is bound at the top by the thermogenic ceiling. The second level directly above the thermogenic kitchen is a region which includes a

combination of thermogenic gas and biogenic gas. The top level is where the biogenic gas is produced and this is bounded at the bottom by the biogenic floor.

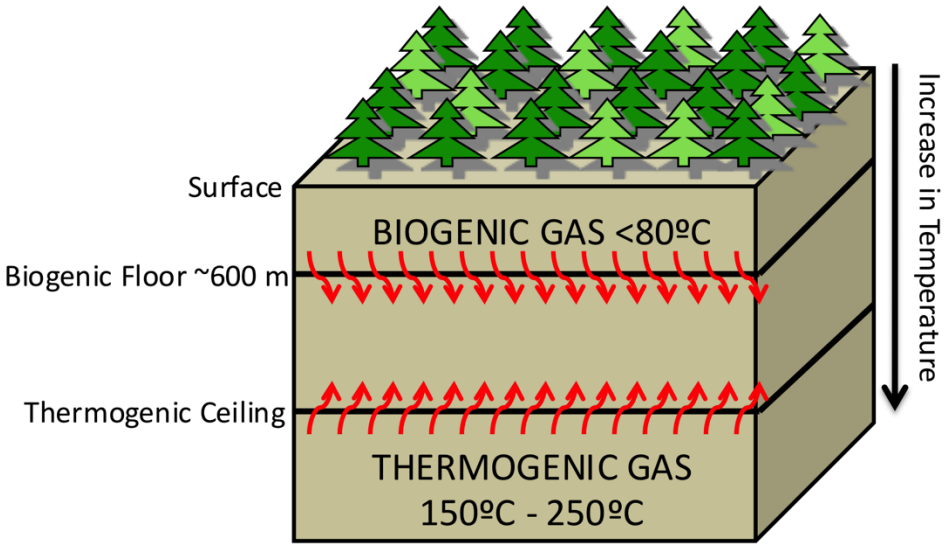

Figure 1.2. Relative depths of biogenic floor and thermogenic ceiling.

1.2.1 Thermogenic Gas Production

Thermogenic gas is produced by thermal cracking of kerogen (Behar et al., 1997). The majority of gas produced in deep conventional reservoirs is by thermogenic gas production which essentially involves high temperature and pressure thermal cracking of kerogen and petroleum deep within the earth over millions of years. This occurs at temperatures above 150ºC to about 250ºC (Pepper and Corvi, 1994). Organic material comprised of ancient algae, wood, and plants, on the surface get buried and after millions of years they reach depths of hundreds to thousands of meters below the surface, where the temperatures and pressures are high enough to allow the organic content to crack and generate gas.

1.2.2 Biogenic Gas Production

Biogenic gas generation occurs by anaerobic microbial degradation of organic matter and typically occurs within reservoirs at shallower depths less than about 550 m (Curtis, 2002; Shaw, 2006). The maximum temperature at which these microorganisms can survive is approximately 80ºC and shallower shale gas reservoirs provide an ideal environment for microbial growth (Larter et al., 2006). Gas production is mainly methane and carbon dioxide but it can also contain up to 2% of ethane, propane, butane and pentane (Rice and Claypool, 1981). It is hypothesized that biogenic gases account for 20% of the worldwide natural gas resource (Rice and Claypool, 1981; Rice, 1993).

Gas produced from Upper Cretaceous shale gas reservoirs in Saskatchewan and Alberta, Canada and Montana, USA is largely believed to be biogenic in origin (Rice and Claypool, 1981; Rice and Spencer, 1996; Ridgley et al., 1999). Vitrinite reflectance, thermal alteration index (TAI), pyrolysis, clay mineralogy and reconstructed depths of burial history suggest that these reservoirs have not yet reached the temperatures required for thermal cracking of the organic material (Cokar et al., 2012).

The main microbial families that are found in shale gas reservoirs are fermentative, syntrophic and methanogenic microbes. Methanogens are the microorganisms that produce methane and they are classified as Archaea. There are six main environmental and physiological constraints on methane producing Archaea:

- **Anoxic environment –** these microorganisms are anaerobic and need an oxygen-free environment.

- **Sulfate-deficient environment –** methane will accumulate in areas where there is little or no sulfate.
- **Temperature –** temperatures between 0 to about 80°C are required.
- **Organic Matter –** organic matter is the main carbon source and is metabolized by several oxidation - reduction reactions.
- **Water –** the bioconversion processes require water as a source of hydrogen.
- **Space –** the size of individual bacteria is 1 to 10 μm, therefore they cannot live in highly compacted shale environments.

1.3 Gas Production Rates

Gas production from shale gas reservoirs initially show high production rates, and usually decline and level off after a certain amount of time as shown in Figure 1.3 (Nexen, 2011). Gas production rates in these reservoirs could be as low as 500 m^3/day (17,600 scf/day) and as high as around 30,000 m^3/day (1,000,000 scf/day). Gas production rates from these reservoirs are typically very low and are discouraging to some operators. Although gas production rates from these reservoirs are much smaller than that typically observed in conventional reservoirs, since these reservoirs are shallow, well completion costs are relatively low and they are also in areas where leases can be easily obtained, so they could still be economic (Shurr and Ridgley, 2002).

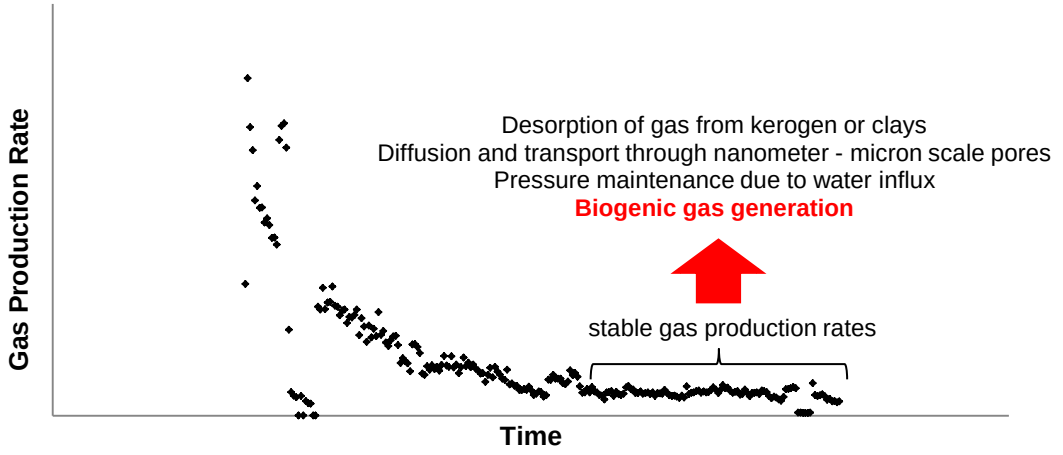

Figure 1.3. Typical gas production rates versus time for a shallow shale gas well (Nexen, 2011).

As shown in Figure 1.3, the gas production rate behaviour of these reservoirs is different than conventional reservoirs in the sense that there is a stable gas production rate period that persists until the well is abandoned. Essentially, the pressure within the system is being maintained; there are several mechanisms that can explain why these stabilized rates could occur:

- Desorption of gas from kerogen or clays that provides gas to the well at a nearly constant rate depending on the extent of reservoir drained by the production well.
- Diffusion and transport through nanometer to micron scale pores at nearly constant rate.
- Water influx into the reservoir from adjacent aquifers maintains pressure thus causing stabilized gas production rates.
- Biogenic gas generation occurs at constant rate and ultimately flows into the production well.

It remains unresolved which one or more of the above mechanisms contributes to stabilized gas production. The results from this thesis show that there is evidence of microbial gas production within these shallow shale gas reservoirs. In the early stages of production, gas contained in pores, water, and fractures as well as biogenic gas is produced to surface. As inventoried gas is depleted from the reservoir, the production rate declines. After the gas has been depleted from the reservoir and it has completely desorbed from the surfaces, the production rate declines until it equals the biogenic gas rate.

1.4 Transport of Natural Gas within the Reservoir

The permeability of these unconventional shale gas reservoirs is very low making it extremely difficult for the gas to flow in the matrix and be produced without any permeability enhancements. In order to optimize the amount of gas produced within the reservoir, well and reservoir completion methods as well as reservoir fracturing methods are being used to optimize gas production from these reservoirs.

1.4.1 Well and Reservoir Completions

Natural gas will not normally flow from vertical wells that are drilled through shale reservoirs due to its low permeability (typically less than 100 mD) and poor pore connectivity. Thin sandy and silty layers can provide horizontal connectivity within the reservoir system and natural fractures can connect more distant parts of the reservoir in both vertical and horizontal directions. The low permeability and connectivity of the system is resolved to some extent by drilling horizontally within the formation and increasing the well length to about one to two kilometres thus increasing well-reservoir

contact volume, this can increase the effective production well length from 5 to 10 times. The direction of the horizontal drill path can also be directed based on the natural fracture trends within the formation to increase pore connectivity. Another means to improve transport and contact is by hydraulically fracturing the reservoir.

1.4.2 Natural Fractures and Induced Fractures

Although natural fractures exist in shale wells they are often very thin, limited in extent, and not always where one wants them to be. Often they can be parallel to each other and thus their ability to connect the reservoir volume can be limited as well. Hydraulic fracturing, also commonly referred to as fracking, can be carried out within these reservoirs to improve permeability and pore connectivity from the reservoir to the well. Often fluid containing water, carbon dioxide, natural gas and sand (often referred to as proppant) is injected into the reservoir at pressures exceeding the fracture pressure of the reservoir. As a result, the injectant flows into the reservoir rock and fractures it. The proppant fills the fracture and thus when the injection period stops, the fracture is held open, in other words, propped open, by the sand. Depending on the depth, the fractures will grow either vertically (typically deeper than 350 m) or horizontally (typically shallower than 350 m). The main intent of hydraulic fracturing is to raise the permeability in the reservoir adjacent to the production well and increase the connectivity of the formation (Kerr, 2010).

1.5 Thesis Objectives

The overall goal of the research documented in this thesis was to develop a better understanding of biogenic methane production capabilities of shallow biogenic shale

reservoirs in the WCSB with a focus on the Colorado Shale Formation in southern Alberta and Saskatchewan. The outcomes of this thesis will further support the existence of methane producing microorganisms in shallow shale gas reservoirs. The following is a list of the main findings obtained from this study:

- The amount of biogenic gas generated within these reservoirs through a new gas material balance theory was determined. The modified gas material balance theory for quantification of biogenic gas during the resource lifetime of a well can be used by oil and gas producers to determine the amount of gas within their reservoirs that is produced biogenically. This will help them with production strategies and methods that they can use to enhance bacterial production of methane within these reservoirs.
- The biogenic gas generation rates were determined through experimentation and incubation of produced water samples and shale core samples from a shallow shale gas reservoir in western Canada. With this information a kinetic model of shale gas production was developed.
- The existence of viable bacteria within the reservoir core inoculations and produced water incubations was established and the microorganisms present within the reservoir were identified at the family level using 16S rRNA gene sequencing. It was also determined that the microorganisms present within the serum bottles did indeed consume the hydrocarbons that were available to them within the reservoir cores.

- The amount of methane gas produced in the serum bottles for the produced water and core inoculations could be enhanced via substrate addition.
- A reaction simulation model was developed using experimental reaction rate kinetics, and it was calibrated to field data to predict the maximum amount of amenable total organic carbon (TOC_A) present within the field, as well as determine the amount of biogenic gas that could be produced within a reactor model.
- A numerical model of shallow biogenic shale gas reservoirs which includes experimental biogenic gas production kinetics and gas desorption isotherms was developed. This was used to history match a shallow shale gas reservoir, and determine the percentage of gas produced by microorganisms during the resource life of the well.

1.6 Organization of Thesis

This thesis is comprised of the following chapters.

Chapter Two – This chapter is a literature review of biogenic gas production. It summarizes what has been discovered about biogenic shale gas systems and what still needs to be explored in these systems.

Chapter Three – This chapter describes a new gas material balance theory that can be used to differentiate between the percentage of gas that is produced biogenically versus the free gas that is present within the reservoir. This chapter also presents novel Langmuir adsorption curves for shale gas reservoirs in western Canada.

Chapter Four – This chapter outlines the experiments that were carried out to quantify the amount of methane produced by the methanogens, and also identifies the microorganisms present through a 16S rRNA gene sequencing study. It also includes a study on the metabolites present within the samples, the ability of microorganisms to consume hydrocarbons, and the ability of different substrates to enhance methane gas production.

Chapter Five – This chapter presents a reaction engineering model that uses experimental methane production kinetics and Darcy flow to model the amount of gas that can be produced biogenically within a reservoir.

Chapter Six – This chapter is the application of the previous chapters. Experimental data were used to develop a kinetic model which was input into a reactive reservoir numerical simulation model to understand biogenic gas production from the reservoir. The methodology used for modelling and the data collected within this research show that direct modelling of the reservoir can be done to both history match and predict biogenic shale gas production.

Chapter Seven – This chapter presents the concluding remarks for this research and it includes recommendations for future studies.

Chapter Two: Literature Review

2.1 Introduction

Microbial methane production was first discovered in 1776 by an Italian physicist by the name of Alessandro Volta. He found "combustible air" in sediments of streams, bogs and lakes that contained rich decaying organic matter (Balch et al., 1979). Since then, many discoveries have been made into the existence of methane producing archaea in anaerobic environments deep within the subsurface. Methanogens are responsible for the production of methane in many shallow gas reservoirs all around the world. Biogenic shale reservoirs have been studied in the past geologically by monitoring hydrocarbon composition, isotopic composition of methane, carbon dioxide and hydrogen, and organic and inorganic carbon compositions. Biodegradation of oils by methanogens and other microbial consortia have also been studied, however currently little is known about the microorganisms responsible for gas production in shale reservoirs, the rates of gas production due to biogenic gas in shale gas reservoirs or the metabolic pathways of methane production.

Currently there has been some research on microbial generation of methane gas from hydrocarbons using experimental bioassays (Gieg et al., 2008; Jones et al., 2008a). However, very little is known about methane generation kinetics from biogenic shale in the WCSB. This thesis explores methane generation kinetics from biogenic shale gas reservoirs in western Canada, and also estimates the amount of biogenic gas present within the reservoir. This literature review presents a summary of all of the data currently available on biogenic shale gas reservoirs and methanogenesis in these reservoirs.

2.2 Properties of Shale

The reservoir of interest in this thesis is located in the WCSB in the Alderson member more commonly known as the Milk River formation. This reservoir contains mostly sandstone with interbedded layers of shale. The sandstone part of the reservoir has larger pore spaces and gas within the reservoir is initially produced through the larger permeability sandstone regions of the reservoirs. The shale intervals have a much lower permeability on the order of (nano Darcy) nD and the sandstone has higher permeabilities on the order of (milli Darcy) mD. Shale is a fine-grained sedimentary rock that is formed by compaction of silt and clay. It is in a category of sedimentary rocks known as mudstones, which are rocks that are formed from clay and mud. Shales are generally fissile and laminated with thin beds of sandstone, limestone or dolostone and they can easily break along these laminations. Shales are composed of a combination of organic matter, carbonate, clay, and silica. The ratio of each constituent is variable depending on where the shale is found.

Black organic shales are known as the source rock for production of hydrocarbons (oil and gas) therefore understanding how they contribute to hydrocarbon production in different reservoirs is of interest. The black color is obtained from tiny organic matter that is deposited within the mud when the shales are formed. The shallow shale gas reservoir in this study is interesting because the shales are both the source and the reservoir rock for the methane gas.

2.3 Properties of Kerogen

The microorganisms that live within the reservoir need to consume organic matter or inorganic compounds like H_2 and CO_2 to produce methane. Organic material found in shales is either bitumen or kerogen. Kerogen is formed by the decomposition or degradation of organic matter. Kerogen is a high molecular weight (>1000 Daltons), insoluble, polymeric organic component of shale (Stanton, 1991). It is primarily made up of carbon, oxygen, hydrogen, nitrogen and sulphur compounds. Kerogen can be classified into three main types depending on hydrogen/carbon and oxygen/carbon ratios as shown in Figure 2.1.

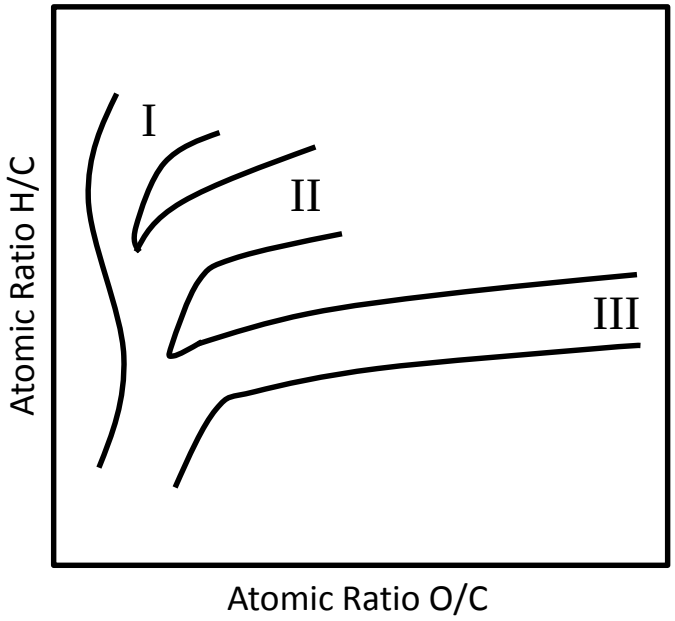

Figure 2.1. Van Krevelen diagram (modified from Behar et al., 2003).

1. Type I kerogen has a high initial H/C ratio and a lower initial O/C ratio. It consists mainly of aliphatic or straight chain hydrocarbons. This type of kerogen has a tendency to produce oil, and it is the rarest of the three main types.

2. Type II kerogen also has a high initial H/C ratio and a lower initial O/C ratio. This type of kerogen can produce both oil and gas. Type II kerogen can contain a large amount of sulfur, and this type of kerogen is termed Type II sulfurous kerogen.
3. Type III kerogen has a low initial H/C ratio and a high initial O/C ratio. It is made up of mainly terrestrial plants and contains aromatic compounds.

2.4 World Wide Biogenic Gas Deposits

Methane gas of biogenic origin accounts for at least 20% of all of the known gas resources (Rice and Claypool, 1981). As shown in Figure 2.2, there are many biogenically productive basins around the world. A significant amount of biogenic methane in addition to thermogenic methane gas is present in some of the most productive reservoirs in the world (Martini et al., 1998). These include the West Siberian sedimentary basin (Cramer et al., 1996), the U.S. Gulf Coast (Rice, 1992) and the Po Basin in Italy (Mattavelli et al., 1992).

Natural gas deep within these reservoirs can be generated microbially by methanogens in shallower reservoirs, thermal cracking of kerogen or coal deep within the reservoirs, or by secondary cracking of oil. The gas in the reservoirs shown in Figure 2.2 is characterized as methanogenic by its low $\delta^{13}C$ values and the presence of methane within the reservoir. $\delta^{13}C$ is the ratio of carbon 13 to carbon 12 present within the sample over the ratio of carbon 13 to carbon 12 present within a standard material as shown in Equation 2.1. These reservoirs also contain a large quantity of gas that has

migrated from different areas, therefore, it is hard to determine the percentage of gas that is thermogenic or biogenic.

$$\delta^{13}C = \left(\frac{\left(\frac{^{13}C}{^{12}C}\right)_{sample}}{\left(\frac{^{13}C}{^{12}C}\right)_{standard}} - 1 \right) \times 1000\ ‰ \qquad (2.1)$$

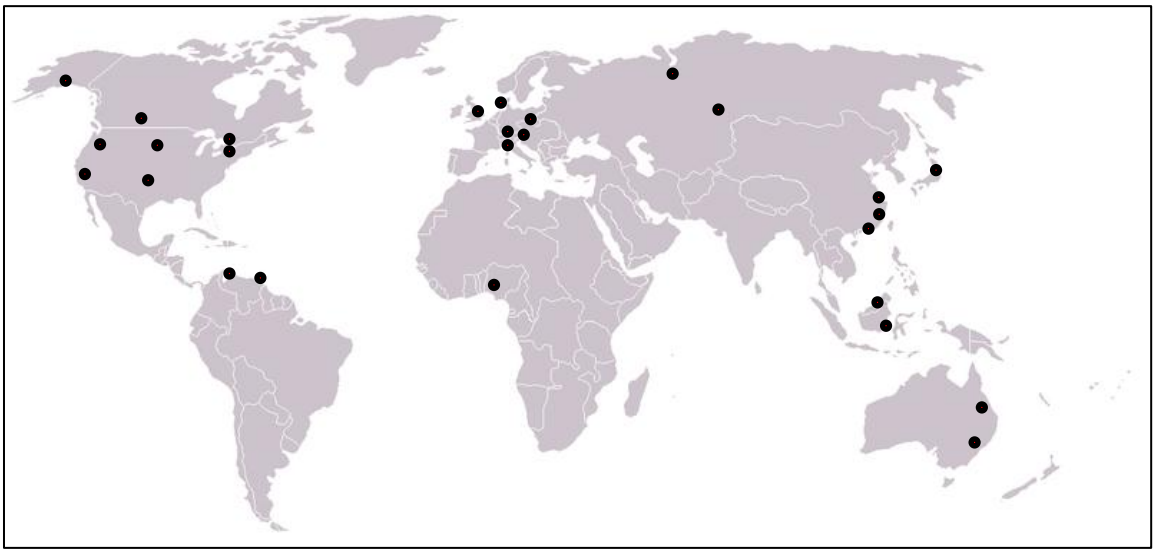

Figure 2.2. Known biogenic methane reservoirs around the world (data obtained from Martini et al., 1998).

Another important characteristic of these unconventional reservoirs is their low permeabilities. The permeability, pore connectivity and transport of the gas from where it is produced to another location is very poor, thus these shales are not only producing the gas but they are also storing the gas. Gas produced in shale reservoirs does not tend to migrate easily from one location to another, therefore the gas produced from a specific reservoir was most likely also generated from that same reservoir.

2.5 Geochemical Evidence of Methanogenesis

Gas production from the Northern Great Plains of Alberta, Saskatchewan and Montana are characterized by early-generation biogenic gas systems (Shurr and Ridgley, 2002). These reservoirs are typically of very low permeabilities, and the gas generation begins very soon after the deposition of the reservoir and source rocks. Biogenic gas accumulations can be present in regions where there is biogenic gas in the shallower portion of the reservoir, with thermogenic gas deeper within the same reservoir. For example, the Alberta basin has biogenic gas on the southeastern margin (Ridgley et al., 1999) and thermogenic gas in the center of the basin. Biogenic gas is found at depths of less than 600 m and at an average depth of 490 m in gas fields in western United States (Rice and Claypool, 1981; Shurr and Ridgley 2002). Biogenic gas is dominantly composed of methane however smaller amounts of (up to 2%) of ethane, propane, butane and pentane can also be found (Rice and Claypool, 1981).

Methane produced by biogenic gas contains isotopically lighter carbon, and thermogenic gas has isotopically heavier carbon. The lighter isotopes are a result of kinetic isotope fractionation by the methanogenic bacteria, essentially, the methanogens enrich the lighter isotopic carbons. The carbon isotopic compositions are compared to the Pee Dee Belemnite standard on a per mil basis according to Equation 2.1 (Dave et al., 2005). The international standard for carbon isotopes is the Vienna Pee Dee Belemnite (VPDB) ratio of $^{13}C/^{12}C$ which has a value of 0.0112372 (Dave et al., 2005). A positive ratio means the ratio of what is being measured is larger than VPDB and is termed “enriched” and a negative ratio means that the sample has a ratio less than VPDB and is called “depleted”

(Dave et al., 2005). Thermogenic gas is characterized by heavier carbon isotopes because during thermal cracking the lighter carbon chains are broken preferentially over the heavier carbon isotope chains (Hoefs, 2004). The carbon isotopes that are present in the CH_4 and CO_2 gases within the reservoir are a result of the mechanisms by which the gas was produced. Isotope analyses have been used in the past to determine the origin of gases, however they are not an exact method for determination of the origin of natural gas. The isotopic compositions of both carbon 13-isotope ratio ($\delta^{13}C$) and deuterium-isotope (δD) relative to analytic standards can be used to characterize a field as either thermogenic, mixed or biogenic, as shown in Figure 2.3.

Studies of gas that are produced from shallow Cretaceous reservoirs in Saskatchewan, Alberta, and Montana have been determined to be of biogenic origin based on their carbon-isotope ratios of methane ranging between -65 and -77.4‰ (per mil) (Ridgley, 2002). Migration of thermogenic gas into the reservoir, and also production of methane via the CO_2 reduction pathway may also produce carbon isotopes similar to those seen in thermogenic reservoirs (about -55 to -40‰ relative to the Pee Dee Belemnite (PDB) standard) (Martini et al., 1998). Other factors such as mixing of gas from different sources, gas migration, and bacterial oxidation of thermogenic gas can produce varying isotopic and compositional data (Martini et al., 1998). There are many factors that can complicate the differentiation of these gases solely based on isotopic studies, therefore the geology, chemical composition and isotopic evidence should all be considered to determine the origin of the gas (Rice, 1981).

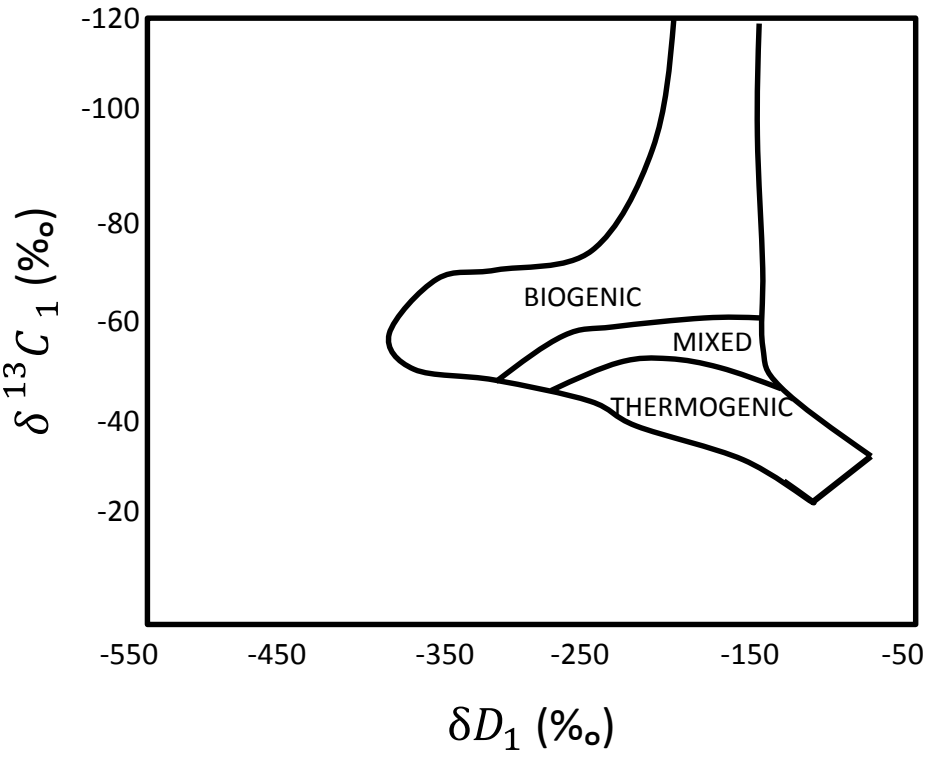

Figure 2.3. Cross plot of carbon-isotope ratio (δ^{13}C) and deuterium-isotope ratio (δD) (modified from Shurr and Ridgley, 2002). Biogenic shales exist in the biogenic envelope.

These common indicators of $\delta^{13}C$ in the methane and the $C_1/[C_2 + C_3]$ ratios have been found to be somewhat unreliable in these systems (Martini et al., 1998). However, there are many other geochemical analyses that can be carried out on the gas and produced water to determine the origin of the gas they are; the alkalinity and $\delta^{13}C$ of dissolved inorganic carbon (DIC) in the coproduced water, δD of the methane and coproduced water and $\delta^{13}C$ of the carbon dioxide produced. In some reservoirs coproduced water and dissolved inorganic carbon can provide even stronger indicators of gas origin (Rice, 1984; Whiticar et al., 1986; Scott et al., 1994; Smith and Pallasser, 1996; Martini et al., 1998). Also, the hydrogen composition of water can also be used to provide an origin of the gas since one of the methanogenic pathways uses CO_2 reduction and in this pathway

hydrogen which most likely comes from formation waters is converted into methane (Shurr and Ridgley, 2002). Basically if the methanogens are indeed using the hydrogen from the formation waters then the deuterium isotope ratio within the formation water and the produced hydrogen should be similar. The amount of salinity within a reservoir will also help determine the origin of the gas (Martini et al., 1998). Chloride concentrations of 3 molal or greater will hinder microbial activity, and chloride concentration above 4 molal will be too high for any type of methanogenic activity (Zinder, 1993).

2.5.1 Milk River Formation Geology and Geochemistry

The Alderson member, more commonly referred to as the Milk River formation, has an estimated 0.5 Tcf of producible gas within the Abbey pools (Pedersen, 2003). The reservoir is a shallow sandstone reservoir with interbedded shale bits located in southwestern Saskatchewan and southeastern Alberta. The interbedded shales are 1 to 20 mm thick interbedded with very fine-grained sandstone (Pedersen, 2003). The porosity of the system is between 12 to about 20% and the total organic content of this reservoir is quite low compared to biogenic reservoirs found in the United States ranging between 0.4 - 1.5 wt% (Ridgley, 2000). Although the weight percent of organic matter is very low within this formation, only 0.5 wt% of total organic carbon (TOC) is required for methanogenic activities (Clayton, 1992; Ridgley, 2000). Figure 2.4 shows a core obtained from the Milk River formation from depth 264.7 – 271.96 m. As seen in Figure 2.4 the reservoir appears to be essentially homogeneous with very thin layering of the different sandstone and siltstone layers.

Figure 2.4. Core image from the Alderson Member from depths of 267.4 to 271.96 m.

2.5.2 Microbial Generation Rates in the New Albany Shales

A study conducted by Schlegel et al. (2011) investigated microbial methane generation rates in the New Albany Shales by using noble gases. The New Albany Shales located in the Illinois Basin are known to contain both thermogenic and biogenic gas accumulations. Currently little is known about the origins of this gas, residence times, and the gas production rates within the reservoir. Correlations between the deuterium ratio (δD) values in the low salinity formation waters and the methane show that the methanogens extract hydrogen from the formation waters (Schoell, 1980; Martini et al., 1998). Using this knowledge of the hydrogen source for methanogenesis constrains the source and timing of ground water recharge enabling researchers to estimate a minimum in-situ metabolic methane production rate. The age of the recharging produced water was calculated using ^{4}He and this was used with other indicators in the water and gas such as stable isotopes of oxygen and hydrogen, chloride , tritium, ^{14}C, and noble gases (Schlegel et al., 2011). It is believed that the fresh meteoric water transported the methanogens deep into the organic-rich New Albany Shales. Schlegel et al. (2011) estimated that the rates of gas production within this reservoir range between 10 to 100 Tcf/Ma for 20% microbial methane to 100 to 1000 Tcf/Ma for 80% microbial methane. These rates are much lower than the rates that were found in other laboratory studies (Jones et al., 2008a). Jones et al. (2008a) calculated biogenic gas generation rates to be approximately 10 Tcf/year, which is a difference of 4 – 6 orders of magnitude higher than the study done by Schlegel et al. (2011). There are three possibilities for this discrepancy; (a) laboratory experiments are fundamentally different than reservoir conditions, (b) microbial systems are very diverse, or (c) there is room for improvement

in one or both of the methods. Schlegel et al. (2011) also mention that in the actual reservoir microbial production of methane could be slower in-situ due to a limited supply of nutrients, substrate, transport or because of the presence of toxic environments that could hinder methanogenesis.

2.5.3 Geochemical Evidence of Methanogenic Activity in the Antrim Shale

In the United States a relatively new black shale play known as the Antrim Shale in the Michigan basin produces predominantly biogenic gas (Shurr and Ridgley, 2002). Wells within this play exhibit the highest natural gas production rates within the basin. The gas produced from this play is thought to be biogenic and there is isotopic and geochemical evidence that the methane gas produced within this basin is of microbial origin. Evidence from active wells within this region show evidence of gas being generated actively within the reservoir as opposed to microbial methane generation from the past (Martini et al., 2004). Evidence of known methanogens from production and formation waters have been found to further support the theory of active natural gas production within this formation.

A lot of research has been done on the Antrim Shale in the United States (Shurr and Ridgley, 2002; Martini et al., 1998; Martini et al., 2004). Most of the work has been based on geochemical analysis of the formation and produced water. In a study conducted by Vugrinovich (1988), the importance of the relationship between hydrology and hydrocarbon deposits is explored. Freshwater charge into the Antrim Shale is very important, because it may oxidize higher chain hydrocarbons such as C_2H_6 and C_3H_8, and

leave behind more methane rich gas (Martini et al., 1998). Also, once the O_2 has been spent, anaerobic microorganisms will become active in the reservoir. Sulfate reducing bacteria will then remove the SO_4^{-2} from the system and once the sulfate has been removed the methanogens will most likely move in and begin producing methane by metabolizing either CO_2 or organic matter (Martini et al., 1998).

One geochemical indicator that is used to determine methanogenic activity within a formation is the amount of dissolved inorganic carbon (DIC). DIC is also known as alkalinity. In nature, alkalinity is buffered by carbonate minerals that are present within the rock through an equilibrium process, thus concentrations of DIC are quite low (Martini et al., 1998). The opposite tends to happen when organic matter degradation occurs. In this case the DIC concentrations tend to rise. The ratio of ^{13}C to ^{12}C in the DIC can also be used as an indicator of biogenic versus thermogenic natural gas (Martini et al., 1998). Ratios of $^{13}C/^{12}C$ are calculated and measured against a standard $\delta^{13}C$ scale. In formation waters where microbial activity is not dominant, the carbon isotope ratios $\delta^{13}C$ are similar to those found in the carbonate rocks within the formation. However, in waters where microbial activity is dominant, the microbial process will consume DIC that is selective for ^{12}C leaving behind an environment that is increasingly more enriched in ^{13}C. Thus calculating carbon isotope ratios is a method that can be used to predict whether or not the natural gas present within a reservoir is of microbial or thermogenic origin (Martini et al., 1998). Extremely high amounts of ^{13}C are present within the Antrim Shale further supporting evidence of microbial activity.

2.6 Crude Oil Biodegradation

Biodegradation of oil occurs naturally within the environment. Currently, biodegraded oils represent a large fraction of the oil found within reservoirs, and will only increase as more reserves are discovered. The largest amount of biodegraded oils are found within the oil sands of North and South America. Anaerobic degradation of oils is supported by the lack of oxygenated formation waters (Horstad et al., 1992), the presence of anaerobic microorganisms in formation waters (Bastin, 1926), and anaerobic hydrocarbon degradation experiments in laboratories (Gieg et al., 2008; Rueter, 1994; Zengler et al., 1999; Jones et al., 2008a). Although there is evidence for anaerobic degradation of oils, there is a very limited understanding of the metabolic pathway through which the oil is degraded. There is current evidence of anaerobic biodegradation of crude oils that have very slow reaction rate kinetics deep within the subsurface (Jones et al., 2008b and Head et al., 2003). Biodegradation of oils is linked with dry methane rich gases (Jones et al., 2008b). This could be attributed to either degradation of oil by the methanogens within the reservoir, or biodegradation of the C_2-C_5 alkanes present within the reservoir.

Evidence of oil biodegradation is clear, and some researchers are looking into intentionally degrading oils within the reservoir (Gieg et al., 2008). Oil recovery techniques are only able to extract about 40% of the oil that remains in the ground (U.S. Department of Energy, 2006). Research to investigate the ability of methanogenic consortia to produce methane gas from the oil that remains trapped within the reservoir was done by Gieg et al. (2008). In the study conducted by Gieg at al. (2008), through experimental studies the researchers hypothesized that the oil trapped within a mature reservoir could be converted into methane gas by the addition of a methanogenic

consortium. All of the samples in the experiment were provided with additional nutrients such as nitrogen, phosphorus, CO_2, trace elements and vitamins, however there was no discernible amount of methane observed unless the samples contained hydrocarbons. This shows the potential for methane production from oil reservoirs where oil has already been produced and residual oil remains. According to the experimental rates reported by Gieg et al. (2008), the researchers estimated that an additional 1 to 5 Tcf of methane gas per year could be produced in the United States – this is significant given that current natural gas production in the United States is equal to 30 Tcf per year (Energy Information Administration, 2007).

Another way to detect hydrocarbon biodegradation in reservoirs is by examining the consumption of hydrocarbons through time as the microorganisms consume them. Usually, the most degradable compounds within a reservoir are the straight-chained hydrocarbons (Jones et al., 2008b). Two or three ringed aromatics are generally not degraded in oil fields (anaerobic conditions) until all of the n-alkanes have been degraded. However, if these oils are degraded in the laboratory under aerobic conditions there is removal of aromatics. Also, the conditions for biodegradation will also determine which hydrocarbons are consumed from the system. In areas where sulfate reducers are present with methanogens, degradation of larger aromatics will also occur (Jones et al., 2008b).

16S ribosomal RNA gene sequences were analyzed for the different cultures in the study by Gieg et al. (2008). Sulfate reducing bacteria were found in the oil degrading

consortium. These include *Desulfobulbus*, *Desulfosporosinus*, and *Desulfovibrio*. Also, syntrophic bacteria *Desulfotomaculum* and *Smithella* were also found. Fermentative bacteria were also found. The dominant methanogen present was *Methanosaeta*, an acetoclastic methanogen, and H_2/CO_2 utilizing methanogens were also present within the inoculum such as *Methanoculleus* and *Methanomicrobiales*.

In a study by Larter et al. (2006), the authors investigated the controls on the composition of biodegraded oils deep within the subsurface. They found that the most biodegraded oils are found near the oil water contact and the compositional changes observed in shallow petroleum reservoirs caused by biodegradation are much more different than alterations caused by physical processes. An oil charge biodegradation model was used by Larter et al. (2006) to determine typical biodegradation fluxes in fresh petroleum clastic reservoirs to be 10^{-3} to 10^{-4} kg petroleum m^{-2} oil water contact $year^{-1}$.

2.7 Biogenic Methane Production in Coal

A few studies have been conducted on biogenic generation amounts from coal bed methane and gas production from coal beds currently accounts for about 10% of the total natural gas production in the United States (Jones et al., 2008a; Fletcher, 2005; Petzet, 2005). Natural gas that is present in coals can be of either biogenic or thermogenic origin and the biogenic gas typically comes from shallow depths where the temperature is less than 80°C. The biogenic methane generating potential of coal was evaluated in the laboratory for coal samples obtained from Texas, Wyoming, Alaska and Pennsylvania by Jones et al. (2008a). A well characterized consortium of bacteria and methanogens was

added to the coal samples, and new biogenic methane production was observed in many of the coal samples. These results provide an important insight into potential biogenic methane generation from coals. Coal bed methane is currently a very important economic activity, therefore the direct economic impact of this research is quite clear since coal can be converted into methane gas by the addition of microorganisms. The study by Jones et al. (2008a) is mainly concerned with secondary biogenic gas generation. Primary methane gas generation within coals occurs during initial peat deposition, but is essentially lost during burial and coal formation. The actual mechanisms involved and the controls on secondary biogenic gas generation are unknown. The fraction of the coal that is biodegraded is unknown. This also holds true for many other studies, it is unclear which hydrocarbon within either coal, shale or oil is being used by the bacteria to form methane gas, and the quantity of the hydrocarbon that is consumed. Currently there is little knowledge of the bacterial consortia that are metabolizing complex materials within the coals to produce methane. The maximum methane gas production reported by Jones et al. (2008a) was 1.75 cm^3/g of core.

2.8 Methanogens and Syntrophy

Several different communities of bacteria and archaea work together and cooperate in methanogenic degradation. Methanogenic degradation of hydrocarbons or organic matter involves the cooperation of three different groups of organisms these are primary fermenters, secondary fermenters and methanogens (Worm et al., 2010). Primary fermenters form products such as alcohols, fatty acids, branched and aromatic fatty acids, and long chain fatty acids from hydrolysis. They produce substrates that can be used

either directly by methanogens or need to be further metabolized by secondary fermenters. Methanogenesis is the final step of anaerobic degradation of organic matter. As shown in Equations 2.2 and 2.3, one group of methanogens use H_2/CO_2 and another group use acetate or methanol to produce methane. Presently there are only two known genera of acetoclastic methanogens; these are *Methanosarcina* and *Methanosaeta*. *Methanosarcina* is a versatile methanogen they can grow with different substrates such as methanol, methylamines, H_2/CO_2 and acetate (Worm et al., 2010).

$$4H_2 + CO_2 \rightarrow CH_4 + 2H_2O \quad (2.2)$$

$$CH_3COO^- + H^+ \rightarrow CH_4 + CO_2 \quad (2.3)$$

Syntrophism is referred to as the ability of an organism to transfer electrons to another organism (Worm et al., 2010). This is a special type of symbiosis where the growth of one microorganisms is dependent on the supply of nutrients or removal of products by another microorganism. Cooperation of the bacteria is essential for the production of methane in subsurface environments. For example, the Gibbs free energy for certain hydrogen generating fermentation reactions are positive, which means they will not take place spontaneously, however, the Gibbs free energy can become negative if the partial pressure of hydrogen decreases, then the reaction becomes spontaneous, which will happen with methanogens present because they consume the hydrogen (Worm et al., 2010). Therefore, methanogens are dependent on fermenters to produce their by-

products but the fermenters are dependent on the methanogens to actually consume their products so that they may produce the required substrates for the methanogens.

Methanogenic archaea use simple carbon compounds as substrates including H_2/CO_2 and acetate (Worm et al., 2010). They can also use some other substrates such as methanol, formate, methylamines, dimethyl sulfide, ethanol and isopropanol (Gilcrease, 2007). For the actual conversion of more complicated organic substrates to methane other microorganisms such as acetogenic bacteria and fermentative bacteria are needed, and thus are present in methanogenic environments (Gilcrease, 2007). The simple compounds that the methanogens need such as H_2, single carbon compounds, or acetate are not abundant in environments where there is little or no biological activity. Thus microbial methane generation is dependent on a consortium of microorganisms to produce these compounds from organic matter such as kerogen, bitumen or other hydrocarbons within a formation. Methanogenesis is not limited by what fuels the methanogens but by what fuels the precursors that drive methanogenesis.

Figure 2.5 shows the complexity of anoxic decomposition and the multitude of microorganisms that are involved in the production of methane gas. This shows how various different anaerobes work together to convert complex organic compounds into CH_4 and CO_2. There are only a limited amount of metabolic reactions that can produce methane. These archaea can generate methane via two metabolic pathways: carbon dioxide reduction or acetate fermentation (See Equations 2.2 and 2.3) (Martini et al., 1998). Most of the methane is produced via carbon dioxide reduction, except for fresh

water environments where acetate fermentation is more common (Shurr, 2002; Martini et al., 1998).

Experimental evidence shows that the hydrogen needed by methanogens is derived from the formation water of the reservoir (Daniels et al., 1980; Balabane et al., 1987). The microorganisms are also capable of consuming other organic compounds. Although the exact mechanism by which these bacteria produce methane gas varies from organism to organism, the net gas production within the reservoir is:

$$C_nH_{2n+2} + \frac{(n-1)}{2}H_2O \rightarrow \frac{(n-1)}{4}CO_2 + \frac{(3n+1)}{4}CH_4 \quad (2.4)$$

where n is the number of carbons in the hydrocarbon that is being consumed in the process.

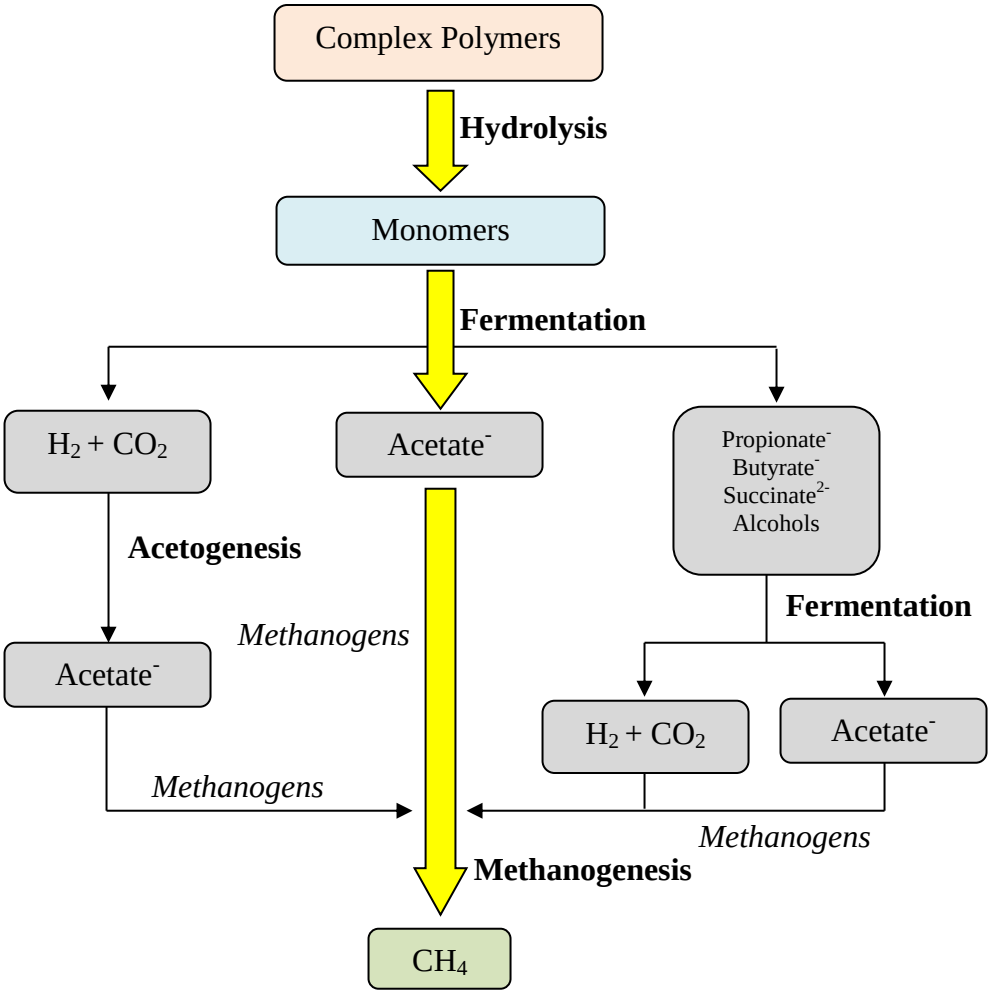

Figure 2.5. Overall process of anoxic decomposition (Modified from Madigan et al., 1997).

Biological formation of methane is understood for easily degradable molecules such as carbohydrates, proteins, and lipids, however very little is known about consumption of organic compounds that lead to methane production (Zengler et al., 1999). In the research conducted by Zengler et al. (1999), biological conversion of a long chain alkane by anaerobic microorganisms is studied. It is known that methane is the terminal process in the biological degradation within aquatic habitats. This usually occurs once the oxygen in the reservoir is depleted and nitrate, ferric iron and sulfate have also been

depleted. Evidence of hexadecane being converted into methane is shown in Zengler et al. (1999).

A study of the microorganisms involved in the conversion of hexadecane into methane were investigated by 16S ribosomal RNA gene sequencing obtained from the enrichment cultures (Zengler et al., 1999). Some of the microorganisms identified in the enrichment cultures include *Desulfovibrio*, a hydrogen utilizing sulfate reducing bacterium, *Methanosaeta*, which is an acetoclastic methanogen, *Methanospirillum* and *Methanoculleus* which are H_2/CO_2 consuming methanogens. The findings in the study by Zengler et al. (1999) are very valuable because they are the first to directly show biodegradation of long chain alkanes, and provide an insight into different microorganisms that may be involved in the production of methane. In many deep reservoirs the depletion of oxygen, nitrate, ferric iron and sulfate leads to methane production.

2.9 Gas Transport Mechanisms

Shale gas reservoirs are known for gas flows in really tiny tight shales resulting in nanoscale gas flows. As described by Javadpour (2007) the actual mechanisms by which stored gas is released and transported to the well is not well understood. There are several nanopore networks involved, and the use of Darcy's law solely is not the best way to model these reservoirs. Although there are natural fractures and induced hydraulic fractures, that increase permeability, present within these reservoirs modelling these reservoirs using only Darcy's law is not sufficient.

The production of gas along with the mechanisms by which it is transported to the well and how it is stored within the reservoir is also of great importance. Figure 2.6 outlines the various gas storage and transport mechanisms from deep within the reservoir to the production well. The production of gas from these reservoirs depends not only on how the gas is formed in the reservoir, but also how it is stored within the reservoir. The gas can be stored within the inorganic matter or organic matter or both, and transport from this solid material is governed by Fick's law of diffusion. Diffusion is governed by the diffusion coefficient and the concentration gradient between the gas phase and the solid phase. In addition to this, surface diffusion or adsorption and desorption from the surface of organic and inorganic material also controls the mass transport process.

Desorption can be described by either the Freundlich isotherm, Henry's law type isotherm, or the Langmuir isotherm as described by King (1990). Knudsen diffusion is also present in the nanopores, mesopores and macropores, since in these pores the mean free path of the molecules is approximately the same size of the pore diameters. Gas is also present within the water that is in the pores. The amount of gas that is present within the water depends on the solubility of methane in water at a particular temperature and pressure. The amount of gas that is present within the formation waters can represent a significant portion of the total gas produced.

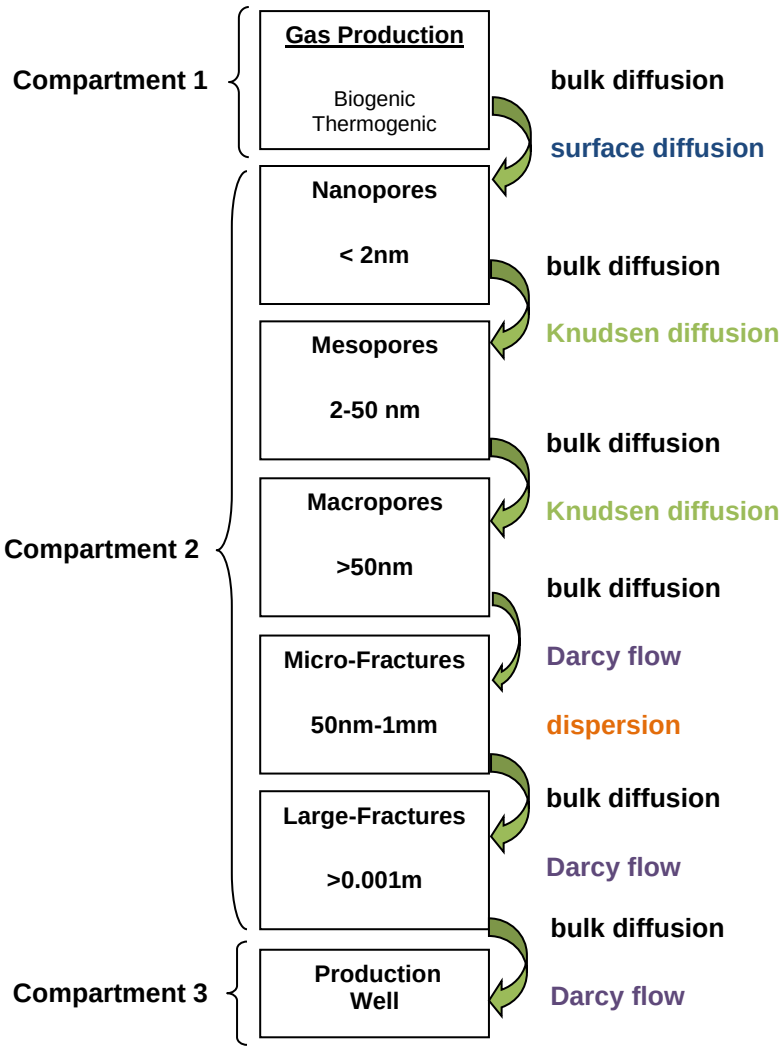

Figure 2.6. Multiscale mass transport of gas in shale gas reservoirs.

2.9.1 Knudsen Diffusion

Knudsen diffusion is present in systems where the mean free path of a molecule is on the same order of magnitude as the pore space through which it is travelling. The Knudsen diffusion coefficient can be described by (Javadpour, 2007):

$$D_{kn} = \frac{d}{3}\sqrt{\frac{8RT}{\pi M}} \tag{2.5}$$

where, D_{kn} is the Knudsen diffusion coefficient, d is the diameter of nanopores, R is the ideal gas constant, T is the temperature and M is the molar mass. Gas within tiny pore spaces does not have the same properties (i.e. density) as gas within larger pore spaces, because it is no longer acting as a bulk fluid.

2.9.2 Darcy Flow

Once gas molecules reach micro-fractures where inertial flow contributions are small and flow is dominated by viscous and pressure forces, Darcy's law applies. Darcy's law takes into account flow of homogeneous fluids through porous media and can be used once the mobility (k/μ) of the system has been determined. The flow rate is defined as:

$$q = -\frac{kA}{\mu}\frac{\Delta P}{L} \tag{2.6}$$

where ΔP is the pressure drop, L is the length of the reservoir, μ is the viscosity of the fluid, k is the permeability of the reservoir, A is the cross sectional area and q is the flow rate. If there are inertial contributions present within the flow, the Forchheimer approximation can be used.

2.10 Gas Storage in Shales

Gas within shale gas reservoirs can be stored as either adsorbed gas on organic or inorganic surfaces, it can be found as free gas within the reservoir, or it can be absorbed into the formation waters. Roughly 70-75% of the adsorbed gas produced in the Antrim Shales is desorbed from both organic and inorganic matter in the reservoir (Martini et al., 2003). Gas in place calculations can become very difficult since the amount of gas that is adsorbed versus the amount of free gas within the system is relatively unknown (Ambrose et al., 2010). Ambrose et al., (2010) propose a new pore-scale model for gas in place within shales. Their new gas material balance incorporates Langmuir equilibrium adsorption isotherms with volumetrics and it accounts for the amount of pore space that is taken up by the sorbed phase. In deeper shale gas systems the inorganic phase has relatively small pore sizes, and the organic phase (kerogen) has larger pore spaces which can store lots of gas, however this organic pore space taken up by the sorbed gas needs to be subtracted from the calculations. The study by Ambrose et al., (2010) essentially found that a significant level of adjustment is required in the volume calculations for shale gas reservoirs with a high total organic amount. They found a decrease in 10 – 25% of total gas storage capacity by using the new gas material balance over the conventional gas material balance.

2.11 Summary of Literature Review

As shown in the literature review research has currently been done in two main areas regarding microbial conversion of hydrocarbons into methane gas. The first is using geochemical indicators such as carbon and deuterium isotopes found in hydrocarbons, produced waters, methane gas, and carbon dioxide gas to identify a gas as biogenic or thermogenic (Martini et al., 1998, Shurr and Ridgley, 2002). The second are methane generation curves for biodegradation using samples of oil and coal in the laboratory to determine methane gas production rates (Gieg et al., 2008; Jones et al., 2008a). Geochemical indicators are not always the best tool to characterize a gas or formation as being biogenic or thermogenic because of mixing of gases within the system and migration of the gases from different sources. There is a need for better indicators to determine the gas generation mechanism within a reservoir. Methane generation curves and gas chromatograms of substrate utilization through experimental studies enable researchers to understand the ability of the hydrocarbon sources to be utilized as substrates for methane production. Evidence from these studies has shown that methanogens are capable of consuming hydrocarbons at considerable rates and that they are able to produce methane at sustainable rates within the laboratory. However, there is very little known about the actual metabolic processes of methane production in situ, the fraction of the hydrocarbon consumed by the microorganisms, the limits on microbial methane production and the ability to verify the rates.

Although laboratory experiments on oil and coal samples have been performed previously, there is currently little information, to the author's knowledge, of

experimental methane production from shallow organic shale reservoirs. Also, information is lacking regarding methane production reaction kinetics from shale gas reservoirs, the ability to quantify the amount of new biogenic gas produced during a resource well lifetime through either experimental studies, analytical models, or numerical modelling and simulation. This thesis attempts to fill in the gaps revealed from this literature review.

Chapter Three: New Gas Material Balance to Quantify Biogenic Gas Generation Rates from Shallow Organic-Matter-Rich Shales

Cokar M., Ford, B., Kallos, M.S., and Gates, I.D. "New Gas Material Balance to Quantify Biogenic Gas Generation Rates from Shallow Organic-Matter-Rich Shales," *FUEL*, vol. 104, pp. 443 - 451, 2012.

3.1 Abstract

With increased demand for fossil fuels of more than 50% in the next 25 years, several methods of either enhancing oil and gas production from existing fields or finding new fields and tackling unconventional sources, such as shale gas reservoirs, are currently underway. Microbially-generated methane gas is a significant portion of commercial gas production around the world. At least 20% of the world's methane originates from methanogens that reside within organic matter rich shales and coals. The metabolic processes and chemical reactions carried out by microorganisms in shale gas reservoirs are currently unknown making it difficult to predict or enhance gas generation rates within a given reservoir. Field production data reveal that gas production from these reservoirs declines initially and then stabilizes after a specified time. The stabilized rate is controlled by contributions from biogenic gas generation, desorption of gas from kerogen, and diffusion and transport of gas through nanometer to potentially even micron scale pore systems. It still remains unclear which one of microbial gas generation or gas transport is the key limitation on production of biogenic gas from shale gas reservoirs. This chapter presents a modified gas material balance on production data for shale gas wells to account for biogenic gas generation. Although the gas material balance approach

is well established, it has not been used to estimate biogenic gas generation amounts. By using actual gas production data from a field where biogenic gas production is known to be the main source of gas generation, the amount of biogenic gas that was produced within the reservoir during the resource lifetime of the well could be determined. The results of the theory presented here were compared to gas production data from Nexen's Bigstick Field and Husky's Abbey Field. The results reveal that a significant fraction, up to about one-third, of gas production is sourced from constant biogenic gas generation. The implication is that biogenic shale gas productivity can be potentially enhanced if microbes are stimulated.

3.2 Introduction

Shale gas is an unconventional gas resource that is found in organic rich, fine grained low permeability formations. It is estimated that the WCSB contains over 1,000 trillion cubic feet of gas in its shale deposits. Shales are the source rock for hydrocarbon production and are known to produce methane gas through biogenic, thermogenic or combination mechanisms (Curtis, 2002). Biogenic gas is generated from anaerobic bacteria that produce methane during early diagenesis. Thermogenic gas originates from thermal cracking of kerogen at extremely high temperatures and pressures (Shaw et al., 2006). With increasing natural gas demands within Canada and North America and beyond, shallow biogenic gas reserves are viable sources for natural gas (Shurr and Ridgley, 2002). Within biogenic shale gas formations, the natural gas can be stored as free gas within fractures or rock pores, adsorbed gas on organic materials such as kerogen or inorganic materials such as clays, or gas that has been dissolved into water within the reservoir (Curtis, 2002).

Natural gas systems are usually placed into three categories, illustrated in Figure 1.2. The first category, the deepest one, is the thermogenic kitchen where temperatures are relatively hot and gas is produced by thermogenesis, this region is capped off by the thermogenic ceiling. The depth of the thermogenic ceiling varies with temperature and geothermal gradient, and does not always occur at the same depth. Thermogenic gases are produced by degradation of kerogen or oil at temperatures above 150 - 160°C up to about 250°C (Pepper and Corvi, 1994). In the second category, the shallowest one, is a favorable environment for microbes to generate methane gas; the bottom of this level is known as the biogenic floor. The depths of the biogenic floor and the thermogenic ceiling will vary between reservoirs, but on average the biogenic floor is about 550 m below the surface (Shurr and Ridgley, 2002). The third category sits between the thermogenic and biogenic categories and contains thermogenic gas that has been displaced from deeper intervals and some biogenic gas. Biogenic gases originate from bacterially-mediated anaerobic mineralization of organic matter in sediments up to about 75°C. Microorganisms in the reservoirs produce biogenic gas, which is mainly made up of methane, however it can also contain up to 2% of other gases such as ethane, propane, butane, and pentane (Rice and Claypool, 1981; Whiticar et al., 1986). More than 20% of all natural gas in reservoirs in the world are from biogenic gas (Rice and Claypool, 1981).

A series of microbial ecosystems are involved in the production of biogenic gas. Initially, if present, oxygen is consumed by aerobic bacteria. After the oxygen is depleted, sulfate reduction from the pore water becomes the dominant form of respiration within the system. After the sulfate is consumed, then methane generation occurs mainly by reduction of CO_2 by hydrogen (Rice and Claypool, 1981). Hydrogen is produced by

bacteria that metabolize organic materials that are present within the reservoir. Although biogenic gas is generated relatively slowly inside shale formations, economic amounts of methane have already accumulated within these reservoirs.

There are several limitations in our understanding of production, storage and transport mechanisms of natural gas in shallow biogenic gas systems. Production of methane by microbial activity depends on geochemical, geological, hydrological and biochemical properties of the formation. However, storage and transport of biogenic gas depends on rock permeability and porosity (Shaw et al., 2006). For biogenic shale gas reservoirs, production data typically follows a decline from an initial peak production rate which stabilizes to a nearly constant value after a specified time. The stabilized rate is controlled by contributions of biogenic gas generation, desorption of gas from kerogen, and diffusion and transport of gas through nanometer to potentially even micron scale pore systems. It still remains unclear which one of gas generation versus gas transport limits production from shale gas reservoirs. Here, we present a modified gas material balance on production data for shale gas wells to account for biogenic gas generation to examine contributions from biogenic gas generation. More specifically, we derive a modified gas material balance that includes a biogenic gas generation term, porosity compressibility, and an adsorption isotherm. From the modified gas material balance, gas transport mechanisms can be ranked. Once the amount of gas produced by microorganisms was determined, these values were compared to biogenic gas generation amounts from literature.

3.2.1 Field Geology

Two shallow shale gas reservoirs were evaluated in this study. The first is Nexen's Bigstick Field and the second is Husky's Abbey Field, both located near the Alberta/Saskatchewan border in Canada shown in Figure 3.1 and Figure 3.2, respectively.

The data from 9 wells were used to analyze biogenic gas production from Nexen's Bigstick Field. In this field, gas is sourced from the upper Colorado shales, lower Second White Specks interval. The production of gas from this interval is from three stacked sand units, the upper two units consisting of transgressive shoreface sands, and the lower unit is a highstand shoreface sand.

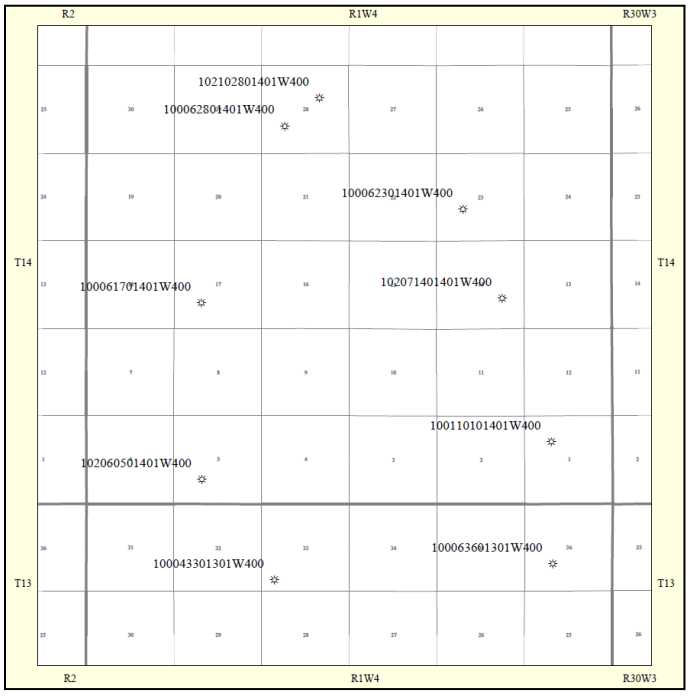

Figure 3.1. Map of all nine wells used in study for Nexen's Bigstick Pool.

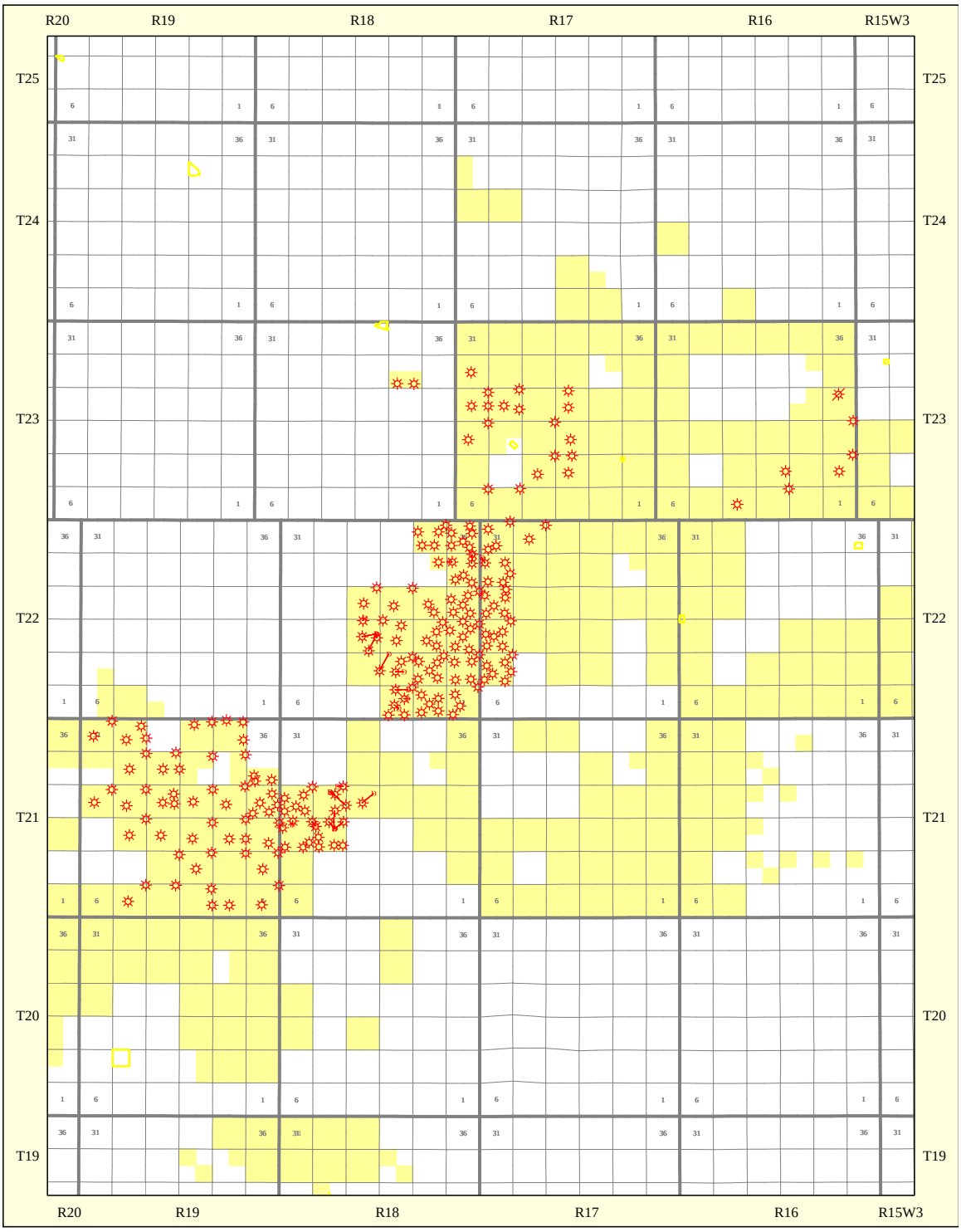

Figure 3.2. Map of all 223 wells used in study for Husky's Abbey Field.

This formation is shallow with depths typically between 300 and 800 m. The ultimate source of the gas and the reservoir are interbedded and the migration of gas from source to reservoir is not significant. In the Bigstick Field, gas production rates range from low to relatively high of about 20,000 to 1,000,000 ft^3/day (566 to 28, 317 m^3/day).

The data from 223 wells were used to analyze Husky's Abbey Field. The main producing zone in this field is a laminated fine sand and a silty/shaley interbedded zone considered to be a prodelta plume of sediment deposited in a deeper shelf environment. The sandstone layers act as a pipeline to produce adsorbed gas in the finer-grained sediments and initial free gas in the higher porosity sand layers. These interbeds are sealed vertically by intraformational mudstone and overlain by tighter bioturbated shales and silts. The individual thin beds are linked vertically by a required fracture treatment that induces a near-vertical fracture. It is this action that allows a large initial production rate, up to 1,000,000 ft^3/day (28,317 m^3/day), from a small perforation interval (often ~2 metres long) to accumulate gas in a vertical and horizontal reach from the wellbore. Production without a fracture treatment yields small amounts of gas for short periods only. Unravelling the complex history of the late-occurring Abbey structure versus the early generation of biogenic gas at 88-66 m.y.a (Fishman et al., 2001) and its subsequent migration into its current setting is still unknown. It would appear that early deeper burial shortly after deposition has generated this biogenic gas, this generation would be terminated when temperatures got too hot with increased burial depths. After migration into this late structure and sitting only at 300 - 400 m depth it would appear that once again temperatures are appropriate to resume biogenic gas generation with current

reservoir temperatures of 14 - 15ºC. Thus current gas production that is shown in this thesis is likely to be a mix of ancient and contemporary methane.

3.2.2 Gas Generation Rates and Storage within the Reservoir

In general, shale gas reservoirs display variable production rates due to changes in near wellbore permeability, fracture width of natural fractures, and hydraulically induced fractures. Gas production rates, at standard conditions, often range between 0.5 and 15 $x10^3$ m^3/d (Shaw et al., 2006). The wells from these formations usually produce low gas rates, however since the wells are quite shallow they are less expensive to drill and complete, thus making them economical (Shurr and Ridgley, 2002). Gas production rates usually decline quickly and then flatten out for the remainder of the well life. The flat decline area is believed to be a result of desorbed gas and gas generation from microorganisms. Gas generation rates and gas reserves are difficult to calculate in unconventional gas reservoirs such as tight gas and shale gas systems (Cox et al., 2002).

Shale gas reservoir production is distinguished by multiple gas storage mechanisms, reservoir heterogeneities, and other unique characteristics that manage gas production (Jenkins and Boyer, 2008). One of these characteristics is the variation in porosity within the reservoir: porosity can vary greatly over a one meter interval. The porosity for these shale systems can be split into two main categories: primary and secondary porosity (King, 1990). Primary porosity is the matrix porosity between rock molecules and is smaller than secondary porosity. Secondary porosity refers to pore space contained in natural fractures within the system. It is believed that as the pressure within the reservoir decreases the gas molecules first desorb from the matrix surface and thereafter diffuse

through the primary porosity regions following Fick's First Law, these molecules then move towards the secondary porosity regions where they are transported using Darcy's Law to the production well (King, 1990). There are three different mechanisms by which gas can be stored within the formation. First, gas can be present in the open spaces between the rock (known as free gas). Second, it can also be trapped within tiny pore spaces which are not connected to each other (non-effective porosity). Third, it can be found as adsorbed methane in kerogen or clay. The matrix has a large amount of surface area, and since it is composed of organic matter it is able to effectively adsorb methane gas (Fathi and Akkutlu, 2009). Almost 50% of the gas that is found in these reservoirs is adsorbed onto kerogen present within the reservoir. Therefore, the total amount of kerogen found within a reservoir greatly affects the adsorption of gas molecules on the matrix (Shaw et al., 2006).

The transport of methane gas through the primary porosity region can follow any of the following diffusion mechanisms either simultaneously or individually depending on the rock or gas properties (King, 1990):

- Surface diffusion: movement of gas molecules along a surface
- Bulk diffusion: movement of gas molecules, where molecular interactions are dominant
- Knudsen diffusion: movement of gas molecules, where molecule-surface interactions are dominant

3.3 Methods

The moles of gas produced are equivalent to the moles of gas initially present in the primary and secondary porosity system plus the moles of biogenic gas produced within the reservoir minus the amount of gas that is left in the primary and secondary porosity system at the end of the production period:

$$n_p = n_{2i} + n_{1i} + \gamma - (n_2 + n_1) \tag{3.1}$$

where n_p is moles of produced gas, n_{2i} is moles of gas in secondary porosity initially, n_{1i} is moles of gas in primary porosity initially, n_2 is moles of gas in secondary porosity, n_1 is moles of gas in primary porosity, and γ is moles of gas generated. The modified gas law can be used to determine moles from the pressure and temperature:

$$PV = znRT \tag{3.2}$$

where P is the pressure, V is the volume, z is gas compressibility, n is the total number of moles, R is the ideal gas constant, and T is the temperature. Equation 3.2 can be substituted into Equation 3.1 to yield:

$$\frac{P_{sc}G_p}{z_{sc}RT_{sc}} = \left(\frac{PV}{zRT}\right)_{2i} + n_{1i} + \gamma - \left[\left(\frac{PV}{zRT}\right)_2 + n_1\right] \tag{3.3}$$

where G_p is the volume of gas produced, P_{sc} is the pressure at standard conditions, z_{sc} is the compressibility at standard conditions and T_{sc} is the temperature at standard

conditions. The gas stored in the primary-porosity matrix can be found from the following equation describing the equilibrium adsorption isotherm (King, 1990):

$$V_E = \frac{V_L P}{P_L + P} \tag{3.4}$$

where V_E is volume of gas stored, V_L is the volume constant for the Langmuir isotherm, and P_L is the Langmuir pressure constant. This volume can be converted to moles by the following equation:

$$C_E = \frac{P_{sc}}{z_{sc} R T_{sc}} V_E \tag{3.5}$$

where C_E is the moles of gas stored. Re-arranging Equation 3.3, and performing substitutions for saturations (see below) we get the following:

$$\frac{P_{sc} G_p}{z_{sc} T_{sc}} = \left(\frac{V_{b2} \phi_i (1 - S_{wi}) P_i}{z_i T}\right) + R V_{b2} C_{Ei} + R\gamma - \left[\left(\frac{V_{b2} \phi (1 - S_{wavg}) P}{zT}\right) + R V_{b2} C_E\right] \tag{3.6}$$

where S_{wi} is the initial water saturation, S_{wavg} is the average water saturation, V_{b2} is the bulk volume of the secondary porosity region, ϕ is the porosity, ϕ_i is the initial porosity, z_i is the initial gas compressibility and C_{Ei} is the moles of gas stored as calculated using the initial equilibrium isotherm. If we assume that the water saturation stays constant and that there is no oil in the reservoir then $(1 - S_{wi})$ and $(1 - S_{wavg})$ are equal to S_{gi} the initial gas saturation (Seidle, 1993). Equation 3.6 then becomes:

$$\frac{P_{sc}G_p}{z_{sc}T_{sc}} = \left(\frac{V_{b2}S_{gi}\phi_i P_i}{z_i T}\right) + RV_{b2}C_{Ei} + R\gamma - \left[\left(\frac{V_{b2}\phi S_{gi}P}{zT}\right) + RV_{b2}C_E\right] \tag{3.7}$$

Re-arranging Equation 3.7 yields:

$$G_p = \frac{V_{b2}z_{sc}\phi_i T_{sc}}{P_{sc}T}\left\{\left[\frac{S_{gi}P_i}{z_i} + \frac{RTC_{Ei}}{\phi_i} + \frac{RT\gamma}{V_{b2}\phi_i}\right] - \left[\frac{\phi S_{gi}P}{\phi_i z} + \frac{RTC_E}{\phi_i}\right]\right\} \tag{3.8}$$

The change of the porosity is given by:

$$\frac{\phi}{\phi_i} = 1 - c_\phi(P_i - P) \tag{3.9}$$

where c_ϕ is the pore compressibility which when substituted into Equation 3.8 leads to:

(3.10)

$$G_p = \frac{V_{b2}z_{sc}\phi_i T_{sc}}{P_{sc}T}\left\{\left[\frac{S_{gi}P_i}{z_i} + \frac{TP_{sc}}{\phi_i z_{sc}T_{sc}}\left(\frac{V_L P_i}{P_L+P_i}\right) + \frac{RT\gamma}{\phi_i V_{b2}}\right] - \left[\frac{[1-c_\phi(P_i-P)]S_{gi}P}{z} + \frac{TP_{sc}}{\phi_i z_{sc}T_{sc}}\left(\frac{V_L P}{P_L+P}\right)\right]\right\}$$

Equation 3.10 can be simplified:

$$G_p = \frac{V_{b2}z_{sc}\phi_i T_{sc}}{P_{sc}T}\left[\frac{P_i}{z_i^*} - \frac{P}{z^*}\right] \tag{3.11}$$

where

$$z_i^* = \frac{z_i}{S_{gi} + \frac{RT\gamma z_i}{\phi_i V_{b2}P_i} + \frac{TP_{sc}z_i}{\phi_i z_{sc}T_{sc}P_i}\left(\frac{V_L P_i}{P_L+P_i}\right)} \tag{3.12}$$

and

$$z^* = \frac{z}{[1-c_\phi(P_i-P)]S_{gi}+\frac{TP_{sc}z}{\phi_i z_{sc}T_{sc}P}\left(\frac{V_L P}{P_L+P}\right)} \tag{3.13}$$

From Equation 3.11, G_p can be plotted versus $\frac{P}{z^*}$ to give V_{b2} (slope) and γ (intercept). The biogenic gas generated, γ, represents the total amount of biogenic gas generated as the reservoir changes from the initial pressure P_i to the final pressure of the well P. This theory categorizes the total amount of methane gas produced as free, desorbed or biogenic. Therefore, knowing the reservoir parameters such as temperatures, pressures, Langmuir constants, reservoir compressibility, porosity, etc. not only can the total amount of gas within the reservoir be determined, but also the amount of gas that is considered free gas within the reservoir, desorbed gas and also microbially generated gas within the reservoir.

3.4 Results and Discussion

As described above, two field cases were analyzed: first, the Bigstick Field operated by Nexen Inc. and second, the Abbey Field operated by Husky Energy Inc. In addition to these two case studies, a high pressure methane adsorption analyses was carried out to determine the amount of methane gas that adsorbed on to the reservoir surfaces. This analysis was carried out on a well located in the Milk River Formation of Husky's Abbey Field. Adsorption data was obtained from two different depths within the formation as described below. The amount of gas produced through microbial activity for these two fields as obtained from the new gas material balance theory was then compared to

Clayton, (1992). Clayton, (1992) reports estimates for the maximum biogenic gas yield given a reservoir volume depending on the total organic carbon within the reservoir.

3.4.1 High Pressure Methane Adsorption Analyses

High pressure methane adsorption analyses were carried out on two different sections of core from two different zones in the Milk River obtained from Husky's Abbey Field. The Milk River D sample was taken from the 313.45 - 314.0 m depth interval whereas the Milk River E sample was from the 324.8 - 325.2 m depth interval. Two grams of the core samples were used for the analysis. The methane adsorption was analysed by using a high-pressured volumetric adsorption technique that employs Boyles' Law $P_1V_1 = P_2V_2$. Basically a known volume of gas was put into a cell with the sample, and the amount of gas that was adsorbed onto the sample material was measured by monitoring the change in pressure in the cell, which was then converted to a volume by using the real gas law. As gas was adsorbed onto the sample the pressure within the cell dropped until equilibrium was reached. The results of this analysis are displayed in Figure 3.3 and Figure 3.4. The Langmuir volume constant and Langmuir pressure constants V_L and P_L were obtained from Figure 3.3 and Figure 3.4. These variables were needed to complete the gas material balance as shown in Equations 3.1 to 3.13.

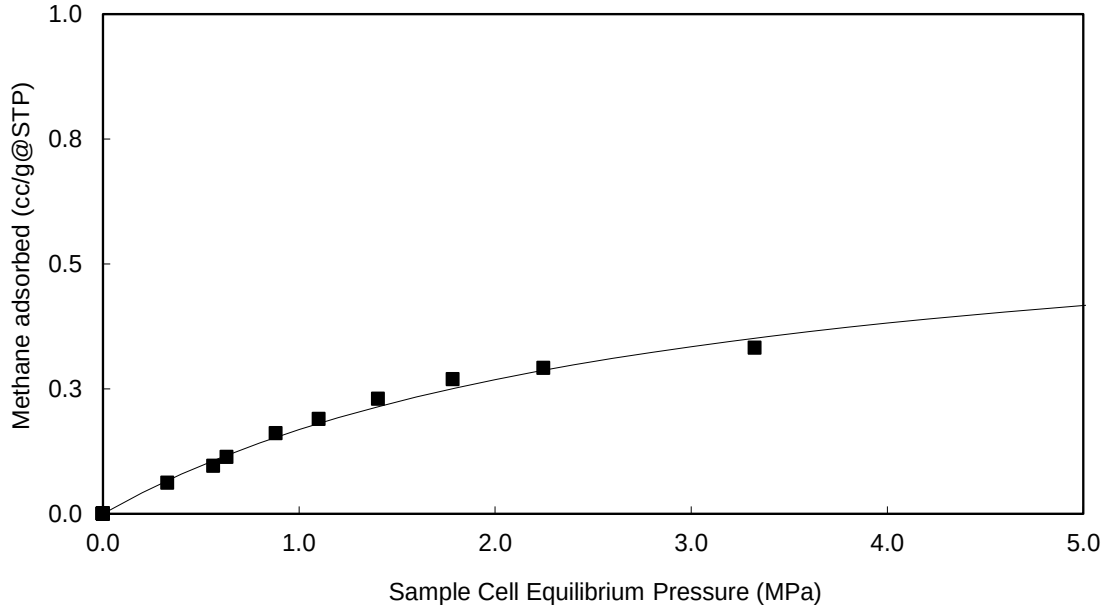

Figure 3.3. Langmuir isotherm Husky Milk River D 313.45-314.0m (CBM Solutions, 2011).

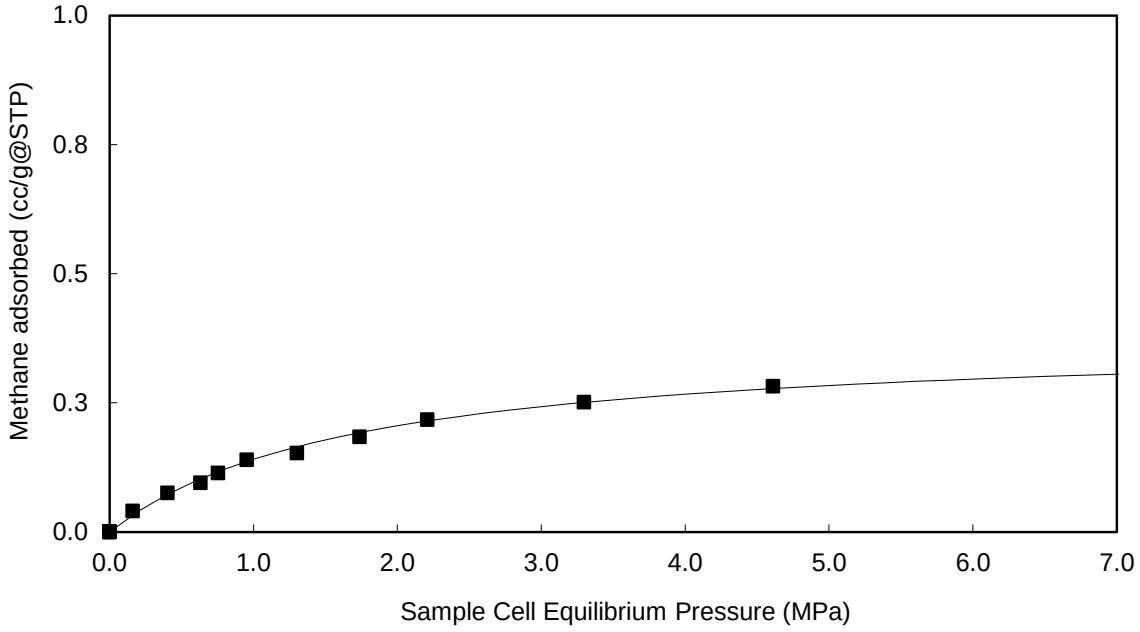

Figure 3.4. Langmuir isotherm Husky Milk River E 324.8-325.2m (CBM Solutions, 2011).

3.5 Case 1 – Nexen's Bigstick Field

Nine wells operated by Nexen in the Bigstick Field were used to evaluate the theory formulated above. These wells produce from the Colorado shale formations. Although these are conventional gas wells, it is believed that the formation from which the gas is produced is sourced from a shale gas formation and the gas production rates observed in these wells are similar to those that would be seen in shale gas wells. The shale gas wells in this area have only been producing since about 2007, therefore there is not enough pressure data from shale gas fields to do a similar analysis, and that is why conventional gas wells adjacent to shale formations were used in the current study. Figure 3.1 shows the location of the wells used in this study.

All volumes were normalized to 288.15K. The pressure and z^* value as obtained from Equation 3.13 was known at different times throughout the well, this was then used to calculate P/z^*. If the gas produced and P/z^* of the nine wells were pooled together, essentially an average pseudo well and pseudo reservoir were created. The data listed in Table 3.1 was then used to construct a single G_p versus P/z^* plot, shown in Figure 3.5 and Figure 3.6 for the Langmuir parameters for zones D and E in the Milk River, respectively, which a linear best fit line was drawn through. The input data for the model is listed in Table 3.1.

Table 3.1. Values used in the equations.

Symbol	Property	Nexen's Bigstick Field		Husky's Abbey Field	
		Value	**Reference**	**Value**	**Reference**
c_ϕ	Porosity compressibility (1/Pa)	1.09 x 10^{-9}	(King, 1990)	1.09 x 10^{-9}	(King, 1990)
P_i	Initial reservoir pressure (Pa)	4,900,000	Field	3,200,000	Field
P_{sc}	Pressure at standard conditions (Pa)	101,325			
P_L	Langmuir pressure constant (Pa)	2.92 x 10^6	Milk River D	2.92 x 10^6	Milk River D
		1.70 x 10^6	Milk River E	1.70 x 10^6	Milk River E
R	Universal gas constant (J/mol K)	8.314			
S_{gi}	Initial gas saturation	0.5	Field	0.6	Field
T	Temperature (K)	288.15			
T_{sc}	Temperature at standard conditions (K)				
V_L	Volume constant for Langmuir isotherm (standard m^3/m^3)	1.485	Milk River D	1.485	Milk River D
		0.893	Milk River E	0.893	Milk River E
z_{sc}	Gas compressibility at standard conditions	1			
ϕ_i	Initial Porosity	0.20	Field	0.20	Field

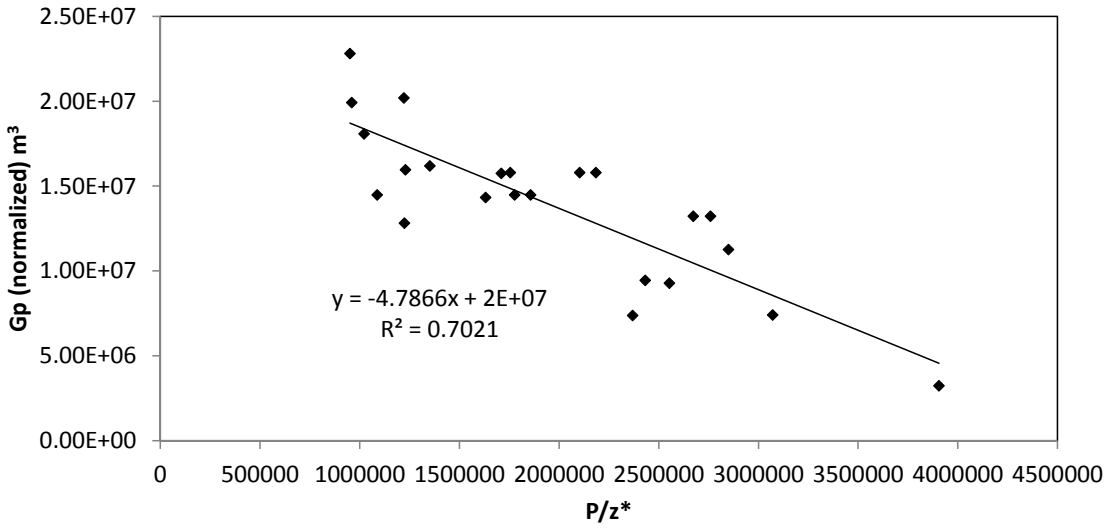

Figure 3.5. Gas produced versus P/z* for Nexen's Bigstick Field with Milk River D Langmuir isotherms. The volumes have been normalized to 288.15K.

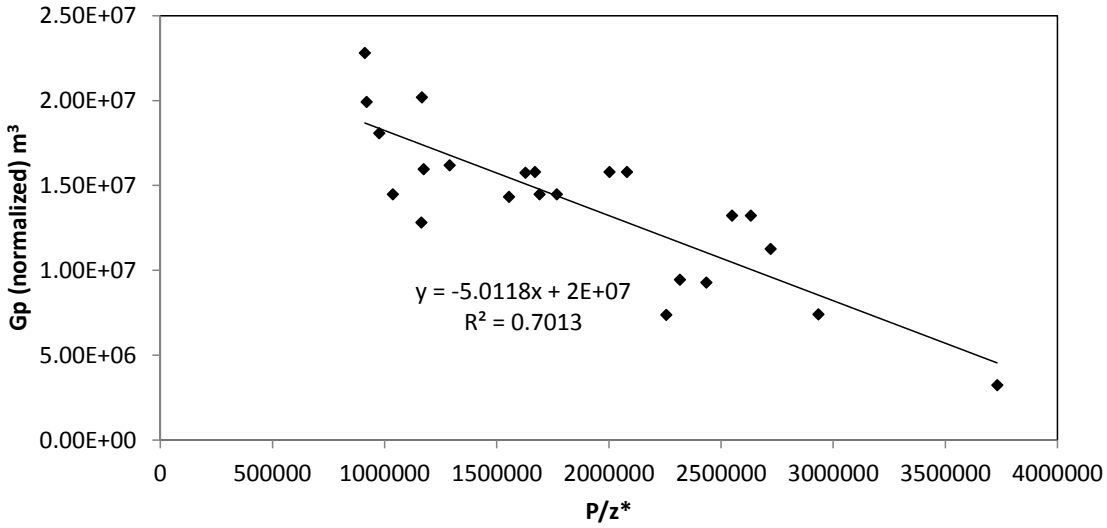

Figure 3.6. Gas produced versus P/z* for Nexen's Bigstick Field with Milk River E Langmuir isotherms. The volumes have been normalized to 288.15K.

This yielded the slope (bulk volume for the pseudo reservoir) and intercept (total amount of biogenic gas produced for the pseudo well), presented in Table 3.2. In other words, a pseudo well was created, representing all of the pressure and total gas production data from this reservoir, to apply the new gas material balance theory. The amount of gas produced from this well was then essentially an average value for the entire field.

To compare the amount of gas produced by microorganisms during the entire production period of the reservoir to the amount of gas produced that was free, and desorbed from the surrounding material within the reservoir, the following analysis was used. An abandonment pressure for the reservoir was taken to be 101,325 Pa (the initial pressure was 4.9 MPa) and the final reservoir compressibility, z, was set equal to 1 (essentially gas behaves as an ideal gas). The analysis was completed with the Langmuir parameters for both zones D and E in the Milk River. When these values were used, it was found that the total amount of gas produced was approximately 2.29×10^7 m^3, and when the Langmuir constants for zone D were used, 36.9% of the gas produced was from microbial activity during the production period, 53.8% was free gas already present within the secondary porosity region, and 9.3% was gas desorbed from different surfaces, and when the Langmuir constants for zone E were used 36.8% of the gas produced could be attributed to microbial activity during the production period, 56.4% was free gas already present within the secondary porosity region, and 6.8% was gas desorbed from different surfaces. The results are tabulated in Table 3.2 for more clarity. The results from the two zones were similar. Also for this field, the amount of gas produced biogenically by

Table 3.2. Properties calculated from theory.

Values	Nexen's Bigstick Field (Milk River D)	Nexen's Bigstick Field (Milk River E)	Husky's Abbey Field (Milk River D)	Husky's Abbey Field (Milk River E)
Intercept (m^3)	2.33×10^7	2.32×10^7	4.68×10^7	4.69×10^7
Slope (m^3/Pa)	-4.79	-5.01	-1.57×10^1	-1.64×10^1
V_{b2} **(m^3)**	2.42×10^6	2.54×10^6	7.96×10^6	8.31×10^6
z_i	0.934	0.934	0.94	0.94
z_i^*	1.01	1.06	1.07	1.12
Moles of biogenic gas produced	3.57×10^8	3.56×10^8	3.60×10^8	3.61×10^8
Volume of biogenic gas produced (m^3)	8.44×10^6	8.41×10^6	8.52×10^6	8.53×10^6
Volume of free gas (m^3)	1.23×10^7	1.29×10^7	3.11×10^7	3.25×10^7
Volume of gas produced by desorption (m^3)	2.14×10^6	1.56×10^6	5.78×10^6	4.43×10^6
Total gas produced if final reservoir pressure is 101,325 Pa (m^3)	2.29×10^7	2.29×10^7	4.54×10^7	4.55×10^7
Volume biogenic gas/total gas	0.369	0.368	0.188	0.188
Volume free gas/total gas	0.538	0.564	0.685	0.715
Volume gas desorbed/total gas	0.093	0.068	0.127	0.097

microorganisms during the resource lifetime of a well was more than a third of the total gas produced.

The results found in this study were then compared with another set of data using the amount of gas that was produced by microorganisms in a study completed by Clayton, (1992). In the current study the maximum yield of biogenic methane as a function of the total reservoir volume was calculated for a 10% conversion of organic matter into methane, as shown in Figure 3.7. This was considered the upper limit. If the bulk volume as calculated from Equation 3.13 was used for the combined data set and the average total organic carbon of the source was between 1% and 50%, the maximum amount of methane produced for this pseudo reservoir volume from Figure 3.7 was between 10^7 m^3 and 10^9 m^3. Since all of the gas in this pseudo reservoir came from microbial degradation, the total volume of gas of 2.29×10^7 m^3, from analyses D and E separately, fell in between the upper and lower limits of Figure 3.7. This shows that the calculation based on the combined data set provides good agreement between the field data and Clayton's results.

In conclusion, after the above analysis was carried out on Nexen's Big Stick field it was clear that 37% of the gas produced during the resource lifetime of a well in this reservoir was directly derived from ongoing biogenic gas generation.

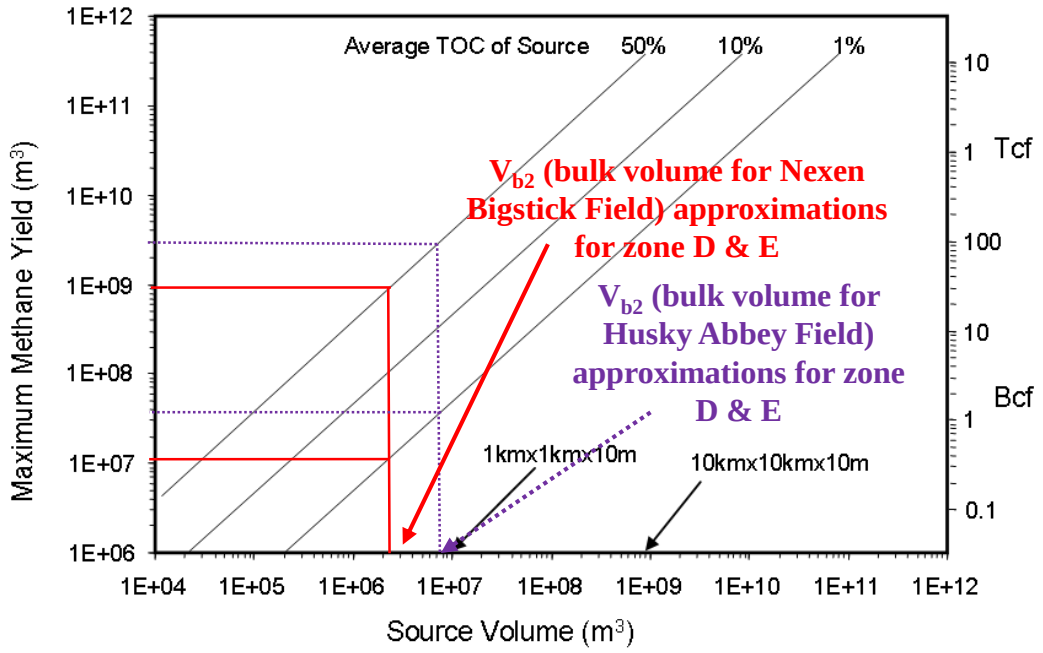

Figure 3.7. Maximum yield of biogenic methane as a function of source sediment volume (Clayton, 1992).

3.5.1 Case 2 – Husky's Abbey Field

The same analysis, as described for the Bigstick Field, was carried out on Husky's Abbey Field. However, in this case the bottom-hole pressure for 223 wells was measured. These wells produce from the Milk River formation, Alderson member. The wells in this area have been producing since about 2002. The static bottom hole pressure was approximated from the shut-in casing pressure (SICP) for a new well that was drilled in a specific section before that well was fractured. The SICP was then corrected for depth and lack of build-up time. This corrected bottom-hole pressure was plotted against the cumulative production for offsetting wells within the section at the fracture. All 223 pseudo section-wells were plotted to create a section-sized final combined well plot. Equation 3.11 was then used and a plot of G_p vs. $\mathrm{P/z}^*$ was plotted as shown Figure 3.8

and Figure 3.9. Figure 3.8 plots the produced gas versus pressure using the Langmuir isotherm constants for zone D and Figure 3.9 is for the case with the Langmuir isotherm for zone E. From the slope and intercept of this graph, along with Equations 3.12 and 3.13, the following information was obtained. Using the Langmuir isotherm constants for zone D and E, it was found that 4.54 x 10^7 m^3 and 4.55 x 10^7 m^3 of gas was produced, respectively in this pseudo reservoir. Of the gas produced using the data from zone D Langmuir constants, 18.8% was produced from microbes during the well life, 68.5% was free gas in the system, and 12.7% of the gas was desorbed from surfaces. Using zone E Langmuir constants, 18.8% was biogenic gas produced during the resource lifetime of the well, 71.5% was free gas contained within the reservoir and 9.7% was desorbed gas.

The results from this analysis were also compared with Clayton's values as shown in Figure 3.7. The average value from both Langmuir constants of V_{b2} is marked on Figure 3.7, and according to this the amount of gas produced should be between 4 x 10^7 and 2 x 10^9 m^3. And as shown in Table 3.2 the amount of gas produced shown was 4.54 x 10^7 m^3 for Milk River (D Langmuir constants) and 4.55 x 10^7 m^3 Milk River (E Langmuir constants), which are between the two values shown in Figure 3.7. These values are close to the 1% TOC line and from laboratory analysis it is known that the TOC content for this reservoir is approximately 1%, so this is indeed a very good match to Clayton's data.

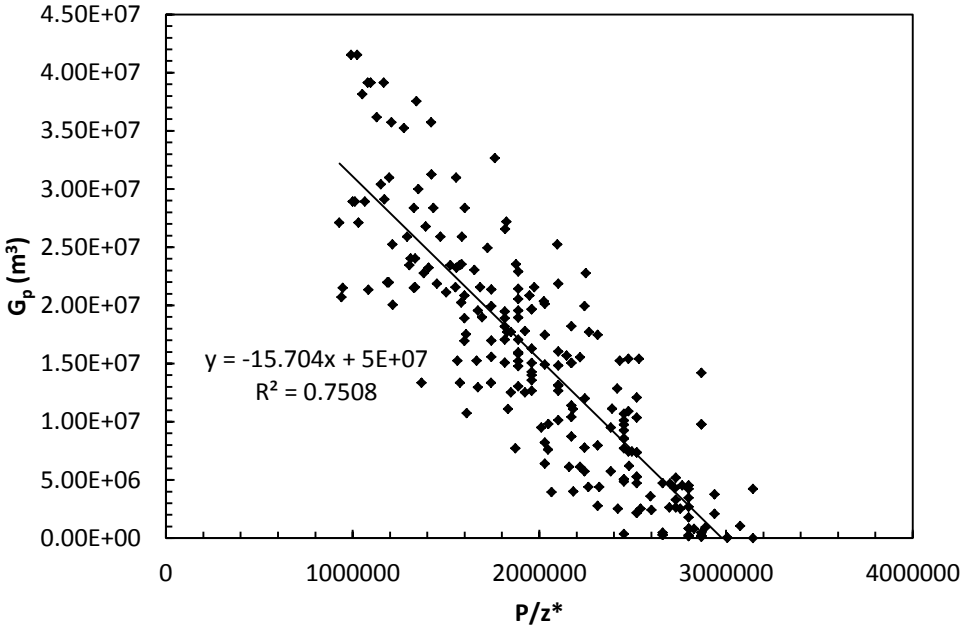

Figure 3.8. Gas produced versus P/z* for Husky's Abbey Field with Milk River D Langmuir isotherms.

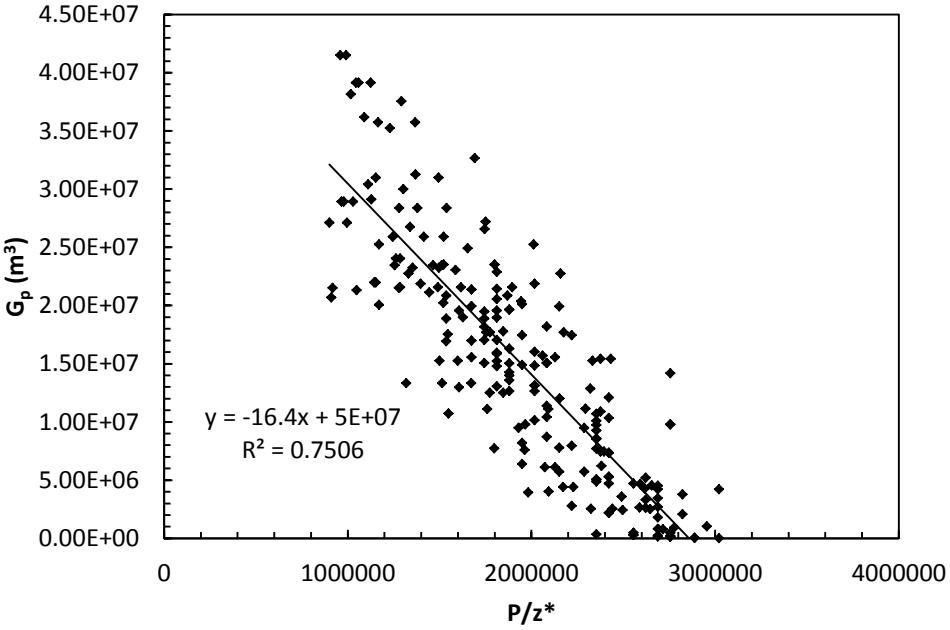

Figure 3.9. Gas produced versus P/z* for Husky's Abbey Field with Milk River E Langmuir isotherms.

3.6 Conclusions and Recommendations

The conclusions are as follows:

- A new gas material balance theory has been derived for shale gas reservoirs that includes terms for biogenic gas generation, along with a term for the free gas present within the reservoir and a term which represents the amount of gas that was desorbed within the reservoir.
- More pressure data needs to be collected from shale gas wells to complete an accurate gas material balance that includes the biogenic gas production term.
- The biogenic gas produced during the production life of a well from shale gas can be significant, as shown in this chapter for Nexen's Bigstick Field it accounts for about 37% of gas production and for Husky's Abbey Field it accounts for 19% of gas production during the resource lifetime of a well. This is important from a gas production point of view – if the microbes could be stimulated by adding nutrients to the system, then the gas yield could be improved.
- New high pressure methane gas adsorption curves are shown in this chapter. These curves were obtained from cores in Husky's Abbey Field, which represent the typical behavior of gas adsorption in a shallow shale system in western Canada.

Chapter Four: Biogeochemical Analysis of Shale Gas Systems Reveals Links Between Geology, Biology and Reservoir Engineering

Cokar, M., Wilson, S., Ford, B., Gieg, L.M., Kallos, M.S., and Gates, I.D., "Biogeochemical Analysis of Shale Gas Systems Reveals Links Between Geology, Biology and Reservoir Engineering," to be submitted, 2012.

4.1 Abstract

The world's largest bioreactor is right below our feet. The largest fraction of anaerobic microorganisms on earth live underground for example in soils, shale intervals, oil and gas reservoirs, and coal seams. The by-product of their metabolic activities are methane and carbon dioxide. The economic potential of this self-renewing natural energy resource is immense and it is of enormous value to study and understand a) methane producing archaeal communities that exist in these underground environments, b) what limits growth of these microbial communities, and c) which substrates enhance their metabolic by-products. An increase of their metabolism will enable greater methane gas production from these systems. The focus of the study documented here is a shallow biogenic shale gas formation. This study is the first of its kind to document methane production curves from microorganisms in produced water and inoculated core samples obtained from a shale gas reservoir in the WCSB. 16S rRNA gene sequencing identified different organisms at the family level present within these samples. In addition, insights into the relationships between geochemistry, methane substrate utilization, and methanogenic substrates were investigated. This study reveals biological evidence of methanogenic activity in a shallow shale gas reservoir in western Canada. The WCSB

contains over 1,000 Tcf of methane in its shale deposits, and evidence of microbial activity within shallow shale reservoirs opens a huge window of opportunity. The actual gas potential of these reservoirs is much greater than current estimates because present-day methanogenic activity can generate a significant fraction of the total gas production from the reservoir. The implication is that methane production rates from biogenic shale gas reservoirs could be enhanced significantly with substrate stimulants injected into a reservoir.

4.2 Introduction

Natural gas is among the cleanest and most abundant fuels available for human consumption. Historically, a transition from heavier fuels to lighter ones has occurred, e.g. wood to coal (solids) to oil (liquid) and eventually to natural gas. Although conventional gas resources are on the decline in North America, unconventional gas reservoirs have become the focal point. Methane gas within these reservoirs can be generated from organic matter both thermogenically and biogenically. Thermogenic gas is found deeper underground where higher temperatures and pressures (>150°C and > 5,000 kPa) (Pepper and Corvi, 1994) provide an ideal environment for natural gas generation through chemical processes. Biogenic gas, on the other hand, is found in more shallow environments which exist at lower temperatures (<80°C) and pressures (<5,000 kPa) where anaerobic microbes are capable of degrading hydrocarbon substrates (Aitken, 2004 and Connan, 1984). Here, the focus of the research documented is on shallow biogenic shale gas reservoirs. These reservoirs are essentially massive biological reactors where indigenous microbes consume kerogen to generate carbon dioxide and

methane and a small fraction of ethane, propane, butane, and pentane. These types of reservoirs represent a key element in the development of petroleum – they are the bioactive source systems that generate oil and gas. The physical, chemical and biological processes of gas generation and nutrient, waste, gas, and water transport and flow, and the interaction between these biological and physical phenomena are currently not well understood. This is compounded by the complexity of the system; biogenic gas generation and its desorption from kerogen, diffusion and convection through nanometer to micron to meter porous systems and the connections between the porous systems make biogenic shale gas reservoirs difficult to analyze.

4.2.1 Shale Gas Formation Geology

The shallow shale gas formation focused on in the research documented here is from the Milk River Formation (also commonly known as the Alderson Member in the oil and gas industry, often referred to as the Abbey Field). It is located in south-eastern Alberta and south-western Saskatchewan (See Figure 4.1) and was deposited in the western Interior Seaway during the late stages of the Upper Cretaceous Mesozoic Era. The productive zones of the Abbey Field are thought to be the leading edges of a prodelta plume of fine-grained sediment deposited in a deeper water marine environment. This formation contains an enormous amount of natural gas with estimates greater than 15 Tcf of natural gas (Fishman et al., 2001). This formation is essentially both a source and reservoir rock that contains the natural gas.

All core and water samples used in this study were obtained from the productive biogenic shallow gas zones in the Alderson Member of the Milk River Formation. The productive

zones of the Abbey Field are split by stratigraphy into Zones B, C, D, E and F depending on the depth. Bedding dip angles show the source of these clastics to be generally from the south or south-west shoreline location. Within each zone of the Abbey Gas Field, each plume of clastics tends to get thinner and more fine-grained basinward. This leads to generally thinner alternating beds of sands, silts and clays in an easterly direction. The bedding is further complicated by varying amounts of worm-burrowing which results in relatively preserved distinct bedding in the E interval to less defined more homogenized bedding in the B, C, and D intervals. Consequently, the permeability (with respect to air) in the horizontal direction within the E interval is equal to on average 3.16 mD versus 0.2-0.4 mD in the other zones. Produced gas rates from the E interval are an order of magnitude higher than that in the B, C, and D intervals.

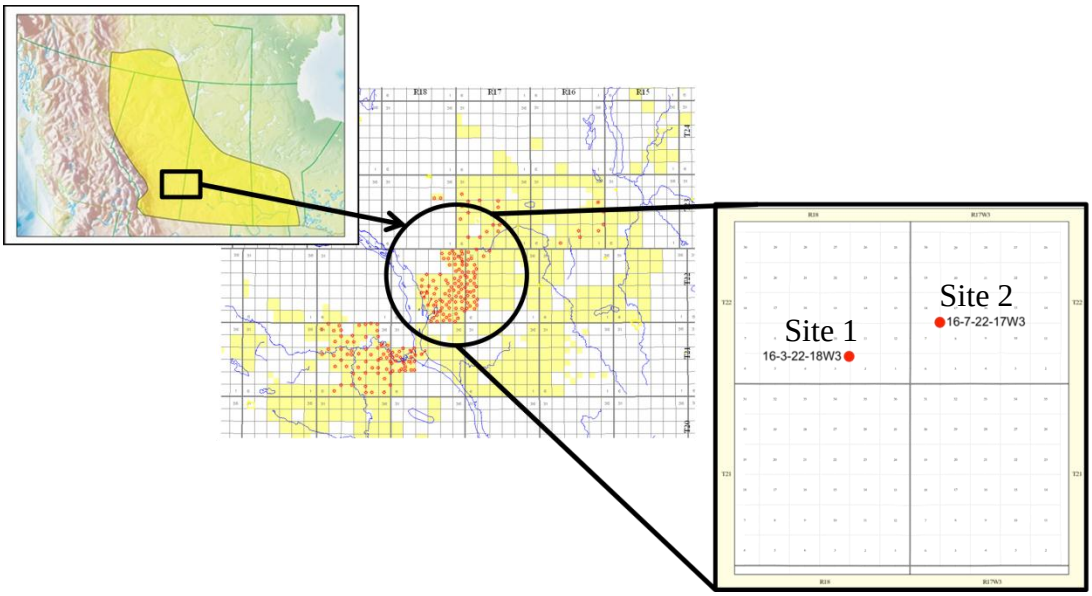

Figure 4.1. Location of the WCSB (National Energy Board, 2011) and locations of wells from which produced water samples Site 1 (16-7-22-17W3) & Site 2 (16-3-22-18W3) and core samples Site 1 (16-3-22-18W3) were obtained.

As shown on the Zone D section at 304.25 m (Figure 4.2a), the clastics and shale/silt areas are more mixed and the darker shale in the lower right quadrant is disturbed from its near horizontal bedding plane by mixing and reworking after deposition by pelagic-burrowers. Note the fine-grained angular and sub-angular clastics in white are less than 0.1 mm in size. Remnant bedding is seen in the upper third of the slide where less burrowing has occurred. In contrast the section of Zone E at 322.49 m (Figure 4.2b) shows much more pronounced bedding planes and more clastic laminations of better reservoir as illustrated by the porous (blue colour) oval section of reservoir in the middle of the slide. Also note that at 322.98 m (Figure 4.2c), similar bedding laminations of reservoir "pipeline" for moving methane gas into the hydraulic fracture created to produce the well. These laminations are typically between 0.25 - 0.33 mm thick.

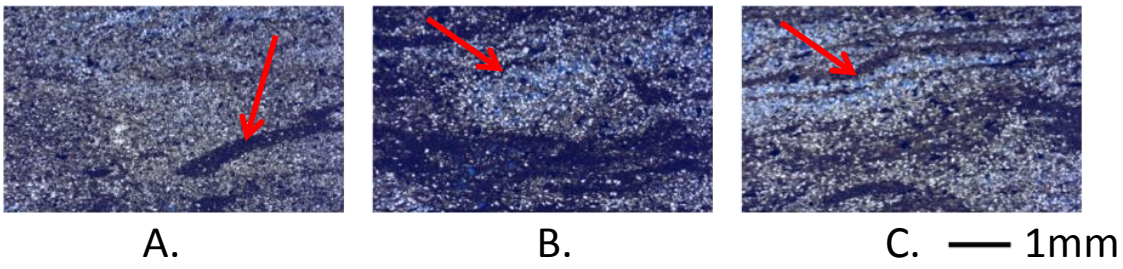

Figure 4.2. Thin sections of zones D and E from left to right at a depth of (A) 304.25 m (Zone D), (B) 322.49 m (Zone E), and (C) 322.98 m (Zone E).

4.2.2 Gas Production Rates

Canadian shale gas resources are much newer than those found south of the border in the United States. Although some fields have been producing gas for several decades, the remainder of the resource is relatively unexplored. Natural gas can be termed either biogenic or thermogenic depending on whether it comes from microorganisms or through

high temperature and pressure processes deep within the subsurface. Thermogenic gas is found several kilometers below the surface where high temperature and pressure thermal cracking converts organic matter and oil into gas whereas biogenic gas can be found at depths above 500 m and are found in reservoirs with temperatures less than 80°C (Larter et al., 2006; Shurr and Ridgley, 2002). The optimum temperature for these types of reservoirs appears to be between 40 and 60°C. There must be organic matter present within these reservoirs for microorganisms to consume and the sulfate content of these reservoirs is generally low, and as these are tight reservoirs there still needs to be adequate permeability to allow for the flow of water that carries nutrients for the microorganisms as well as adequate pore space for the microorganisms to grow (Fishman et al., 2001). The gas production rates within these reservoirs can be initially as high as 20,000 m^3/day (706,000 scf/day) and can fall down to less than 1,000 m^3/day (35,300 scf/day) near the end of the well's production life. These reservoirs are generally characterized by relatively high flow rates in the beginning with a sharp decline and then stabilized flow near the end of the well's life. The stabilized flow can be attributed to very low permeabilities within the nanopores, diffusivity of methane from the formation water, desorption of gas from both organic and inorganic surfaces, pressure maintenance due to water influx, or ongoing biogenic gas generation.

4.2.3 Shale Gas Reservoir Biology

Anaerobic production of methane can be found in a wide variety of places, which include marine environments, petroleum environments, digestive tract of animals, and deep sea hydrothermal vents (Bapteste, 2005; McDonald et al., 1999; Takai and Horikoshi, 1999; and Florin et al., 2000). Biological methane producers are known as archaeal

methanogens which consists of five phylogenetically divergent orders: *Methanobacteriales*, *Methanopyrales*, *Methanococcales*, *Methanomicrobiales* and *Methanosarcinales*. All of these microorganisms have the ability to metabolically produce methane in the absence of oxygen (Bapteste, 2005). There are a limited amount of metabolic reactions that can generate methane. The two most predominant pathways are hydrogen consumption, wherein methanogens are CO_2 reducing prokaryotes, and they use hydrogen as the electron donor or energy source and CO_2 as the electron acceptor (hydrogenotrophic) as described in Equation 2.2 of Chapter 2. Alternatively, acetate can be fermented, which uses acetate and hydrogen to produce methane and carbon dioxide as seen in Equation 2.3 of Chapter 2.

Materials and Methods

Figure 4.3 outlines the three sets of experiments that were performed in this study. The first set of experiments involved incubation of produced water samples from two different sites within the Milk River formation. The produced water from all of the experiments was taken from two different wells located within the Milk River formation. The first well will be herein referred to as 'Site 1' has Unique Well Identifier (UWI) 16-3-22-18W3 and the second well referred to as 'Site 2' has UWI 16-7-22-17W3. The location of these wells is shown in Figure 4.1. There were four runs setup up for each site, with each having a different substrate added to the produced water. The second set of experiments involved incubating core samples without any inoculation, and the third set of experiments involved inoculation of the incubated core samples from the produced water enriched with H_2/CO_2.

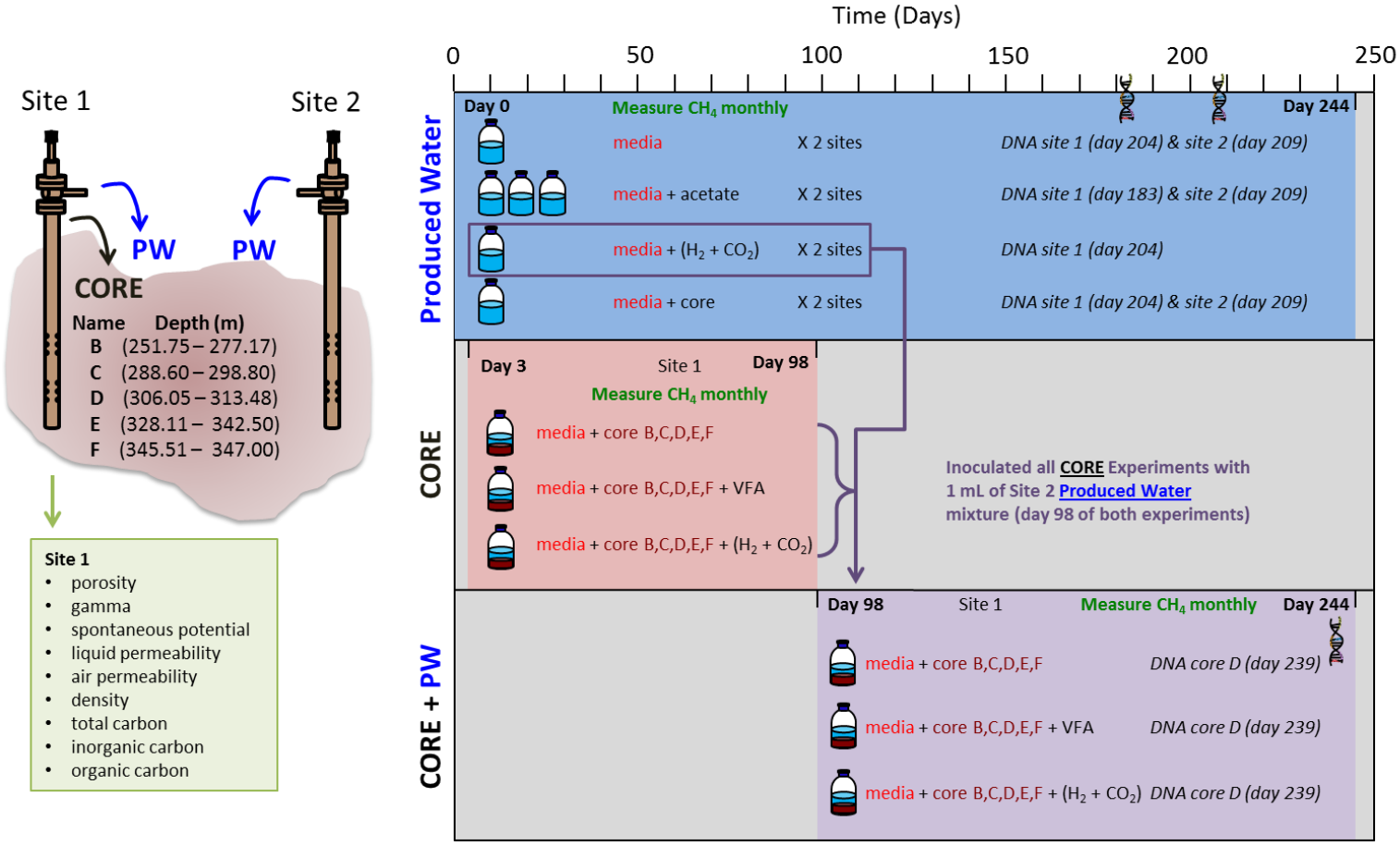

Figure 4.3. Outline of experiments: the first experiment lasted 244 days, which involved produced water from two different sites. The second experiment ran from Day 3 to Day 95 and involved only core samples. The third experiment ran from Day 98 to Day 244, and core was inoculated with 1 mL of produced water that was enriched with H_2/CO_2.

4.2.4 Sample Gathering and Handling

The produced water samples were collected from the wellhead and the experiments started within three days of collection. The produced water samples were stored in an anaerobic chamber (Vinyl Coy Anaerobic Chamber, containing 90% N_2:10% CO_2). Additionally, core was received from the Site 1 well. However, the core was drilled in 2002 and stored in a core storing facility where it was open to atmospheric conditions before being transported to the laboratory. The core was sectioned into five different zones labeled B, C, D, E and F, as shown in Figure 4.3. These zones correspond to different regions within the reservoir that share similar geochemical and geological characteristics.

4.2.5 Core and Produced Water Preparation

The external surface of the cores were scraped off in order to remove any contaminants that were introduced during coring, handling, and storage. This was done in an anaerobic chamber (Vinyl Coy Anaerobic Chamber, containing 90% N_2:10% CO_2) with a knife that was sterilized in an autoclave. The core was then crushed by using a mortar and pestle (which was also sterilized) until it was in a coarse powdered form. All equipment that came into contact with the core was sterilized by using an autoclave to prevent external bacterial contamination of the cores.

Produced Water

As soon as the produced water samples were received they were put into an anaerobic chamber (Vinyl Coy Anaerobic Chamber, containing 90% N_2:10% CO_2). A 20 mL

sample of the produced water was added to 5 mL of mineral salts medium (prepared without rumen fluid) to establish four sets of enrichment cultures (McInerney et al., 1979). The materials and methods for the preparation of the mineral salts medium is listed in Appendix B. These enriched cultures were incubated in the following four different conditions anaerobically: (a) an N_2/CO_2 headspace with no additional electron donors, (b) H_2/CO_2 at a ratio of 80:20 (28 mL and 7 mL) was added to the headspace with no additional electron donors, (c) N_2/CO_2 headspace with 0.5 mL of 100 mM of acetate, and (d) N_2/CO_2 headspace with 5 g of core from Site 1.

Core Incubations

Core samples (5 g) were added to 15 mL mineral salts medium (prepared without rumen fluid) to establish three sets of enrichment cultures starting 3 days after the produced water experiments (Figure 4.3). These enrichments were incubated anaerobically under three different conditions: (a) an N_2/CO_2 headspace with no additional electron donors; (b) H_2/CO_2 at a ratio of 80:20 (16 mL and 4 mL) was added to the headspace with no additional electron donors; and (c) N_2/CO_2 headspace amended with volatile fatty acids (VFA's) (0.1 mL for a 1M VFA solution that consisted of equimolar concentrations of acetate, butyrate and propionic acid). All three sets of enrichments were carried out in either duplicate or triplicate depending on the amount of core material available at each depth. They were separated by depth of formation as shown in Figure 4.3.

Core Inoculations with Produced Water

The core incubations after 95 days (Day 98 of experiment) showed no discernible amount of methane produced. This was most likely attributed to the lack of microorganisms present in core stored since 2002 at atmospheric conditions, most likely any strictly anaerobic microorganisms present would have not survived. These samples were then inoculated with 1.0 mL of Site 2 H_2/CO_2 enriched produced water sample, since this sample showed the largest amount of methane production out of all of the experiments.

4.2.6 Gas Analysis

Methane formation in the bottles was monitored by injecting a 0.2 mL sample of gas from the headspace in each bottle into a gas chromatograph on a monthly basis. A sterile syringe (BD Syringe, 1 mL, Ref. 309659) was used and it was pre-flushed with a 90:10 mixture by volume of N_2/CO_2 to ensure anaerobic conditions. A HP Series 5890 gas chromatograph equipped with a flame ionization detector at a temperature of 200°C was used. Methane gas was injected at a temperature of 150°C into a packed stainless steel column (6ft. x 1/8 in., Poropak R, 80/100, Supelco) that was maintained isothermally at a temperature of 100°C. Methane standards at a known concentration were then used to calculate methane levels from calibration curves. These methane standards were made in the laboratory by using Praxair mixture of CH_4.

4.2.7 Sample Preparation and Analysis by Gas Chromatography-Mass Spectrometry (GC-MS)

To identify the water-soluble shale components that could be driving syntrophic methane production (and any putative metabolites), the supernatants (15 mL) from each replicate

were subsampled, acidified, extracted with ethyl acetate, and prepared for low resolution GC-MS analysis (Gieg and Suflita, 2002). Briefly, samples were concentrated by rotary evaporation and under a gentle stream of N_2 to a volume of 100 mL, and then silylated using 50 mL BSTFA (N,O- bis(trimethylsilyl) trifluoroacetamide, Thermo Fisher, CAS 25561-30-2). Samples were analyzed via autoinjection on an Agilent GC-MS system (Model 7890A GC, Model 5975C inert XL MSD) equipped with an HP-1 capillary column (50 m x 0.32 mm i.d. x 0.2 μm film, Agilent Technologies, Inc.). The samples were analyzed in splitless mode, with the inlet held at 270°C. The oven was initially held at 50°C for 5 min, then increased at a rate of 8°C/min to a final temperature of 270°C that was held for 20 min. The method used for the solvent extraction is described in Appendix B.

4.2.8 Analysis of Microbial Community

The microbial community composition of all of the produced water samples (with the exception of Site 2 H_2/CO_2 enriched culture) and the core at Zone D for all three substrates indicated in Figure 4.3 were determined via 454 pyrosequencing. Genomic DNA (gDNA) was extracted (0.3 mL per sample with three replicates) with the 'FastDNA SPIN kit for soil'; MP biomedicals (Solon, OH), as per the manufacturer's protocol. A fragment of the 16S rRNA gene was amplified by polymerase chain reaction (PCR) (95 °C, 3 mins; 25 cycles of 95 °C 30 s; 55 °C 45 s; 72 °C 10 min), and primers 926f (aaa ctY aaa Kga att gac gg) (Brigman et al., 2002) and 1392 r (acg ggc ggt gtg tRc) (Lane et al., 1985). The resultant ~500bp (base pair) fragments were confirmed by agarose electrophoresis (1% agarose gels) and purified (Qiagen PCR purification kit;

Qiagen, Mississauga, ON), as per the manufacturer's protocol. The 454 pyrosequencing was done similar to the method described by Ramos-Padron *et al*. (2011). The purified amplicons were subsequently re-amplified for 454 pyrosequencing. The FLX Titanium amplicon primers 454T-RA had a 25 nucleotide A-adaptor sequence of CGTATCGCCTCCCTCGCGCCATCAG (Berdugo-Clavijo et al., 2012) and 454T-FB had a 25 nucleotide B-adaptor sequence of CTATGCGCCTTGCCAGCCCGCTCAG (Berdugo-Clavijo et al., 2012) were used. The PCR products were then purified by using a commercial kit 'QIAquick PCR Purification Kit: Qiagen'(Maryland, USA); and/or EZ-10 spin column PCR purification kit (BioBasic Inc., Markham, ON). A fluorometer (Qubit Fluorometer using a QuantiTTM dsDNA HA Assay Kit; Invitrogen, Eugene, USA) was used to determine the concentration of the sample. All of the samples were sent to Genome Quebec Innovation Centre for pyrosequencing.

4.3 Results and Discussion

4.3.1 Log and Core Analysis of Reservoir Data (Day 0)

A geochemical analysis of Well 16-3-22-18W3 (Site 1) was conducted. The neutron porosity, gamma ray, and spontaneous potential (SP) were determined by downhole logging tools after the well was cored and before production. The air and liquid permeabilities along with the density of the formation, total carbon, organic carbon and inorganic carbon were determined in the laboratory (CBM Solutions, 2004). For each section of the reservoir labeled B, C, D, E and F the average value of the property is displayed in Figure 4.4. As can be seen from Figure 4.4, geologically the formation does not vary significantly with depth except for the air and liquid permeabilities in Sections E and F, which are significantly higher than the other zones.

The inorganic content of the reservoir however varies between the zones. The order of the zones from the highest inorganic carbon content to the lowest inorganic carbon content is C, E, D, F and B. The inorganic carbons consist of carbonates such as calcite, dolomite, and siderite. The organic carbon is the highest in Zones F, B and C, and the lowest in Zones E and D as seen in Figure 4.4.

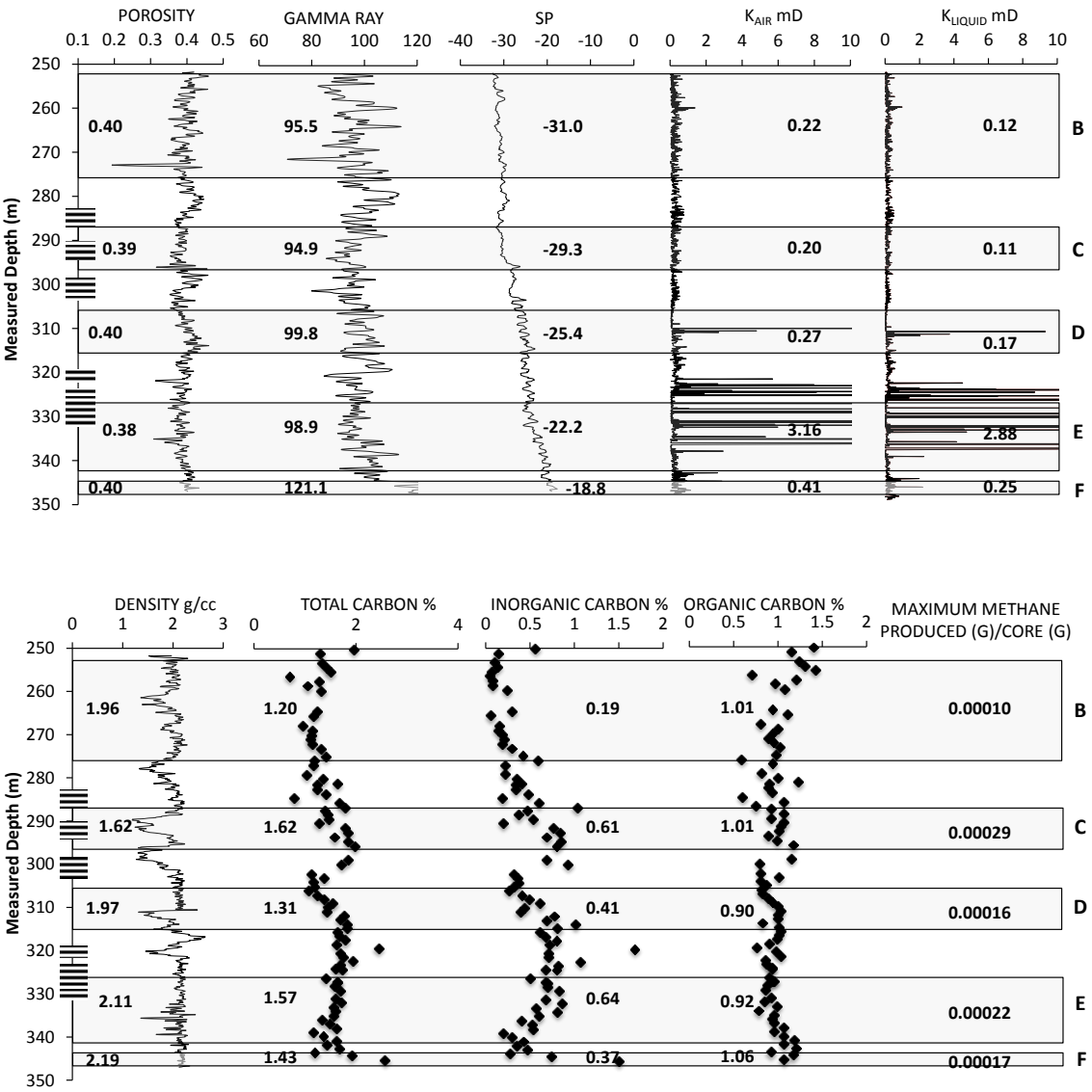

Figure 4.4. Log and core analysis of Site 1 well 16-3-22-18W3. From left to right is the formation neutron porosity, gamma ray, spontaneous potential (SP), air (K_{AIR}) and liquid (K_{LIQUID}) permeability, density, total carbon weight percent (wt%), inorganic carbon (wt%), organic carbon (wt%), and maximum methane produced (g)/core (g). The data for each zone of the formation B, C, D, E and F is averaged over that range and shown on the figure. The perforations are shown on the axis on the left hand side labeled measured depth.

4.3.2 SEM Images of Core (Day 0)

Understanding shale properties are complicated by their anisotropy in composition, pore size, permeability, and pore connectivity. Shales are defined by a grain size of less than 39 μm. Clays are also approximately of the same size and thus are commonly found in the same vicinity of shales. Other minerals such as quartz and calcite are also present within shales. Visualization of shales helps to understand their texture and pore structure.

A Phillips XL30ESEM scanning electron microscope (SEM) was used to obtain images taken for Site 1 core at a magnification of 1000x and 10000x. The images are shown in Figure 4.5. The shale images are similar to those presented by Sondergeld (2010). Images were also taken of inoculated core samples with no additional substrate added at a magnification of 1000x and 10000x after the experiments were completed. The core samples were coated with gold-paladium using a sputter coater, whereas the bacterial samples were dried out and imaged immediately. As can be seen in Figure 4.5a, shale gas reservoirs are complex with a high degree of variability and complexity and contain many tiny pores where gas can be trapped. The pore sizes vary between nanometers and micrometers. Figure 4.5a reveals that clay platelets within all of these samples are ubiquitous. These images provide insight on shale gas microstructure. The samples are mostly just clays which are very fissile and the layering of the clays is evident in Figure 4.5a. Figure 4.5b shows the different consortia of microorganisms in the inoculated cores at each depth. In addition to methane production curves, these SEM images provide qualitative evidence of microorganisms growing within the inoculated core samples.

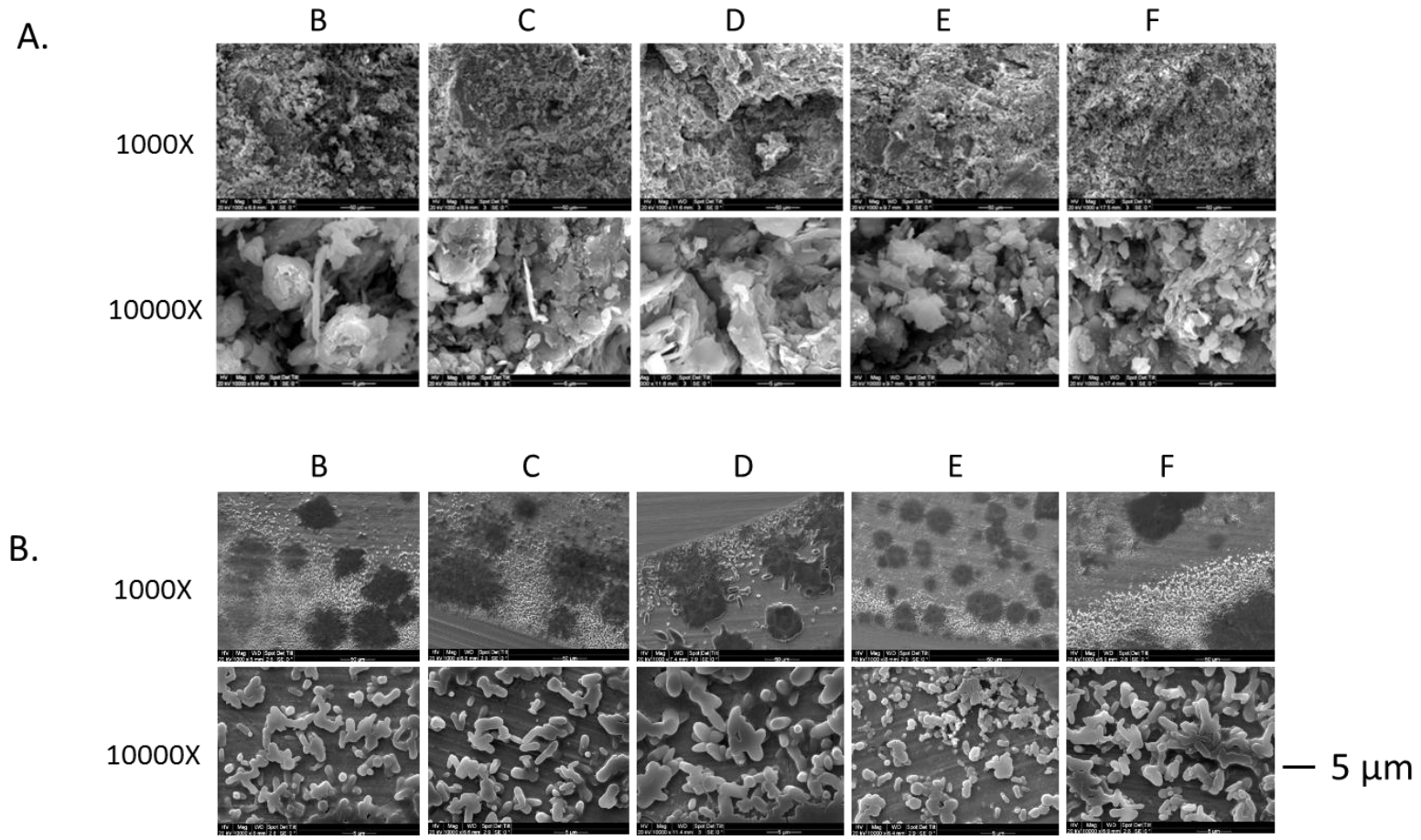

Figure 4.5. (A) SEM images of core at depths B, C, D, E, and F at 1000x and 10000x magnification. (B) Microorganisms from the inoculated core samples with no additional substrate samples that were grown with the cores at depths B, C, D, E, and F at a magnification of 1000x and 10000x.

4.3.3 Produced Water Incubations (Day 0 -244)

There were four types of enrichments incubated for this experiment for both Sites 1 and 2. These four incubations were: (a) an N_2/CO_2 headspace with no additional electron donors (no substrate), (b) N_2/CO_2 headspace with 5 g of core from Site 1 (core), (c) H_2/CO_2 at a ratio of 80:20 was added to the headspace with no additional electron donors (H_2/CO_2), and (d) N_2/CO_2 headspace with acetate (acetate). The four samples described will be herein referred to as no substrate, core, H_2/CO_2 and acetate. Methane production from these serum bottles was measured on a monthly basis and 454 pyrosequencing of a fragment of the 16S rRNA gene was performed for all of these samples except for the enriched Site 2 sample with H_2/CO_2.

The acetate cultures for Sites 1 and 2 are also part of a heterogeneity study, and this will be discussed later. The purpose of the heterogeneity study was to see the difference in the microbial consortia in different replicates that were inoculated from the same sample and contain the same amount of acetate. In many biological studies it is common to find differences in samples even if they are obtained from the exact same source; the reason behind this is currently unknown. The concentration of the samples sent out for 454 sequencing and the original number of reads as well as the ones that passed quality control for all of the samples are indicated in Table 4.1. Table 4.2 is a list of all the microorganisms present at or above 3% abundance within the samples. Subsequent analysis, with the normalized data, was carried out at the family level. The data shown in the graphs for the family level of microorganisms present within the sample are microorganisms present at 3% or more in at least one of the samples. The results of the 16S rRNA gene sequencing and methane production curves for produced water are

presented in Figure 4.6 - Figure 4.13 and Table 4.3 and Table 4.4, wherein the percent of total reads represented by each particular family are indicated. The results of the 16S rRNA gene sequencing and methane production curves for the inoculated cores samples are presented in Figure 4.14 - Figure 4.20 and Table 4.5.

The average amount of methane produced for all of the samples was calculated by taking the total cumulative methane produced over the entire experimental period and dividing it by the number of days. The average methane production rate for Site 1 and Site 2 samples with no substrate is 9.93×10^{-9} methane(g)/produced water(g)/day and 8.34×10^{-8} methane(g)/produced water(g)/day shown in Figure 4.6 and Figure 4.8. The no substrate sample for Site 2 has more methane than the no substrate sample in Site 1. Additionally, the Site 2 produced water sample also showed more fines within the produced water sample than the produced water sample for Site 1. The fines were most likely from the formation, and may contain hydrocarbons that could be used by the microorganisms for methane production. The microbial communities present within the no substrate sample of Site 1 and Site 2 also reflect what was observed in from the methane production curves. The microbial community within the no substrate sample for Site 1 was predominantly composed of *Anaerolineaceae* (2.1%), *Caulobacteraceae* (3.4%), *Desulfobulbaceae* (0.4%), *Desulfovibrionaceae* (3.2%), *Erysipelotrichaceae* (0.2%), *Eubacteriaceae* (0.1%), *Geobacteraceae* (4.1%), *Methanobacteriaceae* (2.8%), *Methanomicrobiaceae* (0.9%), *Methanosarcinaeceae* (3.1%), *Porphyromonadaceae* (1.0%), *Pseudomonadaceae* (40.4%), *Sphingomonadaceae* (4.3%), *Synergistaceae* (2.9%), *Syntrophomonadaceae* (0.6%). The microbial community within the no substrate

sample for Site 2 was predominantly composed of *Bradyrhizobiaceae* (4.2%), *Burkholderiaceae* (5.1%), *Caulobacteraceae* (6.4%), *Comamonadaceae* (6.4%), *Desulfobulbaceae* (0.2%), *Geobacteraceae* (1.6%), *Methanobacteriaceae* (16.2%), *Methanosarcinaceae* (15.2%), *Pseudomonadaceae* (5.7%) and *Sphingomonadaceae* (7.6%). Site 2 has more methanogens than Site 1 even when no substrate has been added to the samples.

The average methane production rates for enriched Site 1 samples with core and H_2/CO_2 are 3.22 x 10^{-8} methane(g)/produced water(g)/day and 6.92 x 10^{-7} methane(g)/produced water(g)/day respectively shown in Figure 4.6. Relative to the microbial community within the no substrate enrichment in Site 1, there was a shift towards methane producing archaea within the core and H_2/CO_2 enrichments, particularly for *Methanosarcinaceae* (23.7%) and (42.7%), respectively, and in the H_2/CO_2 enrichment there was a shift towards *Methanobacteriaceae* (24.9%). Clearly there are methanogens present within the produced water samples as shown by the methane generation curves as well as the 16S rRNA gene sequencing data.

The average methane production rates for enriched Site 2 samples with core and H_2/CO_2 are 5.38 x 10^{-8} methane(g)/produced water(g)/day and 1.03 x 10^{-6} methane(g)/produced water(g)/day as shown in Figure 4.8. Relative to the microbial community within the no substrate enrichment in Site 2, there was a shift towards methane producing archaea and iron reducing bacteria within the core, particularly *Methanobacteriaceae* (17.7%),

Methanosarcinaceae (35.5%), and iron reducing bacteria *Geobacteraceae* (16.1%). 16S rRNA gene sequencing data for the enriched Site 2 H_2/CO_2 sample is not available.

Table 4.1. Number of 16S rRNA gene pyrosequencing reads for the produced water (PW) sample and core samples.

Sample	Concentration of Sample Sent (µg DNA/mL)	Number of Reads	
		Raw	Passed Quality Control
PW - Site 1 No Substrate	6.88	8111	5678
PW - Site 1 Core	10.00	8322	6273
PW - Site 1 H_2/CO_2	10.00	8697	6336
PW - Site 1 Acetate 1	10.00	8750	6403
PW - Site 1 Acetate 2	10.00	8725	6367
PW - Site 1 Acetate 3	10.00	9414	6724
PW - Site 2 No Substrate	2.55	2126	1327
PW - Site 2 Core	7.20	7719	5735
PW - Site 2 Acetate 1	9.28	9998	7648
PW - Site 2 Acetate 2	10.00	10129	7900
PW - Site 2 Acetate 3	10.00	9990	7894
Core - No Substrate	10.00	6179	4647
Core - H_2/CO_2	10.00	8012	5915
Core - VFA	10.00	8469	6392

Table 4.2. Family name of microorganisms present at 3% abundance or above in all of the samples, their description and reference.

Family Name	Description	Reference
Anaerolineaceae	anaerobic microorganisms	(Yamada et al., 2006)
Bradyrhizobiaceae	nitrogen fixation	(Ge et al., 2012)
Burkholderiaceae	pathogen	(Deng, et al., 2012)
Caulobacteraceae	aerobic non photosynthetic found in natural bodies of water	(Poindexter et al., 1964)
Clostridiaceae	fermenters	(Wust et al., 2011)
Comamonadaceae	hydrocarbon degradation	(Rouviere et al., 2003)
Desulfobulbaceae	sulfate reducer	(Jehmlich et al., 2010)
Desulfomicrobiaceae	sulfate reducer	(Dias et al., 2008)
Desulfovibrionaceae	sulfate reducer	(Lodowska et al., 2009)
Erysipelotrichaceae	metabolism is respiratory and weakly fermentative	(Verbarg et al., 2004)
Eubacteriaceae	acetogenic bacteria	(Allen et al., 2009)
Geobacteraceae	iron reduction and hydrocarbon degradation	(Snoeyenbos-West et al., 2000)
Methanobacteriaceae	methanogen	(Xing et al., 2012)
Methanocorpusculaceae	methanogen	(Xing et al., 2012)
Methanomicrobiaceae	methanogen	(Xing et al., 2012)
Methanosarcinaceae	methanogen	(Xing et al., 2012)
Porphyromonadaceae	anaerobic sugar fermenters	(Jabari et al., 2011)
Pseudomonadaceae	capable of degrading long chain alkanes and crude oil	(Liu et al., 2012)
Sphingomonadaceae	degrade aromatic compounds	(Balkwill et al., 2006)
Synergistaceae	anaerobic thiosulfate reducing bacterium	(Labutti et al., 2010)
Syntrophomonadaceae	syntrophic butyrate oxidizers	(Liu et al., 2011)

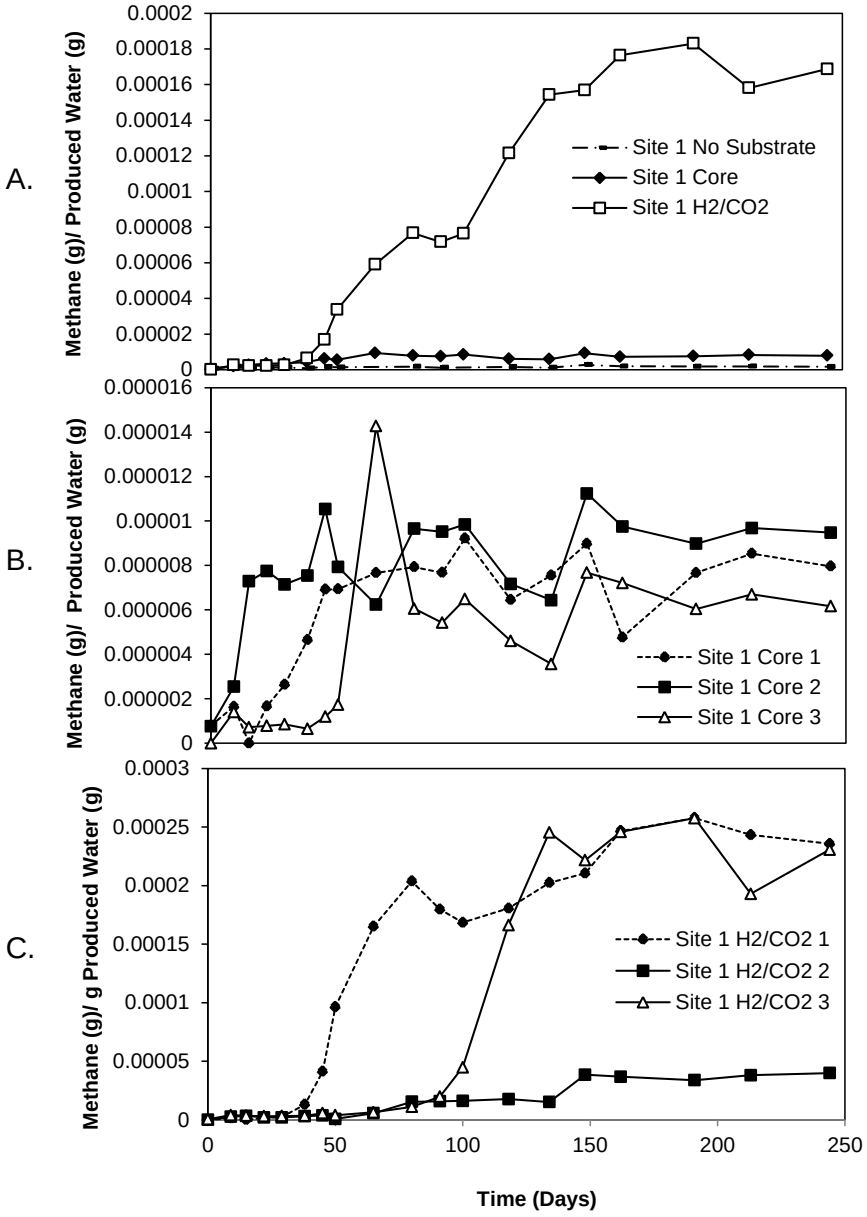

Figure 4.6. Site 1 produced water methane growth curves in methane (g)/produced water (g) as a function of time (days) for Site 1. (A) all of the samples no substrate, core and H_2/CO_2, (B) triplicate samples for Site 1 Core, and (C) triplicate samples for Site 1 H_2/CO_2.

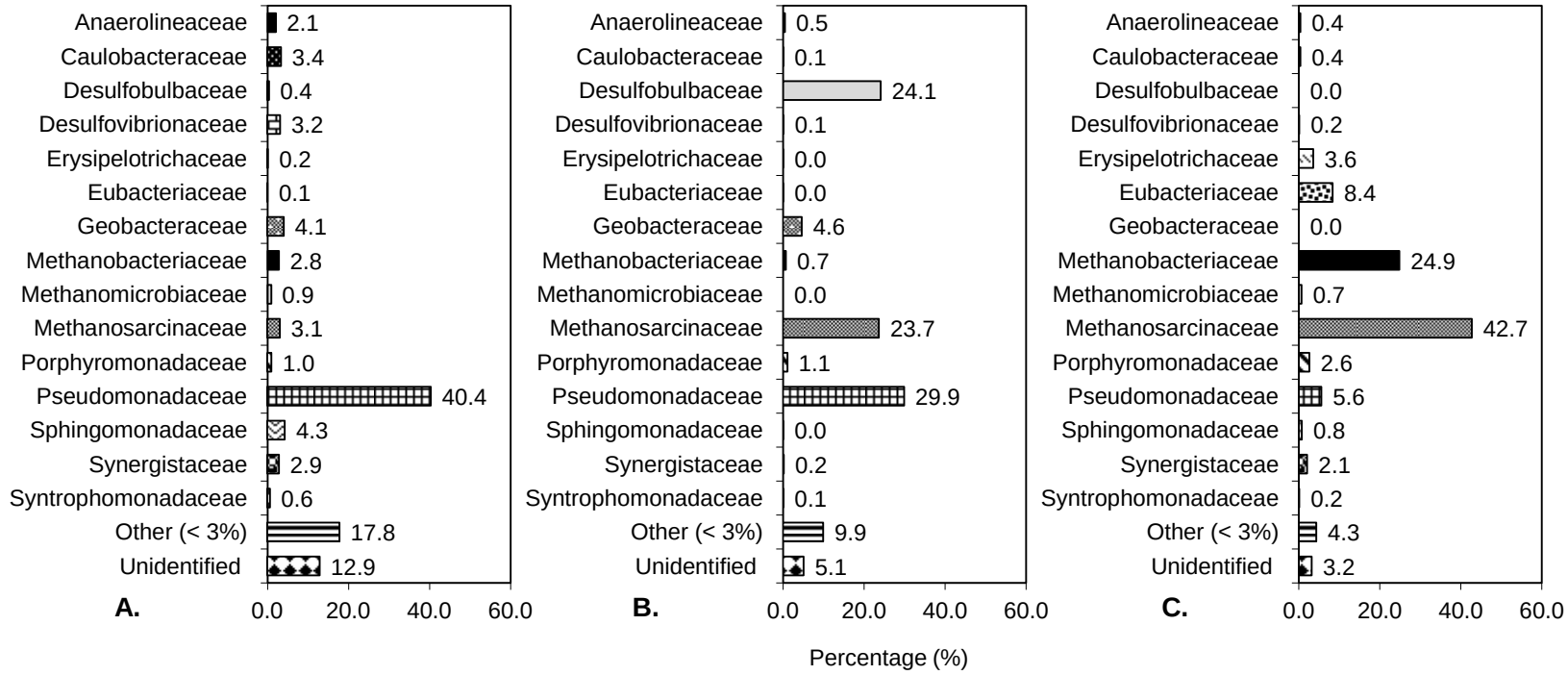

Figure 4.7. Site 1 produced water 16S rRNA gene sequence results. (A) Site 1 no substrate, (B) Site 1 core, and (C) Site 1 H_2/CO_2.

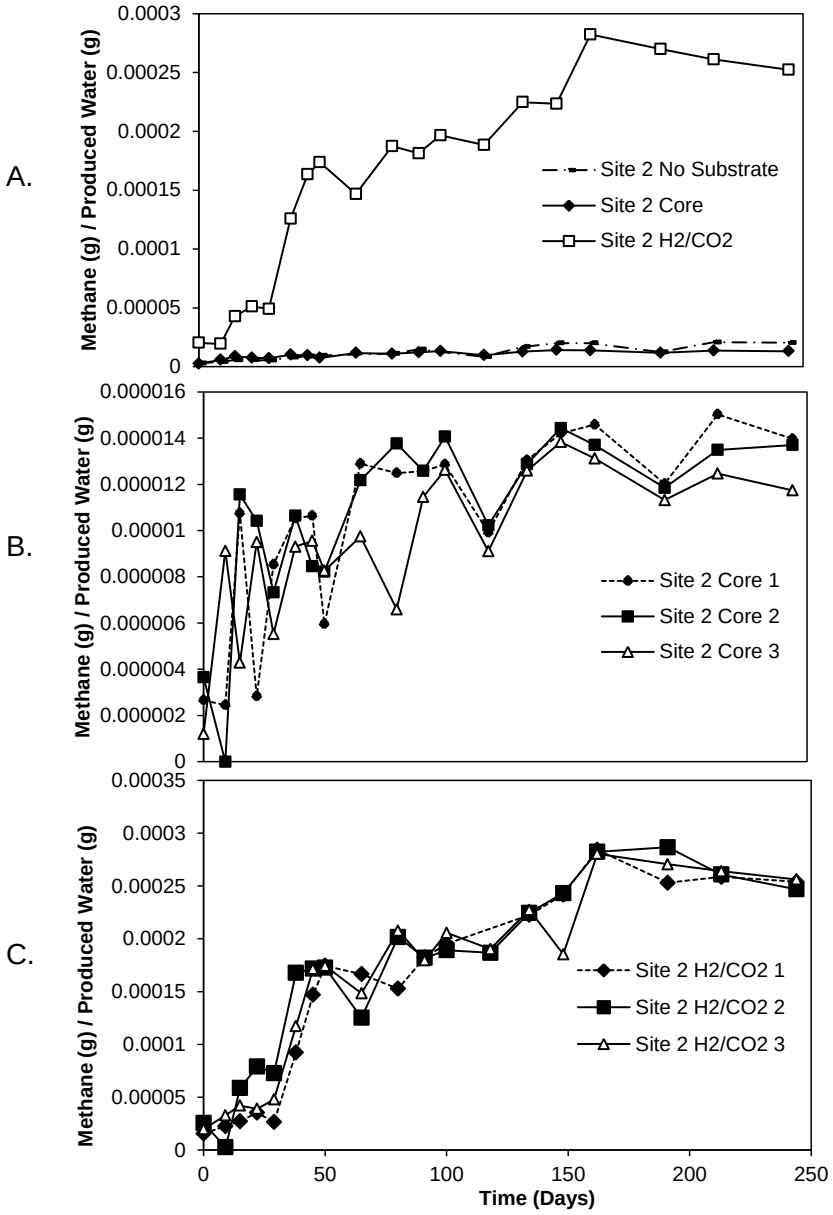

Figure 4.8. Site 2 produced water methane growth curves in methane (g)/produced water (g) as a function of time (days) for Site 2. (A) all of the samples no substrate, core and H_2/CO_2, (B) triplicate samples for Site 2 Core, and (C) triplicate samples for Site 2.

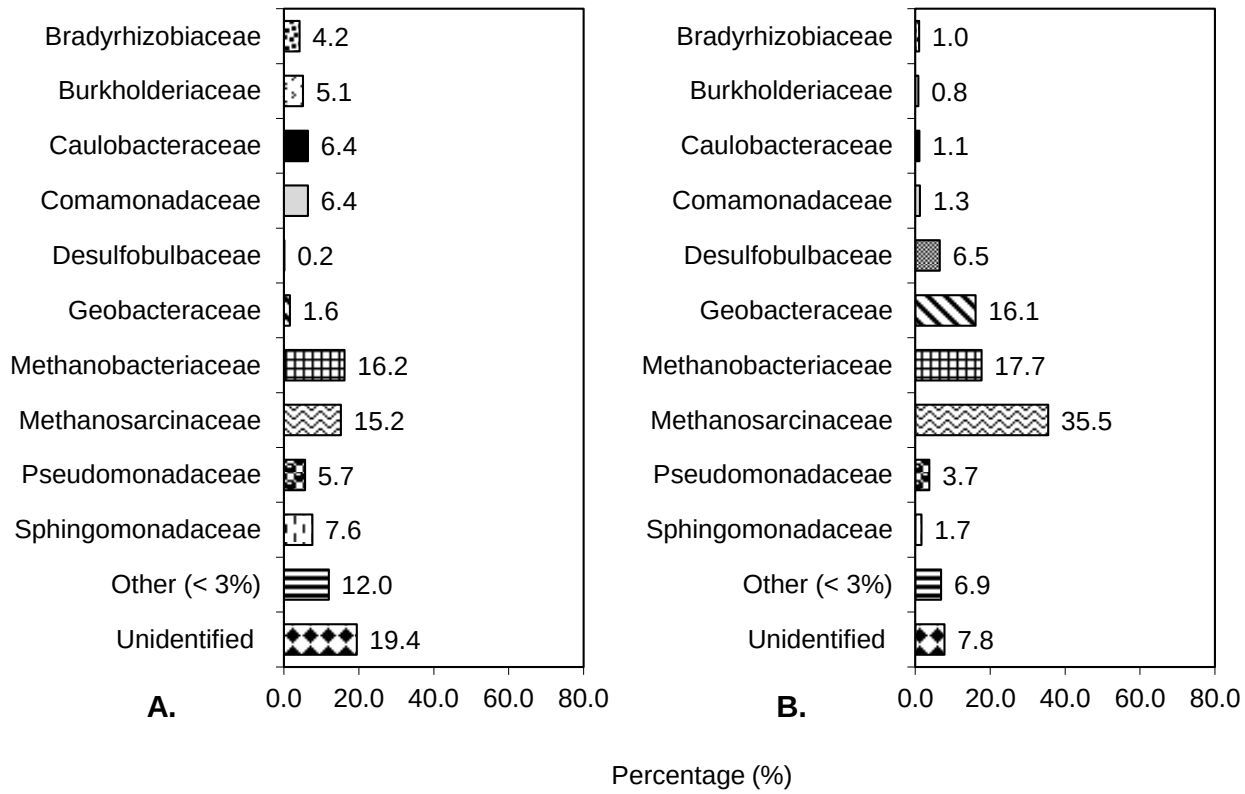

Figure 4.9. Site 2 produced water 16S rRNA gene sequence results. (A) Site 2 no substrate, (B) Site 2 core.

4.3.4 Produced Water Incubations – Heterogeneity Study (Day 0 -244)

A variability study was carried out on the produced water cultures enriched with acetate for both Sites 1 and 2 over the course of the experiment. The variability study was done to understand the differences in both methane production and microorganisms present within the same replicates. Often times in environmental samples it is observed that not all of the replicates give the same results, the reason for this is currently unknown, however this can make environmental samples more difficult to study at times. Figure 4.10 to Figure 4.13 show the 16S rRNA gene sequence results and the methane production curves for enriched Site 1 and 2 cultures with acetate.

The average methane production rate throughout the experiment for Site 1 Acetate as shown in Figure 4.10 for Acetate 1, 2 and 3 is 7.07×10^{-7} methane(g)/produced water(g)/day, 3.78×10^{-8} methane(g)/produced water(g)/day and 8.03×10^{-7} methane(g)/produced water(g)/day, respectively. Although the replicates were all incubated using the same sample and with the same procedure there is a distinguishable variability in terms of methane production and family of organisms present within each sample. Both Site 1 Acetate 1 and Site 1 Acetate 3 samples have a significant presence of *Methanosarcinaceae* (55.6 % and 84.5 %), respectively. Essentially, both Acetate 1 and Acetate 3 samples from Site 1 also show higher amounts of methane produced per gram of core compared to the Site 1 Acetate 2 sample.

A similar trend is seen with the Site 2 samples as shown in Figure 4.12. The average acetate production rate throughout the experiment as shown in Figure 4.12 for Site 2 Acetate 1, 2 and 3 is 1.97×10^{-8} methane(g)/produced water(g)/day, 7.79×10^{-7}

methane(g)/produced water(g)/day and 7.87 x 10^{-7} methane(g)/produced water(g)/day, respectively. Once again, only two (Site 2 Acetate 2 and Acetate 3) of the three replicates show similar trends in the amount of methane produced. The analysis of the family of organisms present within these three samples also show that the percentage of *Methanosarcinaceae* present within Site 2 Acetate 2 and Site 2 Acetate 3 samples are 74.7 and 75.8 %, respectively, which is much higher than the Site 2 Acetate 1 sample. This suggests that the *Methanosarcinaceae* are contributing to a larger amount of methane being present within the bottles.

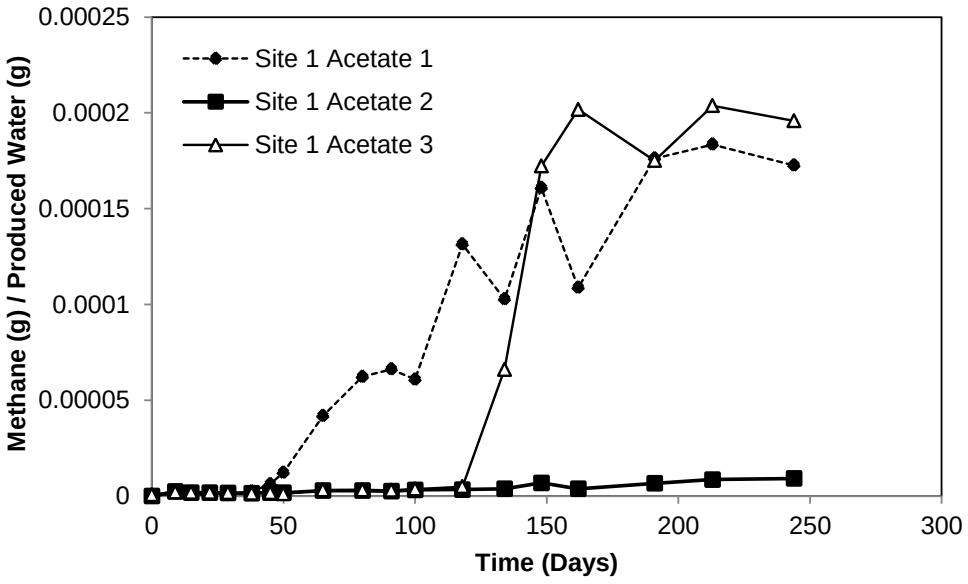

Figure 4.10. Site 1 Acetate methane production curve methane (g)/ produced water (g) as a function of time (days).

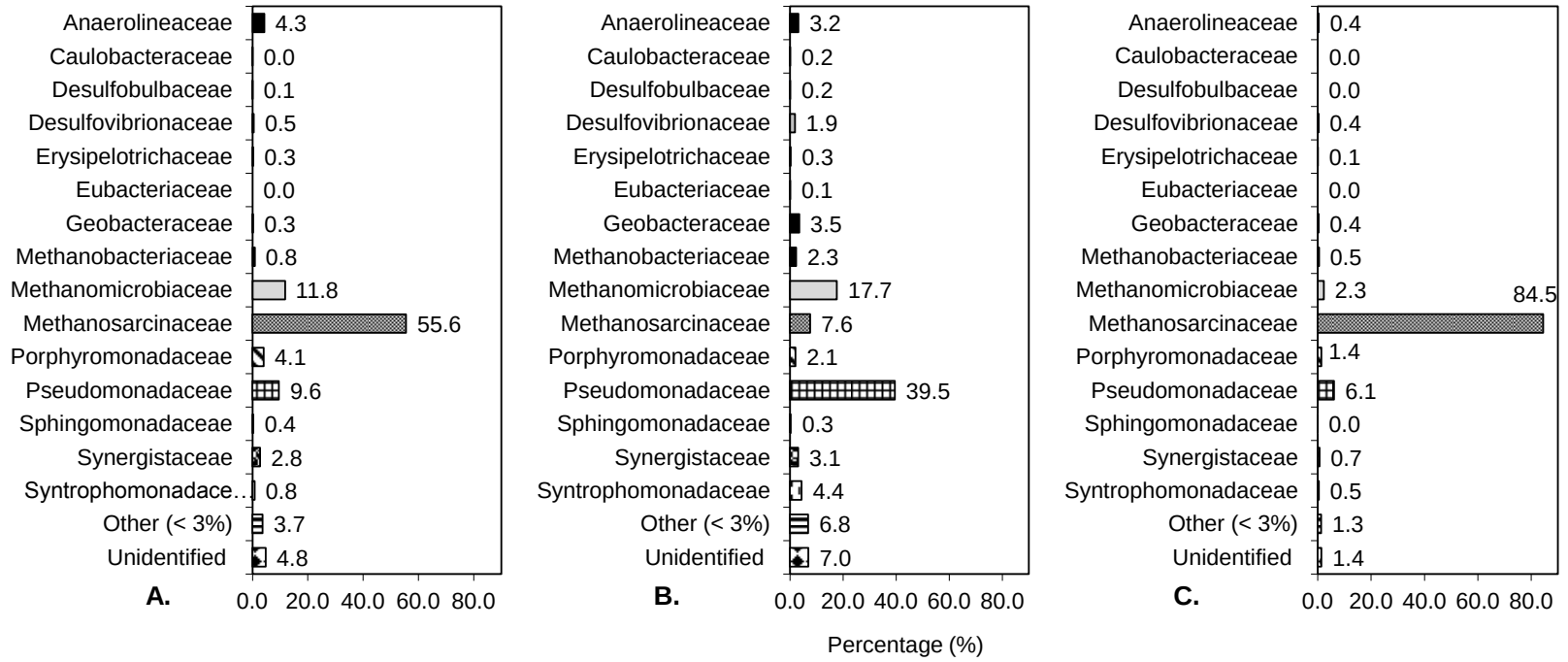

Figure 4.11. Site 1 Acetate, 16S rRNA gene sequence results. Percentage of microorganisms present within the sample (A) Site 1 Acetate 1, (B) Site 1 Acetate 2, and (C) Site 1 Acetate 3.

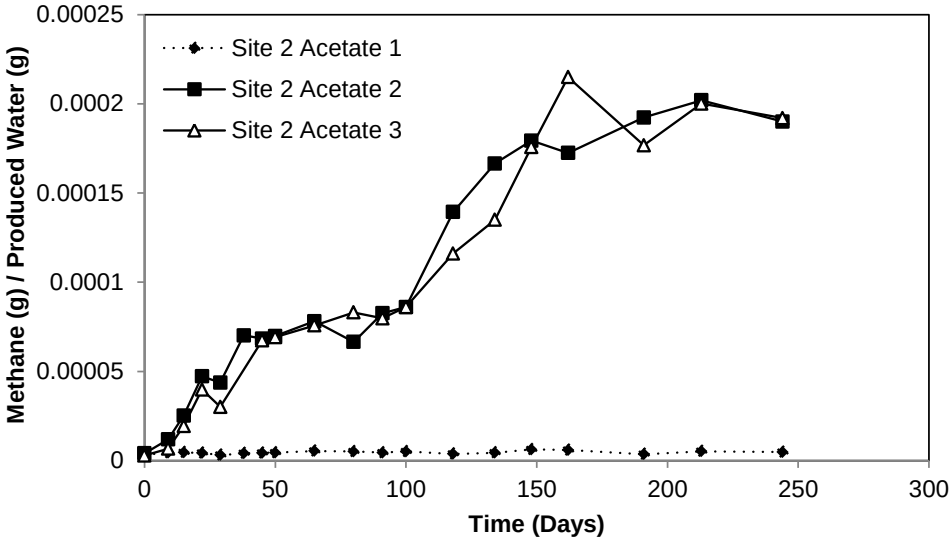

Figure 4.12. Site 2 Acetate methane production curve methane (g)/ produced water (g) as a function of time (days).

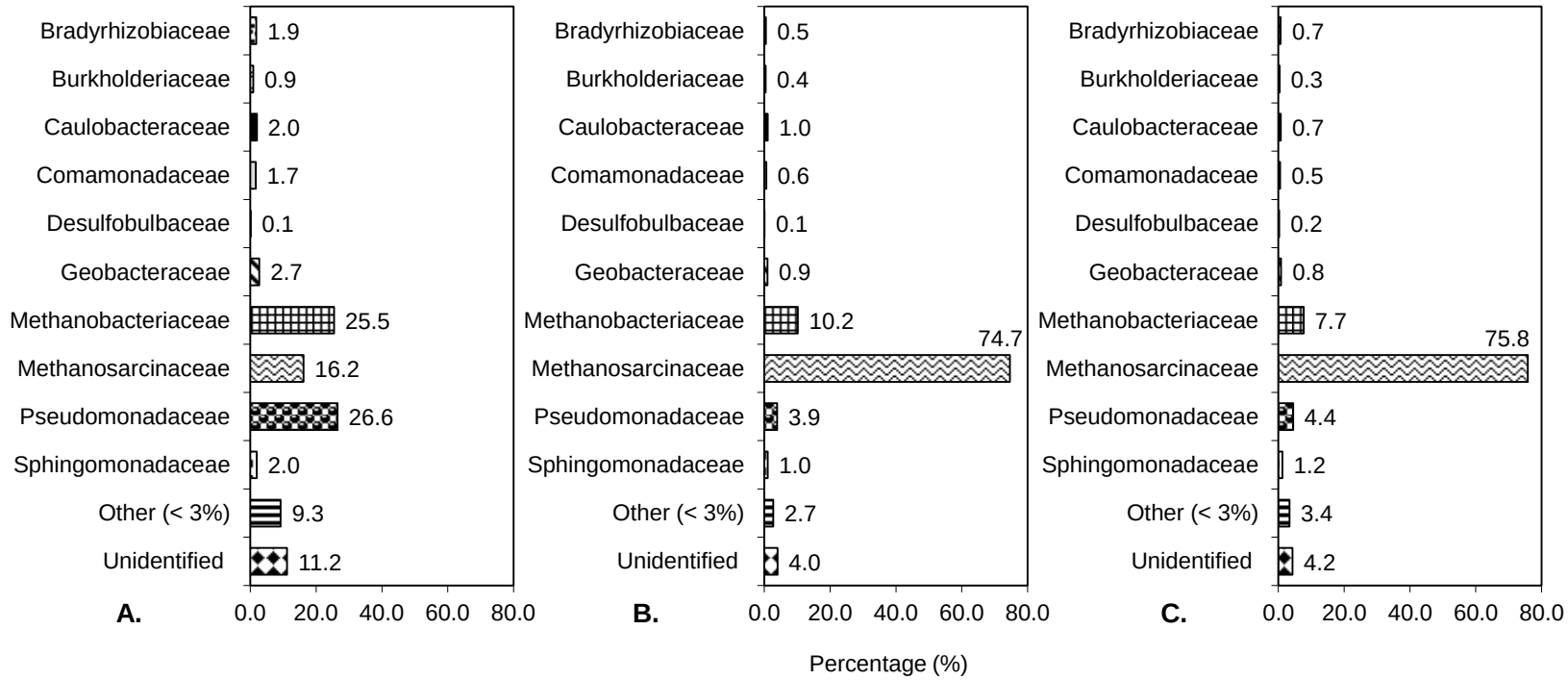

Figure 4.13. Site 2 Acetate, 16S rRNA gene sequence results. Percentage of microorganisms present within the sample (A) Site 2 Acetate 1, (B) Site 2 Acetate 2, and (C) Site 2 Acetate 3.

For Site 1, overall 40.4% of the enriched, no substrate consortia was comprised of *Pseudomonadaceae* which is a family of microorganisms found deep within the subsurface, and they are capable of degrading long chain alkanes and crude oil (Liu et al., 2012). *Pseudomonadaceae* decreased from 40.4 to 29.9% or 5.6% in the Site 1 core and H_2/CO_2 samples, as well as the Site 1 Acetate 1 and 3 samples from 40.4 to 9.6% or 6.1% respectively. However, *Pseudomonadaceae* was present at 39.5% in the Site 1 Acetate 2 sample. *Methanosarcinaceae* remained the most predominant methanogen, increasing from 3.1 to 23.7 or 42.7%, respectively, within the no substrate, core and H_2/CO_2 enrichments. Similarly, there was an increase in *Methanosarcinaceae* in the Site 1 Acetate 1, 2 and 3 samples from 3.1 to 55.6%, 7.6% and 84.5%.

All three enrichments contained microorganisms affiliated with sulfur and iron cycling (e.g. *Geobacteraceae*, *Desulfobulbaceae* and *Desulfovibrionaceae*) and methanogenesis (*Methanosarcinaceae*, *Methanobacteriaceae*, and *Methanomicrobiaceae*), suggesting that these may be important processes within the shale reservoir from which the produced water samples were obtained.

The no substrate core was comprised predominantly of *Pseudomonadaceae* and amending the enrichments with core, H_2/CO_2 or acetate selected for a shift towards an increase in the proportion of methanogens. Therefore, methanogens were present within the samples, and the enrichment conditions did in fact select for an increased proportion of methanogens.

4.3.5 Core Incubations (Day 3 – 98)

There was no discernible amount of methane observed in the cores samples. This can be attributed to the fact that the core used in the experiment was subject to atmospheric conditions since it was cored in 2002.

4.3.6 Core Inoculations (Day 98 – 144)

There were three types of enrichments incubated with cores samples from Zones B, C, D, E and F obtained from Site 1 but inoculated with Site 2 produced water on Day 98. These three incubations were: (a) an N_2/CO_2 headspace with no additional electron donors (no substrate); (b) H_2/CO_2 at a ratio of 80:20 was added to the headspace with no additional electron donors (H_2/CO_2); and (c) N_2/CO_2 headspace amended with volatile fatty acids (VFA's) (0.1 mL for a 1M VFA solution that consisted of equimolar concentrations of acetate, butyrate and propionic acid) (VFA). The three samples listed will be herein referred to as no substrate, H_2/CO_2, and VFA. Methane production from these bottles was measured on a monthly basis and 454 pyrosequencing of a fragment of the 16S rRNA gene was performed for all of the samples in Zone D (10 µg DNA/mL of the no substrate, H_2/CO_2 and VFA sample were sent out for core D 16S rRNA gene sequencing analysis) .

Subsequent analysis, with the normalized data, was carried out at the family level. The results of the 454 pyrosequencing are presented in Figure 4.20 and Table 4.5, wherein the percent refers to the percent of total reads represented by each particular family of organism. Figures 4.14 - Figure 4.19 show the methane production curves for all of the samples at depths B, C, D, E and F with enriched samples of no substrate, H_2/CO_2, and

VFA . There were 8 families of organisms that were present at 3% abundance or more in at least one of the enrichment conditions. These are bolded in Table 4.5 and further discussion will be limited to these organisms.

The methane production curves are shown in Figures 4.14 - Figure 4.19. The no substrate samples demonstrated the least methane production (g) per gram of core present, while core enrichment with H_2/CO_2 and VFA's greatly increased the amount of methane produced.

In the no substrate culture methane gas was the highest at depth C followed by depth E, depths D and F are very similar and depth B showed the smallest amount of methane produced (See Figure 4.14). This is reflective of what was actually seen in this field through a spinner study. Depth C and E showed most of the methane production within the field. Also, as shown in Figure 4.4 depths C and E have more inorganic carbon relative to the other depths. The presence of inorganic carbon could be indicative of microbial activity within that region.

With the addition of H_2/CO_2 and VFA's to the core samples, all of the methane production shifted upwards. In the samples with H_2/CO_2 all of the samples in Zones B, C, D and E produced similar amounts of methane (around 0.0004 methane(g)/core(g)) except for sample F (which is much lower around, 0.00025 methane(g)/core(g)), and in the VFA samples essentially all of the samples in zones B, C, D, E and F produced the same amount of methane (around 0.0005 methane(g)/core(g)). The average methane gas

production rates for the entire 146 days of experiment for all the different zones in the no substrate, H_2/CO_2 and VFA cultures are 1.20 x 10^{-6} methane(g)/core(g)/day, 2.78 x 10^{-6} methane(g)/core(g)/day, and 3.36 x 10^{-6} methane(g)/core(g)/day, respectively. The bottles containing VFA clearly show an increase in the amount of methane produced, this suggests that VFA could potentially increase the methanogenic yield of shale reservoirs.

The microbial community within the no substrate core was predominately composed of *Clostridaceae* (3.5%), *Desulfomicrobiaceae* (0.8%), *Geobacteraceae* (24.3%), *Methanobacteriaceae* (3.4%), *Methanomicrobiaceae* (0.4%), *Methanosarcinaceae* (27.9%), and *Pseudomonadaceae* (17.3%). Relative to the microbial community within the no substrate enrichment, there was a shift towards a predominately methanogenic community within the H_2/CO_2 enrichment, particularly *Methanosarcinaceae* (50.7%). The proportion of *Clostridaceae* (0.2%), *Geobacteraceae* (4.7%), and *Pseudomonadaceae* (8.2%) decreased and the proportion of *Desulfomicrobiaceae* (3.8%) slightly increased, while there were more minor changes in the other predominant consortia members. Similarly, relative to the no substrate core enrichment, the VFA enrichment also shifted towards a primarily methanogenic consortium, particularly *Methanocorpusculaceae* (3.8%), *Methanomicrobiaceae* (5.5%), and *Methanosarcinaceae* (36.6%). There was a decrease in the *Clostridiaceae* (0.7%), *Geobacteraceae* (2.8%), and *Pseudomonadaceae* (0.4%). Other predominant organisms included *Desulfomicrobiaceae* (2.0%) and *Methanobacteriaceae* (2.1%).

Overall, 52% of the enriched, no substrate consortium comprised microorganisms involved in iron reduction (*Geobacteraceae*) and methanogenesis (*Methanosarcinaceae*), suggesting that these are key metabolic functions within the core. *Methanosarcinaceae* remained the most predominant methanogen, increasing from 27.9 to 50.7 or 36.6%, respectively, within the no substrate H_2/CO_2 and VFA enrichments.

All three enrichments contained microorganisms affiliated with sulfur and iron cycling (e.g. *Geobacteraceae* and *Desulfomicrobiaceae*) and methanogenesis (*Methanosarcinaceae*, *Methanobacteriaceae*, *Methanomicrobiaceae, and Methanocorpusculaceae*), suggesting that these may be important processes within the core.

The no substrate core was predominantly *Geobacteraceae* and *Methanosarcinaceae*, and amending the enrichments with H_2/CO_2 or VFA's selected for a shift towards an increase in the proportion of methanogens. Therefore, methanogens were present within the samples, and the enrichment conditions did in fact select for an increased proportion of methanogens.

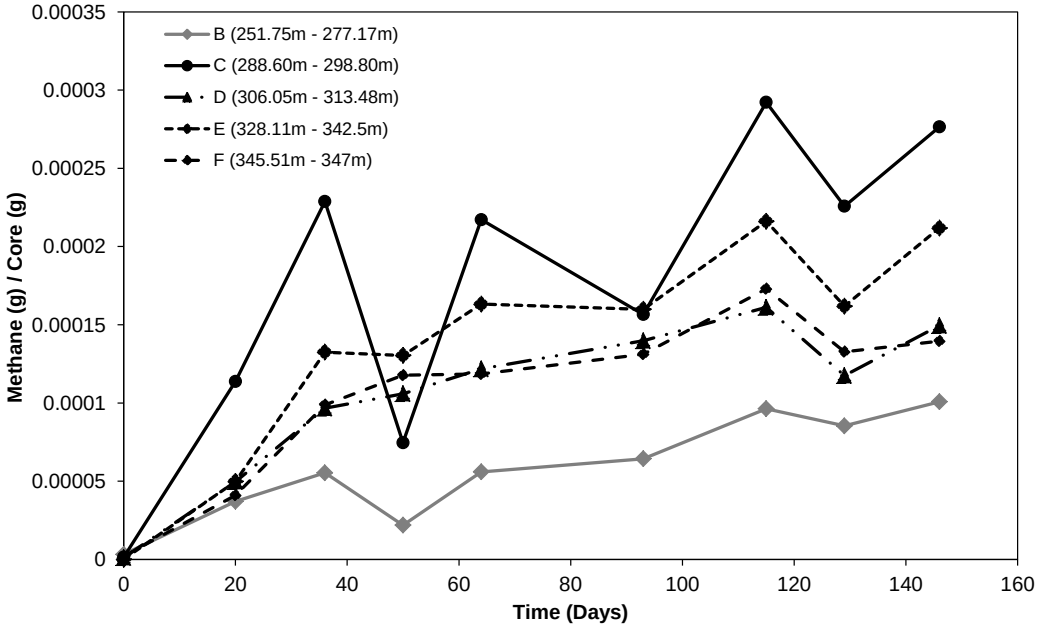

Figure 4.14. measured methane (g)/ core (g) as a function of time in days for sample depths B, C, D, E and F for core inoculations with no substrate.

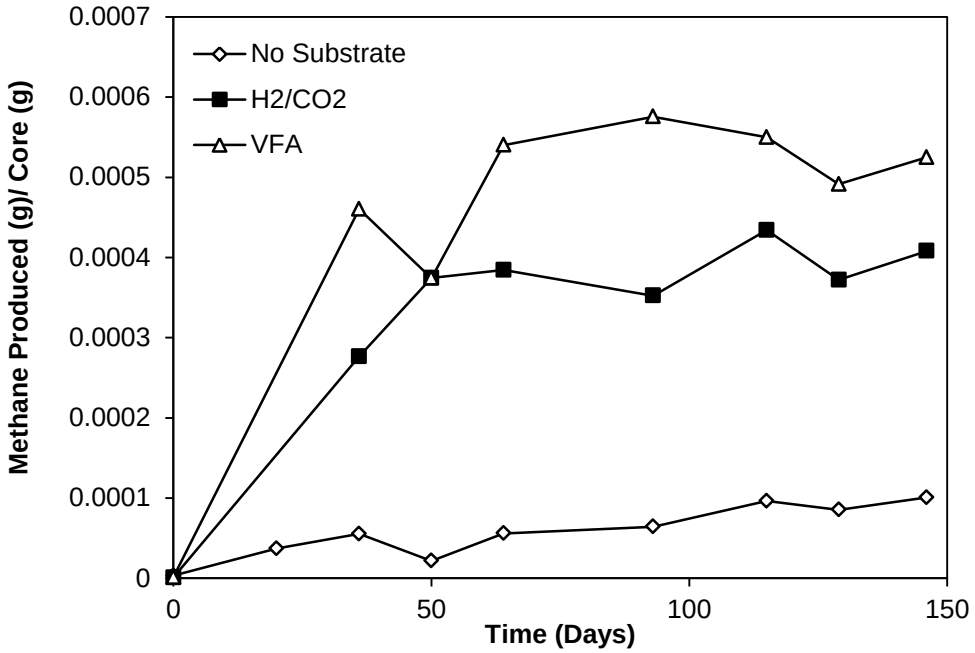

Figure 4.15. Depth B measured methane (g)/core (g) as a function of time in days for core inoculations with no substrate (A) no substrate, (B) H_2/CO_2, and (C) VFA.

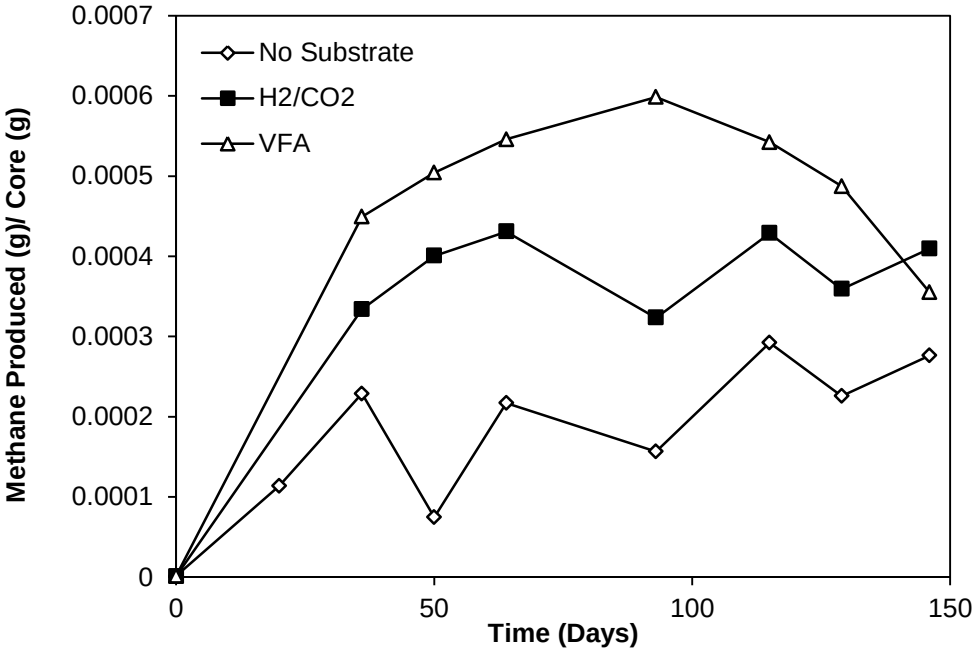

Figure 4.16. Depth C measured methane (g)/core (g) as a function of time in days for core inoculations with no substrate (A) no substrate, (B) H_2/CO_2, and (C) VFA.

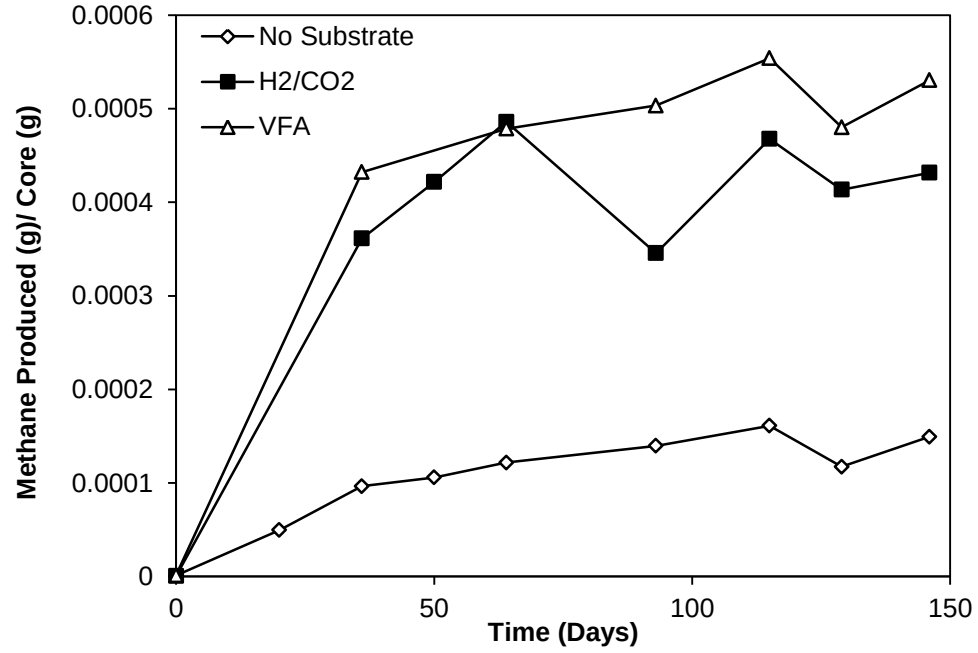

Figure 4.17. Depth D measured methane (g)/core (g) as a function of time in days for core inoculations with no substrate (A) no substrate, (B) H_2/CO_2, and (C) VFA.

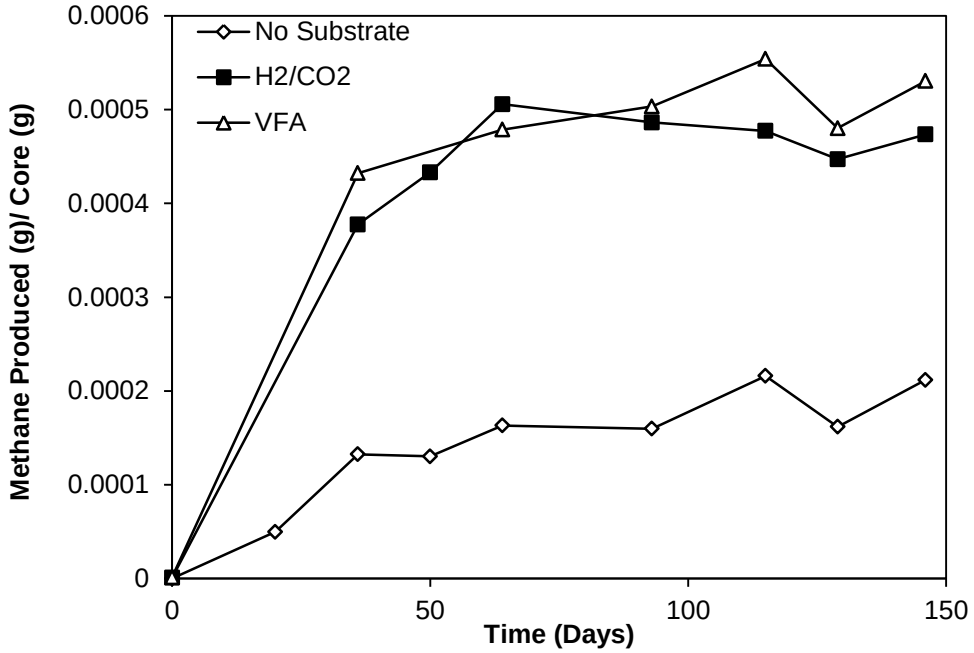

Figure 4.18. Depth E measured methane (g)/core (g) as a function of time in days for core inoculations with no substrate (A) no substrate, (B) H_2/CO_2, and (C) VFA.

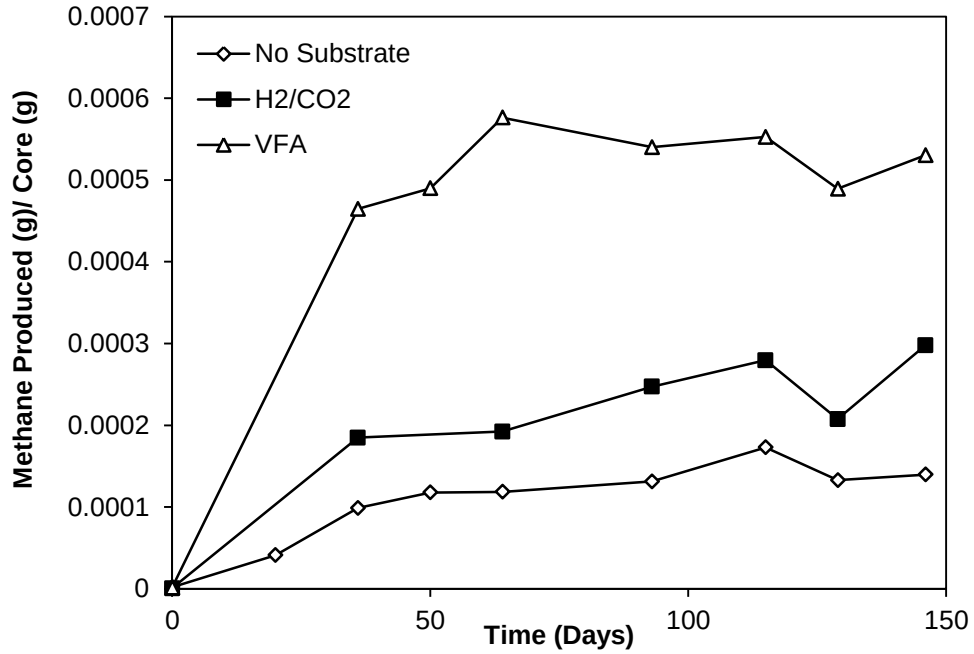

Figure 4.19. Depth E measured methane (g)/core (g) as a function of time in days for core inoculations with no substrate (A) no substrate, (B) H_2/CO_2, and (C) VFA.

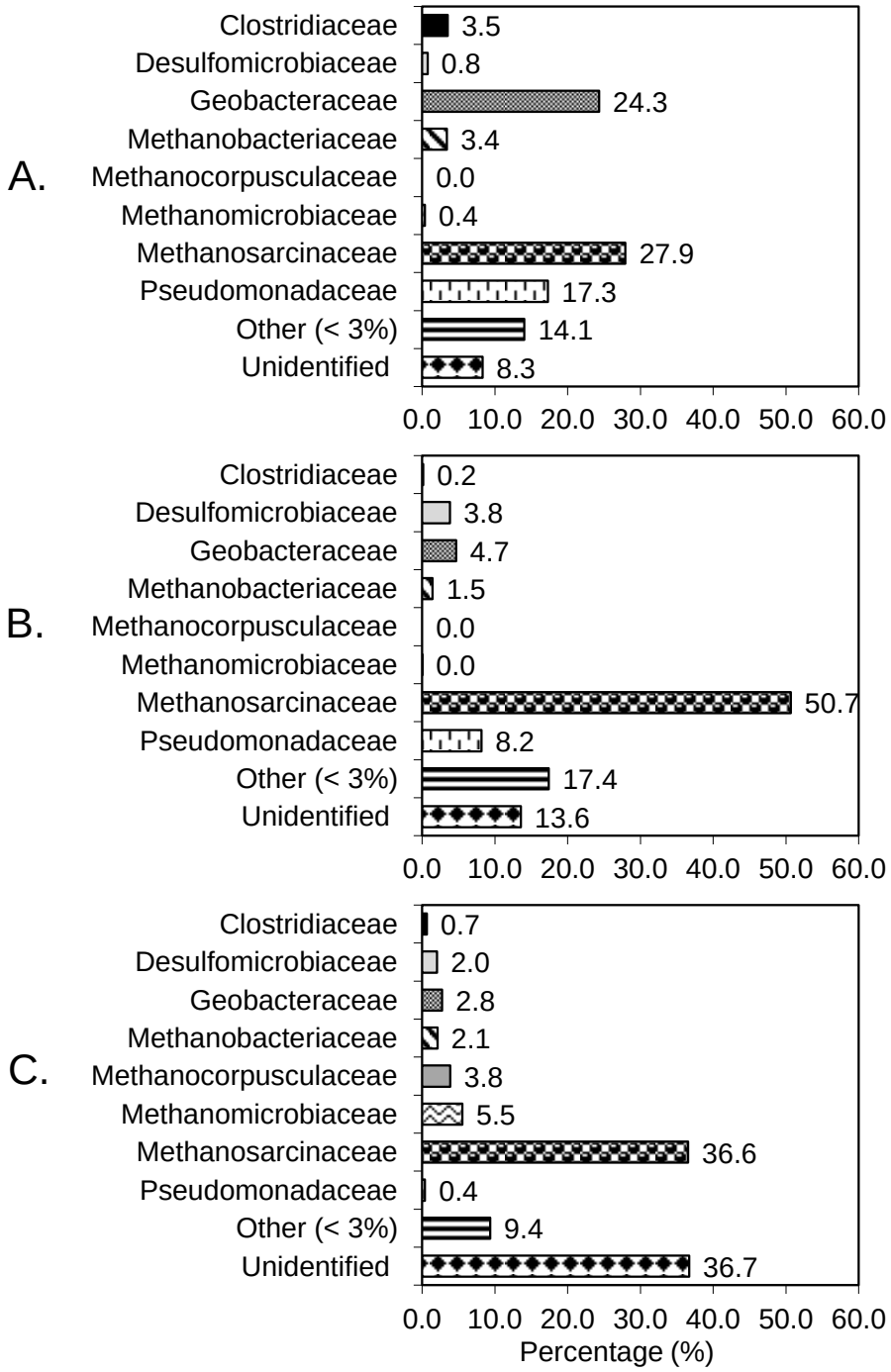

Figure 4.20. 16S rRNA gene sequence results for core samples from zone D. Percentage of microorganisms present within the sample (A) no substrate, (B) H_2/CO_2, and (C) VFA.

4.3.7 Analysis of Inoculated Core-Containing Incubations for Evidence of Substrate Biodegradation

None of the initial core-containing incubations produced discernible amounts of methane after approximately 3 months of incubation (Experiment 2). In contrast, in the produced water incubations amended with H_2/CO_2 or VFA, substantial amounts of methane were produced relative to the no substrate controls (Experiment 1), showing that the microbes associated with the shale formation were active and methanogenic. Thus, to assess whether such microbial populations from the formation could utilize shale components found in the cores, the methanogenic produced water samples from Experiment 1 (pre-incubations with H_2/CO_2) were used to inoculate the inactive core incubations from Experiment 2. One replicate prepared from core material sampled from each depth was inoculated, while the second replicate remained uninoculated. Methane was monitored for several months, and the replicate containing the inoculum produced significantly higher levels of methane above that of the inoculant-free control. Even after 244 days, the uninoculated replicate produced little methane. Thus, we hypothesized that components in the shale core material were being utilized in the inoculated replicates, leading to the enhanced levels of methane. Shale is comprised largely of kerogen, which is known to be solvent-insoluble, refractory organic matter that is formed during diagenesis at relatively shallow depths (Petsch et al., 2001). The organic matter is largely undefined, although some recent analyses have shown that shale can contain some compounds like alkanes, polycyclic aromatic hydrocarbons (PAH), and S-heterocycles that can feasibly serve as microbial substrates in shale formations (Formolo et al., 2008; Matlakowska and Sklodowska, 2011). For our study, water-soluble components of the

shale core-containing incubations were determined using gas chromatography-mass spectrometry (GC-MS) at the end of the incubation period.

4.3.8 Water-Soluble Substrate/Metabolite Identification by GC-MS

Medium-only controls were prepared alongside inoculated and uninoculated core samples. All three samples were compared for differences in the resulting peaks that appeared during GC-MS analysis. Total ion chromatograms, as well as selected ions indicative of hydrocarbons such as alkanes (m/z 57) and trimethylsilylated carboxylic acids or hydroxyl groups (m/z 73) were compared. In addition, each sample was probed for the fragment ions characteristic of anaerobic aromatic or alkane metabolites such as fumarate addition products and downstream metabolites (Gieg and Suflita, 2005; Wawrik et al., 2011).

Water extract analysis from incubations containing sample E shale core material showed many differences between the uninoculated and inoculated core samples. For example, when uninoculated and inoculated water extracts were probed for a characteristic alkane fragment ion (m/z 57), numerous peaks indicative of alkanes ranging from C_{22} to C_{30} were evident in the uninoculated sample, while these were largely absent in the inoculated sample (Figure 4.21a). These alkanes were depleted relative to other compounds such as hexadecanoic and octadecanoic acid that were present in the samples at near equivalent amounts (Figure 4.21b), suggesting that the alkanes associated with the E core sample served as a carbon source for syntrophic conversion of shale to methane. In addition, several other compounds were present in the water extract of the uninoculated core-containing replicate that were depleted in the inoculated core-

containing replicate (based on a comparison of the m/z 73 fragment analysis indicating the presence of compounds containing a –COOH or –OH group). These differences suggest that a variety of other non-alkane shale components also served as carbon sources for syntrophic shale conversion to methane (Figure 4.22). Identified components based on mass spectral matches with authentic standards are shown in Figure 4.22. For samples containing core material from Zones B, C, D, and F, similar albeit fewer differences were seen in the inoculated versus uninoculated replicates when targeted fragment analyses were conducted. Alkanes were not present in the water extracts from these shale core samples (based on a search for the distinct m/z 57 fragment ion). However some changes in other peaks after a specific search for the m/z 73 fragment ion were observed. Some components positively identified in the uninoculated cores but that were absent in the inoculated cores included a variety of dicarboxylic acids (succinic acid, methylsuccinic acid, glutaric acid, adipic acid, pimelic acid), phthalic acid, and hydroxybenzoic acid. None of the identified components were present in the medium only controls. Collectively, these data suggest that several organic acids and/or alkanes associated with shale can serve as carbon sources to drive syntrophic conversion of shale organic matter to methane. Core sample E showed the greatest number of changes in putative shale substrates in the inoculated versus uninoculated core samples, which positively correlates with the observation that the highest amount of methane was also produced from this core sample.

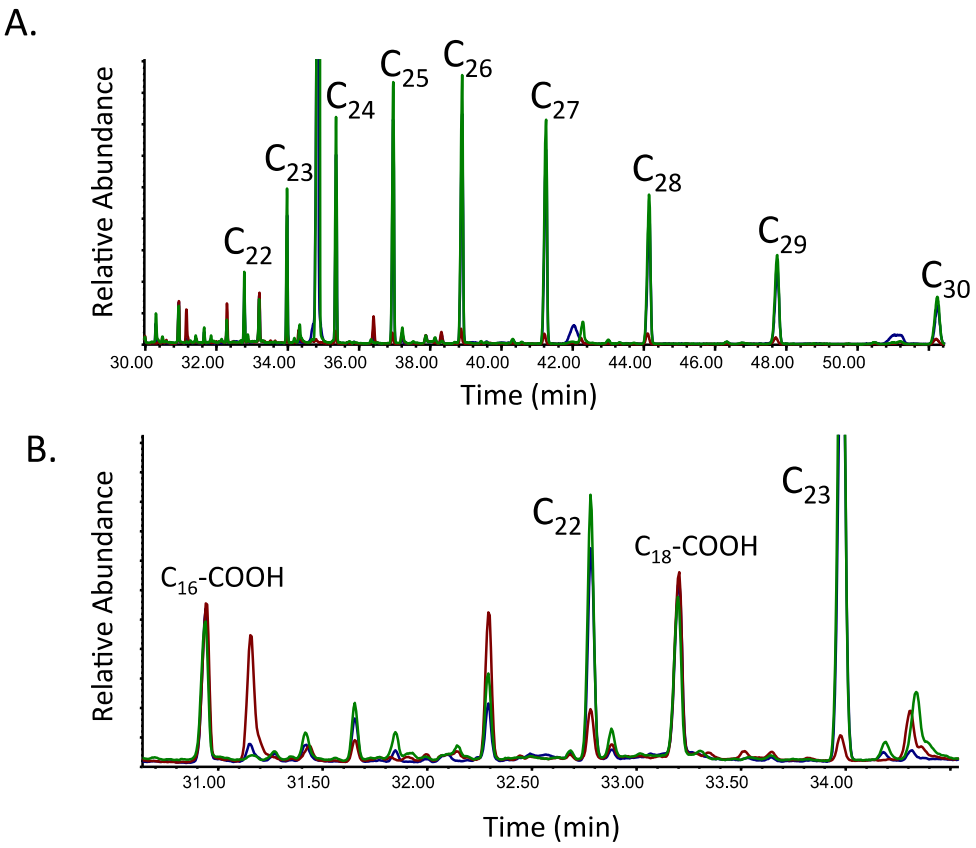

Figure 4.21. (A) A portion of the m/z 57 fragment analysis of the organic extract of the water-soluble components from inoculated (red) and uninoculated (green) shale core E-containing samples. The alkanes ranging from C_{22}-C_{30} are depleted in the inoculated sample versus the uninoculated sample. (B) A zoomed-in portion of A, showing that similar responses of other components were seen (hexadecanoic and octadecanoic acids) in the extracts. Blue trace is an additional water extract of an uninoculated core E sample.

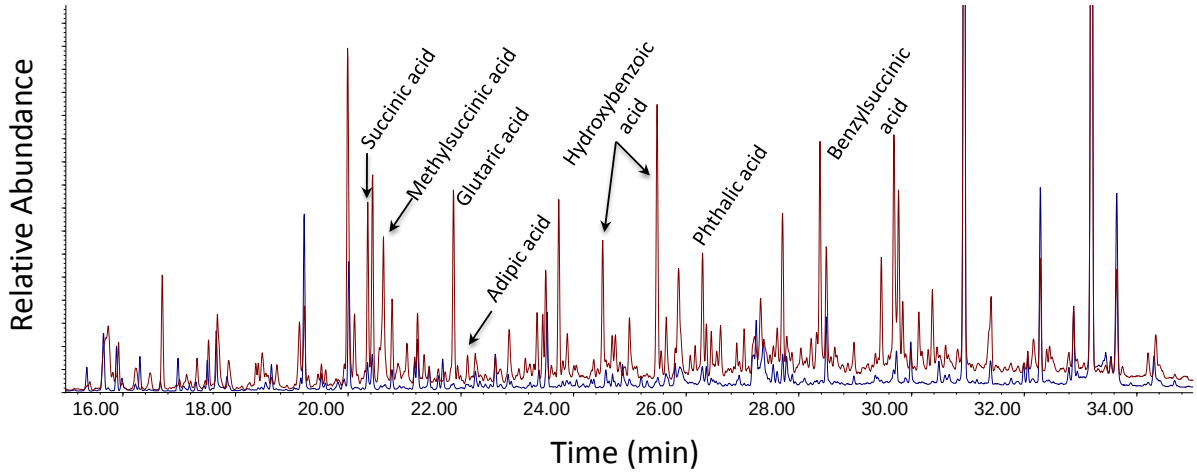

Figure 4.22. A portion of the m/z 73 fragment analysis of the organic extract of the water-soluble components from inoculated (blue) and uninoculated (red) shale core E-containing samples, showing that numerous compounds in the uninoculated sample are depleted in the inoculated sample. Positively identified compounds are indicated.

4.4 Conclusions and Recommendations

- Within the shale gas formation, there is no significant difference in geology between the different depths within the well, however there is a difference in the amount of methane that is produced at different depths. Depths C and E have the highest percentage of inorganic carbon as compared to the other depths, and are also producing more methane at these depths both within the laboratory and within the field.
- The 16S rRNA gene sequencing data of the produced water samples show evidence of methanogens within the cultures. There is also a clear shift towards methanogenic communities with the addition of H_2/CO_2 and acetate in the produced water samples.

- None of the initial core-containing incubations produced discernible amounts of methane after approximately 3 months of incubation. This was most likely because the shale samples were obtained from core previously extracted in 2002 and were subject to atmospheric conditions.
- Within the inoculated core cultures there is a clear shift towards a methanogenic community with the addition of H_2/CO_2 and VFA. This is reflected both in the 16S rRNA gene sequencing analysis and the methane production curves. The enrichment core samples with VFA show the highest amount of methane produced at all depths.
- Analysis of alkanes in the uninoculated and inoculated cores samples indicate that several organic acids and/or alkanes associated with shale can serve as carbon sources to drive syntrophic conversion of shale organic matter to methane.

Table 4.3. Overview of the community analysis as determined by 454 pyrosequencing of the 16S rRNA gene for Site 1 Produced Water. Family of organisms present at or above 3% in at least one of the samples are bolded.

Family	Site 1 Acetate 1		Site 1 Acetate 2		Site 1 Acetate 2		Site 1 No Substrate		Site 1 Core		Site 1 H_2/CO_2	
	No. Reads[A]	Percent[B]	No. Reads[A]	Percent[B]	No. Reads[A]	Percent[B]	No. Reads[A]	Percent[B]	No. Reads[A]	Percent[B]	No. Reads[A]	Percent[B]
Acetobacteraceae	0	0.0	0	0.0	0	0.0	4	0.1	0	0.0	0	0.0
Acholeplasmataceae	1	0.0	42	0.7	0	0.0	0	0.0	1	0.0	0	0.0
Acidimicrobiaceae	0	0.0	1	0.0	0	0.0	0	0.0	0	0.0	0	0.0
Acidobacteriaceae	1	0.0	0	0.0	0	0.0	12	0.2	0	0.0	2	0.0
Aerococcaceae	0	0.0	0	0.0	0	0.0	0	0.0	0	0.0	0	0.0
Aeromonadaceae	0	0.0	6	0.1	0	0.0	1	0.0	0	0.0	0	0.0
Alcaligenaceae	3	0.0	0	0.0	0	0.0	14	0.2	30	0.5	1	0.0
Anaerolineaceae	**260**	**4.3**	**193**	**3.2**	**26**	**0.4**	**127**	**2.1**	**28**	**0.5**	**24**	**0.4**
Aurantimonadaceae	0	0.0	0	0.0	0	0.0	3	0.1	0	0.0	0	0.0
Bacillaceae	1	0.0	3	0.0	0	0.0	1	0.0	0	0.0	0	0.0
Bacteroidaceae	0	0.0	0	0.0	0	0.0	0	0.0	0	0.0	0	0.0
Bradyrhizobiaceae	8	0.1	23	0.4	0	0.0	144	2.4	7	0.1	26	0.4
Brucellaceae	0	0.0	1	0.0	0	0.0	26	0.4	16	0.3	27	0.4
Burkholderiaceae	11	0.2	22	0.4	4	0.1	101	1.7	7	0.1	25	0.4
Caldilineaceae	1	0.0	0	0.0	0	0.0	0	0.0	0	0.0	0	0.0
Caldisericaceae	0	0.0	0	0.0	0	0.0	1	0.0	0	0.0	0	0.0
Campylobacteraceae	2	0.0	4	0.1	0	0.0	8	0.1	2	0.0	3	0.0
Carnobacteriaceae	9	0.1	12	0.2	5	0.1	63	1.0	4	0.1	2	0.0
Caulobacteraceae	**3**	**0.0**	**10**	**0.2**	**2**	**0.0**	**205**	**3.4**	**4**	**0.1**	**25**	**0.4**
Cellulomonadaceae	0	0.0	1	0.0	0	0.0	2	0.0	1	0.0	1	0.0
Chrysosaccaceae	0	0.0	0	0.0	0	0.0	0	0.0	0	0.0	0	0.0
Clostridiaceae	4	0.1	30	0.5	5	0.1	2	0.0	47	0.8	2	0.0
Comamonadaceae	14	0.2	14	0.2	4	0.1	152	2.5	43	0.7	21	0.3
Coriobacteriaceae	1	0.0	3	0.0	0	0.0	0	0.0	3	0.0	4	0.1
Corynebacteriaceae	0	0.0	1	0.0	0	0.0	0	0.0	0	0.0	1	0.0
Cytophagaceae	0	0.0	0	0.0	0	0.0	1	0.0	0	0.0	0	0.0
Deferribacteraceae	0	0.0	47	0.8	5	0.1	20	0.3	17	0.3	0	0.0
Desulfobacteraceae	2	0.0	5	0.1	1	0.0	40	0.7	48	0.8	0	0.0

Family	Site 1 Acetate 1		Site 1 Acetate 2		Site 1 Acetate 2		Site 1 No Substrate		Site 1 Core		Site 1 H_2/CO_2	
	No. Reads[A]	Percent[B]	No. Reads[A]	Percent[B]	No. Reads[A]	Percent[B]	No. Reads[A]	Percent[B]	No. Reads[A]	Percent[B]	No. Reads[A]	Percent[B]
Desulfobulbaceae	**4**	**0.1**	**11**	**0.2**	**0**	**0.0**	**25**	**0.4**	**1467**	**24.1**	**0**	**0.0**
Desulfomicrobiaceae	20	0.3	17	0.3	3	0.0	6	0.1	2	0.0	1	0.0
Desulfovibrionaceae	**32**	**0.5**	**115**	**1.9**	**22**	**0.4**	**192**	**3.2**	**6**	**0.1**	**10**	**0.2**
Desulfuromonadaceae	1	0.0	25	0.4	0	0.0	107	1.8	48	0.8	5	0.1
Dietziaceae	0	0.0	0	0.0	0	0.0	0	0.0	0	0.0	0	0.0
Enterobacteriaceae	9	0.1	10	0.2	0	0.0	19	0.3	2	0.0	25	0.4
Enterococcaceae	0	0.0	0	0.0	0	0.0	0	0.0	0	0.0	0	0.0
Equidae	0	0.0	0	0.0	0	0.0	4	0.1	0	0.0	0	0.0
Erysipelotrichaceae	**21**	**0.3**	**16**	**0.3**	**7**	**0.1**	**10**	**0.2**	**1**	**0.0**	**219**	**3.6**
Erythrobacteraceae	0	0.0	0	0.0	1	0.0	0	0.0	0	0.0	0	0.0
Eubacteriaceae	**0**	**0.0**	**8**	**0.1**	**0**	**0.0**	**3**	**0.1**	**1**	**0.0**	**510**	**8.4**
Exobasidiaceae	0	0.0	0	0.0	0	0.0	0	0.0	0	0.0	0	0.0
Flavobacteriaceae	1	0.0	1	0.0	1	0.0	8	0.1	1	0.0	1	0.0
Geobacteraceae	**19**	**0.3**	**211**	**3.5**	**22**	**0.4**	**248**	**4.1**	**281**	**4.6**	**0**	**0.0**
Geodermatophilaceae	0	0.0	0	0.0	0	0.0	1	0.0	0	0.0	0	0.0
Gracilibacteraceae	4	0.1	12	0.2	4	0.1	24	0.4	17	0.3	12	0.2
Halomonadaceae	4	0.1	5	0.1	1	0.0	16	0.3	1	0.0	1	0.0
Hydrogenophilaceae	0	0.0	0	0.0	0	0.0	3	0.1	0	0.0	1	0.0
Hyphomicrobiaceae	0	0.0	0	0.0	0	0.0	3	0.1	0	0.0	0	0.0
Lachnospiraceae	7	0.1	7	0.1	2	0.0	6	0.1	2	0.0	4	0.1
Legionellaceae	0	0.0	0	0.0	0	0.0	12	0.2	0	0.0	0	0.0
Leptospiraceae	0	0.0	0	0.0	0	0.0	0	0.0	0	0.0	0	0.0
Marinilabiaceae	10	0.2	11	0.2	3	0.0	34	0.6	84	1.4	9	0.1
Methanobacteriaceae	**49**	**0.8**	**141**	**2.3**	**30**	**0.5**	**172**	**2.8**	**44**	**0.7**	**1514**	**24.9**
Methanocorpusculaceae	0	0.0	0	0.0	0	0.0	0	0.0	0	0.0	0	0.0
Methanomicrobiaceae	**717**	**11.8**	**1076**	**17.7**	**141**	**2.3**	**55**	**0.9**	**0**	**0.0**	**42**	**0.7**
Methanosaetaceae	6	0.1	25	0.4	15	0.3	43	0.7	3	0.0	0	0.0
Methanosarcinaceae	**3387**	**55.6**	**463**	**7.6**	**5143**	**84.5**	**189**	**3.1**	**1441**	**23.7**	**2601**	**42.7**
Methylobacteriaceae	1	0.0	1	0.0	1	0.0	30	0.5	0	0.0	6	0.1
Methylocystaceae	6	0.1	8	0.1	0	0.0	4	0.1	3	0.0	3	0.0

Family	Site 1 Acetate 1		Site 1 Acetate 2		Site 1 Acetate 2		Site 1 No Substrate		Site 1 Core		Site 1 H_2/CO_2	
	No. Reads[A]	Percent[B]	No. Reads[A]	Percent[B]	No. Reads[A]	Percent[B]	No. Reads[A]	Percent[B]	No. Reads[A]	Percent[B]	No. Reads[A]	Percent[B]
Microbacteriaceae	3	0.0	2	0.0	0	0.0	15	0.2	0	0.0	1	0.0
Micrococcaceae	1	0.0	0	0.0	0	0.0	1	0.0	4	0.1	2	0.0
Moraxellaceae	1	0.0	5	0.1	0	0.0	10	0.2	1	0.0	1	0.0
Mycobacteriaceae	0	0.0	0	0.0	0	0.0	0	0.0	0	0.0	0	0.0
Nitrosomonadaceae	0	0.0	0	0.0	0	0.0	1	0.0	0	0.0	1	0.0
Nocardiaceae	0	0.0	0	0.0	0	0.0	1	0.0	0	0.0	0	0.0
Nocardioidaceae	0	0.0	0	0.0	0	0.0	0	0.0	3	0.0	0	0.0
Oxalobacteraceae	1	0.0	6	0.1	2	0.0	5	0.1	88	1.5	0	0.0
Paenibacillaceae	0	0.0	0	0.0	0	0.0	0	0.0	0	0.0	0	0.0
Peptococcaceae	20	0.3	10	0.2	4	0.1	8	0.1	61	1.0	4	0.1
Phyllobacteriaceae	0	0.0	1	0.0	0	0.0	4	0.1	0	0.0	1	0.0
Planctomycetaceae	0	0.0	7	0.1	4	0.1	1	0.0	7	0.1	2	0.0
Planococcaceae	0	0.0	0	0.0	0	0.0	1	0.0	0	0.0	0	0.0
Polyangiaceae	3	0.0	0	0.0	0	0.0	3	0.1	0	0.0	1	0.0
Porphyromonadaceae	**248**	**4.1**	**125**	**2.1**	**85**	**1.4**	**61**	**1.0**	**66**	**1.1**	**160**	**2.6**
Propionibacteriaceae	0	0.0	0	0.0	0	0.0	2	0.0	0	0.0	0	0.0
Pseudomonadaceae	**586**	**9.6**	**2406**	**39.5**	**373**	**6.1**	**2458**	**40.4**	**1820**	**29.9**	**342**	**5.6**
Rhizobiaceae	1	0.0	0	0.0	1	0.0	3	0.1	0	0.0	0	0.0
Rhodobacteraceae	6	0.1	14	0.2	3	0.0	48	0.8	8	0.1	11	0.2
Rhodocyclaceae	0	0.0	4	0.1	0	0.0	1	0.0	0	0.0	1	0.0
Rikenellaceae	39	0.6	10	0.2	6	0.1	0	0.0	0	0.0	35	0.6
Ruminococcaceae	1	0.0	2	0.0	0	0.0	2	0.0	1	0.0	9	0.1
Saccharomycetaceae	0	0.0	1	0.0	0	0.0	0	0.0	0	0.0	0	0.0
Shewanellaceae	7	0.1	8	0.1	1	0.0	26	0.4	42	0.7	4	0.1
Sinobacteraceae	0	0.0	2	0.0	0	0.0	16	0.3	0	0.0	2	0.0
Sphingobacteriaceae	0	0.0	0	0.0	0	0.0	0	0.0	0	0.0	4	0.1
Sphingomonadaceae	**24**	**0.4**	**19**	**0.3**	**1**	**0.0**	**263**	**4.3**	**2**	**0.0**	**47**	**0.8**
Spirochaetaceae	3	0.0	2	0.0	0	0.0	4	0.1	0	0.0	0	0.0
Staphylococcaceae	0	0.0	0	0.0	0	0.0	2	0.0	0	0.0	0	0.0
Streptococcaceae	1	0.0	0	0.0	0	0.0	0	0.0	0	0.0	0	0.0

Family	Site 1 Acetate 1		Site 1 Acetate 2		Site 1 Acetate 2		Site 1 No Substrate		Site 1 Core		Site 1 H_2/CO_2	
	No. Reads[A]	Percent[B]	No. Reads[A]	Percent[B]	No. Reads[A]	Percent[B]	No. Reads[A]	Percent[B]	No. Reads[A]	Percent[B]	No. Reads[A]	Percent[B]
Synergistaceae	**169**	**2.8**	**188**	**3.1**	**43**	**0.7**	**174**	**2.9**	**11**	**0.2**	**128**	**2.1**
Syntrophaceae	2	0.0	1	0.0	3	0.0	5	0.1	0	0.0	0	0.0
Syntrophobacteraceae	0	0.0	1	0.0	0	0.0	1	0.0	0	0.0	0	0.0
Syntrophomonadaceae	**50**	**0.8**	**267**	**4.4**	**30**	**0.5**	**39**	**0.6**	**5**	**0.1**	**10**	**0.2**
Syntrophorhabdaceae	14	0.2	2	0.0	1	0.0	2	0.0	2	0.0	4	0.1
Veillonellaceae	0	0.0	1	0.0	0	0.0	3	0.1	0	0.0	1	0.0
Vibrionaceae	0	0.0	5	0.1	1	0.0	0	0.0	0	0.0	0	0.0
Victivallaceae	0	0.0	0	0.0	0	0.0	0	0.0	0	0.0	0	0.0
Xanthomonadaceae	1	0.0	0	0.0	0	0.0	0	0.0	0	0.0	0	0.0
Unidentified	292	4.8	424	7.0	86	1.4	787	12.9	310	5.1	194	3.2
Total	**6089**	**100.0**	**6089**	**100.0**	**6089**	**100.0**	**6089**	**100.0**	**6089**	**100.0**	**6089**	**100.0**

[A] The total number of reads were normalized to the average number of reads from each sample (6089 reads).
[B] Percent of total reads per family as determined with the normalized data.

Table 4.4. Overview of the community analysis as determined by 454 pyrosequencing of the 16S rRNA gene for Site 1 Produced Water. Family of organisms present at or above 3% in at least one of the samples are bolded.

Family	Site 2 Acetate 1		Site 2 Acetate 2		Site 2 Acetate 2		Site 2 No Substrate		Site 2 Core	
	No. Reads[A]	Percent[B]	No. Reads[A]	Percent[B]	No. Reads[A]	Percent[B]	No. Reads[A]	Percent[B]	No. Reads[A]	Percent[B]
Acetobacteraceae	0	0.0	0	0.0	0	0.0	0	0.0	0	0.0
Acholeplasmataceae	0	0.0	0	0.0	0	0.0	0	0.0	0	0.0
Acidimicrobiaceae	0	0.0	0	0.0	0	0.0	0	0.0	0	0.0
Acidobacteriaceae	5	0.1	2	0.0	2	0.0	14	0.2	6	0.1
Aerococcaceae	0	0.0	0	0.0	1	0.0	0	0.0	3	0.1
Aeromonadaceae	0	0.0	0	0.0	0	0.0	0	0.0	0	0.0
Alcaligenaceae	6	0.1	4	0.1	4	0.1	18	0.3	5	0.1
Anaerolineaceae	25	0.4	7	0.1	6	0.1	32	0.5	14	0.2
Aurantimonadaceae	0	0.0	0	0.0	0	0.0	0	0.0	0	0.0
Bacillaceae	5	0.1	0	0.0	2	0.0	0	0.0	0	0.0
Bacteroidaceae	2	0.0	0	0.0	0	0.0	0	0.0	0	0.0
Bradyrhizobiaceae	**113**	**1.9**	**29**	**0.5**	**41**	**0.7**	**257**	**4.2**	**61**	**1.0**
Brucellaceae	1	0.0	0	0.0	0	0.0	0	0.0	0	0.0
Burkholderiaceae	**57**	**0.9**	**25**	**0.4**	**21**	**0.3**	**312**	**5.1**	**48**	**0.8**
Caldilineaceae	0	0.0	0	0.0	0	0.0	0	0.0	0	0.0
Caldisericaceae	1	0.0	0	0.0	0	0.0	0	0.0	0	0.0
Campylobacteraceae	2	0.0	0	0.0	1	0.0	0	0.0	2	0.0
Carnobacteriaceae	8	0.1	0	0.0	5	0.1	83	1.4	14	0.2
Caulobacteraceae	**119**	**2.0**	**62**	**1.0**	**45**	**0.7**	**390**	**6.4**	**68**	**1.1**
Cellulomonadaceae	0	0.0	0	0.0	0	0.0	0	0.0	0	0.0
Chrysosaccaceae	0	0.0	0	0.0	1	0.0	0	0.0	0	0.0
Clostridiaceae	2	0.0	0	0.0	0	0.0	9	0.2	21	0.3
Comamonadaceae	**101**	**1.7**	**36**	**0.6**	**30**	**0.5**	**390**	**6.4**	**76**	**1.3**
Coriobacteriaceae	10	0.2	8	0.1	4	0.1	5	0.1	6	0.1
Corynebacteriaceae	1	0.0	0	0.0	0	0.0	0	0.0	0	0.0
Cytophagaceae	0	0.0	0	0.0	0	0.0	0	0.0	0	0.0
Deferribacteraceae	0	0.0	0	0.0	0	0.0	0	0.0	0	0.0
Desulfobacteraceae	0	0.0	0	0.0	0	0.0	0	0.0	7	0.1

Family	Site 2 Acetate 1		Site 2 Acetate 2		Site 2 Acetate 2		Site 2 No Substrate		Site 2 Core	
	No. Reads[A]	Percent[B]	No. Reads[A]	Percent[B]	No. Reads[A]	Percent[B]	No. Reads[A]	Percent[B]	No. Reads[A]	Percent[B]
Desulfobulbaceae	**6**	**0.1**	**5**	**0.1**	**12**	**0.2**	**9**	**0.2**	**398**	**6.5**
Desulfomicrobiaceae	23	0.4	2	0.0	11	0.2	14	0.2	16	0.3
Desulfovibrionaceae	2	0.0	1	0.0	0	0.0	0	0.0	5	0.1
Desulfuromonadaceae	16	0.3	4	0.1	2	0.0	9	0.2	7	0.1
Dietziaceae	2	0.0	0	0.0	1	0.0	0	0.0	0	0.0
Enterobacteriaceae	9	0.1	3	0.1	2	0.0	0	0.0	6	0.1
Enterococcaceae	0	0.0	0	0.0	0	0.0	0	0.0	2	0.0
Equidae	0	0.0	0	0.0	0	0.0	0	0.0	0	0.0
Erysipelotrichaceae	27	0.4	3	0.1	2	0.0	14	0.2	5	0.1
Erythrobacteraceae	0	0.0	0	0.0	0	0.0	0	0.0	0	0.0
Eubacteriaceae	32	0.5	18	0.3	12	0.2	37	0.6	44	0.7
Exobasidiaceae	0	0.0	0	0.0	0	0.0	0	0.0	1	0.0
Flavobacteriaceae	4	0.1	0	0.0	1	0.0	32	0.5	5	0.1
Geobacteraceae	**167**	**2.7**	**57**	**0.9**	**49**	**0.8**	**96**	**1.6**	**979**	**16.1**
Geodermatophilaceae	0	0.0	0	0.0	0	0.0	0	0.0	0	0.0
Gracilibacteraceae	14	0.2	7	0.1	9	0.2	0	0.0	11	0.2
Halomonadaceae	0	0.0	0	0.0	0	0.0	5	0.1	0	0.0
Hydrogenophilaceae	0	0.0	0	0.0	1	0.0	5	0.1	1	0.0
Hyphomicrobiaceae	2	0.0	1	0.0	1	0.0	5	0.1	1	0.0
Lachnospiraceae	2	0.0	1	0.0	0	0.0	5	0.1	3	0.1
Legionellaceae	3	0.1	0	0.0	2	0.0	9	0.2	1	0.0
Leptospiraceae	0	0.0	0	0.0	0	0.0	0	0.0	0	0.0
Marinilabiaceae	0	0.0	0	0.0	0	0.0	0	0.0	0	0.0
Methanobacteriaceae	**1550**	**25.5**	**620**	**10.2**	**467**	**7.7**	**987**	**16.2**	**1077**	**17.7**
Methanocorpusculaceae	5	0.1	5	0.1	0	0.0	0	0.0	0	0.0
Methanomicrobiaceae	25	0.4	7	0.1	10	0.2	0	0.0	21	0.3
Methanosaetaceae	3	0.1	0	0.0	8	0.1	41	0.7	39	0.6
Methanosarcinaceae	**989**	**16.2**	**4547**	**74.7**	**4617**	**75.8**	**927**	**15.2**	**2162**	**35.5**
Methylobacteriaceae	29	0.5	9	0.2	1	0.0	50	0.8	15	0.2
Methylocystaceae	3	0.1	1	0.0	0	0.0	14	0.2	1	0.0

Family	Site 2 Acetate 1		Site 2 Acetate 2		Site 2 Acetate 2		Site 2 No Substrate		Site 2 Core	
	No. Reads[A]	Percent[B]	No. Reads[A]	Percent[B]	No. Reads[A]	Percent[B]	No. Reads[A]	Percent[B]	No. Reads[A]	Percent[B]
Microbacteriaceae	9	0.1	8	0.1	5	0.1	5	0.1	8	0.1
Micrococcaceae	2	0.0	1	0.0	0	0.0	0	0.0	0	0.0
Moraxellaceae	2	0.0	0	0.0	2	0.0	5	0.1	6	0.1
Mycobacteriaceae	2	0.0	0	0.0	0	0.0	9	0.2	1	0.0
Nitrosomonadaceae	0	0.0	0	0.0	1	0.0	0	0.0	0	0.0
Nocardiaceae	0	0.0	0	0.0	0	0.0	9	0.2	0	0.0
Nocardioidaceae	0	0.0	0	0.0	0	0.0	0	0.0	0	0.0
Oxalobacteraceae	0	0.0	0	0.0	0	0.0	0	0.0	1	0.0
Paenibacillaceae	0	0.0	0	0.0	0	0.0	0	0.0	0	0.0
Peptococcaceae	52	0.8	12	0.2	16	0.3	96	1.6	47	0.8
Phyllobacteriaceae	7	0.1	2	0.0	2	0.0	0	0.0	4	0.1
Planctomycetaceae	4	0.1	0	0.0	2	0.0	14	0.2	2	0.0
Planococcaceae	2	0.0	0	0.0	0	0.0	0	0.0	0	0.0
Polyangiaceae	1	0.0	0	0.0	2	0.0	0	0.0	1	0.0
Porphyromonadaceae	25	0.4	5	0.1	5	0.1	14	0.2	4	0.1
Propionibacteriaceae	0	0.0	0	0.0	0	0.0	0	0.0	1	0.0
Pseudomonadaceae	**1618**	**26.6**	**236**	**3.9**	**271**	**4.4**	**344**	**5.7**	**227**	**3.7**
Rhizobiaceae	0	0.0	0	0.0	0	0.0	0	0.0	0	0.0
Rhodobacteraceae	0	0.0	0	0.0	0	0.0	0	0.0	0	0.0
Rhodocyclaceae	2	0.0	0	0.0	0	0.0	9	0.2	1	0.0
Rikenellaceae	62	1.0	5	0.1	22	0.4	5	0.1	1	0.0
Ruminococcaceae	10	0.2	3	0.1	2	0.0	18	0.3	3	0.1
Saccharomycetaceae	0	0.0	0	0.0	0	0.0	0	0.0	0	0.0
Shewanellaceae	0	0.0	0	0.0	0	0.0	0	0.0	0	0.0
Sinobacteraceae	3	0.1	2	0.0	6	0.1	32	0.5	3	0.1
Sphingobacteriaceae	0	0.0	0	0.0	0	0.0	0	0.0	0	0.0
Sphingomonadaceae	**122**	**2.0**	**63**	**1.0**	**74**	**1.2**	**463**	**7.6**	**101**	**1.7**
Spirochaetaceae	46	0.8	25	0.4	25	0.4	46	0.8	31	0.5
Staphylococcaceae	3	0.1	1	0.0	0	0.0	9	0.2	0	0.0
Streptococcaceae	1	0.0	0	0.0	0	0.0	0	0.0	0	0.0
Synergistaceae	53	0.9	5	0.1	9	0.2	14	0.2	8	0.1

Family	Site 2 Acetate 1		Site 2 Acetate 2		Site 2 Acetate 2		Site 2 No Substrate		Site 2 Core	
	No. Reads[A]	Percent[B]	No. Reads[A]	Percent[B]	No. Reads[A]	Percent[B]	No. Reads[A]	Percent[B]	No. Reads[A]	Percent[B]
Syntrophaceae	2	0.0	1	0.0	2	0.0	5	0.1	8	0.1
Syntrophobacteraceae	0	0.0	0	0.0	0	0.0	0	0.0	0	0.0
Syntrophomonadaceae	7	0.1	14	0.2	15	0.3	41	0.7	21	0.3
Syntrophorhabdaceae	0	0.0	0	0.0	0	0.0	0	0.0	0	0.0
Veillonellaceae	0	0.0	0	0.0	0	0.0	0	0.0	0	0.0
Vibrionaceae	0	0.0	0	0.0	0	0.0	0	0.0	0	0.0
Victivallaceae	2	0.0	0	0.0	0	0.0	0	0.0	0	0.0
Xanthomonadaceae	0	0.0	0	0.0	0	0.0	0	0.0	0	0.0
Unidentified	683	11.2	243	4.0	258	4.2	1183	19.4	473	7.8
Total	**6089**	**100.0**	**6089**	**100.0**	**6089**	**100.0**	**6089**	**100.0**	**6089**	**100.0**

[A] The total number of reads were normalized to the average number of reads from each sample (6089 reads).
[B] Percent of total reads per family as determined with the normalized data.

Table 4.5. Overview of the community analysis as determined by 454 pyrosequencing of the 16S rRNA gene for the inoculated core samples. Family of organisms present at or above 3% in at least one of the samples are bolded.

Family	No Substrate Core		H_2/CO_2 Core		VFA Core	
	No. Reads[A]	Percent[B]	No. Reads[A]	Percent[B]	No. Reads[A]	Percent[B]
Acetobacteraceae	0	0.0	0	0.0	0	0.0
Acholeplasmataceae	34	0.6	64	1.0	10	0.2
Acidimicrobiaceae	0	0.0	0	0.0	0	0.0
Acidobacteriaceae	0	0.0	0	0.0	1	0.0
Aerococcaceae	0	0.0	0	0.0	0	0.0
Aeromonadaceae	0	0.0	0	0.0	0	0.0
Alcaligenaceae	0	0.0	0	0.0	0	0.0
Anaerolineaceae	17	0.3	18	0.3	8	0.1
Aurantimonadaceae	0	0.0	0	0.0	0	0.0
Bacillaceae	3	0.0	33	0.5	41	0.7
Bacteroidaceae	0	0.0	0	0.0	0	0.0
Bradyrhizobiaceae	0	0.0	5	0.1	1	0.0
Brucellaceae	0	0.0	0	0.0	0	0.0
Burkholderiaceae	5	0.1	0	0.0	6	0.1
Caldilineaceae	0	0.0	0	0.0	0	0.0
Caldisericaceae	0	0.0	0	0.0	0	0.0
Campylobacteraceae	4	0.1	2	0.0	0	0.0
Carnobacteriaceae	118	1.9	0	0.0	0	0.0
Caulobacteraceae	0	0.0	3	0.1	0	0.0
Cellulomonadaceae	3	0.0	4	0.1	0	0.0
Chrysosaccaceae	0	0.0	0	0.0	0	0.0
Clostridiaceae	**215**	**3.5**	**9**	**0.2**	**40**	**0.7**
Comamonadaceae	0	0.0	1	0.0	0	0.0
Coriobacteriaceae	38	0.6	10	0.2	30	0.5
Corynebacteriaceae	0	0.0	0	0.0	0	0.0
Cytophagaceae	0	0.0	0	0.0	0	0.0
Deferribacteraceae	0	0.0	0	0.0	0	0.0
Desulfobacteraceae	4	0.1	7	0.1	0	0.0
Desulfobulbaceae	109	1.8	81	1.3	34	0.6
Desulfomicrobiaceae	**46**	**0.8**	**234**	**3.8**	**124**	**2.0**
Desulfovibrionaceae	28	0.5	41	0.7	0	0.0
Desulfuromonadaceae	105	1.7	1	0.0	10	0.2
Dietziaceae	0	0.0	0	0.0	0	0.0
Enterobacteriaceae	0	0.0	0	0.0	0	0.0
Enterococcaceae	0	0.0	0	0.0	0	0.0
Equidae	0	0.0	0	0.0	0	0.0
Erysipelotrichaceae	51	0.8	66	1.1	18	0.3

Family	No Substrate Core		H_2/CO_2 Core		VFA Core	
	No. Reads[A]	Percent[B]	No. Reads[A]	Percent[B]	No. Reads[A]	Percent[B]
Erythrobacteraceae	0	0.0	0	0.0	0	0.0
Eubacteriaceae	13	0.2	69	1.1	2	0.0
Exobasidiaceae	0	0.0	0	0.0	0	0.0
Flavobacteriaceae	0	0.0	0	0.0	0	0.0
Geobacteraceae	**1482**	**24.3**	**285**	**4.7**	**168**	**2.8**
Geodermatophilaceae	0	0.0	0	0.0	0	0.0
Gracilibacteraceae	28	0.5	42	0.7	17	0.3
Halomonadaceae	0	0.0	0	0.0	0	0.0
Hydrogenophilaceae	0	0.0	0	0.0	0	0.0
Hyphomicrobiaceae	0	0.0	0	0.0	0	0.0
Lachnospiraceae	3	0.0	2	0.0	1	0.0
Legionellaceae	0	0.0	0	0.0	0	0.0
Leptospiraceae	1	0.0	0	0.0	1	0.0
Marinilabiaceae	0	0.0	0	0.0	0	0.0
Methanobacteriaceae	**207**	**3.4**	**89**	**1.5**	**129**	**2.1**
Methanocorpusculaceae	**0**	**0.0**	**0**	**0.0**	**234**	**3.8**
Methanomicrobiaceae	**24**	**0.4**	**1**	**0.0**	**337**	**5.5**
Methanosaetaceae	0	0.0	2	0.0	0	0.0
Methanosarcinaceae	**1701**	**27.9**	**3086**	**50.7**	**2227**	**36.6**
Methylobacteriaceae	0	0.0	0	0.0	0	0.0
Methylocystaceae	0	0.0	0	0.0	0	0.0
Microbacteriaceae	0	0.0	0	0.0	1	0.0
Micrococcaceae	0	0.0	0	0.0	0	0.0
Moraxellaceae	0	0.0	0	0.0	0	0.0
Mycobacteriaceae	0	0.0	0	0.0	0	0.0
Nitrosomonadaceae	0	0.0	0	0.0	0	0.0
Nocardiaceae	0	0.0	0	0.0	0	0.0
Nocardioidaceae	0	0.0	0	0.0	0	0.0
Oxalobacteraceae	45	0.7	123	2.0	0	0.0
Paenibacillaceae	3	0.0	0	0.0	0	0.0
Peptococcaceae	67	1.1	98	1.6	174	2.9
Phyllobacteriaceae	0	0.0	1	0.0	0	0.0
Planctomycetaceae	0	0.0	0	0.0	0	0.0
Planococcaceae	0	0.0	0	0.0	0	0.0
Polyangiaceae	0	0.0	0	0.0	0	0.0
Porphyromonadaceae	13	0.2	105	1.7	10	0.2
Propionibacteriaceae	0	0.0	0	0.0	1	0.0
Pseudomonadaceae	**1053**	**17.3**	**497**	**8.2**	**25**	**0.4**
Rhizobiaceae	0	0.0	0	0.0	0	0.0
Rhodobacteraceae	0	0.0	0	0.0	0	0.0
Rhodocyclaceae	0	0.0	0	0.0	0	0.0

Family	No Substrate Core		H_2/CO_2 Core		VFA Core	
	No. Reads[A]	Percent[B]	No. Reads[A]	Percent[B]	No. Reads[A]	Percent[B]
Rikenellaceae	4	0.1	28	0.5	9	0.1
Ruminococcaceae	1	0.0	8	0.1	2	0.0
Saccharomycetaceae	0	0.0	0	0.0	0	0.0
Shewanellaceae	0	0.0	0	0.0	0	0.0
Sinobacteraceae	0	0.0	0	0.0	1	0.0
Sphingobacteriaceae	0	0.0	0	0.0	0	0.0
Sphingomonadaceae	0	0.0	5	0.1	2	0.0
Spirochaetaceae	63	1.0	103	1.7	30	0.5
Staphylococcaceae	12	0.2	0	0.0	0	0.0
Streptococcaceae	0	0.0	0	0.0	1	0.0
Synergistaceae	59	1.0	80	1.3	29	0.5
Syntrophaceae	0	0.0	0	0.0	0	0.0
Syntrophobacteraceae	0	0.0	0	0.0	0	0.0
Syntrophomonadaceae	28	0.5	54	0.9	131	2.1
Syntrophorhabdaceae	0	0.0	0	0.0	0	0.0
Veillonellaceae	0	0.0	0	0.0	0	0.0
Vibrionaceae	0	0.0	0	0.0	0	0.0
Victivallaceae	0	0.0	4	0.1	0	0.0
Xanthomonadaceae	0	0.0	0	0.0	0	0.0
Unidentified	505	8.3	827	13.6	2235	36.7
Total	**6089**	**100.0**	**6089**	**100.0**	**6089**	**100.0**

[A] The total number of reads were normalized to the average number of reads from each sample (6089 reads).
[B] Percent of total reads per family as determined with the normalized data.

Chapter Five: Biogenic Shale Gas Reservoirs: Kilometer Scale Biogeochemical Reactors

Cokar, M., Kallos, M.S., and Gates, I.D. "Biogenic Shale Gas Reservoirs: Kilometer Scale Biogeochemical Reactors," submitted to the *American Institute of Chemical Engineering* ID: AIChe-12-14652, 2012.

5.1 Abstract

Methane gas can be found in many different biological and non-biological settings. Methane gas can be produced either thermogenically or biogenically. Thermogenic methane gas is found deep within the subsurface and is a result of high temperature and pressure fractionation of kerogen and organic compounds. Biogenic methane gas on the other hand is produced by anaerobic microorganisms and can be found in any organic-rich anaerobic environment, which includes shallow shale reservoirs, landfills, rice fields and swamps. Biogenic methane gas accounts for about 20% of the world's methane (Rice and Claypool, 1981; Rice, 1993), yet little is known about the kinetics of its production and transport. In the current study, a fixed bed reactor model based on a biological shale gas reservoir was modeled to shed light on these processes. The model used experimental methane generation kinetics and was calibrated against field data to obtain a range of values for amounts of new biogenic methane that could be produced from a shallow shale gas well. The amount of methane was dependent on the amount of amenable total organic carbon (TOC_A) that was present within the reservoir. The maximum amount of TOC_A was determined from the theory to be about 8.9 volume%. The TOC_A was then varied, from a value slightly below the maximum, between 8.5

volume percent down to 1 volume percent to obtain a range of biogenic gas produced during the steady state production period of a well. The results show that between 11% (TOC_A = 1 volume percent) and 96% (TOC_A = 8.5 volume percent) of gas produced at steady state can be attributed to new biogenic gas produced within the reservoir during the stable gas production rate period observed beyond the initial transient declining rate period of the well. Also, the amount of gas produced after substrate addition to the reservoir was also determined using experimental methane production data. The results reveal that with addition of volatile fatty acids (VFA) the amount of gas produced can double. This has a significant implication – if biogenic gas generation can be enhanced within the reservoir by adding nutrients or rate-limiting minerals to the reservoir, then the total gas rate that could be realized from shallow biogenic shale gas reservoirs could be enhanced.

5.2 Introduction

Biogeochemical reservoirs are found in underground systems where biochemical reactions convert a substrate to a set of products over geological length scales (usually of order of kilometers to tens of kilometers) and time scales (typically over millions to tens of millions of years). These systems – for example shallow biogenic shale gas reservoirs, shallow heavy oil reservoirs, coal beds, and sediments at the bottom of water bodies and oceans – abound on the planet. However, little is understood about length and time scales for mass transport, fluid flow and bioconversion especially when we attempt to extract the products of the reactions for our own uses over time scales much smaller than that of the system itself. The focus here is on shallow biogenic shale gas reservoirs where the product is natural gas. Biogenic shale gas reservoirs are typically shallow with

temperatures lower than 80°C and consist of finely distributed organic matter (kerogen), which is buried remains of what was once algae and other plant-based organic materials. Anaerobic microbes, typically buried with the organic matter, evolve and survive in these anoxic environments and convert a fraction of the organic matter through complex reaction pathways eventually to carbon dioxide and methane (Gieg et al., 2008):

$$\text{Amenable Organic Matter in Shale} + H_2O \rightarrow CH_4 + CO_2 \quad (5.1)$$

The methane generated from this microbial action over millions of years is the natural gas which we produce to the surface. A similar process occurs in many petroleum systems including coal beds (which yield on production, coal-bed methane) and heavy oil reservoirs.

Currently, very little is known about methane generation kinetics in shallow shale gas reservoirs. Research has been done in the past which examined methane generation kinetics of oil biodegradation (Larter et al., 2006; Gieg et al., 2008). Simulation and modelling of gas transport within the tiny pore structures of kerogen and shale gas has also been studied by many researchers in North America (Akkutlu and Fathi, 2011; Kalantari-Dahaghi, 2010; Ambrose et al., 2010; Javadpour et al., 2007). Currently, research is focused on understanding the reservoir storage capacity in terms of gas molecules on organic and inorganic surfaces within shale gas materials to determine the fraction of gas considered free gas, adsorbed gas on surfaces as well as absorbed gas. Shale systems with a high percentage of organic carbon are very complex because the gas

can be found within a) isolated pores, b) connected pores and c) within the oil or water phase. In a study by Ambrose et al. (2010), it appears that a significant portion of the total gas in place is found within large inter-connected nano-pores which are found within the organic matter (kerogen). They proposed a modified gas material balance equation that took into consideration the free gas volume taken up by the sorbed gas.

Modelling of gas within these systems becomes more complicated because of the nano-pore sizes. Darcy flow is not always the most accurate way to model flow through nano-pores. Knudsen diffusion is an important transport process in shales and siltstones, because the mean free path of the molecule is the same order of magnitude as the size of the pore. Roy et al. (2003) proposed a model of gas flow in nano-pores by using a diffusive transport regime with a constant diffusion coefficient and negligible viscous effects.

A new gas material balance which estimated current biogenic gas generation rates was developed by Cokar et al. (2012). In this study both gas adsorption onto organic and inorganic surfaces was taken into consideration using Langmuir isotherms as well as a new biogenic gas amount. For the shallow biogenic shale gas reservoirs studied by Cokar et al. (2012), it was assumed that approximately 19 to 37% of the total gas produced during the resource lifetime of the well could be attributed to recently (during production period) or currently generated biogenic gas.

At present, it remains unknown how to deal with these large systems where transport in the natural system has very large time scale (hundreds of thousands to millions of years) whereas for gas production operations (years to tens of years), the time scale is hundreds of thousands to millions of times smaller. Here, we describe a novel simple model to describe the shale gas biogeochemical reaction system with the focus on evaluating bioreaction rate constants and the fraction of produced gas that is being currently generated biogenically.

5.3 Methodology

5.3.1 Methane Production Data - Experimental

Reaction rate data was obtained through experimentally measured methane production from cores as described previously in Chapter 4. Briefly, core and produced water samples were obtained from productive biogenic shallow gas zones in the Alderson Member that the oil and gas industry commonly refers to as the Abbey Field within the Milk River Formation. The productive zones of the Abbey Field are thought to be the leading edges of a prodelta plume of fine-grained sediment deposited in a deeper water marine environment. Core samples from five productive intervals labeled B, C, D, E, and F were added to each serum bottle. Produced water samples (1.0 mL) that were enriched with H_2/CO_2 were used to inoculate all of the five intervals, and the methane production was monitored on a monthly basis for 146 days (details of experimental methods and raw data from experiments see Chapter 4). The field production data from the same well is shown in Figure 5.1.

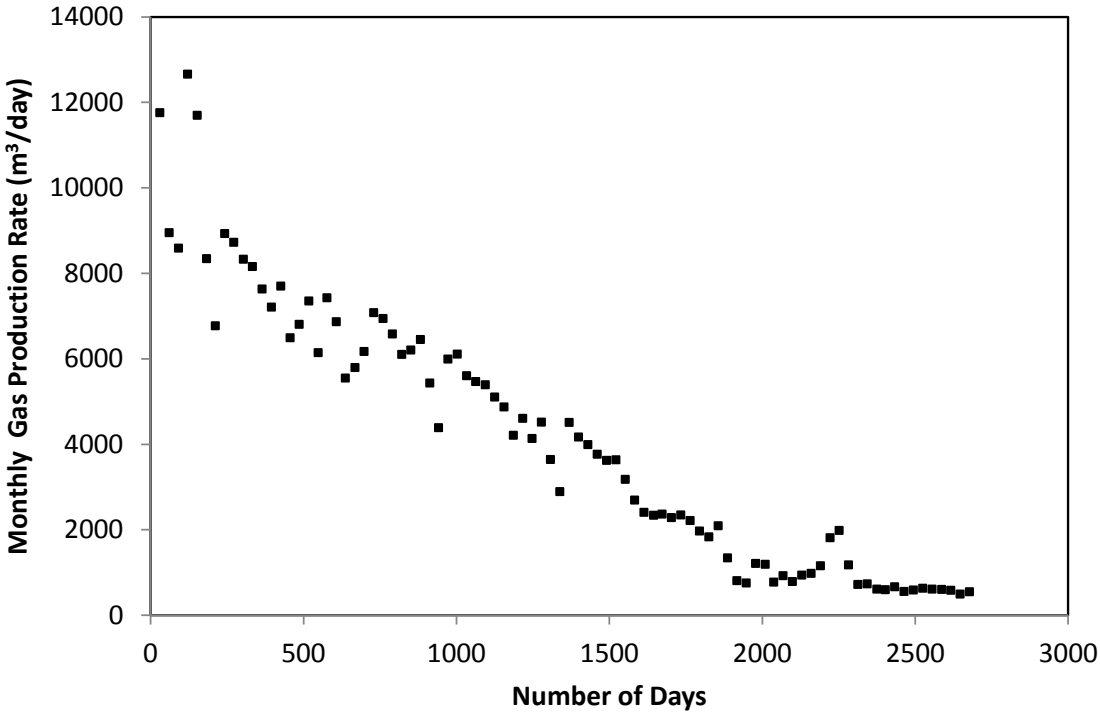

Figure 5.1. Monthly gas production rate (m^3/day) of well 16-3-22-18W3 perforated in the Abbey Field shale gas reservoir that was modeled and history matched in this study. This is a typical gas profile of a shallow shale gas well within this region. There is a tail region at the end that represents a constant gas production rate after about 2,250 days.

There were three sets of experiments set up for the core inoculations at each depth B, C, D, E and F. The first set of experiments is referred to as No Substrate, because it only contains the core, the second set of experiments is called H_2/CO_2, because H_2/CO_2 at a ratio of 80:20 was added to the mixture, and the last set of experiments is referred to as VFA because it contains 0.1 mL of a 1M VFA solution that consisted of equimolar concentrations of acetate, butyrate and propionic acid as described in Chapter 4. The methane produced for all of the serum bottles was monitored on approximately a monthly basis for 146 days, however, the data contained in his chapter is for the initial 64 days, since after this the amount of methane produced becomes dependent on nutrient supplies

within the serum bottles, whereas in the reservoir, it is assumed that there is an unlimited amount of nutrients supply for the microorganisms.

5.3.2 Initia Zero Order Rate Constant

For a zero order reaction, the rate of production of methane would be given by:

$$\frac{dC}{dt} = k_o \tag{5.2}$$

where C is the methane concentration (methane (kg)/(core (m^3) x volume fraction of TOC)), $\frac{dC}{dt}$ is the change in concentration of methane per unit time (methane (kg)/(core (m^3) x volume fraction of TOC x s)), and k_o is the zero order reaction rate constant (methane (kg)/(core (m^3) x volume fraction of TOC x s)). Equation 5.2 can be integrated given an initial condition. Given initial concentration C_o and concentration C at time t, the result is:

$$C - C_o = k_o t \tag{5.3}$$

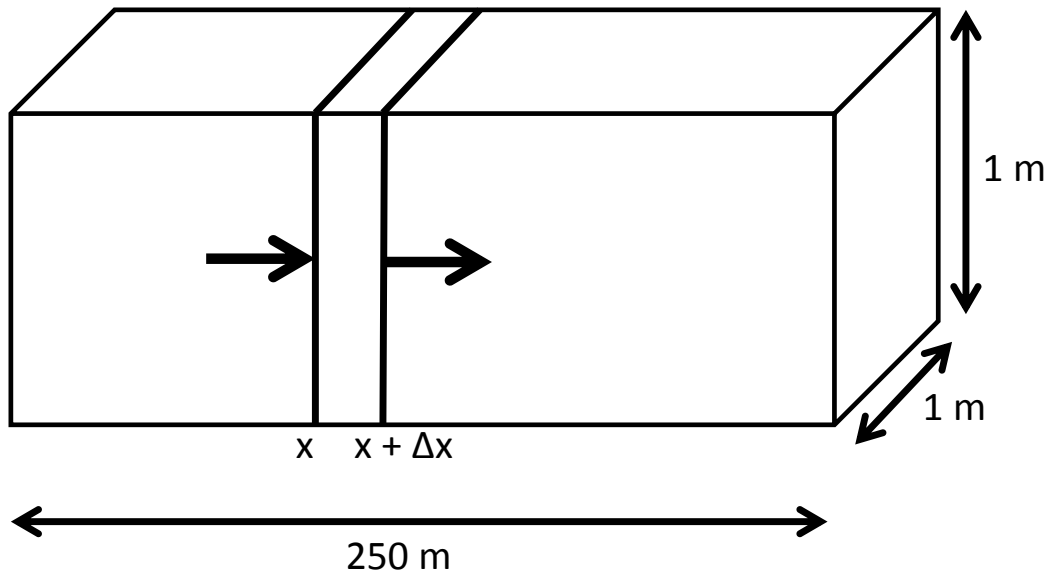

Figure 5.2. Model geometry with differential element: the model area is 1m^2 with a length equal to 250m.

5.3.3 Biogeochemical Model Geometry

The bioreactor reservoir model consisted of a rectangle that was 250 m long with cross-sectional area equal to 1 m^2 as displayed in Figure 5.2. The production well was placed at x = 0 whereas the far field boundary condition is taken to be at x = 250 m. Within the model domain were both kerogen and organic matter and sandstone particles with diameter 0.01 mm with porosity and effective permeability as listed in Table 5.1.

Table 5.1. Reservoir and gas properties.

Property	Value	Source
Temperature (K)	288.15	(Cokar et al., 2012)
Viscosity (Pa·s)	1.16×10^{-5}	(CRC Handbook)
Porosity	0.20	(Cokar et al., 2012)
Pressure (P_{atm}) (kPa)	101.325	(Field Data)
Pressure (P_e) (kPa)	3200	(Field Data)
Density of Kerogen (kg/m^3)	1180	(Okiongbo, 2005)
Density of Rock (kg/m^3)	2300	(CBM Solutions, 2011)
Permeability with TOC_A = 1% (mD)	5.02×10^{-2}	(Calibrated to Field Data)
Permeability with TOC_A = 2% (mD)	4.38×10^{-2}	(Calibrated to Field Data)
Permeability with TOC_A = 4% (mD)	3.11×10^{-2}	(Calibrated to Field Data)
Permeability with TOC_A = 8.5% (mD)	2.47×10^{-3}	(Calibrated to Field Data)
Zone B (251.75 - 277.17m) TOC (wt% / vol%)	1.01 / 1.95	(CBM Solutions, 2011)
Zone C (288.60 - 298.80m) TOC (wt% / vol%)	1.01 / 1.95	(CBM Solutions, 2011)
Zone D (306.05 - 313.48m) TOC (wt% / vol%)	0.90 / 1.73	(CBM Solutions, 2011)
Zone E (328.11 - 342.5m) TOC (wt% / vol%)	0.92 / 1.78	(CBM Solutions, 2011)
Zone F (345.51 - 347m) TOC (wt% / vol%)	1.06 / 2.05	(CBM Solutions, 2011)

5.3.4 Governing Equations

For flow in porous media, Darcy's law is given by:

$$q = -\frac{kA}{\mu}\frac{dP}{dx} \tag{5.4}$$

where q is the flow rate, k is the reservoir permeability, P is the pressure, μ is the methane viscosity, x is the distance, and A is the cross sectional area. The Darcy velocity is given by q/A.

5.3.5 Zero Order Reaction Methane Material Balance

For steady-state flow, the mass balance reduces to *in* + *generation* = *out*. Given a differential element as shown in Figure 5.2, the rate of mass flowing into the element is equal to:

$$(\rho u A)_x = (-\rho \frac{k}{\mu} \frac{dP}{dx} A)_x \tag{5.5}$$

whereas the rate of mass flow out of the element is given by:

$$(\rho u A)_{x+\Delta x} = (-\rho \frac{k}{\mu} \frac{dP}{dx} A)_{x+\Delta x} \tag{5.6}$$

The bioreaction generation term is given by:

$$k_o A \Delta x (TOC)(TOC_A) \tag{5.7}$$

where *TOC* is the total organic carbon content (expressed as a volume fraction) within the reservoir and TOC_A is the volume fraction of the TOC that is amenable TOC (i.e. the fraction of the organic matter that is consumed by microbes). The governing equation is then given by:

$$\frac{Mk}{RT\mu}\left[\left(\frac{dP}{dx}\right)^2 + P\frac{d^2P}{dx^2}\right] + k_0(TOC)(TOC_A) = 0 \tag{5.8}$$

By applying the same boundary conditions as described above, the pressure is then given by:

$$P = \sqrt{-k_o(TOC)(TOC_A)\frac{\mu RT}{kM}x^2 + \left(\frac{P_e^2 - P_{atm}^2}{L} + k_o(TOC)(TOC_A)\frac{\mu RT}{kM}L\right)x + P_{atm}^2} \qquad (5.9)$$

The well rate is given by Darcy's law applied at $x = 0$:

$$q_{x=0} = -\frac{kA}{\mu}\left(\frac{dP}{dx}\right)_{x=o} = -\frac{1}{2}\frac{kA}{\mu}\left(\frac{1}{P_{atm}}\right)\left(\frac{P_e^2 - P_{atm}^2}{L} + k_o(TOC)(TOC_A)\frac{\mu RT}{kM}L\right) \qquad (5.10)$$

The fraction of gas produced from the well that is derived biogenically is then given by:

$$\frac{q_{biogenic}}{q_{x=0}} = \frac{k_o(TOC)(TOC_A)\frac{\mu RT}{kM}L}{\left(\frac{P_e^2 - P_{atm}^2}{L} + k_o(TOC)(TOC_A)\frac{\mu RT}{kM}L\right)} \qquad (5.11)$$

5.3.6 Bioreactor Reservoir Model Assumptions

a. Isothermal Conditions

The reservoir is assumed to be at a constant temperature equal to 288.15K (15ºC). Given that the temperature is set by the geothermal gradient, this assumption is reasonable.

b. One Component Model

In a typical shale gas well in this field, there are three main components in the gas phase - methane, nitrogen, and carbon dioxide. The composition of methane at the wellhead is approximately 95%, therefore in the models developed here, it was assumed that methane was the only gas component in the reservoir, and the other gas components were

neglected. Since the reservoir temperature was constant within the model domain, methane viscosity was assumed to be constant.

c. Steady State Assumption

It was assumed that the reservoir was operating at steady state and the pressure within the reservoir was not changing with time. This implies that the production rate of gas at the well location was equal to the gas flow rate into the far field boundary.

d. Laminar Flow Assumption

A particle Reynold's number was calculated for this porous system since this was a fixed bed reactor model. The particle was taken as the sandstone grain, since the sandstone is the most abundant type of material in this system. To determine if the assumption to use a single effective Darcy flow given typical gas flow rates within the reservoir was valid, the particle Reynold's number was evaluated, given by:

$$Re_p = \frac{\rho u D}{\mu(1-\phi)} \tag{5.12}$$

where Re_p is the particle Reynold's number, ρ is the density, D is the particle diameter, μ is the fluid viscosity and ϕ is the reservoir porosity. Darcy's law only applies to laminar flow. For a radial geometry, since the maximum flow velocity occurs at the well, and given a maximum flowrate of approximately 15,000 m^3/day which is observed in the Abbey Field, the particle Reynold's number was determined to be 0.13 (assuming gas density 0.7 kg/m^3, particle size equal to 0.01 mm, gas viscosity 1.16×10^{-5} Pa·s, flow area is 1 m^2 and porosity 0.2). Since the Reynold's number was less than 1, the flow in the

system was laminar, and it was governed by viscous forces thus Darcy's law applies and a single effective permeability was used.

e. Reservoir Porosity and Effective Permeability

It was assumed that the reservoir had constant porosity and effective permeability. To estimate the effective permeability of the reservoir, constant boundary conditions far from the wellbore (at 250 m was equal to 3,200 kPa) and at the wellbore (wellbore pressure was equal to 101.325 kPa) were maintained and the flow rate was calibrated to the field gas production during the steady state period as shown in Figure 5.1 after about 2,250 days. The values of the porosity and effective permeability used in the models developed here are listed in Table 5.1.

f. Ideal Gas Assumption

In the bioreactor reservoir model, methane in the gas phase was treated as an ideal gas. To verify this was reasonable, the ideal gas compressibility factor of methane gas was calculated by using the Redlich-Kwong equation of state. The critical temperature and pressure of methane are equal to 190.7 K and 45.8 atm, respectively. The compressibility factor of methane was found to be equal to 0.95, 0.982, and 0.998 at 3,200, 1,200, and 101 kPa, respectively. Thus, the assumption of ideal gas behavior was reasonable.

g. Constant Pressure Boundary Condition

Since the reservoir was operating at steady state conditions, it was assumed that the pressure at the edge of the reservoir was constant equal to 3,200 kPa. Given the low permeability of shale gas formations, the length scale of flow and transport over well operation time periods was of the order of several tens of meters.

h. Homogeneity of Total Organic Carbon and Amenable Organic Carbon Content

In real shale gas reservoirs the distribution of organic matter is random. In this model however, it was assumed that the kerogen was homogeneously distributed within the reservoir. As listed in Table 5.1, the total organic carbon content (in weight percent) of the field that was studied ranged between a value of 0.9 and 1.06%. It was known that not all of the hydrocarbon present was consumed by the microorganisms within the shale, however, there was significant uncertainty as to how much was actually consumed by the microbes within the literature (Gieg et al., 2008; Clayton, 1992). Since this amount was unknown, the impact of the amenable TOC on methane production was evaluated in a sensitivity study. The amenable TOC amount was varied between 1 and 8.5 vol% based on the maximum physically possible TOC_A as determined from the theory.

5.4 Results and Discussion

5.4.1 Bioconversion Rates

In the research documented here, a bioreactor reservoir model was developed to simulate the amount of biogenic gas produced in a reservoir at the end of a seven year period of gas production. The gas production profile from the chosen well, which is typical for shallow gas wells, is shown in Figure 5.1. The model treated the entire shale gas reservoir as a single compartment with uniform geological, transport, and bioreaction properties. In this manner, all of the different transport mechanisms including bulk, surface, and Knudsen diffusion and flow in matrix, fractures and faults governed by Darcy's law were combined into an effective Darcy flow governed by a single effective permeability which was calibrated by using field data.

This effective permeability was unknown and had to be determined from tuning the model to field data. Geological properties of the reservoir are listed in Table 5.1. Other key uncertainties were the bioreaction rate constants for conversion of kerogen in the shale to gas (typically a combination of mostly methane with small amounts of carbon dioxide and other components) and the fraction of the TOC_A. Under optimal conditions it is estimated that about 10% of the TOC within the shale can be converted into methane (Clayton, 1992). For oil systems, other studies have estimated that only about 1% of the hydrocarbons present in an oil reservoir can be biologically converted into methane in situ (Gieg et al., 2008). Thus, the value of the TOC_A content is uncertain, and was determined from the theory.

To establish the bioconversion rate law and overall kinetic parameters, a bioreactor model was developed that included an effective porous media model with flow governed by Darcy's law in addition to zero order reaction kinetics with respect to methane generation. In addition, a sensitivity study was also conducted to examine the effect of TOC_A content on methane production rates. All of the models at different TOC_A percentages were calibrated to field shale gas operation data (shown in Figure 5.1) and therefore each model had a different effective permeability as shown in Table 5.1. Thus, the models span the spectrum of transport (effective permeability) to bioreaction rate.

The experimental core production data from Chapter 4 was reported as methane mass produced over time per gram of core. This methane produced in grams per gram of core was first converted on a core volume basis then divided by the fraction of TOC present

within the core and plotted over time for the three different sets of experiments which included No Substrate, H_2/CO_2 and VFA (Figure 5.3 to 5.7) for the first 64 days. Only the initial data points were considered because after about 64 days the rate begins to decrease due to limited nutrient supply in the serum bottles, whereas in the field it is assumed that there is an abundance of nutrients. All of the intervals are capable of generating methane although the gas generation rates for each interval were different. This could be the result of different organic materials within the TOC, inorganic carbon sources, or that the inoculum into each sample was not identical. The serum bottles that were enhanced with H_2/CO_2 and VFA show an increased amount of methane produced. These figures also show best fits of the experimental data with Equation 5.3 for the initial methane gas production curves up to day 64. The slope of the lines yielded the zero order initial reaction rate constants, listed in Table 5.2, for each interval B, C, D, E, and F with different substrates added. As shown in Figure 5.3 to Figure 5.7 the correlation coefficient (r^2) for the difference between the theoretical rate constant and the actual data show a strong correlation between the zero order reaction rate model and the laboratory data, except for the r^2 values for the No Substrate samples for depth B and C were below 0.4.

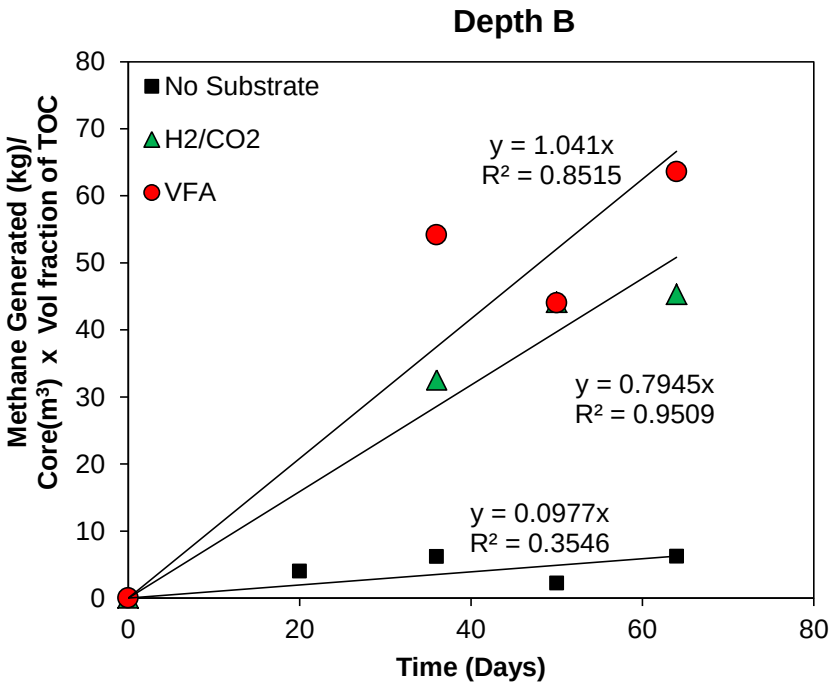

Figure 5.3. Zero order initial reaction rate constants for methane generation curves for depth B.

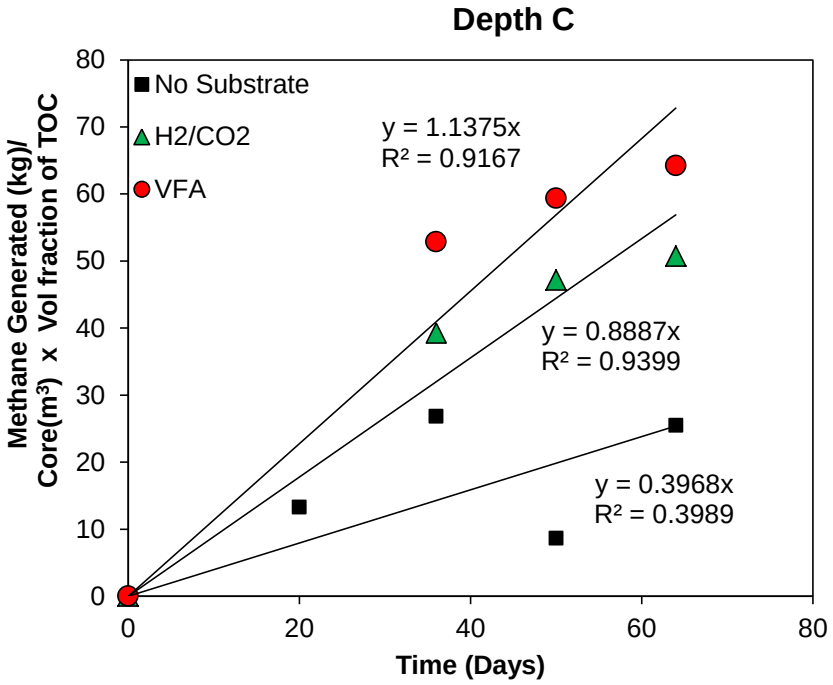

Figure 5.4. Zero order initial reaction rate constants for methane generation curves for depth C.

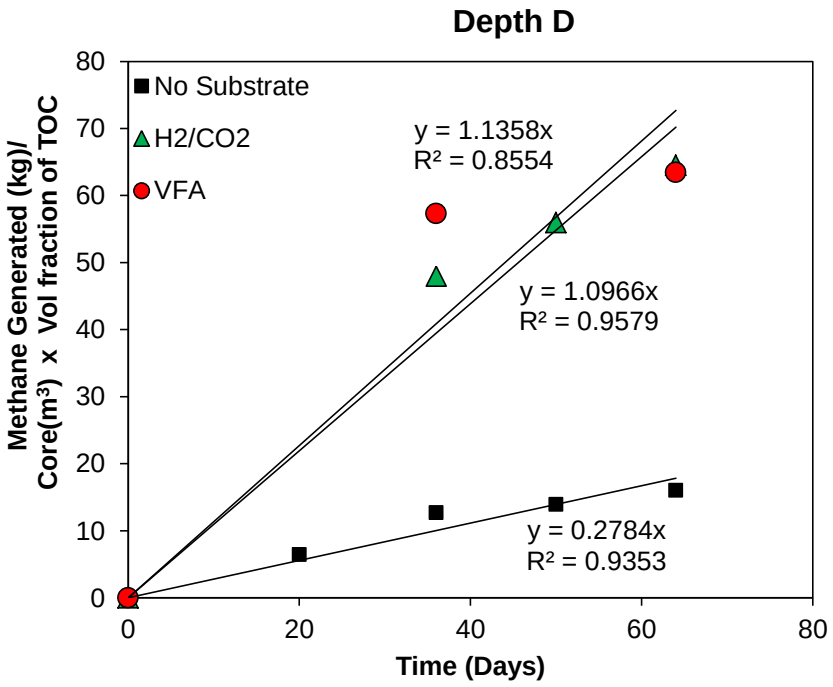

Figure 5.5. Zero order initial reaction rate constants for methane generation curves for depth D.

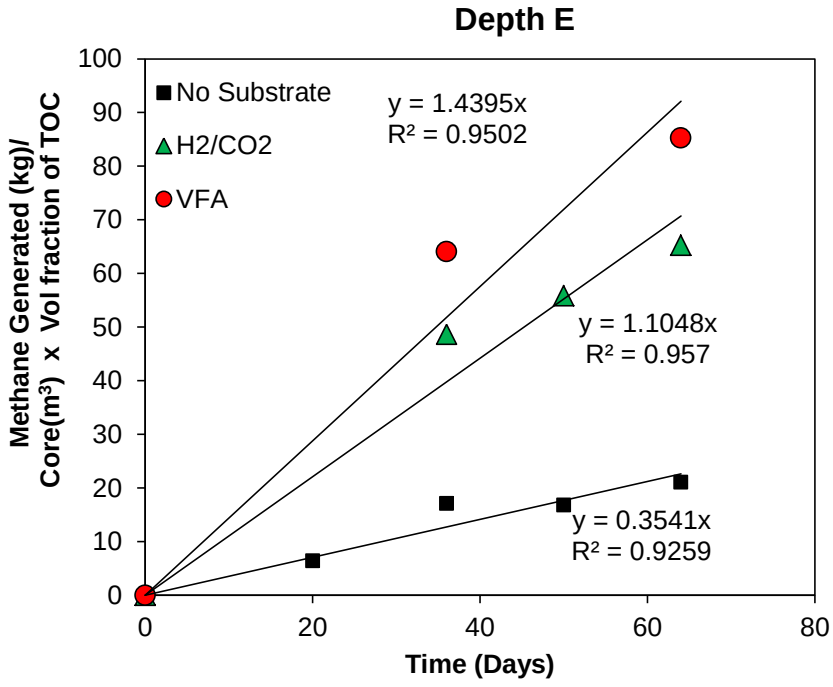

Figure 5.6. Zero order initial reaction rate constants for methane generation curves for depth E.

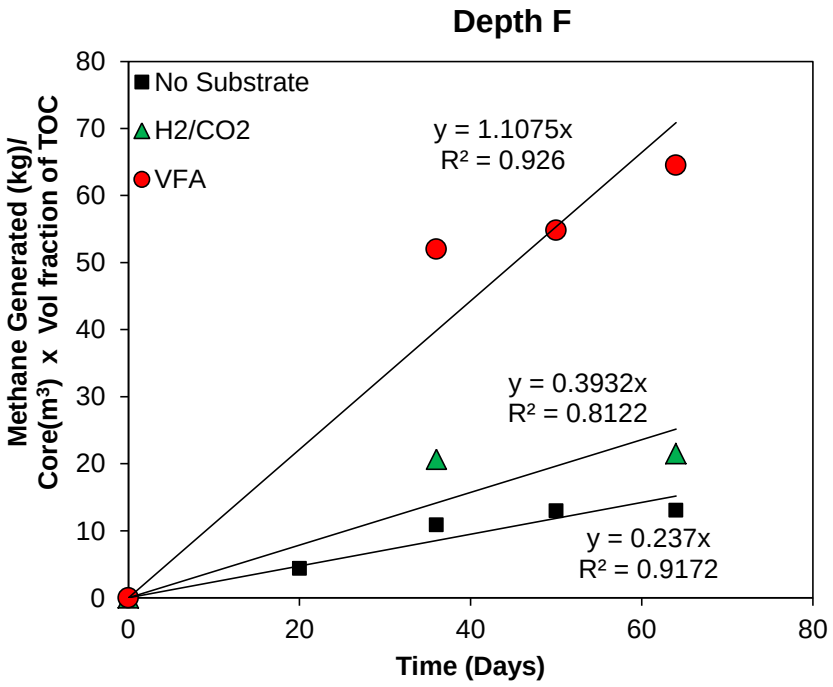

Figure 5.7. Zero order initial reaction rate constants for methane generation curves for depth F.

Table 5.2. Zero order reaction rate constants and average zero reaction rate constants for each interval in the shale gas reservoir.

Substrate	Case	Methane (kg)/(core (m^3) x volume fraction of TOC x day)	Methane (kg)/(core (m^3) x volume fraction of TOC x s)
No Substrate	Depth B	9.77×10^{-2}	1.13×10^{-6}
	Depth C	3.97×10^{-1}	4.59×10^{-6}
	Depth D	2.78×10^{-1}	3.22×10^{-6}
	Depth E	3.54×10^{-1}	4.10×10^{-6}
	Depth F	2.37×10^{-1}	2.74×10^{-6}
	Average	**2.73×10^{-1}**	**3.16×10^{-6}**
H_2/CO_2	Depth B	7.95×10^{-1}	9.20×10^{-6}
	Depth C	8.89×10^{-1}	1.03×10^{-5}
	Depth D	1.10	1.27×10^{-5}
	Depth E	1.10	1.28×10^{-5}
	Depth F	3.92×10^{-1}	4.54×10^{-6}
	Average	**8.55×10^{-1}**	**9.90×10^{-6}**
VFA	Depth B	1.04	1.20×10^{-5}
	Depth C	1.14	1.32×10^{-5}
	Depth D	1.14	1.31×10^{-5}
	Depth E	1.44	1.67×10^{-5}
	Depth F	1.11	1.28×10^{-5}
	Average	**1.17**	**1.36 x 10^{-5}**

The fixed bed zero order reactive model for methane production in shallow shale gas reservoirs described above was used to simulate the steady state gas production period of the well, which occurs beyond about 2,250 days of production as shown in Figure 5.1. The model was calibrated to the field value for gas production near the end of the well life of 1,000 m^3/day and different TOC_A values were simulated to understand the amount of current biogenic gas generated as a fraction of the total gas produced during this steady state period. In order to do this, a TOC_A value was chosen and a permeability was fitted to the model so that the well production rate was equivalent to 1,000 m^3/day. The model also shows that the maximum amount of TOC_A that is physically possible is 8.89 volume

percent, which is similar to what Clayton (1992) estimated. In that study it was estimated a maximum conversion amount of 10%. As shown in Figure 5.8, any value for TOC_A above this value yields physically impossible (negative) reservoir permeability values.

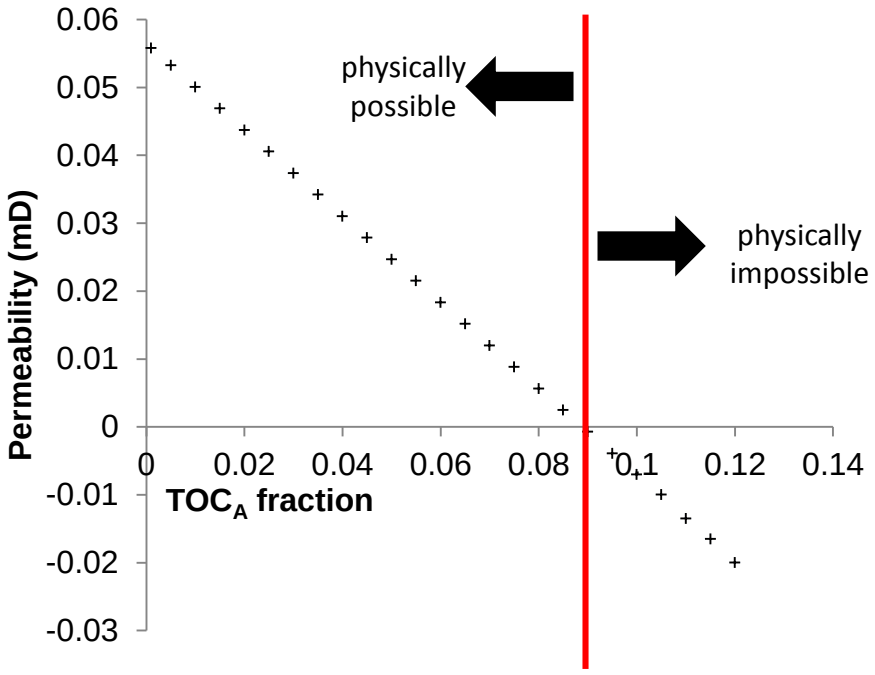

Figure 5.8. Physical range of TOC_A fraction for this field. The results show that a TOC_A fraction of 0.0889 (8.89%) or less is physically possible in this field, any value of TOC_A above this value yields a physically impossible permeability. The TOC_A values were varied between 0% all the way up to 12% and the model permeability was obtained by setting the gas production rate to 1,000 m^3/day and plotted as shown.

Figure 5.9 shows the results for the biologically reactive models with zero order reaction rate constants. As the amount of TOC_A within the model decreased from a value slightly below the maximum of 8.5% to about 1%, the fraction of recent biogenic gas generation that occurred during the production life of the operation also decreased. For a TOC_A amount of 8.5%, 4%, 2% and 1% the amount of recent biogenic gas generation within the

reservoir model was equal to 96%, 45%, 23% and 11%, respectively. These results reveal that a significant fraction of the gas produced within the reactive reservoir model was attributable to recent biogenic gas generated from microbes. This has important implications for production.

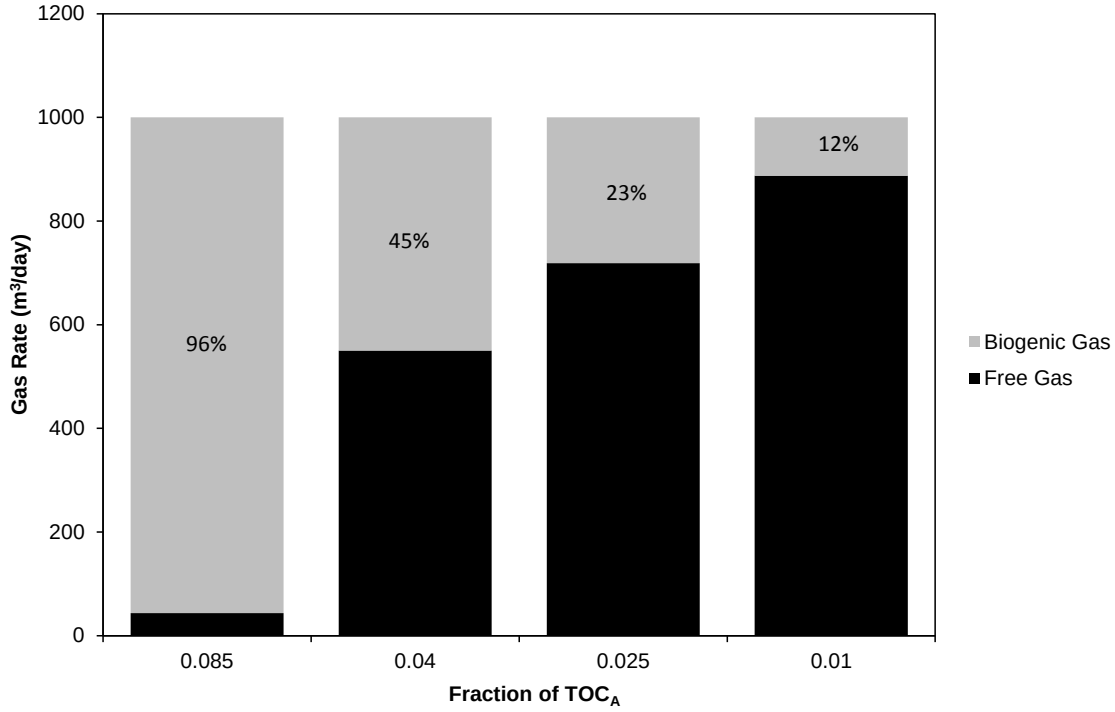

Figure 5.9. Steady state gas flow rate in (m^3/day) for the different models. Biogenic Gas refers to recent gas generated biogenically over the life of the well operation whereas Free Gas refers to gas generated over the past few million years that has been stored in the reservoir (adsorbed on shale solid surfaces, dissolved in shale, water, and free gas).

In the experiments described in Chapter 4, various media ingredients were added to the core and produced water incubations, including volatile fatty acids (VFA) and hydrogen and carbon dioxide (H_2/CO_2), and the methane production was again measured over time. The initial rates for these experiments were used (as shown in Figures 5.3 - 5.7) to generate zero-order rate constants which were then used in the model. In this case the

free gas production was fixed and the biogenic new gas rate was calculated from the model. As shown in Figure 5.10, when H_2/CO_2 and VFA were added as a substrate in addition to the core the reactive model yields much higher rates of biogenic gas production. With a TOC_A value of 2 volume percent, the amount of biogenic gas produced from the No Substrate, H_2/CO_2 and VFA models was 225 m^3/day, 698 m^3/day, and 970 m^3/day, with a free gas rate for all three models equal to 775 m^3/day (Figure 5.10). This shows that with additional substrates, the amount of gas produced within the model can be easily doubled. If biogenic gas generation can be enhanced within the reservoir by adding nutrients or minerals that may be limiting microbe metabolism to the reservoir, for example, in the proppant used to maintain the hydraulic fracture open after the well is stimulated, then the total gas rate that could be realized from shallow biogenic shale gas reservoirs could be enhanced. As shown in the Chapter 4, as well as in this chapter, the addition of VFA and H_2/CO_2 into enriched core samples yielded higher amounts of methane.

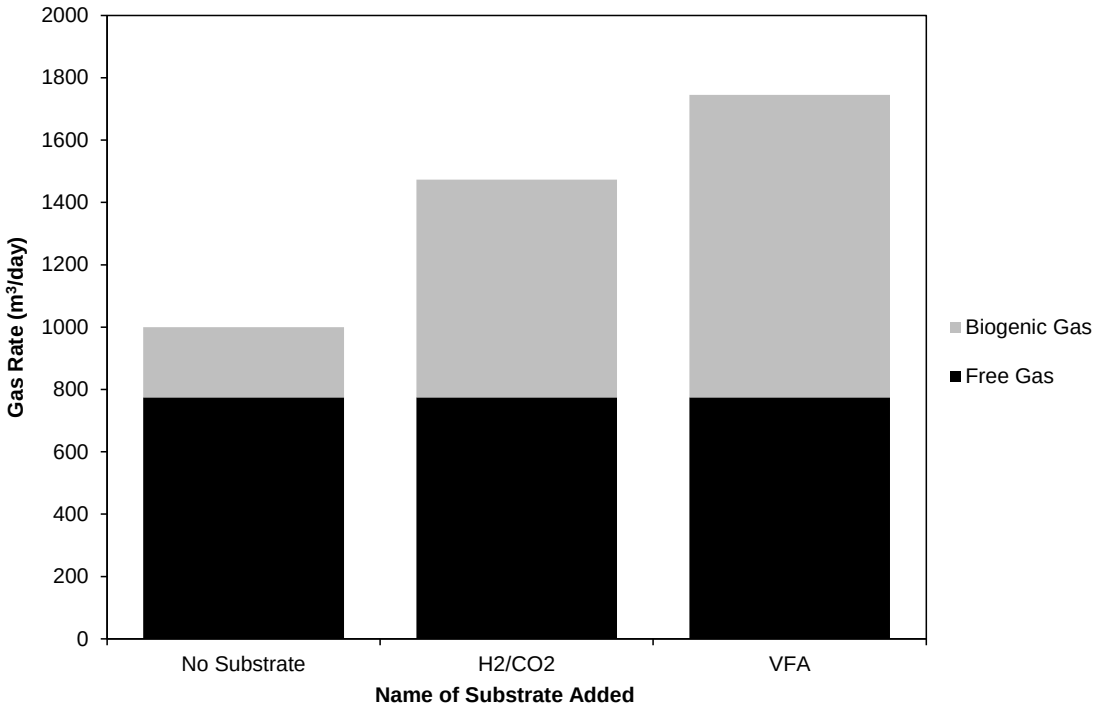

Figure 5.10. Steady state gas flow rate in (m^3/day) for the three different models with No Substrate, H_2/CO_2 and VFA added to them at a TOC_A volume fraction of 0.02.

In a study by Cokar et al. (2012) by using a modified gas material balance method, the fraction of recent biogenic gas generated during the resource lifetime of a well was estimated for two different fields: Nexen's Bigstick field and Husky's Abbey Field. It was found that for the Nexen field approximately 37% of the gas produced was due to recent biogenic gas generation that occurred during the production life of the operation, and in the Abbey field approximately 19% of the gas produced was by recent biogenic gas. Since the core samples for the experimentally generated kinetic data were obtained from the Abbey field, comparison of the recent biogenic gas generation fraction from the reactor model and the Abbey field gas material balance show similar results.

In a study by Gieg et al. (2008), methane generation rates were found from core samples inoculated with oil. The researchers suggested that microorganisms could potentially be added into oil reservoirs which contain residual oil and these microorganisms could convert this immobile oil into methane gas, which would then be produced. They also estimated that approximately 1 to 5 Tcf of CH_4 could be produced each year in the United States by biological transformation. This accounts for approximately 3 to 16%, respectively, of the total methane produced per year within the United States.

If it is biologically possible to stimulate the microbes to produce more methane, then the only factor that could limit production would be the mass transfer of this new methane to the production well. The Damköhler number (dimensionless) represents the ratio of the time scale of the rate of reaction to the time scale of the convective flow within the system, in other words, it compares the time scale of reaction versus that of transport. For continuous flow reactors, the Damköhler number, *Da*, is defined by the ratio of the reaction rate multiplied by the volume over the mass flow rate (Fogler, 1999). We have defined a modified Damköhler number for our system:

$$Da = \frac{k_0 \times V \times (TOC) \times (TOC_A)}{q \times \rho} \tag{5.13}$$

where k_0 is the zero order reaction rate constant (methane (kg)/(core (m^3) x volume fraction of TOC x s)), V is the volume of the reactor model (m^3), TOC is the volume fraction of TOC present within the model, TOC_A is the volume fraction of TOC_A present within the total organic carbon, q is the flowrate of gas through the system (m^3/s) (taken

at the well), and ρ is the density of the gas (kg/m^3). The Damköhler numbers at different volume fractions of TOC_A and reservoir permeabilities are listed in Table 5.3. The Damköhler number for the four TOC_A models were 0.04, 0.02, 0.009 and 0.004 for the 8.5%, 4%, 2% and 1% TOC_A models, respectively. These results reveal that the biogenic shale gas system is essentially controlled by bioconversion rate within the system rather than the transport within the system. In other words, in the stabilized gas rate period, within the connected hydraulically fractured region surrounding the well, transport is not the rate-limiting step for gas production. This is a significant result for increased gas production by enhancing biogenic gas generation since it implies that if the limiting step for bioconversion can be found, providing transport was enhanced to allow it to act with the microbes, then the bioconversion rate could be enhanced. In the stabilized gas production period of the well (after about 2,250 days for the well displayed in Figure 5.1), the system is biogenically controlled. During the initial part of gas production the gas flow rates are much higher because gas is being depleted from connected fractures and silty/sandy beds within the shale gas formation, and at the end of the wells production period the gas production rate has decreased. We have shown here that this long-term steady-state rate has the ability to increase substantially if the biogenic gas generation rate can be increased. The overall recovery of hydrocarbons can be enhanced through more detailed studies on the biology of subsurface shale gas reservoirs coupled with detailed reservoir modelling of bioreaction rates and transport.

Table 5.3. Damköhler numbers, *Da*, for all three models with different TOC_A and permeabilities.

Amenable TOC (Volume Fraction)	*Da*	Permeability (mD)
0.085	3.72×10^{-2}	2.47×10^{-3}
0.04	1.75×10^{-2}	3.11×10^{-2}
0.02	8.75×10^{-3}	4.38×10^{-2}
0.01	4.38×10^{-3}	5.02×10^{-2}

5.5 Conclusions

The bioreaction model developed in this study is the first of its kind to predict the amount of recent biogenic gas that is generated within a shallow biogenic shale gas reservoir during the lifetime of the well operation. The zero order reaction rate constants were determined from experimental methane gas generation data obtained from core and produced water from a field shale gas operation. The bioreactor model used the reaction rate constants and calibrated the effective permeability of the model against field data for a given TOC_A, which was also estimated from this model. The results reveal the fraction of produced gas that is currently generated biogenically. Additionally, the amount of TOC_A was varied to determine the effect of this variable on new biogenic gas production. The main conclusions of this research are as follows:

- This model predicts that the amount of TOC_A within a reservoir in western Canada is less than 8.89 volume percent. This results shows the maximum amount of TOC_A that can be converted to methane gas through microbial activity.
- The amount of currently generated biogenic gas produced was 96%, 45%, 23% and 11% of the total produced gas for TOC_A values of 8.5%, 4%, 2% and 1%, respectively.

- The assumption of a zero order reaction rate model for the production of methane was reasonable because there was general agreement between the zero order reaction rate model and the laboratory model.
- As the amount of TOC_A increased, the fraction of biogenic gas increased.
- Given TOC_A estimates approximately 2% TOC_A for shallow shale gas reservoirs in western Canada, approximately 23% of the total produced gas during the stabilized gas production period was estimated to be generated recently (over the time scale of the operation of the well) by microbes.
- The results suggest that the total gas produced could be enhanced if the rate of bioconversion of the TOC_A could be enhanced. Future studies should focus on the rate-limiting step of bioconversion of shale gas kerogen to methane.

Chapter Six: Reactive Reservoir Simulation of Biogenic Shallow Shale Gas Systems enabled by Experimentally Determined Methane Generation Rates

Cokar M., Ford, B., Kallos, M.S., and Gates, I.D. "Reactive Reservoir Simulation of Biogenic Shallow Shale Gas Systems enabled by Experimentally Determined Methane Generation Rates," revisions submitted to *Energy and Fuels* ID: ef-2012-018223, 2012.

6.1 Abstract

As conventional gas resources in Canada decline, more interest is being given to unconventional shale gas reservoirs. Natural gas also has the potential to overcome other petroleum sources such as coal, heavy oil and conventional oil as the fuel of choice because it is a cleaner source of energy with lower carbon emissions. As the world slowly shifts towards cleaner energy sources it becomes more and more important to study unconventional shale gas reservoirs. Shallow biogenic shale gas reservoirs generate gas by microbial activity implying that current production to surface consists of ancient adsorbed gas as well as recent biogenerated gas. Approximately 20% of all of the methane generated is generally thought to be of microbial origin. Most shallow shale gas reservoirs are less than 80°C and given the supply of carbon, water, and minerals, they are essentially multi-kilometer scale bioreactors. In this study, the reaction rate kinetics for methane production were determined from experimental data by using produced water and core samples from a shallow shale gas reservoir. This data along with Langmuir desorption data was used to model a heterogeneous shale gas reservoir by using reactive reservoir simulation. The results show that biogenic shale gas generation accounts for about 12% of the total gas produced during a period of 2,678 days. This is a

significant percentage of the total gas production and therefore there is great potential to enhance methanogenesis within these reservoirs through substrate addition or other means.

6.2 Introduction

Today, approximately 20% of the gas produced in the United States comes from shale gas reservoirs (EIA, 2011; Wilson and Dulofsky, 2012). The proportion of gas coming from shale gas reservoirs has increased significantly over the past decade with enhancements of hydraulic fracturing procedures, horizontal well drilling, fracture design and stimulation, seismic data, and a better understanding of shale gas geology. Also, a significant amount of organic matter must be present within these systems; this provides a carbon source for deep thermogenic gas production and a feedstock for biogenic gas production (Curtis, 2002). Due to the size of the gas resource, there is increased focus on research to better understand the geological and geochemical nature of these reservoirs. For biogenic shale gas reservoirs, the focus of the research documented here, they can be thought of as immense bioreactors.

For this study, a reaction model was developed by using core and produced water data, along with geological data acquired from log and core analysis obtained from shallow gas zones in the Alderson Member that the oil and gas industry commonly call the Abbey Field within the Milk River Formation, shown in Figure 4.1. The main producing zones within this field are a laminated fine sand interval interbedded with silty/shaley zones. The sandstone acts as a pipeline to produce gas from the other parts of the reservoir. Gas rates within these zones can be initially as high as 20,000 m^3/day (706,000 scf/day) and

fall to less than 1,000 m^3/day (35,300 scf/day) by the end of the well's life. Typical gas production profiles of these wells exhibit a steep decline to a stabilized plateau rate which slowly declines as the well continues to produce fluids as shown in Figure 5.1. Gas production from these reservoirs is sustained by gas flow from very low permeability conduits, desorption of gas from kerogen or clays, diffusive transport through nanometer or micron scale pores, pressure maintenance due to water influx, and biogenic gas generation within the reservoir.

There has been no public data available for the biogenic contribution for modelling shale gas reservoirs at field scale in the past. There is a great need to have recovery process models which include biogenic gas so that these processes can be more accurately designed and optimized. Experimental work has been done in the past to understand methane production curves in oil fields and coal (Gieg et al., 2008; Jones et al., 2008a, Jones et al., 2008b) but there is currently no published data available for methane production rates from a shallow biogenic shale reservoirs in western Canada. We have developed a modified gas material balance theory (Cokar et al., 2012) that included a desorption term and a biogenic gas generation term. This gas material balance calculation was the first of its kind to predict the amount of gas within the reservoir realized from free gas, biogenic gas, and desorbed gas. It was assumed that the initial reservoir pressure in the field of study (Abbey Field) was 3,200 kPa and that it dropped to 101.325 kPa by the end of the reservoir life, and at this point the percent of cumulative gas produced from free, biogenic, and desorbed gas was 72%, 19%, and 10% respectively.

In Chapter 4, long-term laboratory experimental data from produced water and core samples was used to find bioconversion kinetic parameters. The kinetics, together with Langmuir desorption data from Chapters 3 and 4, was then used to construct a reactive reservoir simulation model of the shale gas reservoir.

6.2.1 Biogenic Gas Generation

The discovery of biological methane dates back to 1776 with Alessandro Volta's discovery of "combustible air" which was being formed in bogs, lakes rich in decaying vegetation, and streams (Balch et al., 1979). Biogenic gas is generated by anaerobic microorganisms which live at moderate temperatures below the surface of the earth at about 80°C and typically less than 5,000 kPa. Methane can be produced by microorganisms through predominantly two different metabolic pathways. The first path is via CO_2 reducing prokaryotes, which use hydrogen as the electron donor or energy source and CO_2 is the electron acceptor. The second path is by acetate fermentation. In this case, acetate and hydrogen are used to produce methane and carbon dioxide.

Methanogens can also use some other substrates such as methanol, formate, methylamines, dimethyl sulfide, ethanol and isopropanol to produce methane (Gilcrease, 2007). For the actual conversion of more complicated organic substrates to methane, other microorganisms such as acetogenic bacteria and fermentative bacteria are also present (Gilcrease, 2007). Figure 2.5 displays the overall process of anoxic decomposition demonstrating how different anaerobes work together to convert complex organic compounds into CH_4 and CO_2 (Madigan et al., 1997).

For the microorganisms, the nutrient supply of vitamins and minerals are believed to be provided to them via formation water (Head et al., 2003). It is believed that the main source of organic matter within shallow shale gas reservoirs is derived from kerogen. Kerogen is a high molecular weight (>1,000 Daltons), insoluble, polymeric organic component of shale. It is primarily made up of carbon, oxygen, hydrogen, nitrogen and sulfur compounds. Kerogen can be classified into different types depending on carbon and oxygen ratios. The Abbey Field shallow shale gas reservoir is predominantly made up of Type III kerogen which originates from land plants. For Type III kerogen, the hydrogen-to-carbon ratio is typically less than 1, and its oxygen-to-carbon ratio is generally between 0.03 and 0.3.

6.2.2 Transport and Flow

As described by Javadpour (2007), the actual mechanisms by which stored gas is released and transported to the well are not well understood. Figure 6.1 shows the proposed gas storage and transport mechanisms from deep within the reservoir to the production well. The production of gas from these reservoirs depends on how the gas is generated in the reservoir, stored within the reservoir, and transported out of the reservoir. The gas can be stored as adsorbed or dissolved gas in kerogen, clay and within the organic matter. It can also be dissolved in formation water. There are several transport mechanisms each with different degrees of connectivity to each other. At small length scales (nanometers to tens of nanometers), Knudsen, surface, and bulk diffusion may dominate transport. At larger length scales (microns to tens of microns), bulk diffusion and Darcy flow in interbedded sand layers can occur. At still larger length scales, there are natural fractures and induced hydraulic fractures in the near-well region that increase the effective

permeability of fluids immensely over nanometer and micron length scales. Although fractures can have small apertures in the tens of microns to millimeters, their extents can range from centimeters to meters. Gas production into the well and transport to surface is at larger length scales from centimeters for the well diameter to hundreds of meters for the well length.

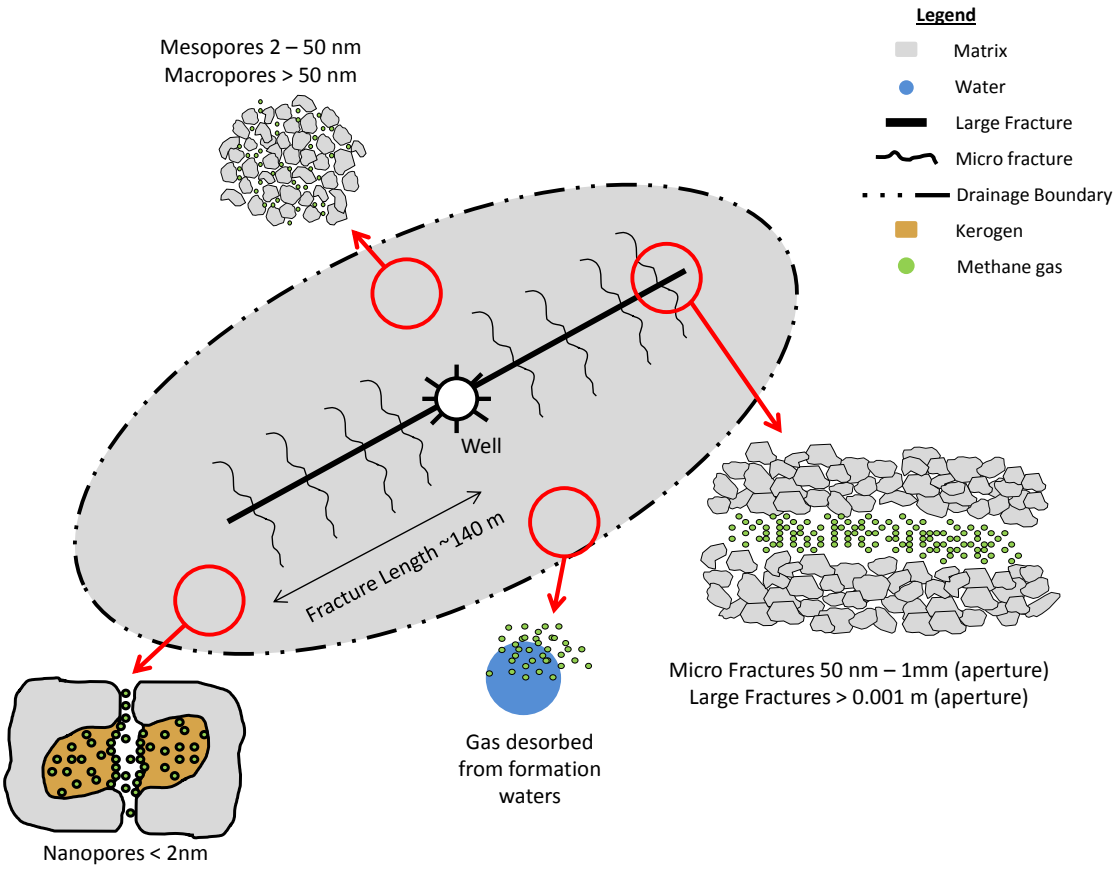

Figure 6.1. Storage and transport of gas in a shale gas reservoir from gas trapped in nanopores, mesopores, macropores, micro fractures, large fractures, and all the way to the production well.

6.3 Materials and Methods

6.3.1 Experimental Data

Data from three sets of experiments was used to determine kinetic parameters for methane generation by using core samples and produced waters from the reservoir. The first set of experiments consisted of cultivation of microorganisms with produced water samples, the second set were done with aged core samples, and the third set were done with both the produced water and core cultures. Produced water was obtained from a Well 16-7-22-17W3 (Well 2) and it was placed into a flask and enriched with a mixture of media and H_2/CO_2. While the microorganisms in this flask were allowed to grow, the second set of experiments was set up using core samples from five different zones from Well 16-3-22-18W3 (Well 1). The core sample was obtained from a core facility where the core had been stored at atmospheric conditions since 2002. The core samples were added to individual flasks each containing media and methane generation was monitored using a HP Series 5890 gas chromatograph. Even after 95 days, the core samples produced no discernible amounts of methane. On Day 98, 1 mL of the produced water/media mixtures enriched with H_2/CO_2 was added to the core sample flasks (the third set of experiments). Methane generated from these bottles was recorded for an additional 146 days. Methane levels were measured during the course of all experiments and are shown in Figure 6.3 of the results section.

6.3.2 Kinetics Model

The kinetic model derived here assumed first order substrate decomposition. Since only methane generation was measured from the experimental curves, the model that was used needed to be able to predict the amount of substrate present within the flask as a function of the amount of methane being produced versus time. Equation 6.1 describes methane production rate versus substrate decomposition as follows:

$$\frac{d[M]}{dt} = k[a_1 e^{-b_1 t}] \tag{6.1}$$

where M is the concentration of methane produced (methane produced (g)/mass of core (g)), a_1 represents the initial amount of substrate present at time zero (which was estimated from TOC data) (mass of substrate (g)/mass of core (g)), b_1 is a constant (1/day), k is the reaction rate constant (1/day) and t is time (day). Equation 6.1 can be integrated with respect to time with an initial condition that the methane concentration is equal to M_o at zero time:

$$M = -ka_1 \frac{1}{b_1}\left[e^{-b_1 t} - 1\right] + M_o \tag{6.2}$$

A least squares parameter estimation procedure using the generalized reduced gradient algorithm (Lasdon et al. 1978) as implemented in Microsoft Excel was used to estimate the three unknown parameters, k, a_1, and b_1. The results are listed in Table 6.4 and displayed in Figure 6.3.

6.3.3 Gas Desorption Model

Gas desorption data for this model was obtained experimentally for Well 1 and is described in Cokar et al. (2012). The data is listed in Table 6.1. To model this behavior, it was assumed that there was a gas component present within a small amount of immobile oil phase in the reservoir whose release into the reservoir was governed by pressure dependent k-values matched to the desorption isotherm data. More specifically, the experimental data in Table 6.1 was used and converted into a ratio of adsorbed gas (cm^3) to pore volume (cm^3) and used as the k-values for methane gas adsorbed into an immobile oil phase. To match the experimental desorption data, the immobile oil saturation was set equal to 0.0001 with a gas composition equal to 0.1 mole% dissolved within the oil phase. The tuned K-values are listed in Table 6.1.

Table 6.1. Gas desorption values for shale gas reservoir well 16-3-22-18W3 (Cokar et al., 2012) (Milk River E).

Pressure kPa	Adsorbed Gas (cc/g @STP)	Adsorbed Gas cm^3/cm^3 Rock Volume	Adsorbed Gas cm^3/cm^3 Pore Volume
161	0.04	0.10	0.48
403	0.08	0.18	0.89
632	0.10	0.22	1.12
754	0.11	0.27	1.34
954	0.14	0.33	1.64
1302	0.15	0.36	1.79
1738	0.18	0.43	2.16
2209	0.22	0.51	2.55
3298	0.25	0.59	2.95
4611	0.28	0.66	3.31
7000	0.38	0.89	4.47

6.3.4 Geological Model

A heterogeneous geological model of the shale gas reservoir was created from log and core data for 31 wells in the neighborhood of Well 1 (average values from log and core data for Well 2 is shown in Table 6.2). The actual thicknesses of Zones B, C, D, E and F are listed in Table 6.3. A heterogeneous model of the reservoir was created by using neutron and density porosity logs (the actual porosity was taken to be equal to the average of the two). The horizontal permeability for each zone was an average of that zone as obtained from core data (See Table 6.2). The vertical permeability was taken to be 25% of the value of the horizontal permeability. Archie's equation was used to determine the water saturation of the field (Archie, 1942). Formation resistivities were obtained from logs and the water formation resistivity was obtained from the water resistivity catalogue (Canadian Well Logging Society, 2002).

Another important input parameter for the model was the initial kerogen solid concentration within the reservoir that is amenable to the microorganisms. As described below, the amenable TOC content was history matched, and it was found that for this model 2% of the total organic carbon (TOC) present in the reservoir can be consumed by the microorganisms. Therefore, at each depth, 2% of the TOC present within that section of the reservoir was used as the initial consumable solid concentration within the zone (see Table 6.3).

Figure 6.2 shows cross-sectional views of the water saturation, gas saturation, porosity, and permeability distributions in the reservoir model. The length and width of the model is 250 m by 250 m, and the height of the model is 114 m. In the vertical direction, each

grid block is 0.5 m thick. In the horizontal directions, the dimensions of the domain are equal to 250 m (30 grid blocks x 8.33 m per grid block) by 250 m (30 grid blocks x 8.33 m per grid block). The initial pressure and temperature at the top of the model is equal to 3,200 kPa and 15°C, respectively.

As was done in field application at all production wells, a hydraulic fracture was created in the reservoir model by introducing an enhanced mobility zone as shown in Figure 6.2. The fracture aperture was taken to be approximately 1 m and the permeability of this zone was enhanced to 200 mD. The fracture area was approximately 150 m x 80 m with a thickness of 1 m. Table 6.2 and Table 6.3 list other required data of the reservoir simulation model.

Table 6.2. Log and core data from well 16-3-22-18W3 this data was used to create a heterogeneous geological model of the reservoir.

Depth Zone (m)	Neutron Porosity	Density (g/cc)	Total Carbon (wt%)	Inorganic Carbon (wt%)	Organic Carbon (wt%)	Air Permeability (mD)
B (251.75-277.17)	0.4	1.96	1.2	0.19	1.01	0.22
C (288.60-298.80)	0.39	1.62	1.62	0.61	1.01	0.20
D (306.05-313.48)	0.4	1.97	1.31	0.41	0.9	0.27
E (328.11-342.5)	0.38	2.11	1.57	0.64	0.92	3.16
F (345.51-347)	0.4	2.19	1.43	0.37	1.06	0.41

6.3.5 History Matching

The porosity, water and gas saturations were obtained from log data, and the permeability within each zone was obtained from core data (see Table 6.2). The history matching parameter in this simulation was the TOC_A present within each layer of the reservoir. After history matching, it was found that 2% of the TOC_A was consumed and this was used as the initial solid concentration of kerogen within the model (see Table 6.3).

6.3.6 Reservoir Simulation Model

The geological model was converted into a reservoir simulation model. The governing equations used in the reservoir simulator for the flowing component *j*, the mass balance is as follows (Bird et al., 1960):

$$\begin{aligned}\nabla\cdot\Bigg[&\frac{k_w\rho_w}{\mu_w}c_{wj}\left(\nabla P_w-\gamma_w\nabla z\right)+D_{wj}\nabla\left(\frac{\rho_w x_{wj}}{MW_w}\right)\\&+\frac{k_o\rho_o}{\mu_o}c_{oj}\left(\nabla P_o-\gamma_o\nabla z\right)+D_{oj}\nabla\left(\frac{\rho_o x_{oj}}{MW_o}\right)\\&+\frac{k_g\rho_g}{\mu_g}c_{gj}\left(\nabla P_g-\gamma_g\nabla z\right)+D_{gj}\nabla\left(\frac{\rho_g y_j}{MW_g}\right)\Bigg]\\&=\frac{\partial}{\partial t}\left[\phi\left(\frac{x_{wj}\rho_w S_w}{MW_w}+\frac{x_{oj}\rho_o S_o}{MW_o}+\frac{y_j\rho_g S_g}{MW_g}\right)\right]+\frac{\dot{m}_j}{MW_j}\end{aligned}\tag{6.3}$$

where k_* is permeability, ρ_* is density, μ_* is viscosity, $\dot{m}_j$ is the removal rate (per unit volume) of component j, MW_* is the molecular weight, D_{*j} is the diffusion-dispersion coefficient for component j in phase *, γ_* is the specific density, P_* is pressure, c_* concentration, φ is porosity, x and y are mole fractions, z is length, * represents the

phase and j represents the component. The flow of each phase is governed by Darcy's law:

$$q_* = -\frac{k_r k_{abs} A}{\mu_*} \nabla P \tag{6.4}$$

where q_i is the volumetric flow rate of component j, A is the area of flow, k_r is the relative permeability of component j in the reservoir, k_{abs} is the absolute permeability of the formation, μ_j is the viscosity of component j, and ∇P is the pressure gradient. The gas generated by microorganisms occurs according to the following first order reaction:

$$\frac{d[M]}{dt} = k_1[S] \tag{6.5}$$

where M is the amount of methane, k_1 is the reaction rate constant, t is time and S is the substrate concentration. The reaction rate constant for this reaction is listed in Table 6.4.

Only one well was simulated in this model. The production well operated at a constant minimum flowing bottom hole pressure equal to 1,100 kPa, which is the current reservoir pressure of the Abbey Field. The specific model properties are shown in Table 6.3.

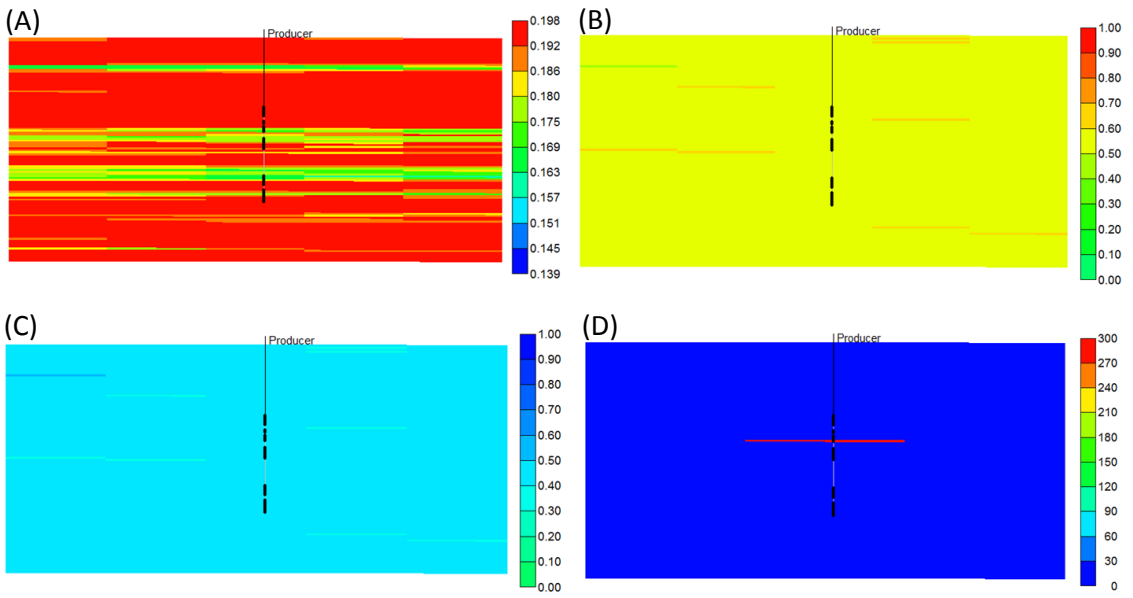

Figure 6.2. Reservoir simulation model (A) porosity, (B) gas saturation, (C) water saturation, and (D) permeability in the i direction (mD) (the fracture layer permeability is shown by the red zone in the middle, the permeabilities of zones B, C, D, E and F can be found in Table 6.2.

Table 6.3. Average values of properties used in reservoir simulation model.

Property	Average Value	Reference
Model Size	30 x 30 x 288	N/A
Block Dimensions	8.3 x 8.3 x 0.5	N/A
Water Saturation	0.44	Field Data
Gas Saturation	0.56	Field Data
Permeability i, j	(see Table 6.2)	Field Data
Permeability k	(0.25 of Table 6.2 permeability for each zone)	Field Data
Porosity	0.19	Field Data
Kerogen concentration and thickness of B	1.36 gmol/m^3 34 m	History Matched
Kerogen concentration and thickness of C	1.15 gmol/m^3 19 m	History Matched
Kerogen concentration and thickness of D	1.21 gmol/m^3 18 m	History Matched
Kerogen concentration and thickness of E	1.41 gmol/m^3 25 m	History Matched
Kerogen concentration and thickness of F	1.59 gmol/m^3 18 m	History Matched

6.4 Results and Discussion

The results for the rate equations (the kinetic model) for the core inoculations are shown in Figure 6.3. This figure shows the amount of methane produced in grams per gram of core present within each flask in zones B, C, D, E and F. It is interesting to note that the amount of methane produced at each depth is different perhaps due to the different organic/inorganic components present in the flasks or because of the bacterial consortia within each flask. Although the samples were inoculated from the same produced water enrichment sample, they may differ within each flask because of the availability of nutrients and different substrates present within each zone. The largest quantity of methane was produced from zones C and E, followed by D and F and finally B. The points in Figure 6.3 represent the experimental data whereas the curved line is the result of the kinetic model given by Equation 6.2. Table 6.4 summarizes the parameters obtained from Equation 6.2 that were used for the line curves in Figure 6.3 for each zone B, C, D, E and F. The least squares parameter estimation method was used to determine the values for k, a_1, and b_1, and the r^2 value is also listed in Table 6.4. The r^2 values were all above 0.64 and fairly close to 1.

The parameter values in Table 6.4 were then used for the simulation model, which was run for 2,678 days on a constant bottom hole pressure of 1,100 kPa. The monthly gas production rate in (m^3/day) as a function of time closely matches the field data (Figure 6.4). The results also reveal that 12% of the gas produced in the 2,678 days was of biogenic origin generated within the production time frame. Approximately 13% of the gas was desorbed from the different sources within the reservoir and about 75% of the gas was free gas that was already present in the reservoir (Figure 6.5). In the gas material

balance presented by Cokar et. al., (2012) we predicted that the biogenic gas amount will equate approximately 19% of the total gas production at the end of a resource well life. Since these wells are known to produce for decades, and it will take decades to decrease the reservoir pressure to about ~100 kPa the results shown in this study are a good match to those calculated with the gas material balance theory, since this model was only run for about 7.3 years. The key addition of mass transfer in the model developed here demonstrate that it plays a role within the system – 19% of the produced gas was recent biogenic gas in the gas material balance (an ideal system with no mass transfer limitations) whereas here 12% of the gas produced was recent biogenic gas.

Figure 6.6 shows the cumulative amount of biogenic gas produced (m^3) as a function of time in days for each zone B, C, D, E and F. The results are for the entire period the model was run, and the rate equations were established from Equation 6.2 and the experimental results obtained from Figure 6.3. At the end of the simulation run at 2,678 days the most amount of gas produced was from zone E, followed by zones C, D, B and F.

The findings in this study can potentially have a huge impact in the methane gas industry especially in shallow reservoirs that contain microorganisms. These microorganisms can produce a significant amount of methane on their own without any stimulation. As shown in the reservoir simulation model they can account for 12% of the total gas production. Shale deposits in the WCSB contain more than 1,000 Tcf of gas. On a large scale if 12% of all of this gas produced from shale reservoirs comes from biogenic gas

this means that 120 Tcf would be coming from microorganisms that are producing methane gas during the resource lifetime of the reservoir. Since all of the organic compounds within the reservoir are not consumed, it may be possible to increase the biogenic production even more by increasing substrate consumption.

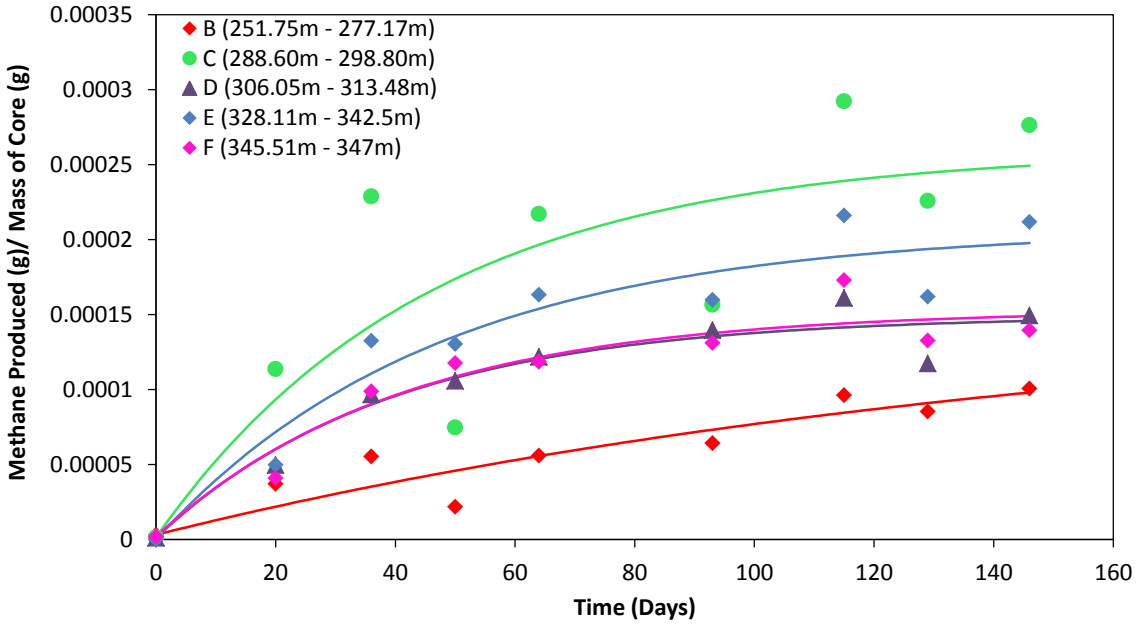

Figure 6.3. Experimental methane production curves versus time for core inoculations.

Table 6.4. Result table for kinetic model showing the variables found for Equation 6.2.

Section Name	Section Depth	k (1/day)	a_1	b_1	r^2
B	251.75-277.17	4.95×10^{-3}	2.02×10^{-4}	6.38×10^{-3}	0.83
C	288.60-298.80	2.82×10^{-2}	2.02×10^{-4}	2.20×10^{-2}	0.64
D	306.05-313.48	2.11×10^{-2}	1.79×10^{-4}	2.54×10^{-2}	0.94
E	328.11-342.5	2.38×10^{-2}	1.85×10^{-4}	2.13×10^{-2}	0.92
F	345.51-347	1.74×10^{-2}	2.12×10^{-4}	2.44×10^{-2}	0.92

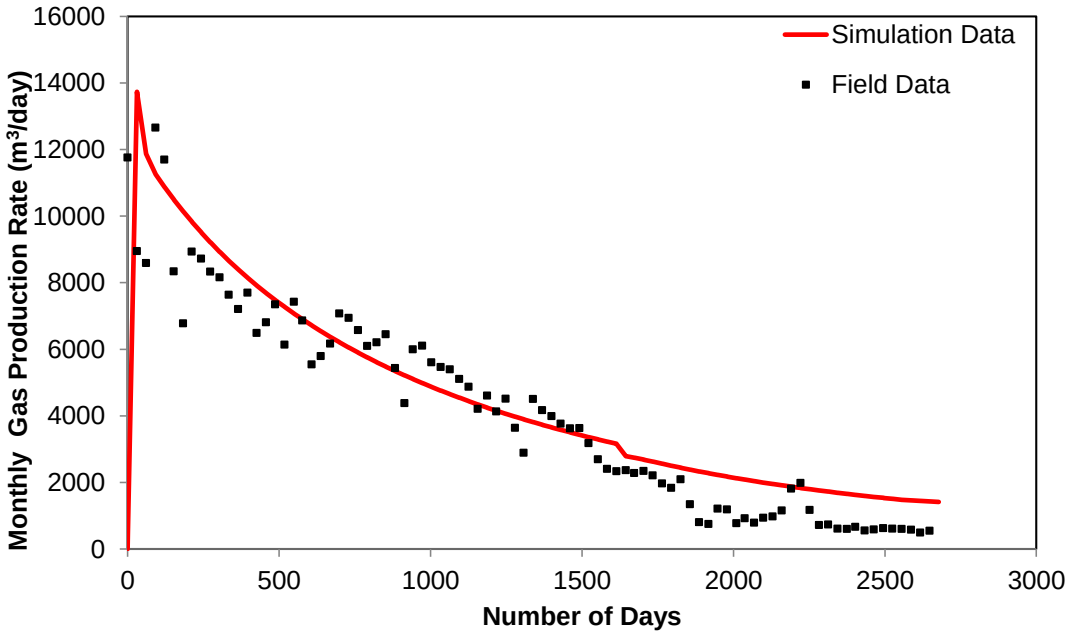

Figure 6.4. Monthly gas production rate (m^3/day) versus number of days for reservoir simulation model.

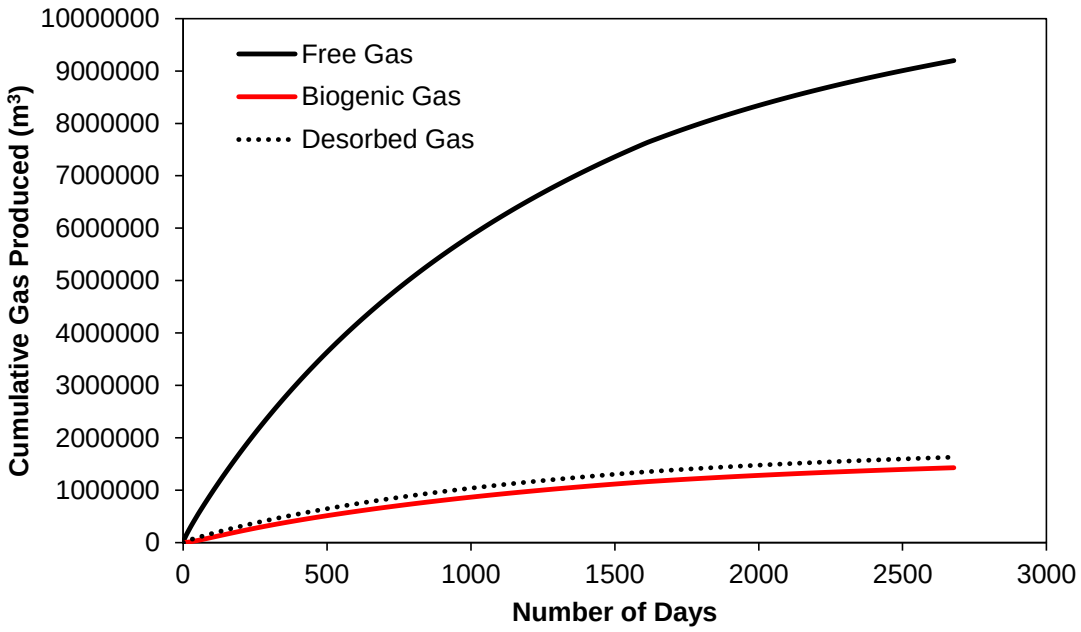

Figure 6.5. Cumulative gas production (m^3) versus number of days from the reservoir simulation model, with free gas present within the reservoir, biogenic gas from each depth, and desorbed gas.

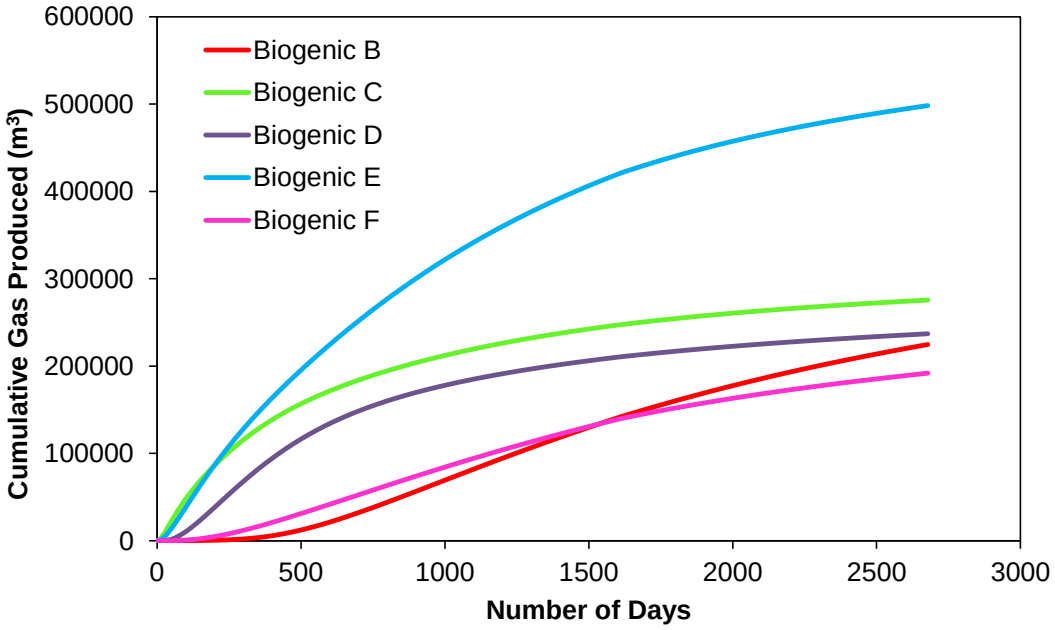

Figure 6.6. Cumulative gas production (m^3) versus number of days from the reservoir simulation model, for biogenic gas produced from each depth.

6.5 Conclusion and Recommendations

- Kinetic parameters were determined using first order substrate utilization for a shallow shale gas reservoir in western Canada using experimental data. This data was used to history match the TOC_A present within these reservoirs. It was found that 2% of the TOC present is amenable for microbial consumption.
- A heterogeneous reservoir simulation model with gas desorption and biogenic gas generation was simulated and history matched to field data. Using the kinetics obtained from the experimental study this model shows that up to a maximum of 12% of the gas present within the reservoir after about 7.3 years of production is due to biogenic gas generation during the wells production

life, the desorbed gas amount is 13% and the free gas accounts for 75% of the total gas produced during this time.

- The history match presented in this study is unique, it is the first history match of its kind for a shallow biogenic shale gas field.
- Further work can be done to determine how to stimulate the microorganisms within the reservoir to consume more of the organic carbon, thus increasing the percentage of TOC_A, so that the microbial gas production rates can increase.

Chapter Seven: Conclusions and Recommendations

7.1 Conclusions

This thesis presents novel data and analysis for biogenic methane generation in shallow shale gas reservoirs in the WCSB. The theory can be extended to other shale gas reservoirs if the kinetics of microbial gas production are known. This study provides three new approaches to estimate new biogenic gas generation amounts: (a) new gas material balance, (b) bioreactor kinetics transport model, and (c) numerical bioreactive reservoir simulation model. The reaction rate kinetics used in the analysis are supported by experimental bioassays which were used to incubate produced water and reservoir core samples from which methane production curves as a function of time were obtained. The sample bottles were then analyzed using 16S rRNA gene sequencing to determine the different microorganisms involved in the production of methane. Also, hydrocarbon utilization by the substrates was studied using a gas chromatograph-mass spectrometer (GC-MS) and it was determined that the microbial consortia present within the shale samples were indeed consuming the hydrocarbons present within the bottles (which was the organics present within the reservoir).

This thesis consists of four main research chapters and a brief summary of each research chapter is described below.

Chapter 3 – A novel gas material balance theory was derived which incorporated experimental gas desorption data (Langmuir desorption isotherms) along with an unknown microbial gas generation amount. Field data from two different fields, Nexen's

Bigstick Field and Husky's Abbey field were calculated from field data of total gas produced as a function of pressure within the reservoir over a period of several years. The results show that if the reservoir pressure was to deplete all the way to approximately 101.325 kPa, which would essentially take many decades, the amount of new microbial gas generated during the production period accounts for about 37% of the total gas produced for Nexen's Bigstick Field and roughly 19% of the total gas produced in Husky's Abbey Field. This chapter also presented gas desorption data obtained from Husky's Abbey Field that followed Langmuir desorption. The amount of gas desorbed from the reservoir was dependent on the reservoir depth (because the reservoir composition was different at each depth) and in Nexen's Bigstick Field the desorption of gas ranged between 9% and 7% of total gas production, and in Husky's Abbey Field the amount of gas desorbed from surfaces within the reservoir ranged from 13% to 10%. Although the new gas material balance theory was applied to field data from shale gas reservoirs in western Canada it can be applied to any reservoir where microbial gas production produces methane gas during the production life of a well.

Chapter 4 – This chapter describes experiments and obtained data which supports the existence of microorganisms within the reservoir. Several experiments were conducted on both core and produced water samples that were received from Husky's Abbey Field. The data is novel, to the knowledge of the author, because it presents the first methane production curves for gas generation in a shale gas reservoir in western Canada. Produced water samples were collected from two different wells within the field and four experiments were done with the produced water samples: (a) an N_2/CO_2 headspace with

no additional electron donors, (b) H_2/CO_2 at a ratio of 80:20 was added to the headspace with no additional electron donors, (c) N_2/CO_2 headspace with acetate, and (d) N_2/CO_2 headspace with 5 g of core from Site 1. The samples with no substrate and just core produced a small amount of methane however in the 16S rRNA gene sequencing analysis for both sites there was a shift towards methanogens when core was added as a substrate to the samples. Also, with the addition of H_2/CO_2 and acetate to the produced water samples there was a definite shift towards higher methane production rates from the samples as well as a shift towards methanogenic communities within the samples. Core inoculations and core incubations were carried out at five depths (labelled B, C, D, E and F, respectively) within the reservoir. There was no discernible methane produced in the core samples but this was most likely because the core had been exposed to atmospheric conditions since 2002. However, when the Site 1 core was inoculated with 1 mL of Site 2 enriched H_2/CO_2 culture there was evidence of methane production. There were three experiments set up for the core inoculation samples: (a) an N_2/CO_2 headspace with no additional electron donors, (b) H_2/CO_2 at a ratio of 80:20 was added to the headspace with no additional electron donors, and (c) N_2/CO_2 headspace amended with volatile fatty acids (VFA's). In the core inoculations with only core present and no additional substrates there was evidence of methane production from the samples. When the substrates H_2/CO_2 and VFA were added to the samples, the amount of methane produced almost doubled. This shows that these substrates were most likely being utilized by the microbial consortia present within the bottle. Water soluble substrate and metabolite identification was performed by using a GC-MS to determine if there was evidence of substrate biodegradation in the inoculated core containing incubation. The evidence from

the GC-MS for Core E samples reveal that many of the alkanes ranging from C_{22} to about C_{30} were present in the uninoculated samples but were largely absent in the inoculated sample suggesting alkanes were indeed consumed by the microbial consortia present within the bottle.

Chapter 5 – A bioreaction transport engineering model was developed to quantify the percentage of biogenic gas that could be produced within a shale gas reservoir. Reaction engineering principles along with methane production data obtained from Chapter 4 were used to create the models. A zero order reaction rate model with transport governed by Darcy flow was developed. Since the amount of TOC_A is not known, a sensitivity analysis was performed on the amount of TOC_A that is present within the reactor model. The TOC_A was varied between 1 and 8.5(vol%). The amount of new biogenic gas produced within the model was equal to 96% at 8.5% TOC_A and 11% at 1%. The Damköhler number, determined for all of the models at different TOC_A's, remained less than 0.04. This is a significant result for increased gas production by enhancement of biogenic gas generation since it implies that if the limiting step for bioconversion can be found, providing transport was enhanced to allow it to act with the microbes, then the bioconversion rate can be enhanced.

Chapter 6 – The final research chapter presented in this thesis is development of a detailed numerical bioreactive reservoir simulation model of a biogenic shallow shale reservoir. This chapter is an amalgamation of all the data obtained from the other chapters. The laboratory methane production curves for the core inoculations with only

core present and no other additional substrates was used to develop a first order substrate consumption reaction model. The first order reaction kinetic parameters were calibrated against experimental data. All of the reservoir properties such as porosity, permeability, water saturations were extracted from well log and core data. The most uncertain parameter of the model was the percentage of TOC that was amenable to the microorganisms. This value was then determined by calibrating the model to the field data. The final matched value for the TOC_A within the reservoir was 2%. This model also included methane desorption from organic and inorganic surfaces within the reservoir. The results reveal that after approximately 7.3 years of simulation, 12% of the total gas produced was biogenic gas generated during the production life of the reservoir, 13% was desorbed from the different surfaces within the reservoir, and 75% was free gas that was already present within the reservoir. This is the first shallow biogenic shale gas reservoir history match reported in the literature.

The main conclusions of the research documented in this thesis are as follows:

1. A modified gas material balance, which included a biogenic shale gas term in addition to gas a desorption term which accounted for the amount of gas that is adsorbed onto surfaces within the reservoir, was used to estimate the percentage of biogenic gas that can be produced from a well during the resource lifetime of that well. For the two wells analyzed with field data, it was found that anywhere between 37 – 19% of the total gas produced is attributable to new biogenic gas.
2. Methane production curves for produced water and core enrichments show that a discernible amount of methane gas is being produced within the bottles. 16S rRNA gene sequencing data further supports these findings by identifying the

methane producing archaea at the family level. Also, an increase in methane production was observed in produced water and core samples when additional substrates were added. This shows evidence that methane production from within the reservoir could be potentially increased via substrate addition.

3. A reaction simulation model with experimental methane production kinetics was used to model the amount of gas that could be produced in a reservoir. The theory also predicted the maximum amount of TOC_A that is physically possible. The maximum amount of TOC_A was determined to be 8.89 volume percent, and biogenic gas generation with a TOC_A value ranging from 8.5 volume percent to 1 volume percent yields a biogenic gas production amount of 96-11%.
4. A numerical reservoir simulation model was used to determine the amount of TOC_A present within a shallow shale gas reservoir in western Canada. It was determined that approximately 2% of the TOC could be converted into methane gas. Additionally, a history match of field data with a first order substrate utilization kinetic models showed that approximately 12% of the total gas produced during a period of approximately 7 years could be attributed to biogenic gas generation.

7.2 Recommendations

The following recommendations arise from the research documented in this thesis:

1. For the gas material balance model, methane solubility in formation water should also be added to evaluate the importance of this storage mechanism.

2. Experimental studies should be conducted to determine more conclusively the actual amount of hydrocarbons within the organic material that are consumed by the microorganisms that live within the reservoir, in other words, the TOC_A.
3. The reservoir simulation model should be used to predict the performance of similar wells in the region to determine how robust the model is.
4. Experimental bioassays have shown that the addition of substrates such as acetate, H_2/CO_2 and VFA's substantially increase methane production within the laboratory. Further research should be done to add substrates containing these chemicals as well as other nutrients into reservoirs that are currently producing biogenic gas to determine the economic impact of substrate addition on a field scale. This field study would definitely lead towards a better understanding of the direct impact substrate and nutrient addition would have on such a field.

All of the above mentioned recommendations should be considered in future research work on the topic of biogenic shale gas production from shallow organic matter rich reservoirs. The research and understanding of this economical and environmentally friendly source of natural gas is just in its infancy and more research is required to really understand the mechanisms of biogenic gas generation as well as the metabolic processes by which gas is produced by the microorganisms within the reservoir.

References

1. Aitken, C.M., Jones D. M., and Larter, S.R. "Anaerobic hydrocarbon biodegradations in deep subsurface oil reservoirs," *Nature*, vol. 431, pp. 291-294, 2004.
2. Allen, T.D., Caldwell, M.E., and Lawson, P.A. "Alkalibaculum bacchi gen. nov., a CO-oxidizing, ethanol-producing acetogen isolated from livestock-impacted soil," *International Journal of Systematic and Evolutionary Microbiology*, vol. 60, no. 10, pp.2483-2489, 2009.
3. Ambrose R., Hartman, R.C., Diaz-Campos, M., Akkutlu, Y., and Sondergeld, C.H. "New Pore-scale Considerations of Shale Gas in Place Calculations," SPE Paper 131772, presented at the SPE Unconventional Gas Conference in Pittsburgh, Pennsylvania, USA, February 23-25, 2010.
4. Archie, G.E. "The electrical resistivity log as an aid in determining some reservoir characteristics." *Transactions, AIME*, vol. 31, pp. 350-366, 1942.
5. Balabane, M., Galimov, E., Hermann, M., and Letolle R. "Hydrogen and carbon isotope fractionation during experimental production of bacterial methane," *Organic Geochemistry*, vol. 11, no. 2, pp. 115-119, 1987.
6. Balch, W.E., Fox, G.E., Magrum, L.J., Woese, C.R., and Wolfe, R.S. "Methanogens: Re-evaluation of a Unique Biological Group," *Microbiological Reviews*, vol. 43, pp. 260-296, 1979.
7. Bapteste, E., Brochier, C., and Boucher, Y. "Higher-level classification of the Archaea: evolution of methanogenesis and methanogens," *Archaea*, vol.1, pp. 353-363, 2005.
8. Bastin, E. "Microorganisms in Oilfields," *Science*, vol. 63, pp. 21-24, 1926.

9. Behar, F., Vandenbroucke, M., Tang, Y., Marquis, F., and Espitalie, J. "Thermal cracking of kerogen in open and closed systems: determination of kinetic parameters and stoichiometric coefficients for oil and gas generation," *Organic Geochemistry*, vol. 26, no. 5/6, pp. 321-339, 1997.
10. Behar, F., Lewan, M.D., Lorant, F., and Vandenbroucke, M. "Comparison of artificial maturation of lignite in hydrous and nonhydrous conditions," *Organic Geochemistry*, vol. 34, no. 4, pp. 575 – 600, 2003.
11. Berdugo-Clavijo, C., Dong, Xiaoli, D., Soh, J., Sensen, C.W., and Gieg, L.M. "Methanogenic biodegradation of two-ringed polycyclic aromatic hydrocarbons," *FEMS Microbial Ecology*, vol. 81, pp. 123-133, 2012.
12. Bird, R. B., Stewart, W. E., and Lightfoot, E.N. Transport Phenomena. New York: John Wiley & Sons, 1960.
13. Brigman, R.L., Furlong, M., Glucksman, A., Skipper, H.D., and Whitman, W.B. "Characterization of Groundwater Microbial Communities from a Chlorinated-Ethene-Contaminated Landfill," US Department of Energy. DE-AC09-96SR18500, 2002.
14. CBM Solutions, 2011. High Pressure Methane Adsorption Analysis. Husky well.
15. Clayton, J.L. "Geochemistry of coal bed gas – A review," *International Journal of Coal Geology*, vol. 35, pp.159-173, 1998.
16. Clayton, C. "Source volumetrics of biogenic gas generation," in Bacterial Gas, Technip Edition, Vially, R. Ed., Paris, pp. 63-74, 1992.
17. CRC Handbook of Chemistry and Physics. 91st Edition, 2009, CRC Press.

18. Cokar, M., Kallos, M.S., and Gates, I.D. "New Gas Material Balance to Quantify Biogenic Gas Generation Rates from Shallow Organic-Matter-Rich Shales," *Fuel*, http://dx.doi.org/10.1016/j.fuel.2012.06.054, 2012.
19. Connan, J. Advances in Petroleum Geochemistry. London: Academic Press, 1984.
20. Cox S.A., Gilbert J.V., and Sutton R.P. "Reserve Analysis for Tight Gas," SPE Paper Number 78695. Presented at the SPE Eastern Regional Meeting, Kentucky, October 23-25, 2002.
21. Cramer, B., Littke, R., Braun, A., Poelchau, H.S., Welte, D.H., Gerling, R. and Lopatin, N.V. "West Siberian Gas Accumulations - the Origin of Methane and Losses to the Atmosphere," AAPG Search and Discover Article #91019, presented at the AAPG Convention and Exhibition, May 19-22, 1996.
22. Curtis, J.B. "Fractured Shale – gas systems," *American Association of Petroleum Geologists Bulletin*, vol. 86, no.11, pp. 1921-1938, 2002.
23. Daniels, L., Fulton, G., Spencer, R.W., and Orme-Johnson, W.H. "Origin of hydrogen in methane produced by methanobacterium thermoautotrophicum," *Journal of Bacteriology*, vol. 141, no. 2, 1980.
24. Balkwill, D.L., Fredrickson, J.K., and Romine, M. F. "Sphingomonas and Related Genera" In: The Prokaryotes, A Handbook of the Biology of Bacteria. Volume 7: Proteobacteria: Delta and Epsilon Subclasses. Deeply Rooting Bacteria ISBN 978-0-387-33493-6, 2006.
25. Davis, J.P., Stuchtemeyer, C.G., Elshaed, M.S. "Bacterial Communities Associated with Production Facilities of Two Newly Drilled Thermogenic Natural

Gas Wells in the Barnett Shale (Texas, USA)," *Environmental Microbiology*, 2012.

26. Dave, S., Madhav, K., and Ray, G.E. "The Science, Impacts and Monitoring of Drought in western Canada," Canadian Plains Research Centre, 2005.
27. Deng, L., Ren, Y., and Wei, C. "Pyrene degradation by Pseudomonas sp. And Burkholderia sp. Enriched from coking wastewater sludge," *Journal of Environmental Science and Health*, vol. 47, pp. 1984-1991, 2012.
28. Dias, M., Salvado, J.C., Monperrus, M., Caumette, P., Amouroux, D., Duran, R. and Guyonead, R. "Characterization of Desulfomicrobium salsuginis sp. nov. and Desulfomicrobium aestuarii sp. nov., two new sulfate-reducing bacteria isolated from the Adour estuary (French Atlantic coast) with specific mercury methylation potentials," *Systematic and Applied Microbiology*, vol. 31, no. 1, pp. 30-7, 2008.
29. EIA. "Review of Emerging Resources: U.S. Shale Gas and Shale Oil Plays. Technical report," Energy Information Administration. U.S. Department of Energy, Washington D.C., 2011.
30. Energy Information Administration, Annual energy outlook. DOE/EIA-0383. U.S. Department of Energy, Washington, DC, 2007.
31. Fathi, E., and Akkutlu, I. "Matrix heterogeneity effects on gas transport and adsorption in coalbed and shale gas reservoirs," *Transport in Porous Media*, vol. 80, no. 2, pp. 281-304, 2009.
32. Fishman, N.S., Ridgley, J.L. and Hall, D.L. "Timing of Gas Generation in the Cretaceous Milk River Formation, Southeastern Alberta and Southwestern

Saskatchewan – Evidence from Authigenic Carbonates," Summary of Saskatchewan Geological Survey, vol. 1, pp. 125-136, 2001.

33. Fletcher, S. "Unconventional gas vital to U.S. supply," *Oil and Gas Journal* , vol. 103, pp. 20–25, 2005.
34. Florin, T.H., Zhu, G., Kirk K.M., and Martin, N.G. "Shared and unique environmental factors determine the ecology of methanogens in humans and rats," *American Journal of Gastroenterology*, vol. 95: pp. 2872-2879, 2000.
35. Formolo, M., Martini, A., and Petsch, S. "Biodegradation of sedimentary organic matter associated with coalbed methane in the Powder River and San Juan Basins, U.S.A." *International Journal of Coal Geology,* vol. 76, pp. 86-97, 2008.
36. Ge, Y., Schime, J.P., and Holden, P.A. "Identification of soil bacteria susceptible to TiO2 and ZnO nanoparticles," *Applied Environmental Microbiology*, vol., 78, no. 18, 2012.
37. Gilcrease, P.C., and Shurr, G.W. "Making Microbial Methane work: The potential for new biogenic gas," *World Oil*, 2007.
38. Gieg, L. M. and Suflita, J.M. "Detection of anaerobic metabolites of saturated and aromatic hydrocarbons in petroleum-contaminated aquifers," *Environmental Science and Technology*, vol. 36, pp. 3755-3762, 2002.
39. Gieg, L. M. and J.M. Suflita. "Metabolic Indicators of Anaerobic Hydrocarbon Biodegradation in Petroleum-Laden Environments," In *Petroleum Microbiology*, Ollivier, B. and Magot, M, Ed. Washington, D. C.: ASM Press, 2005, pp. 337-356.

40. Gieg, L.M., Duncan, K.E., and Suflita, J.M. "Bioenergy Production via Microbial Conversion of Residual Oil to Natural Gas," *Applied and Environmental Microbiology*, vol. 74, no.10, pp. 3022-3029, 2008.
41. Head, I.M., Martin, D., Larter, S.R., and Jones, D.M. "Biological Activity in the deep subsurface. and the origin of heavy oil," *Nature*, vol. 23, pp. 344-352, 2003.
42. Hoefs, J. *Stable Isotope Geochemistry*. Germany: Springer, 2004.
43. Horstad, I., Larter S.R., Mills, N. "A quantitative model for biological petroleum degradation within the Brent Group reservoir in the Fullfaks Field, Norweigian North Sea," *Organic Geochemistry*, vol. 19, pp. 107-117, 1992.
44. Jabari, L., Gannoun, H., Cayol, J-L., Hedi, A., Sakmoto, M., Falsen, E., and Ohkuma, M. "Macellibacteroides fermentans gen. nov., sp. Nov., a member of the family Porphyromonadaceae isolated from an upflow anaerobic filter treating abattoir wasterwaters," *International Journal of Systematic and Evolutionary Microbiology*, vol. 62, no. 10, pp. 2522-2527, 2011.
45. Javadpour, F., Fisher, D., and Unsworth, M. "Nanoscale Gas Flow in Shale Gas Sediments," *Journal of Canadian Petroleum Technology*, vol. 46, no.10, pp. 55-61, 2007.
46. Javadpour, F. "Nanopores and Apparent Permeability of Gas Flow in Mudrocks (Shales and Siltstones)," *Journal of Canadian Petroleum Technology*, vol. 48, no.8, 2009.
47. Jehmlich, N., Kleinsteuber, S., Vogt, C., Benndorf, D., Harms, H., Schimdt, F., Von Bergen, M., and Seifer, J. "Phylogenetic and proteomic analysis of

anaerobic toluene-degrading community," *Journal of Applied Microbiology*, vol. 10, no.6, 2010.

48. Jenkins, C.D., and Boyer, C.M. Coalbed- and Shale-Gas Reservoirs," *Journal of Petroleum Technology*, Distinguished Authors Series, 2008.
49. Jones, E.J.P., Voytek, M.A., Warwick, P.D., Corum, M.D., Cohn, A., Bunnell, J.E., Clark, A.C., and Orem, W.H. "Bioassay for estimating the biogenic methane-generating potential of coal samples," *International Journal of Coal Geology*, vol. 76, pp. 138-150, 2008(a).
50. Jones, D.M., Head, I.M., Gray, N.D., Adams, J.J., Rowan A.K., Aitken, C.M., Bennett, B., Huang, H., Brown, A., Bowler, B.F., Oldenburg, T., Erdmann, M., and Larter, S.R., "Crude-oil biodegradation via methanogenesis in subsurface petroleum reservoirs," *Nature*, vol. 451, 2008(b).
51. Kerr, R.A. "Natural gas from shale bursts onto the scene," *Science*, vol. 328, pp. 1624-1626, 2010.
52. King, G.R., "Material Balance Techniques for Coal Seam and Devonian Shale Gas Reservoirs," Paper SPE 20730 presented at the 65th Annual Technical Conference and Exhibition of the Society of Petroleum Engineers, New Orleans, 23-26 September, 1990.
53. Labutti, K., Mayilraj, S., Clum, A., Lucas, S., Glavina Del Rio, T., Nolan, M., Tice, H., Cheng, J.F., Pitluck, S., Liolios, K., Ivanova, N., Mavromatis, K., Mikhailova, N., Pati, A., Goodwin, L., Chen, A., Palaniappan, K., Land, M., Hauser, L., Chang, Y.J., Jeffries, C.D., Rohde, M., Spring, S., Göker, M., Woyke, T., Bristow, J., Eisen, J.A., Markowitz, V., Hugenholtz, P., Kyrpides, N.C.,

Klenk, H.P., and Lapidus, A. "Permanent draft genome sequence of Dethiosulfovibrio peptidovorans type strains (SEBR 4207)," vol. 3, no. 1, 2010.

54. Larter, S. Huang, H., Adams, J., Bennett, B., Jokanola,O., Oldenburg, T., Jones, M., Head, I., Riediger, C., and Fowler, M. "The controls on the composition of biodegraded oils in the deep subsurface: Part II – Geological controls on subsurface biodegradation fluxes and constraints on reservoir-fluid property prediction," *AAPG Bulletin*, vol. 90, no. 6, pp. 921-938, 2006.
55. Lasdon L.S., Waren A., Jain A. and Ratner M. "Design and Testing of a Generalized Reduced Gradient Code for Nonlinear Programming," *ACM Transactions on Mathematical Software*, vol. 4, no. 1, pp. 34-50, 1978.
56. Lane, D.J, Pace, B., Olsen, G.J., Stahl, D.A., Sogin, M.L., and Pace, N.R. "Rapid-determination of 16s ribosomal-rna sequences for phylogenetic analyses," Proceedings of the National Academy of Sciences of the United States of America, vol. 82, pp. 6955-6959, 1985.
57. Liu, P., Qiu, Q., and Lu, Y. "Syntrophomonadaceae-Affiliated Species as Active Butyrate Utilizing Syntrophs in Paddy Field Soil, " Applied and Environmental Microbiology, 2011. DOI: 10.1128/AEM.00190-11.
58. Liu, H., Liang, R., Tao, F., Ma, C., Liu Y., Liu, X., and Liu J. "Genome sequence of Pseudomonas aeruginosa strain SJTD-1, a bacterium capable of degrading long-chain alkanes and crude oil," Journal of Bacteriology, vol. 194, no. 17, 2012.
59. Lodowska, J., Wolny, D., Jaworska-Kik, M., Dzierzewic Z., and Weglarz, L. "Interstrain diversity of 2-keto-3-deoxyctonate content in lipopolusaccharides of Desulfovibrio desulfuricans," vol., 58, no. 1, pp.21-7, 2009.

60. Madigan, M.T., Martinko, J.M., and Parker, J. Brock biology of microorganisms: Prentice-Hall Inc. 8th Edition, 1997.

61. Martini, A.M.,. Walter, L.M., Budai, J.M., Ku, T.C.W., Kaiser, C.J., and Schoell, M., "Genetic and temporal relations between formation waters and biogenic methane – Upper Devonian Antrim Shale, Michigan basin, USA," *Geochimica et Cosmochimica Acta*, vol. 62, no.11, pp.1699-1720, 1998.

62. Martini, A.M., Walter, L.M., Ku, T.C.W., Budai, J.M., McIntosh, J.C. and Schoell, M. "Microbial production and modification of gases in sedimentary basins: a geochemical case study from a Devonian shale gas play, Michigan Basin," *AAPG Bulletin*, vol. 87, no. 8, pp. 1355-1375, 2003.

63. Martini, A.M., Nusslein, K., and Petsch, S.T. "Final Report Enhancing Microbial Gas From Unconventional Reservoirs: Geochemical and Microbiological Characterization Of Methane-Rich Fractured Black Shales," 2004.

64. Martini, A. "Enhancing Microbial Gas from Unconventional Reservoirs," GasTIPS, 2005.

65. Matlakowska, R., and Sklodowska, A. "Biodegradation of Kupferschiefer black shale organic matter (Fore-Sudetic Monocline, Poland) by indigenous microorganisms," Chemosphere, vol. 83, pp., 1255-1261, 2011.

66. Mattavelli, L., Ricchiuto, T., and Martinenghi, C. "Deep isotopic light methane in northern Italy," in *Bacterial Gas*, Technip Edition, Vially, R., Ed., Paris, 1992.

67. Maestrojuan, G.M., and Boone, D.R. "Characterization of *Methanosarcina barkeri* MS^T and 227, *Methanosarcina mazei* $S\text{-}6^T$, and *Methanosarcina*

vacuolata Z-761^{T}," *International Journal of Systematic Bacteriology*, vol. 41, no.2, pp. 267-274, 1991.

68. McDonald, I.R., Upton, M., Hall, G. Pickup R.W., Edwards C., Saunders J.R., Richie D.A., and Murrell, J.C. "Molecular ecological analysis of methanogens and methanotrophs in blanket bog peat," *Microbial Ecology*, vol. 38, pp. 225-233, 1999.
69. McInerney, M.J., Bryant, M.P. and Pfennig, N. "Anaerobic bacterium that degrades fatty acids in syntrophic association with methanogens." *Archives of Microbiology*, vol. 122, pp. 129-135. 1979.
70. Murrell, J.C. "Molecular ecological analysis of methanogens and methanotrophs in blanket bog peat," Microbial Ecology, vol. 38, pp. 225-233, 1999.
71. McInerney, M.J., Bryant, M.P. and Pfennig, N. "Anaerobic bacterium that degrades fatty acids in syntrophic association with methanogens," *Archives of Microbiology*, vol. 122, pp. 19-135, 1979.
72. Nexen, 2011. Figure 1.3. Typical gas production rates versus time for a shallow shale gas well (Nexen, 2011).
73. National Energy Board. "Northeast British Columbia's Ultimate Potential for Conventional Natural Gas – Fact sheet." Internet: http://www.neb.gc.ca/clf-nsi/rnrgynfmtn/nrgyrprt/ntrlgs/nbcltmtptntl2006/fctsht0609-eng.html, 2011[September 27, 2012].
74. National Energy Board (NEB). " A Primer for Understanding Canadian Shale Gas," 2009.

75. Okiongbo, K.S., Aplin, A.C., and Larter, S.R. "Changes in Type II Kerogen Density as a Function of Maturity: Evidence from the Kimmeridge Clay Formation," *Energy & Fuels*, vol. 19, pp. 2495-2499, 2005.
76. Park, H.S., Chatterjee, I., Dong, X., Wang, S-H., Sensen, C.W., Caffrey, S.M., Jack, T.R., Boivin, J., and Voodruow, G. "Effect of sodium bisulfite injection on the microbial community composition in a brackish-water-transporting pipeline," *Applied and Environmental Microbiology*, vol. 77, no. 9, pp.6908-6917, 2011.
77. Pepper, A.S., and Corvi, P.J. "Simple Kinetic Models of Petroleum Formation: Part 3. Marine and Petroleum Geology," vol.12, no.4, pp. 417-452, 1994.
78. Petsch, S.T., Eglinton, T.I., and Edwards K.J. "14C-Dead Living Biomass: Evidence for Microbial Assimilation of Ancient Organic Carbon During Shale Weathering," *Science*, vol. 292, no. 5519, pp. 1127-1131, 2001.
79. Petzet, A. "Resource plays, CBM to fuel drilling upturns in US, Canada," *Oil and Gas Journal*, vol. 103, pp. 32–34, 2005.
80. Pedersen, P.K. "Stratigraphic Relationship of Alderson(Milk River) Strata Between the Hatton and Abbey-Lacadena Pools, Southwestern Saskatchewan – Preliminary Observations," Saskatchewan Geological Survey, vol. 1, 2003.
81. Poindexter, J.L.S., and Bazire, G.C. "The fine structure of stalked bacteria belonging to the family caulobacteraceae," *The Journal of Cell Biology*, 1964.
82. Ramakrishanan, H., Peza, E., Sinha, S., Woods, M., Ikeocha, C., Mengel, F., Simon, Y., Pearce, P., Kiester, J., McKetta, S., and Jeffers, J. "Understanding and Predicting Fayetteville Shale Gas Production Through Integrated Seismic-to-Simulation Reservoir Characterization Workflow." Presented at the SPE Annual

Technical Conference and Exhibition, Denver Colorado 30 October – 2 November 2011, SPE 147226.

83. Ramos-Padron, E., Bordenage, S., Lin, S., Mani Bhaskar, I., Dong, X., Sensen, C.W., Fournier, J., Voordouw, G., and Gieg, L.M. "Carbon and sulfur cycling by microbial communities in a gypsum-treated oil sands tailings pond," *Environmental Science and Technology*, vol. 45, pp. 439-446, 2011.
84. Rice, D.D. and Claypool G.E. "Generation, accumulation, and resource potential of biogenic gas," *American Association of Petroleum Geologists Bulletin*, vol. 65, pp. 5-25, 1981.
85. Rice, D.D. "Occurrence of indigenous biogenic gas in organic-rich, immature chalks of Late Cretaceous age, eastern Denver Basin," In:Petroleum Geochemistry and Source Rock Potential of Carbonate Rocks, no. 18, Palacas, J.G., Ed., *American Association of Petroleum Geologists Studies in Geology*, pp. 135-150, 1984.
86. Rice, D.D. "Biogenic gas: controls, habitats, and resource potential," in D.G. Howell, ed., The Future of Energy Gases – U.S. Geological Survey Professional Paper 1570, Washington, United States Government Printing Office, pp. 583-606, 1993.
87. Rice, D.D. "Resource Potential of Ancient Bacterial Gas," US Geological Survey, 1992.
88. Rice, D.D. and Spencer, C.W., "Northern Great Plains shallow biogenic gas. In: 1995 National Assessment of United States Oil and Gas Resources –Results, Methodology, and Supporting Data," Gautier, D.L., Dolton, D.L., Takahashi, K.I.,

and Varnes, K.L., Ed. U.S. Geological Survey Digital Data Series DDS-30. Release 2, 1996.

89. Ridgley, J.L., Hester, T.C., Condon S.M., Anna, L.O., Rowan, E.L., Cook, T., and Lillis, P.G. "Re-evaluation of the Shallow Biogenic Gas Accumulation, Northern Great Plains, USA – Is the Similar Gas Accumulation in Southeaster Alberta and Southwestern Saskatchewan a Good Analog?," U.S. Geological Survey, 1999.
90. Ridgley, J.L. "Regional Geochemical Study of the Upper Cretaceous Shallow Biogenic Gas System in Saskatchewan, Alberta, and Montana – Application of Isotope and Compositional Systematics to Understanding the Distribution of Gas Resources," Saskatchewan Geological Survey, vol. 1, pp. 143-150, 2002.
91. Rouviere, P. E. and Chen, M. W. "Isolation of Brachymonas petroleovorans CHX, a novel cyclohexane-degrading beta-proteobacterium," FEMS Microbiology Letters, vol. 227, pp. 101-106, 2003.
92. Ross, J.K., and Bustin, R.M. "The importance of shale composition and pore structure upon gas storage potential of shale gas reservoirs," *Marine and Petroleum Geology*, vol. 26, pp. 916-927, 2009.
93. Rueter, P., Rabus, R., Wilkes, H., Aeckersberg, F., Rainey, F.A., Janasch, H.W., and Widdel, F. "Anaerobic oxidation of hydrocarbons in crude oil by new types of sulphate reducing bacteria," *Nature*, vol. 372, pp. 455-458, 1994.
94. Schoell, M. "Genetic characterization of natural gases," *American Association of Petroleum Geologists Bulletin*, vol. 67, pp. 2225-2238, 1983.

95. Schoell, M. "The hydrogen and carbon isotopic composition of methane from natural gases of various origins," *Geochimica et Cosmichimica Acta*, vol. 44, pp. 649-661, 1980.

96. Schlegel, M.E., Zheng, Z., McIntosh, J., Person, M., and Ballentine, C. "Constraining the timing of microbial methane generation in an organic-rich shale using noble gases, Illinois Basin, USA," *Chemical Geology*, vol. 287, pp. 27-40, 2011.

97. Scott, A.R., Kaiser, W.R., and Ayers Jr., W.B. "Thermogenic and secondary biogenic gases in San Juan basin, Colorado and New Mexico – Implications for coalbed gas producibility," *AAPG Bulletin*, vol. 78, pp. 1186-1209, 1994.

98. Seidle, J.P. "Long-term gas deliverability of a dewatered coalbed," *Journal of Petroleum Technology*, 1993.

99. Shaw, J.C., Reynolds, M.M., and Burke L.H. "Shale Gas Production Potential and Technical Challenges in Western Canada," Paper presented at the Petroleum Society's 7th Canadian International Petroleum Conference, 57th Annual Technical Meeting, Calgary, Alberta, Canada, June 13 – 15, 2006.

100. Shurr, G.W. and Ridgley J.L. "Unconventional Shallow Biogenic Gas Systems," *AAPG Bulletin*, vol. 86, no. 11, pp. 1939-1969, 2002.

101. Smith, J.W., and Pallasser, R.J. "Microbial origin of Australian coalbed methane," *AAPG Bulletin*, vol. 80, no. 6, pp. 891-897, 1996.

102. Snoeyenbos-West, O.L, Nevin, K.P., Anderson, R.T., and Lovley, D.R. "Enrichment of Geobacter Species in Response to Stimulation of Fe(III)

Reduction in Sandy Aquifer Sediments," *Microbial Ecology*, vol. 39, pp. 153-167, 2000.

103. Sondergeld, C.H. "Micro-Structural Studies of Gas Shales," SPE Paper 131771 Presented at the SPE Unconventional Gas Conference, Pittsburgh, Pennsylvania, USA, February, 23-25, 2010.

104. Stanton, B.J., Morris, R.J., and McGowan, C.W. "The characterization of the kerogen of Chattanooga oil shale. Part I-The oxidation of Chattanooga Shale with boiling perchloric acid," *Fuel Processing Technology*, vol. 29 pp. 85-95, 1991.

105. Stasiuk, L.D., and Goodarzi, F. "Organic Petrology of second white speckled shale, Saskatchewan, Canada a possible link between bituminite and biogenic gas?" *Bulletin of Canadian Petroleum Geology*, vol. 36, no. 4, pp. 397-406, 1988.

106. Takai K., Horikoshi, K. "Genetic diversity of archaea in deep-sea hydrothermal vent environments," *Genetics*, vol. 152, pp. 1285-1297, 1999.

107. U.S. Department of Energy. "Undeveloped domestic oil resources: the foundation for increasing oil production and a viable domestic oil industry." Internet:www.fossil.energy.gov/programs/oilgas/eor/Undeveloped_Domestic_Oil_Resources_Provi.html., 2006.

108. Verbarg, S., Rheims, H., Emus, S., Fruhling, A., Kroppenstedt, R.M., Stackebrandt, E., and Schumann, P. "Erysipelothrix inopinata sp. Nov., isolated in the course of sterile filtration of vegetable peptone broth, and description of

Erysipelotrichaceae fam. nov.," *International Journal of Systematic and Evolutionary Microbiology*, vol. 54, no. 1, p. 221-225, 2004.

109. Vugrinovich R. "Relationship between regional hydrogeology and hydrocarbon occurrences in Michigan," vol. 11, no. 4, pp. 429-442, 1988.

110. Water Resistivity Catalogue. [electronic resource]: Rw maps and data for Western Canadian Sedimentary basin and North Dakota, Northern Territories, East Coast. Canadian Well Logging Society, 2002.

111. Wawrik, B., Mendivelso, M., Parisi, V.A., Suflita, J.M., Davidova I.A., Marks C.R., Van Nostrand, J.D., Laign, Y., Zhou, J., Huizinga, B.J., Strapoc, D., and Callaghan, A.V. "Field and laboratory studies on the bioconversion of coal to methane in the San Juan Basin," vol., 81, no. 1, 2012.

112. Wilson, K.C., and Dulofsky, L. J. "Computational Optimization of Shale Resource Development using Reduced-Physics Surrogate Models." Presented at the SPE Western Regional Meeting, 21-23 March 2012, SPE 152946.

113. Whiticar, M. J., "Carbon and hydrogen isotope systematics of bacterial formation and oxidation of methane," *Chemical Geology*, vol. 161, pp. 291-314, 1999.

114. Whiticar, M.J., Faber, E., and Schoell, M. "Biogenic methane formation in marine and fresh-water environments - CO_2 reduction vs acetate fermentation isotope evidence," *Geochimica et Cosmochimica Acta*, vol. 50, pp.693-709, 1986.

115. Worm, P., Plugge, C.M., Stams, A.J., Muller, N., and Schink, B. "Syntrophy in Methanogenic Degradation," in *(Endo)symbiotic Methanogenic*

Archaea. Hackstein, J.H.P., Berlin, Heidelberg: Springer-Verlag, 2010, pp. 143-173.

116. Wust, P.K., Horn, M.A., and Drake, H.L. "Clostridiaceae and Enterobacteriaceae as active fermenters in earthworm gut content," *the International Society of Microbial Ecology Journal*, vol. 5, pp. 92-106, 2011.

117. Yamada, T., Sekiguch, Y., Hanada, S., Imachi, H., Ohashi, A., Harada, H., and Kamagata, Y. "Anaerolinea thermolimosa sp. Nov., Lecilinea saccharolytica gen. nov., sp., nov. and Leptolinea tardivitalis gen. nov., sp. Nov., novel filamentous anaerobes, and description of the new classes Anaerolineae classis nov. and Caldilineae classis nov. in the bacterial phylum Chloroflexi," *International Journal of Systematic Evolutionary Microbiology,* vol. 56, no. 6, 2006.

118. Xing, P., Zheng, J., Li, H., and Liu, Q. "Methanogen genotypes involved in methane formation during anaerobic decomposition of Micrcystis booms at different temperatures," *World Journal of Microbiology and Biotechnology*, 2012.

119. Zengler, K., Richnow, H.R., Rossello-Moro, R., Michaelis, W., and Widdel, F. "Methane formation from long-chain alkanes by anaerobic microorganisms," *Nature*, vol. 401, pp. 266-269, 1999.

120. Zinder S.H.,"Physiological ecology of methanogens," in Methanogenesis Ecology, Physiology, Biochemistry, and Genetics. J.G. Ferry, Ed., Chapman and Hill, pp.128-206, 1993.

APPENDIX A – Contributions to Research

Contributions to Research

a. Articles in or Accepted in Refereed Journals

1. **Cokar, M.,** Kallos, M.S., Gates, I.D. (Accepted October, 2012) Reservoir Simulation of Steam Fracturing in Early Cycle Cyclic Steam Stimulation. *SPE Journal of Reservoir Evaluation and Engineering*. ID: RE-0112-0007, 24pp.
2. **Cokar, M.,** Kallos, M.S., Gates, I.D. (Accepted July, 2012 with revisions) A New Thermogeomechanical Theory for Gravity Drainage in SAGD. Accepted, *SPE Journal,* ID: SJ-02120028.
3. **Cokar, M.,** Ford, B., Kallos, M.S., Gates, I.D. (Accepted June 2012) New Gas Material Balance to Quantify Biogenic Gas Generation Rates from Shallow Organic-Matter-Rich Shales. *FUEL,* vol. 104, pp. 443-451.
4. **Cokar, M.** and Graham, J. (February, 2010) Optimization of SAGD Wellbore Completions: Short Production Tubing String Sensitivities. *SPE Journal of Production & Operations*, vol. 25, no. 1, pp 50-58.

b. Book Chapters

5. Gates, I.D., **Cokar, M.**, Kallos, M.S. (January, 2012) American Association of Petroleum Geologists Special Publication on Oil Sands. Chapter 21: Fundamentals of Heat Transport at the Edge of Steam Chambers in Cyclic Steam Stimulation and Steam-assisted Gravity Drainage. Heavy-oil and oil-sand petroleum systems in Alberta and beyond: *AAPG Studies in Geology* 64, p. 1 – 15.

c. Articles Submitted to Refereed Journals

6. **Cokar, M.,** Wilson, S., Ford, B., Gieg, L.M., Kallos, M.S., Gates, I.D., "Biogeochemical Analysis of Shale Gas Systems Reveals Links Between Geology, Biology and Reservoir Engineering," to be submitted.
7. **Cokar, M.,** Kallos, M.S., Gates, I.D. "Biogenic Shale Gas Reservoirs: Kilometer Scale Biogeochemical Reactors," submitted to *American Institute of Chemical Engineering* ID: AIChe-12-14652, 2012.
8. **Cokar M.,** Ford, B., L., Kallos, M.S., and Gates, I.D. "Reactive Reservoir Simulation of Biogenic Shallow Shale Gas Systems enabled by Experimentally Determined Methane Generation Rates," submitted *to Energy and Fuels* ID: ef-2012-018223, 2012.
9. **Cokar M.,** Kallos, M.S., Gates, I.D. "The social aspects of designing an anaerobic microdigester with combined thermoelectric heat and power generation to convert human excreta to electricity, heat, methane and fertilizer," submitted to the *Journal of Water Sanitation and Hygiene Development*, November 2012.

d. Articles Published and Accepted in Refereed Conferences

10. **Cokar, M.**, Kallos, M.S., Gates, I.D. (October, 2011) Multiscale Probabilistic Mass Transport in Shallow Organic Matter Rich Shales. Canadian Society of Chemical Engineering Conference. London, Ontario.
11. **Cokar, M.**, Kallos M.S., Gates I.D. (June, 2011) Biogenic Potential of Shale Gas and Processes that Stimulates Methanogenesis in Shales. International

Symposium on Applied Microbiology and Molecular Biology in Oil Systems. Calgary, Alberta.

12. **Cokar, M.**, Kallos M.S., Gates I.D. (Mar., 2011) A New Thermogeomechanical Theory for Gravity Drainage in SAGD. World Heavy Oil Congress. Edmonton, Alberta.
13. **Cokar, M.**, Gates, I.D., Kallos, M.S., Larter S., Pedersen, P.K., Huang, H, Laycock, D., Taylor, S., Spencer, R., Allen, N., Thomas, M., Zhao, X., Adamu, M., Aplin, A. (Dec., 2010) Gas Generation and Transport in Shallow Organic-Matter-Rich Shales. AAPG/SEG/SPE/SPWLA Hedberg Conference. Austin, Texas (poster).
14. Pedersen, P.K., Larter, S., Huang, H., Laycock, D., Taylor, S., **Cokar, M.,** Gates, I.D., Spencer, R., Allen, N., Thomas, M., Zhao, X., Adamu, M., Aplin, A. (Dec., 2010) Colorado Group, Western Canada Sedimentary Basin: Controls on a Working Biogenic Shale Gas System. AAPG/SEG/SPE/SPWLA Hedberg Conference. Austin, Texas (poster).
15. **Cokar, M.,** Kallos, M.S., Huang, H., Larter, S.R., and Gates, I.D. (October, 2010) Biogenic Gas Generation from Shallow Organic-Matter-Rich Shales. Canadian Unconventional Resources and International Petroleum Conference. 13pp, Calgary.
16. **Cokar, M.,** Kallos, M.S., Gates, I.D. (April, 2010) Reservoir Simulation of Steam Fracturing in Early Cycle Cyclic Steam Stimulation. SPE Improved Oil Recovery Symposium. 19pp, Tulsa, Oklahoma.

17. **Cokar, M.** and Graham, J. (Oct., 2008) Optimization of SAGD Wellbore Completions: Short Production Tubing String Sensitivities. Int'l Thermal Operations and Heavy Oil Symposium. SPE 117854. 17pp, Calgary, Alberta.
18. Abedi, J., **Cokar, M.,** and Omidyeganeh, O. (June, 2007) Numerical Simulation of the Wind Field around Buildings. 5th International Conference on Computational Heat and Mass Transfer. 6pp, Canmore, Alberta.

APPENDIX B – Experimental Ingredients

Mineral Salts Medium Without Rumen Fluid (McInerney et al., 1979)

The medium that was added into the samples was prepared as follows per 100.0 mL: 5.0 mL of Pfennig I, 5.0 mL Pfennig II, 1.0 mL Wolin metals, 1.0 mL Balch vitamins, 0.1 mL of a 0.1% solution of Resazurin (Sigma-Aldrich, CAS 62758-13-8), 0.005 g of yeast extract (Amresco, J850-500G) and 0.35 g of $NaHCO_3$ ($NaHCO_3$ is used as a buffer in the solution)(EMD Chemicals Inc., CAS 144-55-8). All of the ingredients were mixed together except the $NaHCO_3$. The pH of the system was monitored to ensure it was in between 7.1 – 7.3. The mixture was boiled on a hotplate at a temperature of 325°C for approximately 20 minutes, this helped remove some of the O_2 within the system. The medium was then cooled under 20% CO_2 in N_2. Then the $NaHCO_3$ was added and it was allowed to equilibrate with the gas for a few minutes. Cysteine sulfide was added to the mixture (2.0 mL per 100.0 mL of mixture). The cysteine sulfide was used to reduce the redox potential of the medium to -400 mV. The bottles were then shaken to evenly distribute the cysteine sulfide within the bottles. The medium was autoclaved and sterilized in a 20 min cycle.

Cysteine Sulfide Preparation

Add 1.25 g of NaOH (EMD Chemicals Inc., CAS 1310-73-2) to 200 mL of H_2O. Boil and cool under an N_2 headspace. Now take the mixture into an anaerobic chamber (Vinyl Coy Anaerobic Chamber, 90% N_2:10%CO_2). Dissolve 5 g of cysteine-HCl (Sigma-Aldrich, CAS 345909-32-2) in the NaOH solution, then add the sodium sulfide (Sigma-Aldrich, CAS 1313-84-4) to dissolve.

The ingredients for the Pfennig I, Pfennig II, Wolin metals and Balch Vitamins are listed in Table B1, B2 and B3.

Table B1. Pfennig Mineral Solutions Ingredients

Name	Chemical Name	CAS	Per litre
Pfennig I	K_2HPO_4	7758-11-4	10.0 g
Pfennig II	$MgCl_2$ $6H_2O$	7791-18-6	6.6 g
	NaCl	7647-14-5	8.0 g
	NH_4CL	12125-02-09	8.0 g
	$CaCl_2$ $2H_2O$	10035-04-08	1.0 g

Table B2. Wolin Metals

Chemical Name	CAS	g/L
EDTA	6381-92-6	0.5
$MgSO_4$ 6H2O	10034-99-8	3
$MnSO_4$ H2O	1034-96-5	0.5
NaCl	7647-14-5	1
$CaCl_2$ $2H_2O$	10034-04-08	0.1
$ZnSO_4$ $7H_2O$	7446-20-0	0.1
$CuSO_4$ $7H_2O$	7758-99-8	0.1
Na_2MnO_4 $2H_2O$	10102-40-6	0.01
H_3BO_3	10043-35-3	0.01
Na_2SeO_4	13410-01-0	0.005
$NiCl_2$ $6H_2O$	10101-97-0	0.003

Table B3. Balch Vitamins

Chemical Name	CAS	mg/L
Biotin	58-85-5	2
Folic Acid	59-30-3	2
Pyridoxine-HCl	58-56-0	10
Thiamine-HCl	67-3-8	5
Riboflavin	83-88-5	5
Nicotinic Acid	59-67-6	5
DL Calcium Pantothenate	137-08-6	5
Vitamin B12	68-19-9	0.5
PABA	150-13-0	5
Lipoic Acid	1077-28-	5
Mercaptoehtane-sulfonic acid (MESA)	19767-45-4	5

Organic Extractions for Metabolic Metabolites (Berdugo-Clavijo et al., 2012)

1. Rinse all clean glassware with acetone, and let air dry in the fume hood. This includes separatory funnels, round-bottom flasks, and glass filter funnels.
2. Fold the filter paper in 4, and add enough anhydrous sodium sulfate (Sigma-Aldrich, CAS 7757-82-6) filter paper to ¾ to the top.
3. Add ethyl acetate (Sigma-Aldrich, CAS 141-78-6) 3 x 10 mL of EtOAc. To the acidified sample and shake, pour it into the separatory funnel. Allow the aqueous and solvent layer to separate. Ethyl acetate will be the top layer.
4. Drain the bottom of the aqueous layer back into the same vessel, taking care to not drain out the ethyl acetate layer by closing the stopcock when all the aqueo7us layer has drained out.
5. Drain the ethyl acetate layer through the filter paper containing sodium sulfate, and allow it to collect into the round-bottom flask.
6. Repeat the extraction procedure 2 more times, for a total of 3 times. Rinse the sodium sulfate with several pipets-full of fresh ethyl acetate.
7. Concentrate the collected ethyl acetate layers by rotary evaporation to a volume of about the size of a quarter 1- 2 mL.
8. Quantitatively transfer the concentrated layer into a 4 mL glass vial, rinsing the round-bottom flask a couple o f times with fresh ethyl acetate and adding to the vial.
9. For the core sample use Dichloromethane (VWR International, CAS 75-09-02) instead of the ethyl acetate.

APPENDIX C – CMG STARS™ Simulation Input File

CMG STARS .dat file

```
** 2012-10-09, 8:52:38 PM, cokarm
RESULTS SIMULATOR STARS 201110

INUNIT SI
WSRF WELL 1
WSRF GRID  10
WSRF SECTOR TIME
OUTSRF SPECIAL MATBAL  REACTION 'CH4 bioB'
OUTSRF SPECIAL MATBAL  REACTION 'CH4 bioC'
OUTSRF SPECIAL MATBAL  REACTION 'CH4 bioD'
OUTSRF SPECIAL MATBAL  REACTION 'CH4 bioE'
OUTSRF SPECIAL MATBAL  REACTION 'CH4 bioF'
OUTSRF SPECIAL MATBAL  REACTION 'kerogenE'
OUTSRF SPECIAL MATBAL  REACTION 'kerogenF'
OUTSRF SPECIAL MATBAL  REACTION 'kerogenD'
OUTSRF SPECIAL MATBAL  REACTION 'kerogenC'
OUTSRF SPECIAL MATBAL  REACTION 'kerogenB'

OUTPRN WELL WELLCOMP
OUTPRN GRID PRES TEMP
OUTSRF GRID PRES SG SO SW TEMP W X Y Z
OUTSRF WELL COMPONENT ALL
**WPRN GRID 0
**OUTPRN GRID NONE

WPRN GRID 20
OUTPRN GRID ALL

OUTPRN RES NONE
RESULTS SUBMODEL_REFSS 27566
RESULTS SUBMODEL_REFSS 57853
RESULTS SUBMODEL_REFSS 181
RESULTS SUBMODEL_REFSS 15
RESULTS SUBMODEL_REFSS 10
RESULTS SUBMODEL_REFSS 10
RESULTS SUBMODEL_REFSS 7
RESULTS SUBMODEL_REFSS 27566
**$  Distance units: m
RESULTS XOFFSET           0.0000
RESULTS YOFFSET           0.0000
RESULTS ROTATION           0.0000  **$  (DEGREES)
RESULTS AXES-DIRECTIONS 1.0 1.0 1.0
RESULTS SUBMODEL_REFSS 3
**$ Definition of fundamental corner point grid
GRID CORNER 15 15 114
CORNERS
 682608.4000 2*682625.0667 2*682641.7333 2*682658.4000
2*682675.0667
```

(data removed for space)

```
**$  0 = pinched block, 1 = active block
PINCHOUTARRAY CON            1
**$  0 = null block, 1 = active block
NULL CON            1
POR ALL
 3*0.2816166 3*0.2820237 3*0.2890894 6*0.3 3*0.2816166
3*0.2820237
```

(data removed for space)

```
*MOD

1:15 1:15 1:114 * 0.66
PERMI KVAR
 34*0.218 19*0.197 18*0.269 25*3.155 18*0.407
MOD
6:10 4:12 48:48 = 200
PERMJ EQUALSI
PERMK EQUALSI * 0.25
END-GRID
**$ Model and number of components
**==============================FLUID
DEFINITIONS==================================
**$ Model and number of components

MODEL 14 9 3 1
COMPNAME 'H2O' 'C20H42' 'CH4des' 'CH4 bioB' 'CH4 bioC' 'CH4
bioD' 'CH4 bioE' 'CH4 bioF' 'CH4' 'kerogenE' 'kerogenF'
'kerogenD' 'kerogenC' 'kerogenB'
CMM
0 0.282556 0.01604 0.01604 0.01604 0.01604 0.01604 0.01604
0.01604 1.0928 1.0928 1.0928 1.0928 1.0928
PCRIT
0 1115 4600 4600 4600 4600 4600 4600 4600
TCRIT
0 493.85 -82.55 -82.55 -82.55 -82.55 -82.55 -82.55 -82.55
KVTABLIM 161 4611 5 100
** 161       403       632       754       954      1302
1738      2209      3298      4611
**$ Gas-liquid K Value tables

KVTABLE 'CH4des'
**$
        3.315     2.954     2.554     2.161     1.794
1.638      1.34    1.1197    0.8877     0.478
        3.315     2.954     2.554     2.161     1.794
1.638      1.34    1.1197    0.8877     0.478
GASD-ZCOEF IMPLICIT

SOLID_DEN 'CH4des' 0.66 0 0
SOLID_DEN 'CH4 bioB' 0.66 0 0
SOLID_DEN 'CH4 bioC' 0.66 0 0
SOLID_DEN 'CH4 bioD' 0.66 0 0
SOLID_DEN 'CH4 bioE' 0.66 0 0
```

```
SOLID_DEN 'CH4 bioF' 0.66 0 0
SOLID_DEN 'CH4' 0.66 0 0
SOLID_DEN 'kerogenE' 1158 0 0
SOLID_DEN 'kerogenF' 1158 0 0
SOLID_DEN 'kerogenD' 1158 0 0
SOLID_DEN 'kerogenC' 1158 0 0
SOLID_DEN 'kerogenB' 1158 0 0
MASSDEN
0 800 320.4
CP
0 0 0
CT1
0 0 0
AVG
0 0 0.00010573 0.00010573 0.00010573 0.00010573 0.00010573
0.00010573 0.00010573
BVG
0 0 0.8126 0.8126 0.8126 0.8126 0.8126 0.8126 0.8126
VISCTABLE
**$      temp
            5         0      20e7        14
           10         0      20e7        14
           25         0      20e7        14
**$ Reaction specification


STOREAC
0 0 0 0 0 0 0 0 0 0 0 0 0 1
STOPROD
0 0 0 68.12967581047380 0 0 0 0 0 0 0 0 0 0
FREQFAC 4.95E-3
**$ Reaction specification


STOREAC
0 0 0 0 0 0 0 0 0 0 0 0 1 0
STOPROD
0 0 0 0 68.12967581047380 00 0 0 0 0 0 0 0 0
FREQFAC 2.82E-2
**$ Reaction specification


STOREAC
0 0 0 0 0 0 0 0 0 0 0 1 0 0
STOPROD
0 0 0 0 0 68.12967581047380 0 0 0 0 0 0 0 0
FREQFAC 2.11e-2
**$ Reaction specification


STOREAC
0 0 0 0 0 0 0 0 0 1 0 0 0 0
STOPROD
0 0 0 0 0 0 68.12967581047380 0 0 0 0 0 0 0
```

```
FREQFAC 2.38e-2
**$ Reaction specification


STOREAC
0 0 0 0 0 0 0 0 0 0 1 0 0 0
STOPROD
0 0 0 0 0 0 0 68.12967581047380 0 0 0 0 0 0
FREQFAC 1.74e-2

ROCKFLUID
RPT 1 WATWET
**$        Sw       krw      krow
SWT
          0.0       0.0       1.0
          1.0       1.0       0.0
**$        Sl       krg      krog
SLT
          0.0       0.5       0.0
          1.0       0.0       1.0
**SWR 0.15
**SOIRW 0.10
**SGR 0.10

INITIAL
VERTICAL DEPTH_AVE

INITREGION 1
REFPRES 3200
REFDEPTH -215
SW ALL
 3*0.4339034 3*0.4380528 3*0.423582 3*0.4438123 3*0.4339217
3*0.4339034


SO CON       0.0001
SG ALL
 3*0.5659966 3*0.5618472 3*0.576318 3*0.5560877 3*0.5659783
3*0.5659966


MFRAC_GAS 'CH4' CON           1
CONC_SLD 'kerogenB' KVAR
 34*1.36 80*0
CONC_SLD 'kerogenC' KVAR
 34*0 19*1.15 61*0
CONC_SLD 'kerogenD' KVAR
 53*0 18*1.21 43*0
CONC_SLD 'kerogenE' KVAR
 71*0 25*1.41 18*0
CONC_SLD 'kerogenF' KVAR
 96*0 18*1.59
MFRAC_OIL 'C20H42' CON          0.9
MFRAC_OIL 'CH4des' CON          0.1
```

```
NUMERICAL
**MATBALTOL 1.0E-4
NORM PRESS 1000
CONVERGE TOTRES LOOSE
UPSTREAM KLEVEL
NORTH 300
ITERMAX 300
MINPRES 10
DTMIN 1E-12
TFORM ZT
ISOTHERMAL
NEWTONCYC 30


RUN
DATE 2004 8 1
DTWELL 1e-006
**$
WELL  'Producer'  FRAC  1.
PRODUCER 'Producer'
OPERATE  MIN  BHP  1100.  CONT
**$ UBA       ff  Status  Connection
**$ UBA      ff  Status  Connection
**$          rad  geofac  wfrac  skin
GEOMETRY  K  0.086  0.249  1.  0.
PERF  GEOA  'Producer'
**$ UBA     ff  Status  Connection
    8 8 36  1.  OPEN    FLOW-TO  'SURFACE'  REFLAYER
    8 8 37  1.  OPEN    FLOW-TO  1
    8 8 38  1.  OPEN    FLOW-TO  2
    8 8 39  1.  OPEN    FLOW-TO  3
    8 8 40  1.  OPEN    FLOW-TO  4
    8 8 43  1.  OPEN    FLOW-TO  5
    8 8 44  1.  OPEN    FLOW-TO  6
    8 8 46  1.  OPEN    FLOW-TO  7
    8 8 47  1.  OPEN    FLOW-TO  8
    8 8 48  1.  OPEN    FLOW-TO  9
    8 8 52  1.  OPEN    FLOW-TO  10
    8 8 53  1.  OPEN    FLOW-TO  11
    8 8 54  1.  OPEN    FLOW-TO  12
    8 8 55  1.  OPEN    FLOW-TO  13
    8 8 56  1.  OPEN    FLOW-TO  14
    8 8 57  1.  OPEN    FLOW-TO  15
    8 8 71  1.  OPEN    FLOW-TO  16
    8 8 72  1.  OPEN    FLOW-TO  17
    8 8 73  1.  OPEN    FLOW-TO  18
    8 8 74  1.  OPEN    FLOW-TO  19
    8 8 75  1.  OPEN    FLOW-TO  20
    8 8 78  1.  OPEN    FLOW-TO  21
    8 8 79  1.  OPEN    FLOW-TO  22
    8 8 80  1.  OPEN    FLOW-TO  23
    8 8 81  1.  OPEN    FLOW-TO  24
    8 8 82  1.  OPEN    FLOW-TO  25
```

```
    8 8 83  1.  OPEN    FLOW-TO  26
    8 8 84  1.  OPEN    FLOW-TO  27

time 1.1

(data removed for space)

DATE 2009 1  1.00000


**$
WELL  'Producer'  FRAC  1.
PRODUCER 'Producer'
OPERATE  MIN  BHP  1100.  CONT
**$ UBA       ff  Status  Connection
**$ UBA      ff  Status  Connection
**$          rad  geofac  wfrac  skin
GEOMETRY  K  0.086  0.249  1.  1.
PERF  GEOA  'Producer'
(data removed for space)

DATE 2009 2  1.00000
WELL  'Producer'  FRAC  1.
PRODUCER 'Producer'
OPERATE  MIN  BHP  1100.  CONT
**$ UBA       ff  Status  Connection
**$ UBA      ff  Status  Connection
**$          rad  geofac  wfrac  skin
GEOMETRY  K  0.086  0.249  1.  1.1
PERF  GEOA  'Producer'
**$ UBA     ff  Status  Connection
    (data removed for space)
DATE 2009 3  1.00000
WELL  'Producer'  FRAC  1.
PRODUCER 'Producer'
OPERATE  MIN  BHP  1100.  CONT
**$ UBA       ff  Status  Connection
**$ UBA      ff  Status  Connection
**$          rad  geofac  wfrac  skin
GEOMETRY  K  0.086  0.249  1.  1.2
PERF  GEOA  'Producer'
**$ UBA     ff  Status  Connection
(data removed for space)
DATE 2009 4  1.00000
WELL  'Producer'  FRAC  1.
PRODUCER 'Producer'
OPERATE  MIN  BHP  1100.  CONT
**$ UBA       ff  Status  Connection
**$ UBA      ff  Status  Connection
**$          rad  geofac  wfrac  skin
GEOMETRY  K  0.086  0.249  1.  1.3
PERF  GEOA  'Producer'
(data removed for space)
```

```
DATE 2009 5  1.00000
WELL  'Producer'  FRAC  1.
PRODUCER 'Producer'
OPERATE  MIN  BHP  1100.  CONT
**$ UBA       ff  Status  Connection
**$ UBA      ff  Status  Connection
**$          rad  geofac  wfrac  skin
GEOMETRY  K  0.086  0.249  1.  1.4
PERF  GEOA  'Producer'
(data removed for space)

DATE 2009 6  1.00000
WELL  'Producer'  FRAC  1.
PRODUCER 'Producer'
OPERATE  MIN  BHP  1100.  CONT
**$ UBA       ff  Status  Connection
**$ UBA      ff  Status  Connection
**$          rad  geofac  wfrac  skin
GEOMETRY  K  0.086  0.249  1.  1.5
PERF  GEOA  'Producer'
(data removed for space)

DATE 2009 7  1.00000
WELL  'Producer'  FRAC  1.
PRODUCER 'Producer'
OPERATE  MIN  BHP  1100.  CONT
**$ UBA       ff  Status  Connection
**$ UBA      ff  Status  Connection
**$          rad  geofac  wfrac  skin
GEOMETRY  K  0.086  0.249  1.  1.6
PERF  GEOA  'Producer'
**$ UBA     ff  Status  Connection
(data removed for space)

DATE 2009 8  1.00000
WELL  'Producer'  FRAC  1.
PRODUCER 'Producer'
OPERATE  MIN  BHP  1100.  CONT
**$ UBA       ff  Status  Connection
**$ UBA      ff  Status  Connection
**$          rad  geofac  wfrac  skin
GEOMETRY  K  0.086  0.249  1.  1.7
PERF  GEOA  'Producer'
**$ UBA     ff  Status  Connection
(data removed for space)

DATE 2009 9  1.00000
WELL  'Producer'  FRAC  1.
PRODUCER 'Producer'
OPERATE  MIN  BHP  1100.  CONT
**$ UBA       ff  Status  Connection
**$ UBA      ff  Status  Connection
**$          rad  geofac  wfrac  skin
GEOMETRY  K  0.086  0.249  1.  1.8
```

```
PERF  GEOA  'Producer'
**$ UBA     ff  Status  Connection
(data removed for space)

DATE 2009 10  1.00000
WELL  'Producer'  FRAC  1.
PRODUCER 'Producer'
OPERATE  MIN  BHP  1100.  CONT
**$ UBA       ff  Status  Connection
**$ UBA      ff  Status  Connection
**$          rad  geofac  wfrac  skin
GEOMETRY  K  0.086  0.249  1.  1.9
PERF  GEOA  'Producer'
**$ UBA     ff  Status  Connection
(data removed for space)

DATE 2009 11  1.00000
WELL  'Producer'  FRAC  1.
PRODUCER 'Producer'
OPERATE  MIN  BHP  1100.  CONT
**$ UBA       ff  Status  Connection
**$ UBA      ff  Status  Connection
**$          rad  geofac  wfrac  skin
GEOMETRY  K  0.086  0.249  1.  2.
PERF  GEOA  'Producer'
**$ UBA     ff  Status  Connection
(data removed for space)

DATE 2009 12  1.00000
WELL  'Producer'  FRAC  1.
PRODUCER 'Producer'
OPERATE  MIN  BHP  1100.  CONT
**$ UBA       ff  Status  Connection
**$ UBA      ff  Status  Connection
**$          rad  geofac  wfrac  skin
GEOMETRY  K  0.086  0.249  1.  2.1
PERF  GEOA  'Producer'
**$ UBA     ff  Status  Connection
(data removed for space)

WSRF GRID TNEXT

DATE 2010 1  1.00000
WELL  'Producer'  FRAC  1.
PRODUCER 'Producer'
OPERATE  MIN  BHP  1100.  CONT
**$ UBA       ff  Status  Connection
**$ UBA      ff  Status  Connection
**$          rad  geofac  wfrac  skin
GEOMETRY  K  0.086  0.249  1.  2.2
PERF  GEOA  'Producer'
**$ UBA     ff  Status  Connection
(data removed for space)
```

```
DATE 2010 2  1.00000
WELL  'Producer'  FRAC  1.
PRODUCER 'Producer'
OPERATE  MIN  BHP  1100.  CONT
**$ UBA       ff  Status  Connection
**$ UBA      ff  Status  Connection
**$          rad  geofac  wfrac  skin
GEOMETRY  K  0.086  0.249  1.  2.3
PERF  GEOA  'Producer'
**$ UBA     ff  Status  Connection
```
(data removed for space)

```
DATE 2010 3  1.00000
WELL  'Producer'  FRAC  1.
PRODUCER 'Producer'
OPERATE  MIN  BHP  1100.  CONT
**$ UBA       ff  Status  Connection
**$ UBA      ff  Status  Connection
**$          rad  geofac  wfrac  skin
GEOMETRY  K  0.086  0.249  1.  2.4
PERF  GEOA  'Producer'
**$ UBA     ff  Status  Connection
```
(data removed for space)

```
DATE 2010 4  1.00000
WELL  'Producer'  FRAC  1.
PRODUCER 'Producer'
OPERATE  MIN  BHP  1100.  CONT
**$ UBA       ff  Status  Connection
**$ UBA      ff  Status  Connection
**$          rad  geofac  wfrac  skin
GEOMETRY  K  0.086  0.249  1.  2.5
PERF  GEOA  'Producer'
**$ UBA     ff  Status  Connection
```
(data removed for space)

```
DATE 2010 5  1.00000
WELL  'Producer'  FRAC  1.
PRODUCER 'Producer'
OPERATE  MIN  BHP  1100.  CONT
**$ UBA       ff  Status  Connection
**$ UBA      ff  Status  Connection
**$          rad  geofac  wfrac  skin
GEOMETRY  K  0.086  0.249  1.  2.6
PERF  GEOA  'Producer'
**$ UBA     ff  Status  Connection
```
(data removed for space)

```
DATE 2010 6  1.00000
WELL  'Producer'  FRAC  1.
PRODUCER 'Producer'
OPERATE  MIN  BHP  1100.  CONT
**$ UBA       ff  Status  Connection
**$ UBA      ff  Status  Connection
```

```
**$          rad  geofac  wfrac  skin
GEOMETRY  K  0.086  0.249  1.  2.7
PERF  GEOA  'Producer'
**$ UBA     ff  Status  Connection
(data removed for space)

DATE 2010 7  1.00000
WELL  'Producer'  FRAC  1.
PRODUCER 'Producer'
OPERATE  MIN  BHP  1100.  CONT
**$ UBA       ff  Status  Connection
**$ UBA      ff  Status  Connection
**$          rad  geofac  wfrac  skin
GEOMETRY  K  0.086  0.249  1.  2.8
PERF  GEOA  'Producer'
**$ UBA     ff  Status  Connection
(data removed for space)

DATE 2010 8  1.00000
WELL  'Producer'  FRAC  1.
PRODUCER 'Producer'
OPERATE  MIN  BHP  1100.  CONT
**$ UBA       ff  Status  Connection
**$ UBA      ff  Status  Connection
**$          rad  geofac  wfrac  skin
GEOMETRY  K  0.086  0.249  1.  2.9
PERF  GEOA  'Producer'
**$ UBA     ff  Status  Connection
(data removed for space)
DATE 2010 9  1.00000
WELL  'Producer'  FRAC  1.
PRODUCER 'Producer'
OPERATE  MIN  BHP  1100.  CONT
**$ UBA       ff  Status  Connection
**$ UBA      ff  Status  Connection
**$          rad  geofac  wfrac  skin
GEOMETRY  K  0.086  0.249  1.  3.
PERF  GEOA  'Producer'
**$ UBA     ff  Status  Connection
(data removed for space)

DATE 2010 10  1.00000
WELL  'Producer'  FRAC  1.
PRODUCER 'Producer'
OPERATE  MIN  BHP  1100.  CONT
**$ UBA       ff  Status  Connection
**$ UBA      ff  Status  Connection
**$          rad  geofac  wfrac  skin
GEOMETRY  K  0.086  0.249  1.  3.1
PERF  GEOA  'Producer'
**$ UBA     ff  Status  Connection
(data removed for space)

DATE 2010 11  1.00000
```

```
WELL  'Producer'  FRAC  1.
PRODUCER 'Producer'
OPERATE  MIN  BHP  1100.  CONT
**$ UBA       ff  Status  Connection
**$ UBA      ff  Status  Connection
**$          rad  geofac  wfrac  skin
GEOMETRY  K  0.086  0.249  1.  3.2
PERF  GEOA  'Producer'
**$ UBA     ff  Status  Connection
```
(data removed for space)

```
DATE 2010 12  1.00000
WELL  'Producer'  FRAC  1.
PRODUCER 'Producer'
OPERATE  MIN  BHP  1100.  CONT
**$ UBA       ff  Status  Connection
**$ UBA      ff  Status  Connection
**$          rad  geofac  wfrac  skin
GEOMETRY  K  0.086  0.249  1.  3.3
PERF  GEOA  'Producer'
**$ UBA     ff  Status  Connection
```
(data removed for space)

```
WSRF GRID TNEXT
DATE 2011 1  1.00000
WELL  'Producer'  FRAC  1.
PRODUCER 'Producer'
OPERATE  MIN  BHP  1100.  CONT
**$ UBA       ff  Status  Connection
**$ UBA      ff  Status  Connection
**$          rad  geofac  wfrac  skin
GEOMETRY  K  0.086  0.249  1.  3.4
PERF  GEOA  'Producer'
**$ UBA     ff  Status  Connection
```
(data removed for space)

```
DATE 2011 2  1.00000
WELL  'Producer'  FRAC  1.
PRODUCER 'Producer'
OPERATE  MIN  BHP  1100.  CONT
**$ UBA       ff  Status  Connection
**$ UBA      ff  Status  Connection
**$          rad  geofac  wfrac  skin
GEOMETRY  K  0.086  0.249  1.  3.5
PERF  GEOA  'Producer'
**$ UBA     ff  Status  Connection
```
(data removed for space)

```
DATE 2011 3  1.00000
WELL  'Producer'  FRAC  1.
PRODUCER 'Producer'
OPERATE  MIN  BHP  1100.  CONT
**$ UBA       ff  Status  Connection
**$ UBA      ff  Status  Connection
```

```
**$          rad  geofac  wfrac  skin
GEOMETRY  K  0.086  0.249  1.  3.6
PERF  GEOA  'Producer'
**$ UBA     ff  Status  Connection
(data removed for space)

DATE 2011 4  1.00000
WELL  'Producer'  FRAC  1.
PRODUCER 'Producer'
OPERATE  MIN  BHP  1100.  CONT
**$ UBA       ff  Status  Connection
**$ UBA      ff  Status  Connection
**$          rad  geofac  wfrac  skin
GEOMETRY  K  0.086  0.249  1.  3.7
PERF  GEOA  'Producer'
**$ UBA     ff  Status  Connection
(data removed for space)

DATE 2011 5  1.00000
WELL  'Producer'  FRAC  1.
PRODUCER 'Producer'
OPERATE  MIN  BHP  1100.  CONT
**$ UBA       ff  Status  Connection
**$ UBA      ff  Status  Connection
**$          rad  geofac  wfrac  skin
GEOMETRY  K  0.086  0.249  1.  3.8
PERF  GEOA  'Producer'
**$ UBA     ff  Status  Connection
(data removed for space)

DATE 2011 6  1.00000
WELL  'Producer'  FRAC  1.
PRODUCER 'Producer'
OPERATE  MIN  BHP  1100.  CONT
**$ UBA       ff  Status  Connection
**$ UBA      ff  Status  Connection
**$          rad  geofac  wfrac  skin
GEOMETRY  K  0.086  0.249  1.  3.9
PERF  GEOA  'Producer'
**$ UBA     ff  Status  Connection

DATE 2011 7  1.00000
WELL  'Producer'  FRAC  1.
PRODUCER 'Producer'
OPERATE  MIN  BHP  1100.  CONT
**$ UBA       ff  Status  Connection
**$ UBA      ff  Status  Connection
**$          rad  geofac  wfrac  skin

GEOMETRY  K  0.086  0.249  1.  4.
PERF  GEOA  'Producer'
**$ UBA     ff  Status  Connection
(data removed for space)
```

```
DATE 2011 8  1.00000
ALTER 'Producer'
    1100.
DATE 2011 9  1.00000
ALTER 'Producer'
    1100.
DATE 2011 10  1.00000
ALTER 'Producer'
    1100.
DATE 2011 11  1.00000
ALTER 'Producer'
    1100.
DATE 2011 12  1.00000
WSRF GRID TNEXT
STOP
```

APPENDIX D – Other Journal Papers

This section contains three publications that were written during the duration of the thesis and include research that was completed that was not directly related to the thesis. These papers have been included because although they are not directly related to the thesis, they are loosely related to the topic of both methane generation and unconventional reservoirs. The first paper is a social study on the social impact of an anaerobic microdigester with combined thermoelectric heat and power generation to convert human excreta to electricity, heat, methane and fertilizer. The second paper has been accepted into the *SPE Journal of Reservoir Engineering and Evaluation,* and the last paper has been accepted with revisions to the *SPE Journal*. These last two papers pertain to unconventional heavy oil reservoirs in northern Alberta.

Cokar M., Kallos, M.S., Gates, I.D. "The social aspects of designing an anaerobic microdigester with combined thermoelectric heat and power generation to convert human excreta to electricity, heat, methane and fertilizer," submitted to the Journal of Water Sanitation and Hygiene Development, November 2012.

THE SOCIAL ASPECTS OF DESIGNING AN ANAEROBIC MICRODIGESTER WITH COMBINED THERMOELECTRIC HEAT AND POWER GENERATION TO CONVERT HUMAN EXCRETA TO ELECTRICITY, HEAT, METHANE AND FERTILIZER

ABSTRACT

More than 894 million people do not have access to clean water sources and as a result, 1.6 million children die each year from diseases caused by fecal-oral contamination. Due to poor sanitation practices worldwide roughly two billion people use non-sewered or non-piped sanitation systems that often pollute the water supplies. The solution to this problem is two-fold. The first and most important part is the social aspect of the problem. This includes establishing an adoption plan for the technology in the target community to ensure it is used as intended and not abandoned or scavenged for parts or other uses. Adoption also includes affordability and practicality of the design (local manufacture), and spreading knowledge of how to improve existing sanitary practices. The second part of the solution is the actual technical design of the unit to fit the community where it is to be implemented. To better understand the social and economic aspects of a proposed unit, we interviewed rural and urban individuals in Faisalabad, Pakistan. The results of this survey were used as the basis for a modified engineering design we are currently testing. As a result of the information that was gained from the survey, a very simple engineering design of the unit was created that can be built with limited technology and is practical for the Asian subcontinent. The design is of a single modular unit that will be able to produce heat, electricity, fertilizer, and methane from human excreta. The unit is small in size so that it may fit in any location within a house to enable familial adoption, and it is also simple in design so that it only requires basic maintenance for proper use. Currently there are other more complicated systems that convert human excreta to methane gas, however this unit is unique in the sense that it can be used at the household level both safely and affordably. It is evident that the social aspects of this project, not the technical, dictate the majority of the engineering design constraints of the unit. Finally, once the unit is implemented on site, social work needs to be established to ensure the proper use of the unit and also to determine how well the engineered unit is doing on site.

INTRODUCTION

Currently there are 4.2 billion people around the world that are in need of improved sanitation (Mara, 2003). As a result millions of people worldwide are dying because of lack of clean drinking water due to human waste entering under water streams, as well as the spread of diseases caused by fecal-oral contamination. Most of the disease causing pathogens that are inside drinking water and that are passed on through drinking water are principally of fecal origin (Ashbolt et al., 2001; Hunter et al., 2002). Over 2.6 billion people worldwide live without access to a clean and safe toilet. Diarrheal diseases caused by poor sanitation kill more children than AIDS, malaria, and measles combined (Coombes, 2010). Fecal-oral diseases are a major killer today and about two children under the age of five years dies each minute due to these diseases. Diarrhea in infancy not only can lead to malnutrition, it can also lead to poor cognitive function later on in a child's life (Mara, 2003).

Water and excreta related diseases also have an effect on a countries economy. It is estimated that 360-400 billion working days were lost in developing countries due to fecal-oral diseases keeping people away from work (Pearce, 1993). It is estimated that in Pakistan alone loss of sanitation costs the country 3.9% of its GDP.

The types of water sanitation and toilets developed in North America and other industrialized nations are inadequate for developing nations. Flush toilets on average use about 70 L/person/day of water (Gleick, 1996). So for a population the size of Canada which is about 34 million people that is approximately 2.38 billion liters of water per day just to flush the toilet. This water usage is not practical in many areas, because water is very rare, and there is no infrastructure in place for piping. Also, the throne architecture developed by Thomas Crapper (1884) has been adopted in the Western world but has not been largely adopted in Eastern countries such as China, India, Pakistan, and other Eastern Asian nations. Thus, it is required that new technology to deal with handling of human excreta must be sensitive to the cultures, history, and current practice of waste handling. A Western solution is not necessarily an Eastern one.

The main purpose of the study reported here was to understand the social needs and adoption issues that will be confronted by introducing new toilet technology to people in developing nations. Often times the hardest part of implementing and introducing a new technology in a specific environment is not the actual technology but the social acceptance of the technology.

MATERIALS AND METHODS

Study Population and Setting

The survey developed for this research was conducted in five communities in the city of Faisalabad, Pakistan shown in Figure 1. Pakistan is the sixth largest country in the world by population, with a population of more than 190 million people. The median age of the citizens is 21.9 years of age with a life expectancy of about 66 years. About 36% of the population lives in urban environments, whereas the majority lives in rural environments. The major infectious diseases in Pakistan are often due to poor sanitation practices and lack of clean drinking water due to ground water contamination. Common waterborne and food related illnesses are bacterial diarrhea, Hepatitis A and E, and Typhoid Fever. Literacy within the country is equal to about 54.9% with a large disparity between men and women. Male literacy rates are equal to about 68.6% whereas female literacy rates are around 40.3%. To better understand the economics of the country, the GDP per capita is approximately equal to $2,800 a year, which ranks 174 in the world out of 226 countries (CIA-Factbook, 2012).

The population of Faisalabad is approximately equal to 2.8 million; this is the third largest metropolis in Pakistan located in the province of Punjab. The climate can see extremes ranging from a maximum temperature of 50 °C during the summer months to a minimum of -2°C in the winter. The mean maximum and minimum temperature in the summer months range between 39 to 27°C whereas in the winter they range between 17 and 6°C (It's Pakistan, 2012). Over 91 million people in Pakistan live without improved sanitation (UNICEF & WHO, 2012). Thus, Pakistan is an ideal target nation for new technology to safely handle human excreta. To conduct the survey, a researcher (capable of speaking Urdu) was sent to Faisalabad, Pakistan in November 2011.

Figure 1: Map of Pakistan with the city of Faisalabad highlighted above (CIA Factbook, 2008).

Sampling Procedure

The survey consisted of 20 simple to answer questions that were written in Urdu which is the local language used for reading and writing in Faisalabad. The survey was translated by the researcher that was sent out to Faisalabad, and it was typed in Urdu and individually given out to each participant. Ethics approval from the University of Calgary was granted to carry out the survey. The survey was distributed among middle class families of Faisalabad, and no more than one survey per household was given out. The participants that took the survey were literate and the survey was completed in privacy without any influence of the researcher. The age of the participants ranged between 4 and 70+.

Prior to conducting the survey we had performed a sample size calculation. Assuming we wanted to determine the responses for 91,000,000 Pakistan citizens without access to proper hygiene, with 95% confidence with a confidence interval of 8% we would need a sample size of 150. We surveyed 196 people (154 male, 42 female), giving us a confidence interval of 7% (results presented as percent of population are +/- 7%).

Questionnaire

The following is a list of the 20 questions that were asked in the survey.

1. What is your gender?
2. What is your age?
3. Do you live in the city or the village?
4. What is the name of your city or village?
5. How many people live in your household?
6. What type of toilet do you use?
7. Typically how many times a day do you defecate?
8. How many hours a day is electricity unavailable in your home?
9. How many hours a day is gas unavailable in your home?
10. If you had a toilet that creates electricity, gas and fertilizer without any ongoing cost would you use it?
11. If no why?
12. Would you be willing to purchase this type of toilet?
13. If no why?
14. What is the reasonable cost of this type of toilet?
15. If you had one electronic device that you cannot live without what would it be?
16. If you had one device that runs on gas that you cannot live without what would it be?
17. How many animals do you have in your house? And what types?
18. What do you do with the animal waste?
19. What do you do with your kitchen scraps like fruit and vegetable peels?
20. Additional comments?

Out of all of the surveys that were distributed 196 were returned and analyzed.

RESULTS AND DISCUSSION

Demographics and Baseline Data

The following sections highlight the results of the survey. Figure 2 shows the number of people living in each household for both the city and the village. As can be seen the average family size of people living in a household is typically larger than that found in North America. This is because the family is living as an extended family often with grandchildren and grandparents in the house. Also, on average each woman gives birth to about 3 children, as compared to countries like Canada and the United States it is 1.59 to 2.09 children per mother (CIA Factbook, 2012). There is no significant difference between the number of people living in each household in the city or the village as shown in Figure 2.

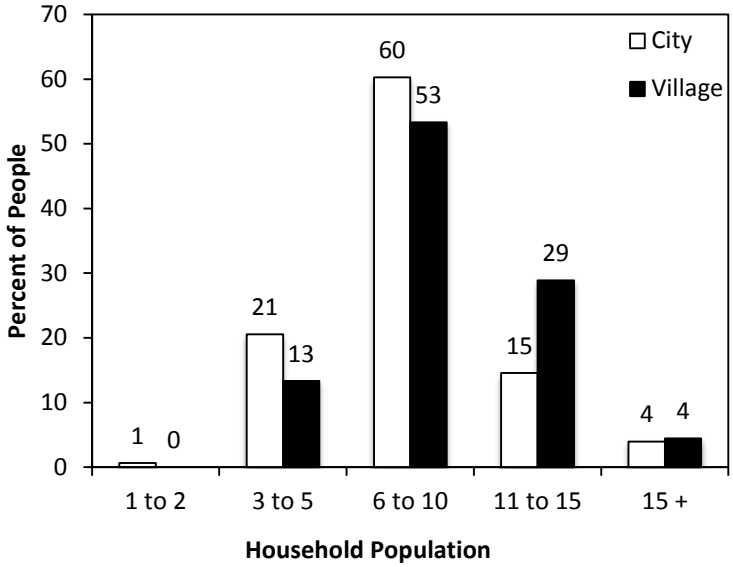

Figure 2: The percent of respondents that stated how many people are living in their home answering the question: Q5: How many people live in your household? (n = 96 responses).

Figures 3 and 4 below show the number of defecations per day for males and females. As shown in Figure 3 most individuals defecate 2 to 3 times daily, also the number of defecations per day between males and females is also approximately the same. This is valuable information that can be used to size out a toilet for this region.

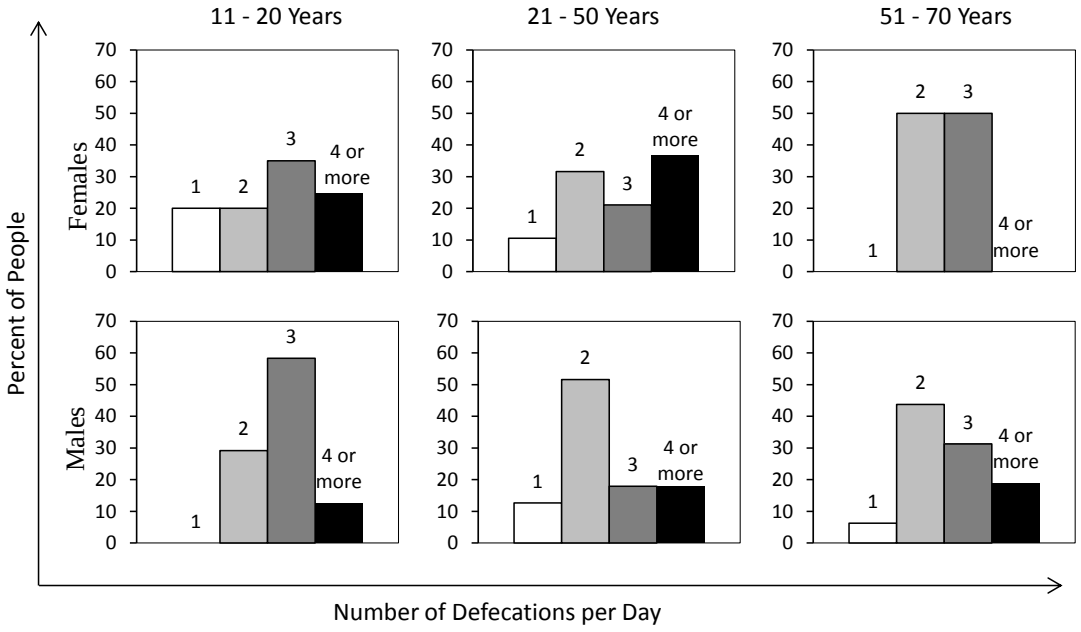

Figure 3: The percent of respondents that answered to the number of defecations per day for males and females between the age of 11 and 70 years answering to the question: Q7: Typically how many times a day do you defecate? (n = 151 responses).

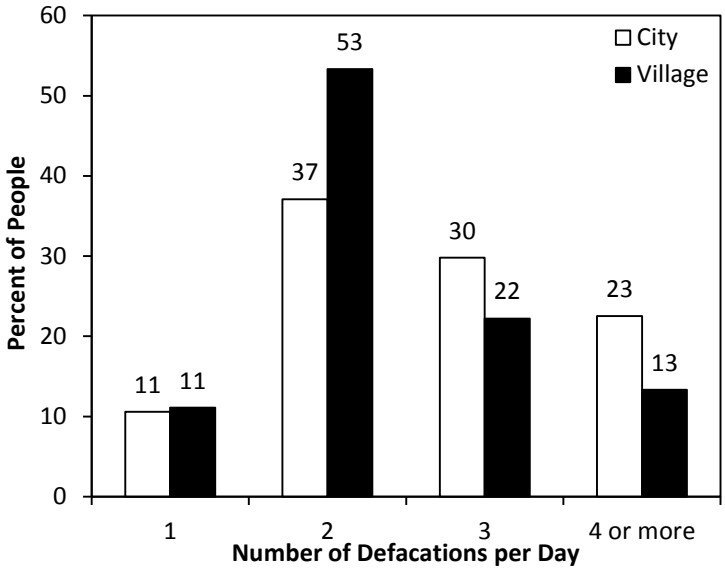

Figure 4: Percent of respondents that answered to the number of defecations per day for people living in the city and village answering to the question: Q7: Typically how many times a day do you defecate? (n = 196 responses).

Figure 5 below shows the methods used for capture of human excreta. For both city and village dwellers it can be seen that preference to a squat toilet, displayed in Figure 6, is given over a sitting (Western throne) toilet. After talking with the participants in the survey it is clear that because the social norm is to use a squat toilet participants also feel that it is more sanitary because no body parts come into physical contact with the toilet.

It is estimated that in Pakistan over 40 million people still practice open defecation. About 4% of the urban population and 34% if the rural population practice open defecation (UNICEF and WHO, 2012), and this is a huge sanitary problem. The data presented in this study shows that approximately 25% of village dwellers and < 2% of city dwellers practice open defecation.

When survey participants were asked whether they would use a toilet that created electricity, gas, and fertilizer, the response was unanimously yes (data not shown). People were very responsive to the idea and they were actually quite surprised that a toilet could produce so many useable things.

Also, another very important point is that people in this area do not use toilet paper to clean themselves as they use the toilets. Due to cultural and religious practices they use water to clean themselves after they have used the toilet to defecate or urinate. However, when water is unavailable then they often resort to leaves or mud.

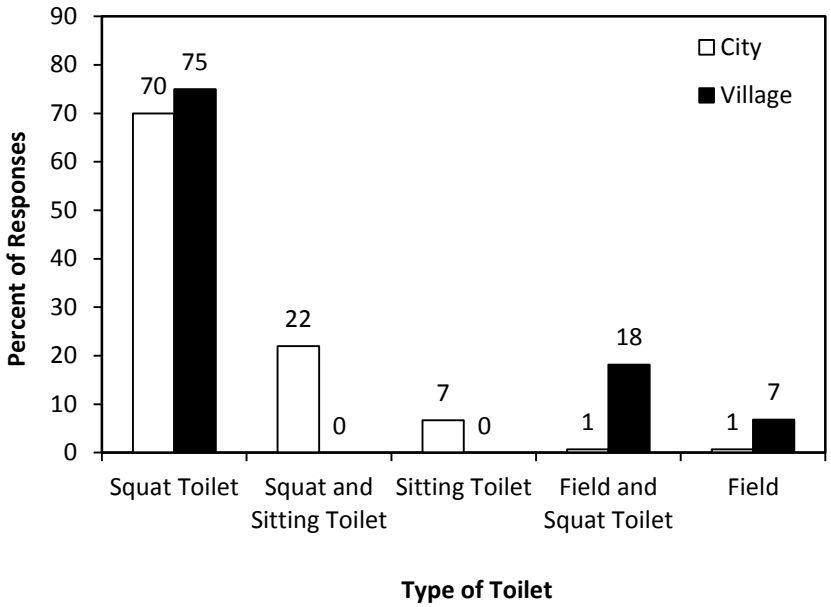

Figure 5: Percent of respondents answering to the method of human waste disposal for the city and village answering to the question: Q6: What type of toilet do you use? (n = 194 responses).

Figure 6: Typical squat toilet in Pakistan.

The average household income for low income families is less than 100 Canadian dollars a month to about 1,000 Canadian dollars for upper middle class families. About one-fifth (22%) of the population lives below the poverty line. The income disparity is quite large and the upper class can make up to several hundred to a few thousand Canadian dollars a month. Figure 7 below shows the amount of money the participants are willing to pay for such a toilet if it were to be sold. This gives an indication of the value perceived for the toilet.

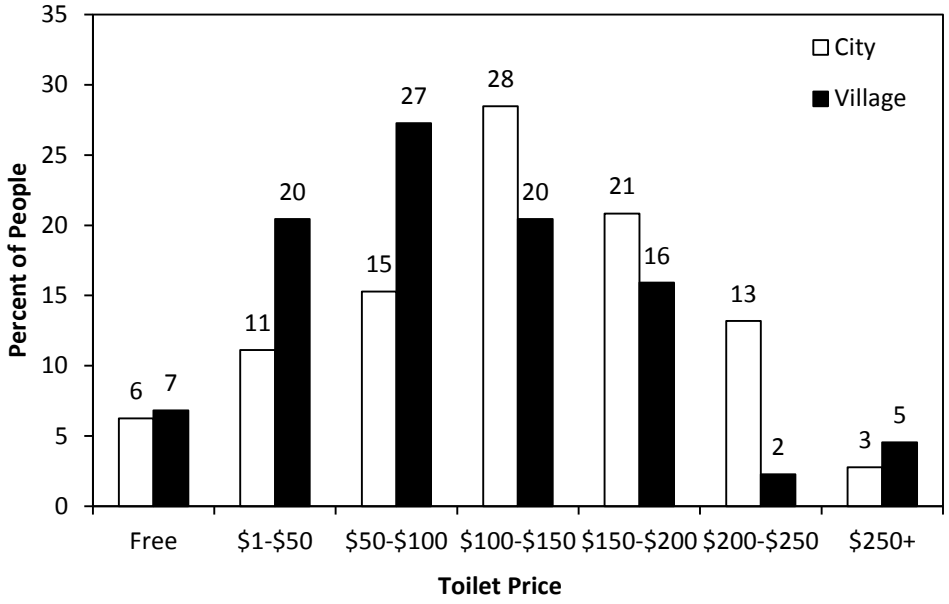

Figure 7: Percent of people answering to the price in Canadian dollars people are willing to pay for the toilet answering to the question: Q14: What is the reasonable cost of this type of toilet? (n = 188 responses).

Although both electricity and gas is widely available in the city, as seen in Figures 8 and 10, each day, electricity and gas supplies are shutdown for several hours. The cause for this is a shortage of resources in the country as well as political problems within the area.

However, as shown in Figure 10, gas is often unavailable in the villages. The gas line infrastructure is not in place to allow gas into the more remote areas. Here the locals are dependent on using cow patties and other sources of fuel to cook their food and warm their houses in the winter.

Figures 9 and 11 reveal which electrical or gas appliance they cannot afford to live without. For electrical device basics, the house fan and motor for the water pump were at the top of the list. Most of the homes in Faisalabad use underground water sources thus requiring a water motor to pump the water from underground aquifers to a container on the roof or higher up where it can be later used. For gas appliances, as shown in Figure 11, a gas stove was the main device that people could not live without since it provides them with the ability to cook food.

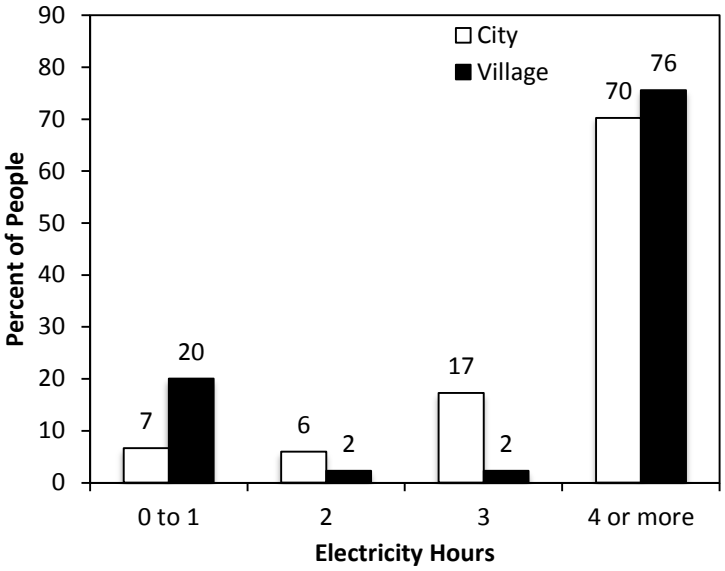

Figure 8: Percent of people answering to the number of hours each day electricity is unavailable in the home answering to the question: Q8: How many hours a day is electricity unavailable in your home? (n = 196 responses).

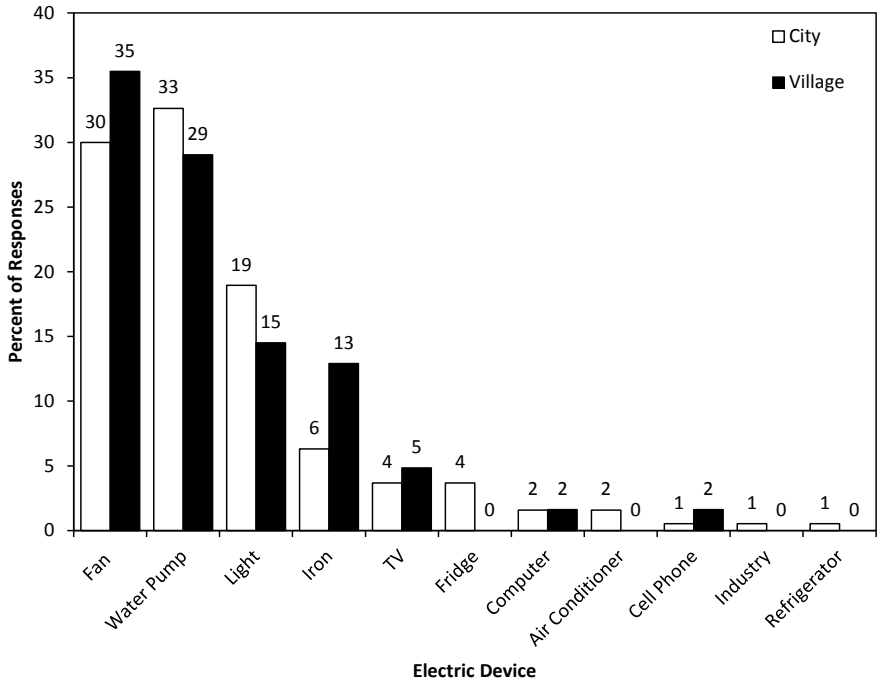

Figure 9: The percent of respondents listing a particular electrical device that they wrote down answering the question: Q15: If you had one electronic device that you cannot live without what would it be? (n= 252 responses).

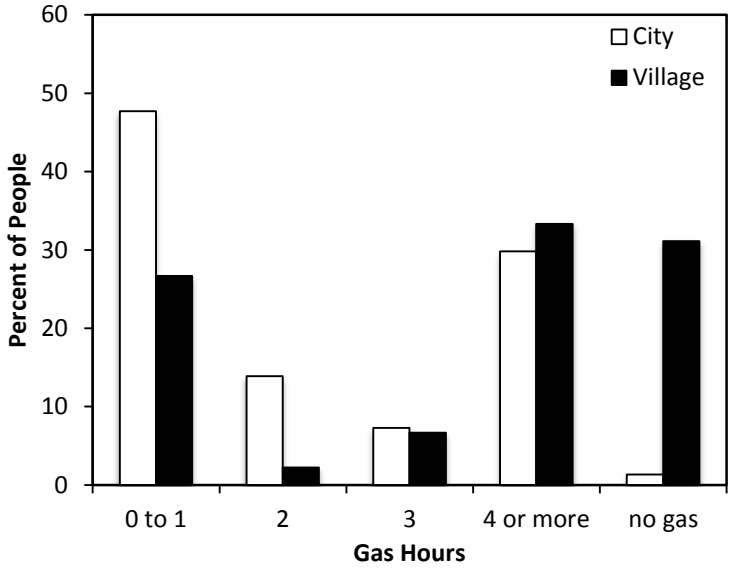

Figure 10: Percent of people answering to the number of hours each day gas is unavailable in the home answering to the question: Q9: How many hours a day is gas unavailable in your home? (n = 196 responses).

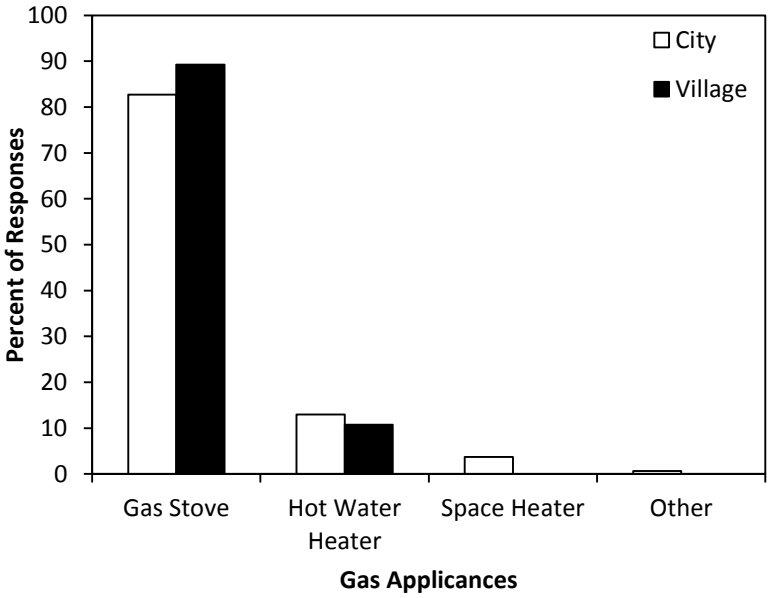

Figure 11: The percent of respondents listing a particular electrical device that they wrote down answering the question: Q15: If you had one electronic device that you cannot live without what would it be? (n = 191 responses).

Figure 12 shows the types of animals that are owned by people living in the city and the village. Also shown in the bottom plot is that the majority of city dwellers do not have animals, whereas a majority of the people living within the villages do have animals. The majority of the animals in the region are goats, water buffalo and cows. These animals provide milk for the people and are still used in farming in rural areas.

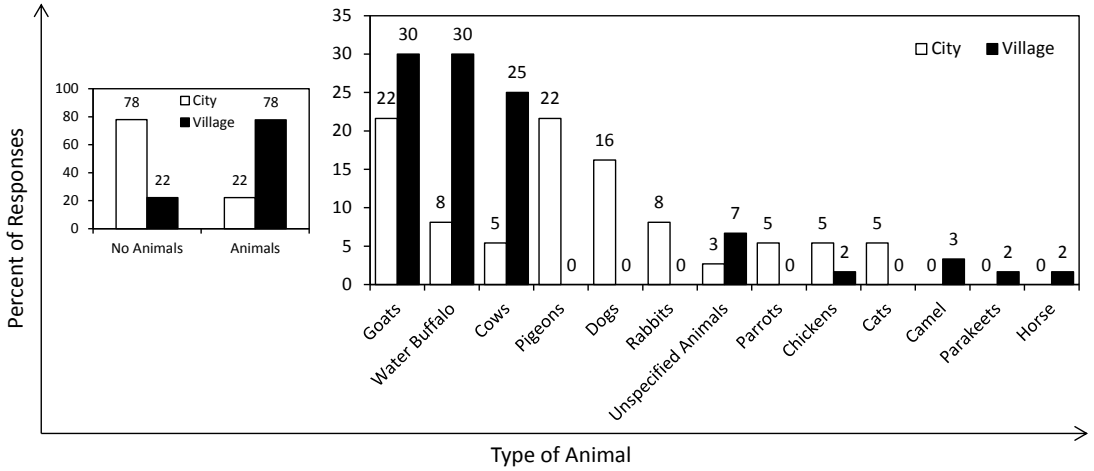

Figure 12: The percent of respondents that have animals in the city and the village that they wrote down answering to the question: Q16: How many animals do you have in your house? (n = 194 responses) and what types? (n = 97 responses).

Most of the waste in urban environments is put away into the landfill sites or is burned. However, in the rural environment the animal waste is used as fertilizer in the field or made into cow patties, illustrated in Figure 13, for fuel to cook their food or heat their homes in the winters. The end use of animal waste is presented in Figure 14. Figure 15 displays the major uses of kitchen organic wastes. The results show that the majority of it is disposed into garbage sites. A much larger amount is used as fertilizer in the village versus that in cities.

Figure 13: Cow patties, cow and water buffalo manure used to make cow patties that are dried out and used as fuel in rural environments.

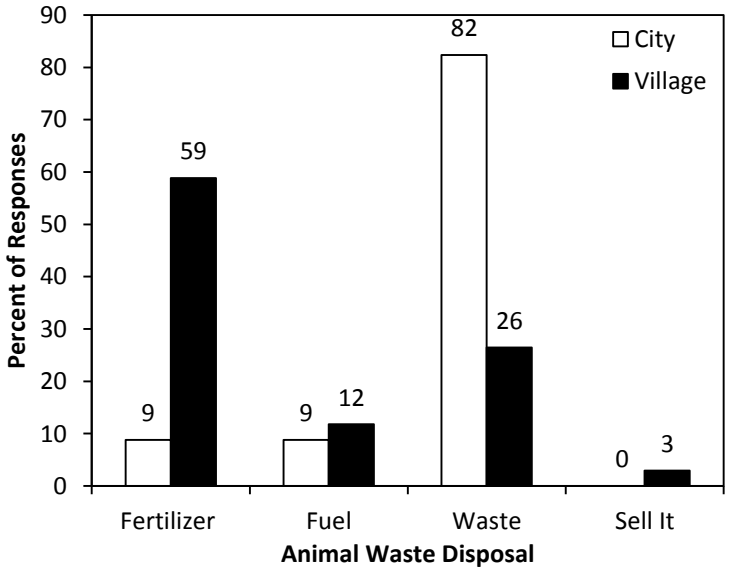

Figure 14: The percent of respondents listing a method of animal waste disposal that they wrote down answering the question: Q18: What do you do with the animal waste? (n = 68 responses).

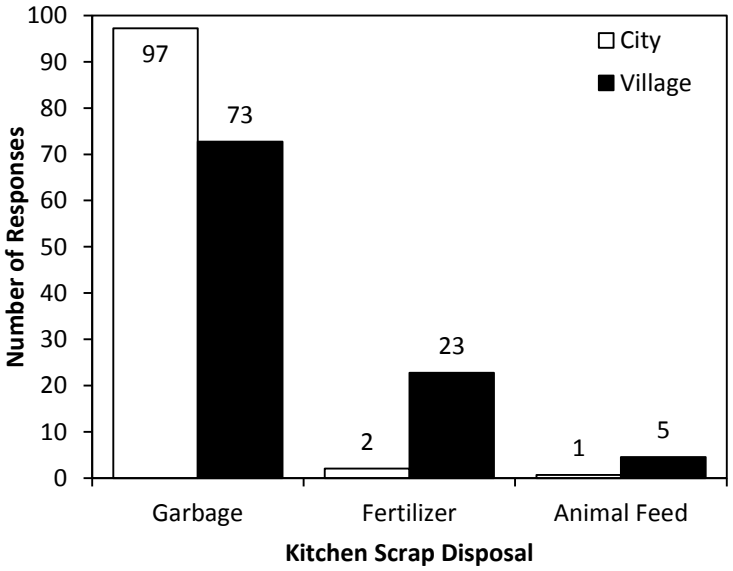

Figure 15: The percent of respondents listing a method of kitchen scarp disposal that they wrote down answering the question: Q19: What do you do with your kitchen scraps like fruit and vegetable peels? (n = 190 responses).

Out of the survey participants only 5% commented in writing. These 5% unanimously agreed that a toilet system that generated biogas, water, electricity, and fertilizer would be beneficial for the country and population, and there is a great need for this technology in the area, due to electricity and gas shortages.

CONCLUSIONS

The conclusions of the study are as follows:

- The survey respondents appear to believe that a toilet technology that produces biogas, water, electricity, and fertilizer would be beneficial. All respondents unanimously agreed that they would want to use such a toilet.
- Given the majority of respondents use squat-style toilets, the toilet technology must use this form of toilet.
- About 78% of village dwellers have animals as compared to only 22% of the city dwellers. The most common types of animals as found in this study were goats, water buffalos and cows.
- The majority of rural respondents indicated that they use animal wastes for fuel and fertilizer whereas respondents from the city stated that they put most of it to garbage.
- For both rural and city respondents, gas stoves was the most needed fuel-based appliance in the household whereas a fan and water pump were the most needed of electrical appliances. Nearly 30% of respondents from the rural areas suggested that they have no access to gas supplies.
- Nearly 30% of respondents, both rural and city, indicated that they have 4 or more hours per day without gas supplies. Nearly 70% of respondents, both rural and

city, stated that they have 4 or more hours per day without electricity. This suggests that there is a market for these resources.

- The largest fraction of city dwellers indicated that they would pay between CAD$100 and $150 for a toilet capable of generating biogas, electricity, water, and fertilizer. The largest fraction of rural dwellers indicated that they would pay between CAD$50 and $100 for such a toilet.
- Nearly 97% of the kitchen scraps are disposed of in the garbage in the city, and only 73% of kitchen scraps are disposed of in the village, the remainder are used as fertilizer or fed to the animals.

ACKNOWLEDGEMENTS
We would like to thank the Bill and Melinda Gates foundation for their financial support in this research.

REFERENCES

Ashbolt, N.J., Grabow, W.O.L, Snozzi, M. 2001 Indicators of microbial water quality. In: Fewtrell, L.,Bartram, J. (Eds.), Water Quality: Guidelines, Standards and Health. Risk assessment and management for water-related infectious disease. IWA Publishing, London (Chapter 13), 289 – 315.

CIA Factbook Pakistan 2012 (online). Available at: https://www.cia.gov/library/publications/the-world-factbook/geos/pk.html (accessed September 12, 2012).

CIA Factbook 2008 Map of Pakistan (online). Available at: https://www.cia.gov/library/publications/the-world-factbook/maps/pk-map.gif (accessed September 12, 2012).

Coombes R. 2010 Toiling for toilets. BMJ 341, 582–583.

Gleick P.H. 1996 Basic Water Requirements for Human Activities: Meeting Basic Needs. Water International. Vol. 21 no.2.

Hunter, P.R., Waite, M., Ronchi, E. 2002 Drinking Water and Infectious Disease: Establishing the Links. IWA Publishing, London.

It's Pakistan 2012 Faisalabad (online). Available at: http://www.itspakistan.net/pakistan/faisalabad.aspx (accessed September 13, 2012).

Mara, D.D. 2003 Water, sanitation and hygiene for the health of developing nations. Public Health 117:452-456.

Pearce D.W., Warford, J.J. 1993 World without end: economics, environment and sustainable development. New york, USA: Oxford University Press.

UNICEF and WHO. 2012 Progress on drinking water and sanitation: 2012 update. New York and Geneva: United Nations Children's Fund (UNICEF) and World Health Organization. Available at: http://www.who.int/water_sanitation_health/publications/2012/jmp_report/en/ (accessed September 5, 2012).

Cokar, M., Kallos, M.S., Gates, I.D. (Accepted October, 2012) Reservoir Simulation of Steam Fracturing in Early Cycle Cyclic Steam Stimulation. *SPE Journal of Reservoir Evaluation and Engineering*. ID: RE-0112-0007, 24pp.

Reservoir Simulation of Steam Fracturing in Early Cycle Cyclic Steam Stimulation

ABSTRACT

In Cyclic Steam Stimulation (CSS), steam is injected above the fracture pressure into the oil sands reservoir. In early cycles, the injected steam fractures the reservoir creating a relatively thin dilated zone which allows rapid distribution of heat within the reservoir without excessive displacement of oil from the neighborhood of the wellbore. Numerical reservoir simulation models of CSS that deal with the fracturing process have difficulty simultaneously capturing flowing bottom hole pressure behaviour and steam injection rate. In this research, coupled reservoir simulation (flow and heat transfer) and geomechanics models are investigated to model dynamic fracturing during the first cycle of CSS in an oil sands reservoir. In Alberta, Canada, in terms of volumetric production rate, CSS is the largest thermal recovery technology for bitumen production with production rates equal to about 1.3 million bbl/day in 2008. The average recovery factor from CSS is between 25 and 28% at the economic end of the process. This implies that the majority of bitumen remains in the ground. Since the mobility of the bitumen depends strongly on temperature, the performance of CSS is intimately linked to steam conformance in the reservoir which is largely established during steam fracturing of the reservoir in the early cycles of the process. Thus, a fundamental understanding of the flow and geomechanical aspects of early cycle CSS is critical. A detailed, thermal reservoir simulation model, including dilation and dynamic fracturing, was developed, using a commercially available thermal reservoir simulator, to understand their effects on bottom hole pressure and injection rate. The results demonstrate that geomechanics must be included to accurately model CSS. The results also suggest that the reservoir dilates during steam injection due to increases in reservoir temperature, which lead to thermal dilation and higher pore pressure.

INTRODUCTION

Oil sands reservoirs in Western Canada hold over 170 billion barrels of recoverable heavy oil and bitumen representing a significant source of unconventional oil. In 2008, oil sands production averaged greater than 1.3 million barrels per day of oil making it about 43% of the total output of crude oil in Canada. At in situ conditions, the majority of this oil has essentially no initial mobility because of its high viscosity which is typically in the hundreds of thousands to millions of cP. Currently, there are two major steam-based bitumen recovery processes in Alberta: Steam Assisted Gravity Drainage (SAGD) and Cyclic Steam Stimulation (CSS). Both processes use steam injection at high pressures to increase bitumen mobility: at over 200°C, the viscosity of bitumen drops to less than 20 cP.

In thermal recovery processes, the distribution of steam injected into the reservoir depends on the steam injection rate and pressure, permeability of the oil sands, the mobility of water and oil in the reservoir, and how changes of the mechanical properties of the oil sand formation impact the permeability of the formation during high pressure steam injection. During steam injection, the reservoir temperature and pressure increase resulting in poroelastic, thermoelastic, and thermal expansion effects which in turn cause formation dilation and compression. These effects are not limited to the near-wellbore region and can extend further into the reservoir depending on the steam injection pressure, quality, and rate (Walters et al., 2000). Hydraulic fracturing, caused by steam injection in a reservoir with relatively immobile oil can take on various orientations depending on the reservoir fluid properties and reservoir state-of-stress. The interactions between heat transfer, multiphase fluid flow, geomechanical behaviour (fracture mechanics, and poroelastic and thermoelastic responses), and gravity override control steam injectivity and the extent of reservoir fracturing (Settari, 1992).

CSS can be carried out with vertical, horizontal or deviated wells (Lebel, 2002). In this paper, we have focused on horizontal well CSS. In CSS, steam injected at high pressure into the reservoir fractures it and distributes heat within the reservoir in the neighborhood of the injection well. The reservoir is dilated with consequent increases in porosity and permeability. The oil is thus mobilized by not only heating of the oil which lowers its viscosity but also by the enhancement of the permeability of the formation near the wellbore. Additional production mechanisms that are involved in CSS include solution gas drive, steam flashing, gravity drainage, fluid expansion, sensible heat from the condensate, and formation recompaction. After the oil production rate has dropped to an uneconomic level, steam injection is resumed and another CSS cycle starts. In a comparison study completed by (Scott, 2002) the results revealed that the CSS process has a 50% higher bitumen production per m^3 of external gas consumed compared to SAGD processes in the Clearwater oil sands Formation. CSS is favored in reservoirs with high solution gas content resilient cap rock above the oil sands formation to prevent losses of high pressure steam and CSS injects at sufficiently high pressures to allow heat to move quickly through lower permeability layers.

Cyclic Steam Stimulation Processes in the Field

Cold Lake – Imperial Oil CSS

In the Cold Lake region of Alberta, bitumen is extracted from the Clearwater Formation. The formation top is roughly 450 m deep, and the formation is a thick unconsolidated sand (up to 45 m thick), with porosities up to 35% and horizontal permeability between 2 and 3 D (Boberg, 1990). The reservoir has an oil saturation of about 11% by weight and the initial viscosity of the bitumen at 13°C ranges from 57,000 to 100,000 cP. Steam injection is done at about 11 MPa and after the injection period, the reservoir temperature rises to over 260°C. At this point, the bitumen viscosity is as low as 5 cP. The majority of wells in Cold Lake are deviated wells arranged in 20 well pads.

Cold Lake – CNRL Primrose CSS

CNRL's Primrose project is located just North of Imperial Oil's Cold Lake operation and extracts oil from the Clearwater Formation. Amoco started a single SAGD well in the Primrose field in July 1998. In May 2001 they converted this well to CSS (Scott, 2002). The properties of the reservoir and fluids are similar to that of Imperial Oil's Cold Lake resource. The process uses horizontal wells and in the current practice at Primrose, injection occurs at the fracture pressure of the reservoir. The well lengths in this area are 600 to 1200 meters with a well spacing of about 60 to 188 meters.

Peace River - Shell CSS

Shell's CSS operation is conducted in the Bluesky Formation in the Peace River area of Alberta. This field has been producing for more than 30 years in a sequence of thermal pilots and demonstration projects. The field contains about 8 billion barrels of 7 °API oil with dead oil viscosities of about 100,000 cP (Brissenden, 2005). The oil is found 600 m below the surface and the net pay is approximately 30 m. The Bluesky Formation consists of estuarine and deltaic zones. The estuarine zone has poorer quality i.e. lower permeability, than the deltaic one. In current operations, closely spaced multilateral J-wells are drilled from a central pad facility (Koci, 2007). Shell is now shifting towards an inverted 7-spot pattern where each pattern will cover 3.4 ha within the Bluesky Formation (Shell Recovery Process, 2009).

Steam Cycle Design

The steam cycle design (time intervals for steaming, soaking, and production for each cycle) should be optimized to produce the maximum amount of oil from the reservoir for the minimum amount of injected steam. Given that steam fracturing occurs in the first or second cycles, the injected volume of steam has to be large enough to contact and mobilize an economic amount of bitumen. However it should not be excessively large that it penetrates too far into the reservoir so that mobilized bitumen cannot be moved back to the production well. On initial production, steam and steam condensate is produced relatively rapidly over a period of days to weeks. After some time, oil production grows and eventually it peaks and then declines as the pressure in the reservoir falls. In multiwell CSS, the configuration, organization, and timing of steam, soak, and production periods is critical given steam generation constraints and pressure management in the reservoir (high pressure injection directly adjacent to low pressure production is undesirable as it would promote steam production to production wells).

Moreover, with each cycle, the steam chambers are growing in the reservoir and thus to maintain the same linear growth rate in the chamber with each cycle, the amount of steam per cycle increases and the length of the production period grows (since it takes longer for mobilized oil to flow back to the production well from a given larger chamber).

Steam Fracturing and Geomechanics

As steam is injected into the reservoir, several changes occur within the sand matrix. These changes include thermal expansion, agitation, and dilation which lead to perturbation of the sand matrix because of the increase in both temperature and pressure (Walters, 2000). Dilation of the reservoir creates zones of increased permeability and porosity which in turn affects steam injection into the reservoir and production of bitumen from the reservoir. Changes to the state of stress and volumetric strain of the oil sand during steam injection are not localized but spread far beyond the steam injection area and not only affect hydraulically connected pores but also unconnected zones as well. Physically, high pressure steam injection can be observed at the surface as heaves of up to 20 to 30 cm (Walters et al., 2000).

If the steam injection pressure exceeds the reservoir fracture pressure, then the reservoir will also steam fracture resulting in steam moving large distances (tens of meters) in short times. The direction and orientation of the fracture depends on the state of in-situ stresses: the fractures propagate with time in the direction normal to the smallest horizontal compressive stress (Lijun, 2004). Steam fracturing, as practiced in CSS, has several benefits with respect to energy delivery into the reservoir. The injected steam parts the formation creating a large permeability conduit for steam. As a result, on steam injection, energy is distributed quickly into the reservoir, through a small conduit, without moving large amounts of bitumen away from the well. If steam was injected at less than fracture pressure, mobilized oil near the injection well could potentially be steam flooded away from the injection well, as the steam would be slowly moving through large conduits, in contrast to a small area as is the case with fractures. Consequently, in the unfractured case, when the well is converted to production, the targeted oil will have been moved away from the well on injection. On the other hand, steam fracturing potentially delivers energy to the formation without excessive displacement of oil away from what will become the production well. As production occurs, the pressure in the formation drops and at the edges of the steam fracture solution gas will evolve and expand thus displacing oil to the production well. Also, steam flashing can occur which leads to further production of fluids from the reservoir.

Figure 1 displays steam conformance zones estimated from seismic data at the end of each of the first three cycles of horizontal well CSS operating in the Clearwater Formation in the Cold Lake oil sands deposit. The images reveal that steam injection is not uniform along the length of the wells and that the steam conformance zone varies significantly along the wells. Figure 2 displays the injection and production dynamics for a typical cycle as reported by CNRL (2007). This plot shows that the steam injection rate ramps up to its maximum value and stabilizes over the injection period. During this injection period the injection pressure also increases, however at a steep rate before reaching the maximum value and then stabilizing during the remainder of the injection

phase. Figure 2 also shows the soak period, after which the fluid production rate begins. To model the actual physics of the reservoir in terms of heat transfer within the reservoir a soak period is not necessary. A soak period is only important due to the logistics of the field in terms of steam distribution between different rows of wells in the field and therefore it was not included in this model. When the fluid production rate is stable, the injection pressure is on a decline. After some time, the fluid production rate falls steeply and then levels off, and during this period the injection pressure plateaus at what appears to be a minimum flowing bottom hole pressure. This data indicates the general pattern that reservoir simulators attempt to replicate during CSS while highlighting the complexity of actual field data.

Current reservoir simulation models cannot take into account the complexity of steam fracturing together with fluid flow as is encountered in CSS. It is unclear how geomechanics should be modeled to represent steam injection with fracturing in the reservoir. In this research, we examine several geomechanical models in early cycle CSS where steam fracturing of the reservoir occurs. Given the complexity of the process, it is not clear what best means is to model this dynamic process.

Previous Work on Numerical Simulation of Steam Fracturing

Quite a bit of work has been done on trying to improve CSS numerical simulation of the Cold Lake area. As mentioned by Lebel and Moriyama (1997) inclusion of petrophysical properties such as bound water, water-oil imbibition relative permeability, increases in matrix compressibilities when the reservoir is in shear failure mode, and the use of a horizontal fracture, 10cm wide and located at the CSS perforations with an increasing transmissibility as a function of pressure, have significantly improved field history matches. In this study, a foamy oil model was also used to obtain a better match of gas produced.

In another study conducted by Koci and Mohiddin (2007), for Shell's Peace River property, the authors outline two different methods in a widely applied simulator that can be used to include geomechanical effects into the model. The first is a reservoir dilation and recompaction model also known as the Beattie-Boberg model, this model is a hysteretic rock compressibility model (see Figure 3) that changes the porosity of the reservoir depending on the pressure, and what state the reservoir is in i.e. dilation or recompaction. The second method that can be used is by creating a fracture within the model. Since the location, depth, and orientation of these hydraulic fractures are difficult to determine, it makes it very difficult to specify the location of these fractures. In the study conducted by Koci and Mohiddin (2007) a horizontal fracture was placed at the top of the reservoir, and a pressure-dependent transmissibility modifier was applied to the top reservoir layer. These fractures will then open or close depending on the reservoir pressure.

The method of using a predefined fracture layer to model the fracture plane for CSS is commonly seen in many previous studies, in another study conducted by Walters et al. (2000), the fracturing process was enabled using a predetermined fracture layer that was determined by assessing the minimum effective stress within the reservoir.

METHODS - RESERVOIR MODEL

The three-dimensional (3D) reservoir simulation model used in this study is based on a geostatistical geological model of the Clearwater Formation in the Cold Lake region of Alberta, Canada. The average porosity, horizontal permeability, and oil saturation are equal to 0.31, 2,829 mD, and 0.64, respectively. Figure 4 displays cross-sections of the porosity, horizontal permeability, and oil saturation. The location of the horizontal well is also displayed. A summary of the properties of the reservoir, including simulation input parameters, is listed in Table 1.

Depending on the length scale for steam transport and fracture propagation in the reservoir, the dimensions of the grid blocks and the reservoir model size itself can impact the pressure evolution and fracture propagation in the reservoir simulation. All of the simulations used a 3D model, and Table 2 describes model dimension and volume. In the reservoir model, the horizontal wellbore is 880 m long. To simplify the analysis and focus on reservoir flow issues, a sink/source well model was used, and this meant that frictional losses occurring along the wellbore were not taken into account.

Simulation Cases

The parameters used for the different simulation cases studied are outlined in Table 3. A thermal reservoir simulator capable of geomechanics was used in this study. The reservoir simulator solves Darcy's law for oil, water, and gas phases, mass continuity, and heat transfer within the reservoir by using the finite volume method. Thermodynamic equilibrium between the oil and gas phases is determined by a flash calculation based on K-values for the solution gas dissolution in the oil phase. The cases listed in Table 3 describe the evolution of geomechanical modelling in this study, and this allows us to understand the ability of the current numerical simulators to accurately model the physics within the reservoir. The cases simulated were as follows:

1. No geomechanics model and no predefined fracture layer,
2. Dilation-recompaction model,
    a. with predefined fracture layer,
    b. no predefined fracture layer,
3. Geomechanics with predefined fracture layer,
        a. coupled geomechanics and fluid flow,
        b. pseudo dilation model,
        c. sensitivity of pressure-dependent transmissibility pressure cutoffs,
        d. sensitivity of results to fracture permeability,
        e. sensitivity of results to pressure-dependent transmissibility, and
4. Geomechanics with no predefined fracture layer.

The well constraints were as follows: ***Injection well:*** Maximum injection pressure of 11,000 kPa with maximum steam rate, expressed as cold water equivalent (CWE), of 1,000 m^3/day. The steam quality equals 0.95. ***Production well:*** Minimum bottom hole pressure (BHP) of 1,000 kPa and a maximum liquid (both oil and water) rate of 750 m^3/day.

RESULTS

In this study, all simulations were run for the first cycle only because the majority of steam fracturing occurs in this cycle. Prior to steam injection, the reservoir model was run for a period of 61 days with no injection or production to ensure that the variables (flow, saturations, pressure, temperature, stresses, etc) in the model were fully equilibrated. Typical of Cold Lake CSS operations, the steam injection period lasted for 38 days (Denbina, 1991). After the steam injection period, no soak period was conducted and the well was converted directly to production which lasted 76 days. In total, five cases were evaluated as shown in the section below.

Case 1 – No Geomechanics Model and No Predefined Fracture Layer

Figure 5 displays the well bottom hole pressure and injection and production rates for this case. The results reveal that after steam injection starts, the reservoir pressure at the well increases rapidly and reaches the maximum BHP constraint of 11,000 kPa. The steam injection rate increases rapidly but after the BHP constraint is reached, it declines within about 2 weeks to less than 100 m^3(CWE)/day. After the well goes on production, the pressure at the well drops rapidly as fluids are removed from the reservoir. The liquid production rate reaches the constraint rate of 750 m^3/day. After 15 days of the production period have elapsed, the minimum BHP constraint (equal to 1,000 kPa) is invoked and the production rate falls and by the end of the production period, it has declined to less than 100 m^3/day. Clearly, a comparison of the steam injection pressure and rate from the simulation and typical field data (Figure 2), demonstrates that the reservoir model without geomechanics fails to represent the injection period dynamics. A comparison of the production dynamics reveals that the simulation results are somewhat similar to the field data: when the pressure is declining, the production rate levels off and when the pressure levels off at an effective minimum BHP, then the production rate falls and then tends to level off.

Figure 5 also displays the temperature distribution along the wellbore in the plane of the well after 31 days of steam injection. The results show that the heated zone has extended about 5 m on each side of the well. The appears to be somewhat smaller than the steam conformance zone displayed in Figure 1 which, in the regions that accepted steam, reached up to 30 m.

Case 2 – Dilation-Recompaction Model

In these models, the Beattie-Boberg dilation-recompaction model (parameters listed in Table 4) is used to represent the dilation behaviour in the reservoir (Beattie and Boberg, 1991). Figure 3 shows a graphical depiction of the Beattie-Boberg dilation-recompaction model.

2a. With Predefined Fracture Layer

A predetermined fracture layer was placed in the layer containing the horizontal well within the reservoir simulation model with enhanced permeability in the layer equal to 10 D. Figure 6 displays the results of this model which exhibit more similar behaviour to what is seen in the field (Figure 2). The bottom hole pressure gradually increases to the

maximum injection pressure of 11,000 kPa, at which it then plateaus. Also, the steam injection rate increases until the maximum injection rate is reached where it remains for the entire injection period, similar to what is observed in the field. Once the steam injection period is over, the bottom hole pressure gradually declines until a minimum flowing bottom hole pressure is reached which is set equal to 1,000 kPa in this model. After production starts, the fluid production rate increases rapidly until it reaches the maximum rate equal to 750 m^3/day which it remains at for about 45 days after which it starts to decline gradually. Figure 6 also shows the steam conformance along the horizontal well. The results show that the heated zone has extended to about 17 m on each side of the well. This is more consistent with the field conformance results than the results obtained with Case 1.

2b. No Predefined Fracture Layer

The results for this case are shown in Figure 7. The BHP does not exhibit a similar trend to the behaviour observed in the field. The BHP profile is more curved than the trend seen in the field data. Also, the pressure does not reach the maximum BHP constraint of 11,000 kPa. However, the pressure decline and steam injection rate profiles are similar to that of the field data shown in Figure 2. The injected steam starts to decline sharply, and this corresponds with a pressure decrease, that is not sharp but gradual and more reflective of what is observed in Figure 2. Also, if the soak period of Figure 2 is ignored, the total fluid production sharply increases at Day 100 when the well is put on production, and then starts a decline period that lasts approximately 50 days after production starts. This decline corresponds to when the well bottom hole pressure is near the minimum flowing bottom hole pressure value of 1,000 kPa which is similar to the field observations shown in Figure 2. Figure 7 shows the temperature distribution after 31 days of steam injection along the wellbore in the plane of the well. The results reveal that the temperatures achieved in the reservoir are higher than that realized by Case 1. Also, the steam conformance zone is slightly larger (about 12 meters on each side of well) but is still much smaller compared to that achieved in the field.

Case 3 – Geomechanics with Predefined Fracture Layer

In this case, there is also a predetermined fracture layer with enhanced permeability in the layer containing the horizontal well where the permeability is set equal to 10 D. The geomechanics are coupled with reservoir flow by using an iterative procedure that updates the porosity of the reservoir from the total mean stress, pressures, and temperatures within the reservoir. A finite-element method is used to solve the stress-strain constitutive equations (Tran et al. 2002). The variables used for this model are listed in Tables 5 and 6. Five different sensitivity analyses were completed for the fracture layer model. In addition, a pressure-dependent transmissibility multiplier was used in the entire reservoir to dynamically alter the permeability of the system as the pressure changed within the reservoir. The multiplying factor for transmissibility in the widely applied simulator, *F*, is given by:

$$F = \frac{1}{1 + e^{\frac{10\left(P - P_{avg}\right)}{P_{UpperCutoff} - P_{LowerCutoff}}}} + \beta\left[1 - \frac{1}{1 + e^{\frac{10\left(P - P_{avg}\right)}{P_{UpperCutoff} - P_{LowerCutoff}}}}\right] \quad (1)$$

where P is the grid block pressure, $P_{UpperCutoff}$ is the pressure at which the fracture opens, $P_{LowerCutoff}$ is the pressure at which the fracture closes, P_{avg} is the average of $P_{UpperCutoff}$ and $P_{LowerCutoff}$, and β is the transmissibility multiplier. For Cases 3a-d, β is set equal to 100. For Cases 3a, 3b, 3d, and 3e the lower cutoff pressure is taken to be 10,500 kPa whereas the upper cutoff value was set to 11,000 kPa. Figure 8 displays the transmissibility multiplier versus pressure. The function essentially models a smoothened step function between 1 and β. This means that as the pressure in a gridblock rises from $P_{LowerCutoff}$ to $P_{UpperCutoff}$, the transmissibility, given for example by $T = (A/l)^{eff} k^{eff}$, where $(A/l)^{eff}$ is the effective area over the effective length, and k^{eff} is an area-weighted harmonic average effective permeability between two adjacent grid blocks, is enlarged smoothly from its initial value to β times its initial value. If the pressure declines below $P_{LowerCutoff}$, then the transmissibility returns to its initial value.

3a. Coupled Geomechanics and Fluid Flow

The well bottom hole pressure, injected steam (CWE) rate, and produced liquid rates are shown in Figure 9. The bottom hole pressure rises quickly to the maximum bottomhole pressure however, not as quickly as Case 1. The steam injection rate does not stay at the maximum rate for the entire period, therefore causing a smaller amount of liquid to be produced. In this model there is a ramp up in the pressure in the beginning of the steam cycle before the pressure plateaus, similar to what is seen in the field (Figure 2), which is more reflective of what is happening in the field. Figure 9 also displays the steam conformance at Day 31 in this run. The steam conformance is smaller and temperatures in the heated zone are lower than that obtained in Case 2 and the conformance zone observed in the field displayed in Figure 1.

3b. Pseudo Dilation Model

This Case is the same as Case 3a with the addition of a pseudo-dilation-recompaction model similar to the Beattie-Boberg model. The parameters of this model are the same as that used in Case 2. Table 5 lists parameter values used in this model. Figure 10 illustrate the results obtained for this Case. For this Case, the BHP behaviour during the injection period obtained is similar to the behaviour observed in the field. Here, the injected steam rate lasts for a longer duration than that exhibited in Case 3a. In Case 3a, the steam rate starts to decline after 9 days of injection whereas in this Case, it starts to decline after 26 days. The current Case 3b behaviour is closer to the behaviour seen in the field. Figure 2 shows that in the field, the steam injection rate declines at about the same time as when the injection pressure falls. During production, unlike Case 3a, the pressure in this Case does not decline as fast and better reflects the behaviour exhibited in field data.

Figure 9 displays the steam conformance and temperature along the wellbore at Day 31. The temperature along the well spreads slightly further away from the well than the previous case and the steam zone extends about 7 m on both sides of the well. This is still much less than the conformance zone observed after Cycle 1 in the field (see Figure 1), however, the steam reaches further away from the wellbore than that seen in Case 3a.

3c. Sensitivity of Pressure-dependent Transmissibility Pressure Cutoffs

This Case is the same as Case 3b but now the lower and upper cutoff pressures are set equal to 6,500 kPa and 7,000 kPa, respectively. Figure 11 shows the results for this Case. The injected steam and produced liquid rates are similar to that of Case 3b, however, the pressure response of the system is highly dependent on the cutoff pressure values. The temperature along the wellbore is shown in Figure 11. Similar to the other models, the steam conformance zone does not match the extent seen in the field as reflected by Figure 1.

3d. Sensitivity of Results to Fracture Permeability

This Case is identical to that of Case 3b except the value of the fracture permeability is raised to 100 D. The results are shown in Figure 12. Once again these results are very similar to that of Case 3b which demonstrates that a 10 times increase in the fracture permeability does not significantly impact the steam injection rate, produced liquid rate, and the well bottom hole pressure. However, the steam conformance in Figure 12 is different than what was observed in Figure 10 (Case 3b): the temperature along the well is higher and the steam reaches further into the reservoir. However, the conformance is still less than what is observed in the field (Figure 1).

3e. Sensitivity of Results to Pressure-dependent Transmissibility

This Case is identical to that of Case 3b except the transmissibility multiplier, β, is lowered to 10. The results for this case are displayed in Figure 13. Figure 13 reveals that the BHP is not affected by a change in the transmissibility multiplier. However, the steam injection rates are different because in Case 3b, the injected steam (CWE) rate drops down vertically, then levels off at a slight slope, whereas in Case 3e, the injected steam (CWE) rate decreases gradually following a curved profile. When the injected steam is compared to Figure 2, it is clear that the rate is more similar to Case 3b, because as shown in Figure 2 the rate drops down vertically without any slope. The produced liquid rate is very similar to that is seen in Case 3b. However, Figure 13 shows that the temperature along the well is much hotter than all of the previous cases. This is because the steam is not penetrating as far into the formation as a result of the reduced transmissibility. Thus, the temperature remains hotter in the near-wellbore region.

Case 4 – Geomechanics with No Fracture Layer

This Case is identical to Case 3b except the predefined fracture layer with its enhanced permeability was removed. Figure 14 shows the BHP, steam injection rate, and the production well liquid rate for this Case. The BHP does not exhibit a similar trend to the behaviour observed in the field. The BHP profile is more curved than the trend seen in the field data. However, the pressure decline and steam injection rate profiles are similar to Figure 2. The injected steam starts to decline sharply, and this corresponds with a pressure decrease, that is not sharp, but gradual and more reflective of what is observed in Figure 2. Also, if the soak period of Figure 2 is ignored, the total fluid production sharply increases at Day 100 when the well is put on production, and then starts a decline approximately 50 days after production. This decline corresponds to when the well bottom hole pressure is near the minimum flowing bottom hole pressure value of 1,000 kPa, similar to what is seen in Figure 2. Also as shown in Figure 14, the temperature

along the well is much higher than what was observed in the previous cases, and the steam is spreading further away from the well than any other of the previous tested cases.

DISCUSSION

Previous studies of steam injection in CSS showed that in order to accurately model the hydraulic fractures in a CSS process it is necessary to have a predefined fracture layer with a pressure dependent transmissibility multiplier or to use the Beattie-Boberg dilation recompaction model, however, from this study it is clear that in order to obtain accurate bottom hole pressure, steam injection and liquid production matches with the field, a predefined fracture layer is not necessary, instead simply the Beattie-Boberg dilation recompaction model can be used, or no predefined fracture layer with a transmissibility multiplier on the entire reservoir can be used. This further supports the suggestion that the actual reservoir physics in terms of real dynamic fracturing which includes fracture formation, location and propagation should be included into the model, instead of just defining a specific layer to be fractured.

The results reveal that if no geomechanics are included in the model, the pressure profile reaches the maximum injection pressure almost instantaneously and the behaviour of the model is quite dissimilar to that observed in the field. However, as additional geomechanical complexity is added, the steam injection rate, injection pressure, and total fluid production trends tend towards the behaviour seen in the field. It is only in the case with full geomechanics without a predefined fracture layer and the dilation recompaction simulation cases that the steam conformance at the end of the steam injection period approaches the conformance observed in the field. All of the cases have difficulty matching steam conformance, and the heated region around the well does not extend far enough away from the well. Although the models simulated in this study follow the trend of what is seen in the field in terms of the steam injection rate, injection pressure and total fluid production, they are missing one essential component - the ability to dynamically model where steam fracturing occurs. Moreover, one interesting result from this study is that the case without a predefined fracture layer yielded results that were more similar to the behaviour observed in the field. This implies that earlier approaches, as done by Lebel and Moriyama (1997), Koci and Mohiddin (2007), Walters et al. (2000), to model CSS by using predefined fracture layers should not be used.

In order to model CSS as shown in this study simpler models that do not have a predefined fracture layer are better at modelling what is actually happening in the field in terms of injection pressures and fluids injected and produced when the dilation-recompaction model is not used as in Case 4. However, in the case 2a and 2b when the dilation-recompaction model is included in the model along with either no predefined fracture layer or defined fracture layer the results are essentially the same. Therefore, it is not recommended to have a higher permeability fracture layer, and instead allow the reservoir's own mechanical properties dictate the flow of steam into the reservoir, and production of fluids from the reservoir. So in general it is recommended not to use a predefined fracture layer since the actual physics of the reservoir are not followed and instead to get a better match in terms of injected and produced fluids it is recommended

to either use a dilation-recompaction model or no fracture layer at all, since Cases 2a, 2b, and 4 are all very similar in their results.

CONCLUSIONS AND RECOMMENDATIONS

In this study, several geomechanical models have been evaluated to attempt to model steam fracturing in the first cycle of cyclic steam stimulation. The conclusions are as follows:

1. Geomechanics must be included for reservoir simulation models of Cyclic Steam Stimulation (CSS) that operate above the fracture pressure of the formation: flow and heat transfer alone are not enough.
2. The models without pre-defined fracture models appear to provide more similar trends and steam conformance to that observed in field CSS data. This is especially true if the actual fracture layer within the reservoir and thus the reservoir physics are not exactly known.
3. The outcomes seems insensitive to permeability multipliers and thus should not be used since they add further unnecessary complexity and associated often-unknown parameters to the geomechanical model.
4. The results suggest that a dilated steam zone forms in the reservoir around the well where the formation fails rather than a thin steam fracture.
5. As shown in Figure 1, with the two horizontal wells at the top of the figure, there is communication between the wells even after the first cycle of cyclic steam stimulation. This suggests that well communication should be taken into consideration starting at the first cycle, in order to develop a better history match and model.

ACKNOWLEDGEMENTS

The authors would like to acknowledge the Alberta Ingenuity Fund (AIF) and NSERC for funding MC, the Computer Modeling Group Ltd. for the use of their thermal simulator, and the Department of Chemical and Petroleum Engineering at the Schulich School of Engineering, University of Calgary.

REFERENCES

Beattie, C.I., Boberg, T.C., and McNab, G.S. Reservoir Simulation of Cyclic Steam Stimulation in the Cold Lake Oil Sands. *SPE Reservoir Engineering*. SPE 18752, 1991.

Beer, F., Johnston, E.R.Jr., and DeWolf, J.T., 2006. *Mechanics of Materials*. New York: McGraw-Hill.

Boberg, T.C., and Rotter, M.B. History Match of Multiwell Simulation Models of Cyclic Steam Stimulation Process at Cold Lake. Paper SPE 20743 presented at the 65th Annual Technical Conference and Exhibition of the Society of Petroleum Engineers, New Orleans, 23-26 September, 1990.

Brissenden, S.J. Steaming Uphill: Using J-Wells for CSS at Peace River. Paper presented at the Canadian International Petroleum Conference, Calgary, 7-9 June, 2005.

Canadian Natural Resource Ltd. (CNRL) Primrose, Wolf Lake, and Burnt Lake Annual Presentation to the EUB (2008), , Retrieved December 2, 2011 from

http://www.ercb.ca/oilsands/insitu-presentations/2007ColdLakeCNRLWolfLakePrimroseCSS9140.pdf. Submitted to the Energy Research and Conservation Board.

Cold Lake Annual Performance Review. Cold Lake Approvals 8558 and 4510. 2007 EUB Annual Performance Review. Jan 23, 2008. Retrieved September 11, 2012 from http://www.ercb.ca/data-and-publications/activity-and-data/insitu-progress. Submitted to the Energy Research and Conservation Board.

Denbina, E.S., Boberg, T.C., Rotter, M.B. Evaluation of Key Reservoir Drive Mechanisms in the Early Cycles of Steam Stimulation at Cold Lake. *SPE Reservoir Engineering.* 1991.

Fjaer, E., Holt, R.M., Horsrud, P., Raaen, A.M., and Risnes, R., 2008. *Petroleum Related Rock Mechanics, 2nd Edition*. Oxford: Elsevier.

Gates, I.D. 2011. *Basic Reservoir Engineering*. Published by Kendall-Hunt Publishing Company, ISBN: 978-0-7575-9062-7.

Koci, P. F., and Mohiddin, J. G. Realistic History Matching of Cyclic Steam Stimulation Performance of Several Groups of Multilateral Wells in the Peace River Field, Canada. Paper SPE 107201 presented at the SPE Europec/EAGE Annual Conference and Exhibition, London, 11-14 June, 2007.

Lebel, J.P. Dynamic Fracture Modeling Approach for Cold Lake Cyclic Steam Stimulation. Paper SPE 79010 presented at SPE/PS-CIM/CHOA International Thermal Operations and Heavy Oil Symposium and International Horizontal Well Technology Conference, Calgary, 4-7 November, 2002.

Lebel, J.P., and Moriyama, R.T. History Match of Mature Cyclic Steam Stimulation Process at Cold Lake. Paper SPE 37549 presented at the SPE International Thermal Operations and Heavy Oil Symposium, Bakersfield, 10-12 February, 1997.

Lijun, J. Settari, A., Sullivan, R.B., and Orr D. Methods for Modeling Dynamic Fractures in Coupled Reservoir and Geomechanics Simulation. Paper SPE 90874 presented at the SPE Annual Technical Conference and Exhibition, Houston, 26-29 September, 2004.

Recovery Process (2009). Application for Approval of the Carmon Creek Project. Volume 1: Project Description. Retrieved December 2, 2011, from http://www.shell.com/static/can-en/downloads/aboutshell/our_business/e_and_p/recovery_process_field_facilities_processing_facilities.pdf.

Scott, G. R. Comparison of CSS and SAGD Performance in Clearwater Formation at Cold Lake. Paper SPE 79020 presented at the SPE International Thermal Operations and Heavy Oil Symposium and International Horizontal Well Technology Conference, Calgary, 4-7 November, 2002.

Settari, A., Ito Y., Fukushima, N., and Vaziri, H., Geotechnical aspects of recovery processes in oil sands. Canadian Geotechnical Journal. Vol. 30, No. 1, pp. 22-23. 1993.

Settari, A., Walters, D.A., and Behie, G.A., Use of Coupled Reservoir and Geomechanical Modelling for Integrated Reservoir Analysis and Management. *JCPT. Vol. 40*, No.12, pp. 55-61. December 2001.

Tran, D., Nghiem, L., Buchanan, L. Improved Iterative Coupling of Geomechanics With Reservoir Simulation. Paper SPE 93244 presented at the SPE Reservoir Simulation Symposium, Texas, 31 January 2005 – 2 February 2005.

Tran, D., Settari, A., Nghiem, L. New Iterative Coupling Between a Reservoir Simulator and a Geomechanics Module. Paper SPE 78192 presented at the SPE/ISRM Rock Mechanics Conference, Irving, 20-23 October, 2002.

Vinsome, P.K.W., and Westerveld, J.D., A Simple Method for Predicting Cap and Base Rock Heat Losses in Thermal Reservoir Simulators. JCPT. Vol. 19, No.3. July-September 1980.

Walters, D.A., Settari, A., Kry, P.R. Poroelastic Effects of Cyclic Steam Stimulation in the Cold Lake Reservoir. Paper SPE 62590 presented at the SPE/AAPG Western Regional Meeting, Long Beach, 19-23 June, 2000.

Table 1: Average reservoir properties of the Clearwater Formation oil sands reservoir model.

Variable	Average Value
Porosity	0.31
Horizontal Permeability	2,829 mD
Vertical Permeability	942 mD
Initial Water Saturation	0.36
Initial Oil Saturation	0.64
Initial Gas Saturation	0

Table 2: Model grid size, dimensions, and volume.

Grid Size	Grid Dimensions (m)	Total Volume (m^3)
52x45x28	1x20x1	1,298,100

Table 3: Properties of simulation cases. Injection well constraint: pressure of 11,000 kPa with maximum steam rate, expressed as cold water equivalent, of 1,000 m^3/day. The steam quality equals 0.95. Production well: minimum bottom hole pressure (BHP) of 1,000 kPa and a maximum liquid (both oil and water) rate of 750 m^3/day.

Case	Description	Pseudo Dilation	Fracture Permeability, mD	Lower Pressure Cutoff, kPa	Upper Pressure Cutoff, kPa	Trans i,j,k
Case 1: No Geomechanics						
1	No Geomechanics	NA				
Case 2: Dilation-Recompaction Model						
2a	Dilation-Recompaction Model with Predefined Fracture Layer	Dilation-Recompaction Model (Beattie et al., 1991)				
2b	Dilation-Recompaction Model and No Predefined Fracture Layer					
Case 3: Fracture Layer Geomechanics Model						
3a	Geomechanic Coupling with Predefined Fracture Layer	NA	10,000	10,500	11,000	100
3b	Pseudo Dilation with Predefined Fracture Layer	Yes	10,000	10,500	11,000	100
3c	Sensitivity of Pressure-Dependent Transmissibility Pressure Cutoffs with Predefined Fracture Layer	Yes	10,000	6,500	7,000	100
3d	Sensitivity of Fracture Permeability with Predefined Fracture Layer	Yes	100,000	10,500	11,000	100
3e	Sensitivity of Transmissibility Multiplier with Predefined Fracture Layer	Yes	10,000	10,500	11,000	10
	Case 4: No Fracture Layer Geomechanics Model					
4	No Fracture Layer	Yes	NA	10,500	11,000	100

Table 4: Model properties for dilation-recompaction model used in Case 2.

Variable	Value	Reference
Reference Pressure	2,650 kPa	Gates (2008)
Dilation Rock Compressibility	1.016E-04 1/kPa	
Residual Dilation Fraction	0.45	
Start Dilation	7,300 kPa	
Start Recompaction	5,000 kPa	
Max. Allowed Proportional Increase in Porosity	1.25	

Table 5: Model properties for pseudo-dilation model used in Cases 3 and 4.

Variable	Value	Reference
Dilation Onset Pressure	7,300 kPa	Gates (2008)
Recompaction Onset Pressure	5,000 kPa	
Young's Modulus Dilation State	100,000 kPa	
Young's Modulus Recompaction State	200,000 kPa	

Table 6: Values for models with geomechanical properties used in Cases 3 and 4.

Variable	Value	Reference
$\sigma_{horizontal\ 1}$ (Initial stress state at well depth)	9,000 kPa	Settari et al. (2001)
$\sigma_{horizontal\ 2}$ (Initial stress state at well depth)	9,000 kPa	
vertical (Initial stress state at well depth)	9,700 kPa	
E linear elastic model	500,000 kPa	
Poisson's Ratio	0.2	

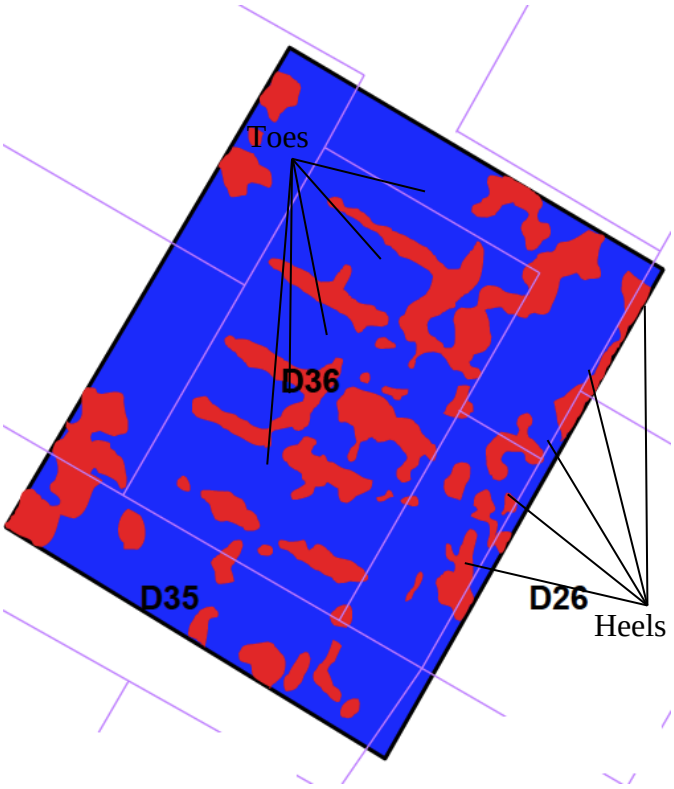

Figure 1: Interpretation of seismic data to indicate hot and cold regions of the reservoir for horizontal well cyclic steam stimulation at the end of the steam injection periods of the first cycle (ERCB (Cold Lake Annual Performance Review) 2008). There are five horizontal wells in the pad aligned at about 30° to the horizontal. The red zones are zones that have been heated (by steam) whereas the blue zones are still cold. The images reveal that heating is not uniform along the wells and that there can be communication between wells after the first steam injection period.

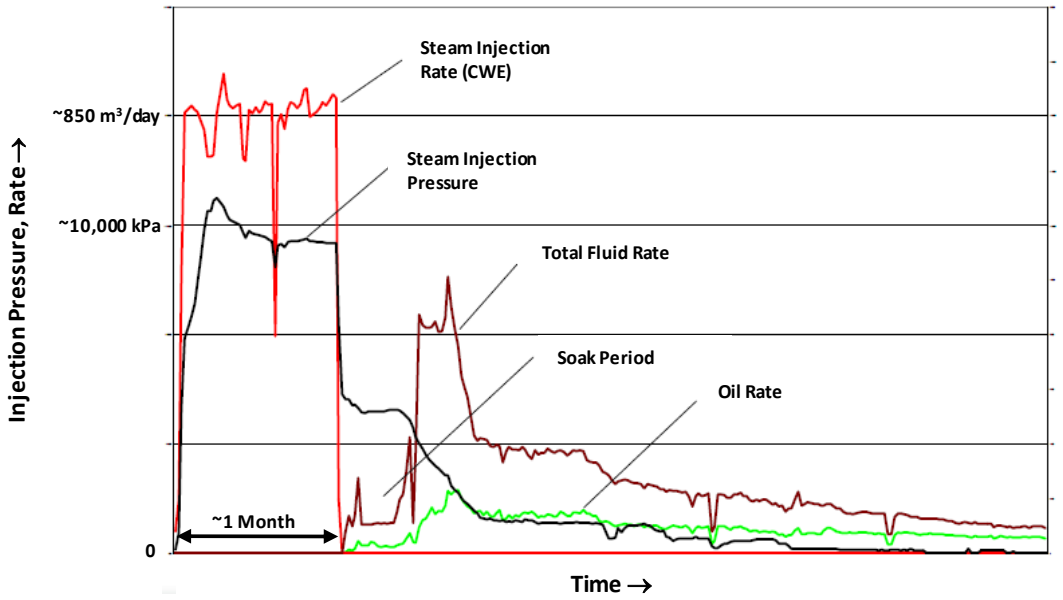

Figure 2: Cyclic steam injection rate, injection pressure, total fluid rate, and oil rate (CNRL, 2007) for CSS in Clearwater Formation oil sands reservoir. The maximum steam injection pressure is about 10,000 kPa. The maximum steam injection rate, expressed as cold water equivalent volume, is between 800 and 1,000 m^3/day.

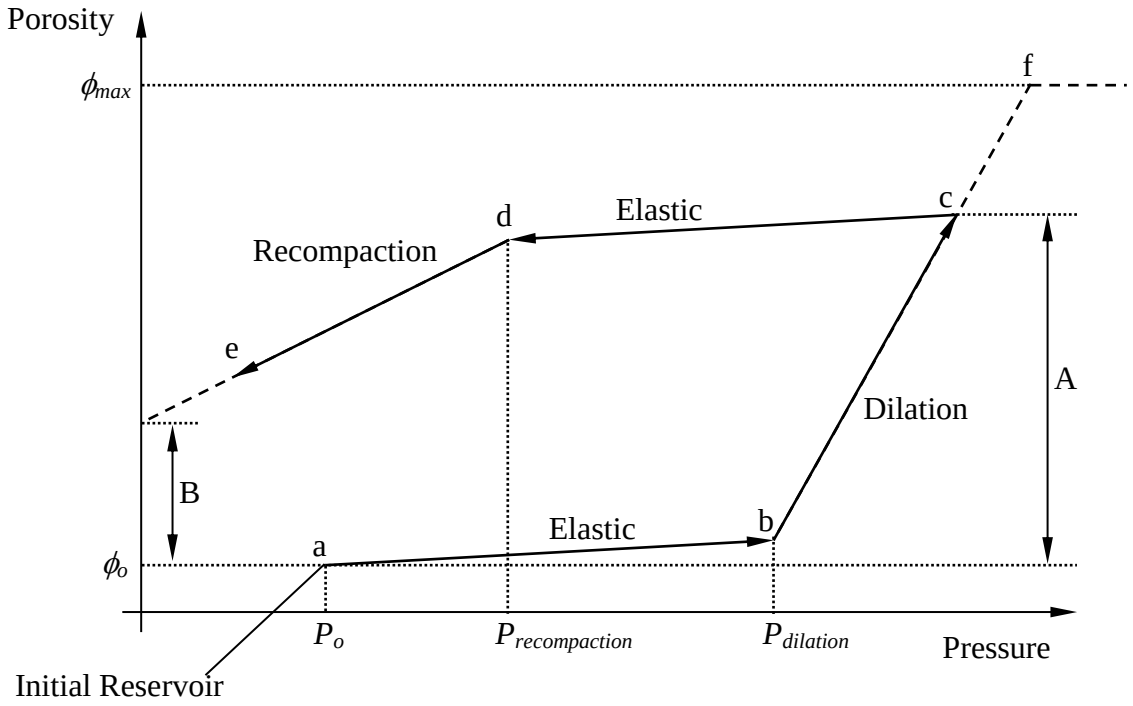

Figure 3: Beattie et al. (1991) dilation-recompaction model. The permeability is modified according to the fluid pressure.

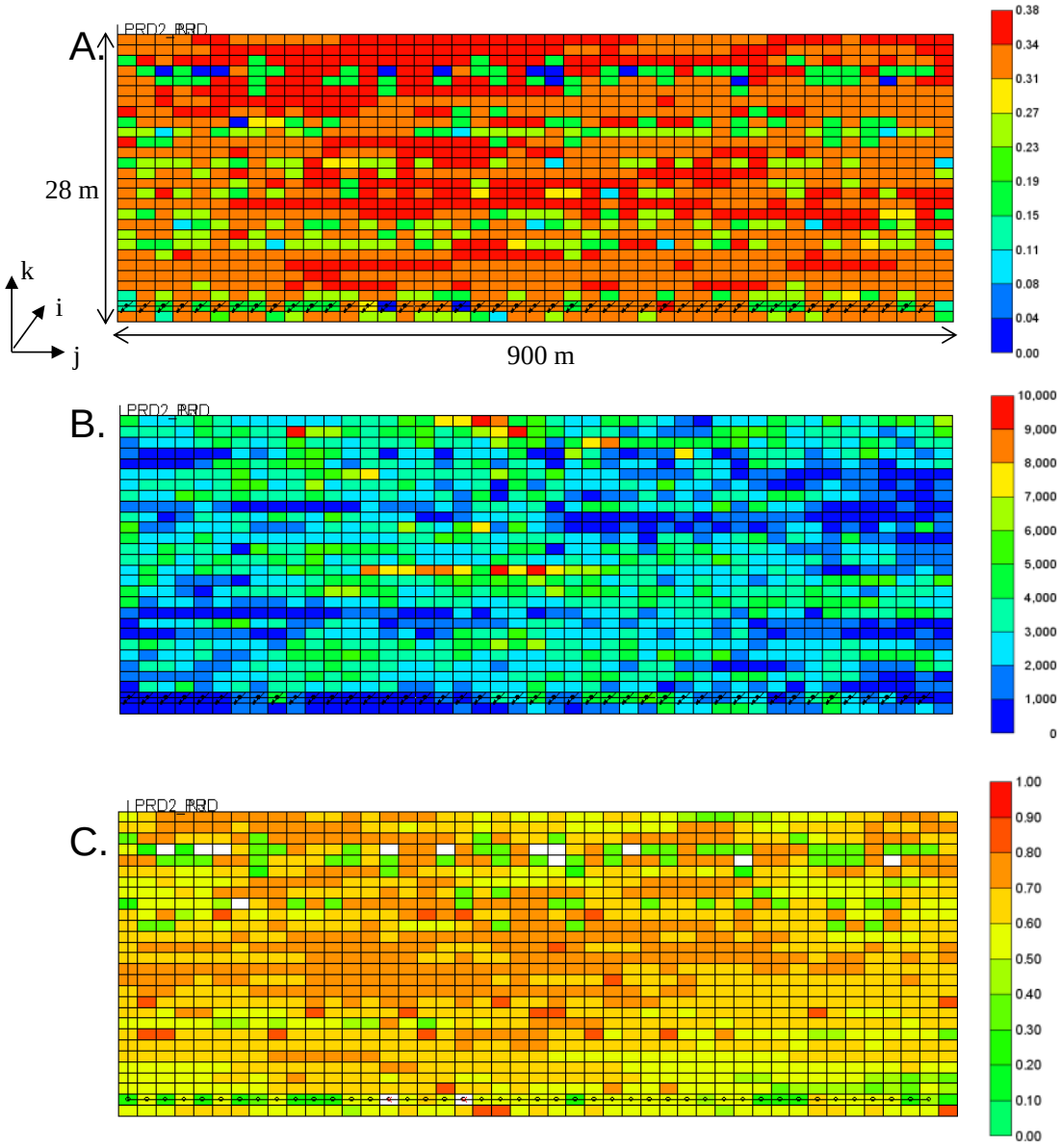

Figure 4: Cross-sections of the (a) porosity, (b) horizontal permeability, and (c) oil saturation of the reservoir simulation model in the plane of the horizontal well. Number of Gridblocks in i (cross-well), j (downwell), and k (vertical) directions are 52, 45, 28, respectively. The grid dimensions in the i, j, k directions are 1, 20, and 1 m, respectively.

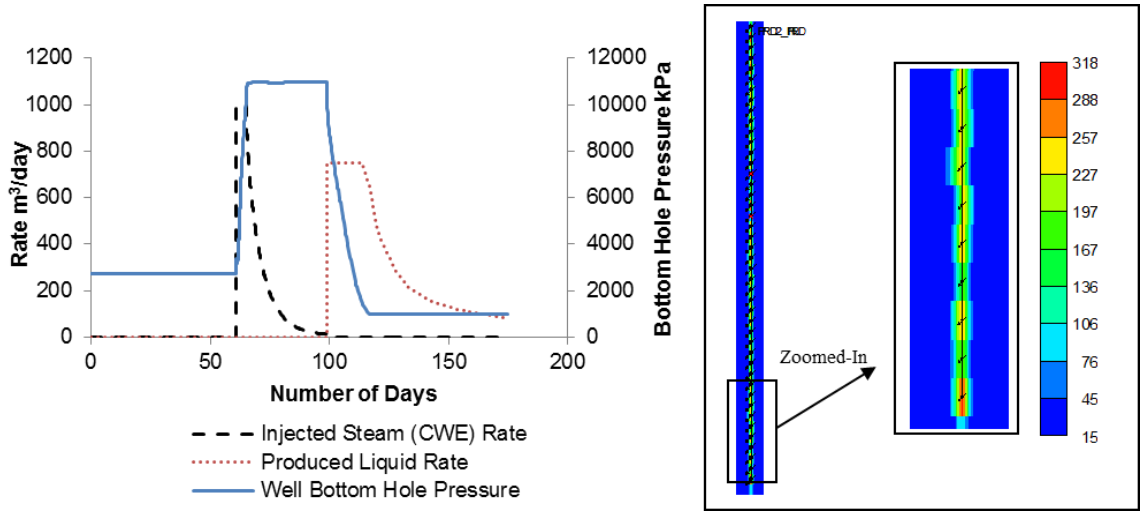

Figure 5: On left: Bottom hole pressure and injection and production rates (for injection, steam expressed as cold water equivalent volume and for production, both oil and water) for Case 1. Steam injection starts on Day 61 and production starts on Day 99. Production continues for 76 days. On right: Temperature (in °C) profile along wellbore for Case 1. The width of the model is 52 m.

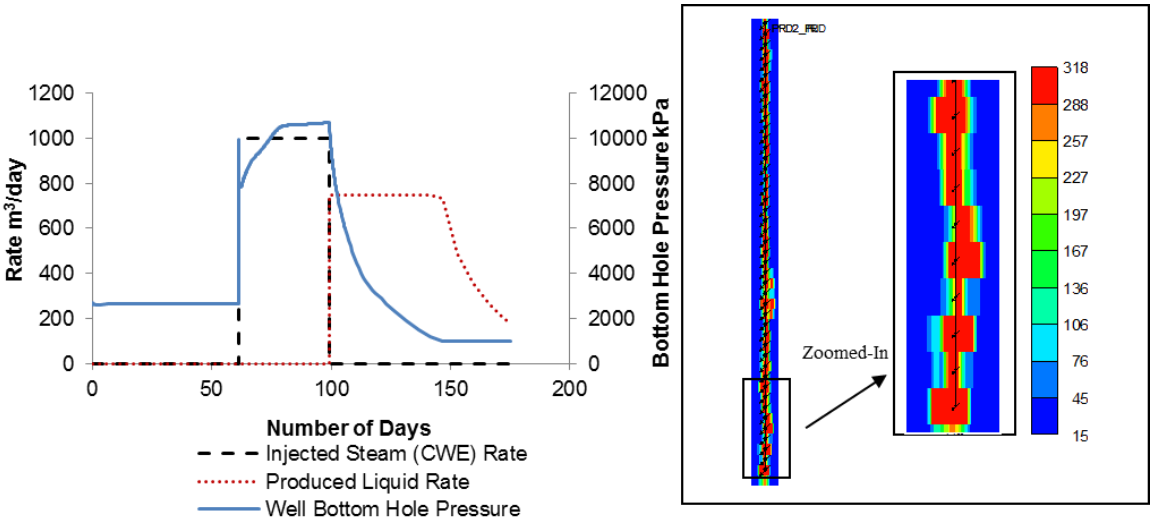

Figure 6: On left: Bottom hole pressure and injection and production rates (for injection, steam expressed as cold water equivalent volume and for production, both oil and water) for Case 2a. Steam injection starts on Day 61 and production starts on Day 99. Production continues for 76 days. On right: Temperature (in °C) profile along wellbore for Case 2a. The width of the model is 52 m.

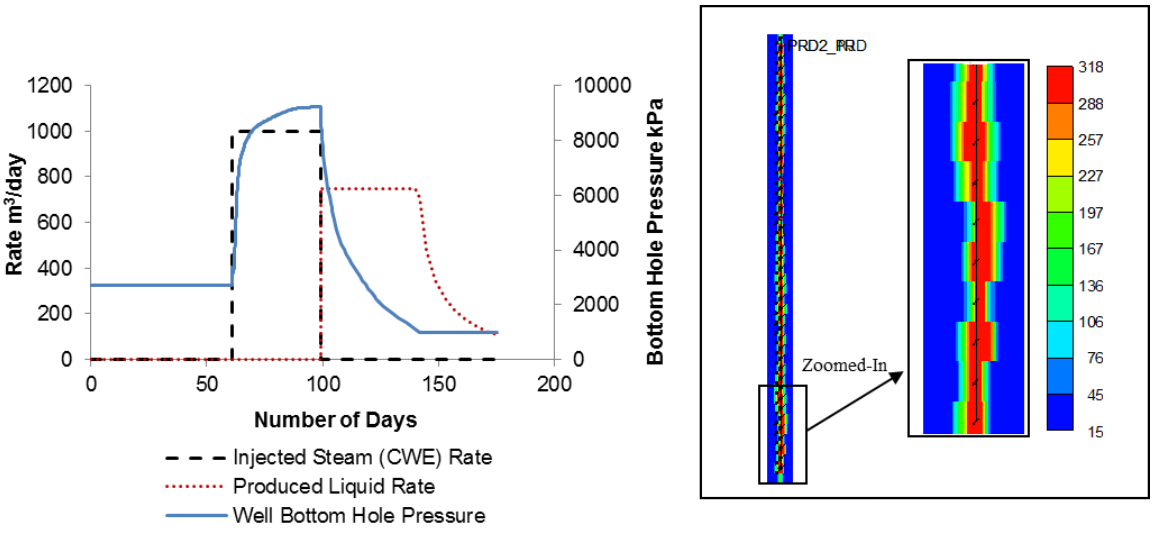

Figure 7: On left: Bottom hole pressure and injection and production rates (for injection, steam expressed as cold water equivalent volume and for production, both oil and water) for Case 2b. Steam injection starts on Day 61 and production starts on Day 99. Production continues for 76 days. On right: Temperature (in °C) profile along wellbore for Case 2b. The width of the model is 52 m.

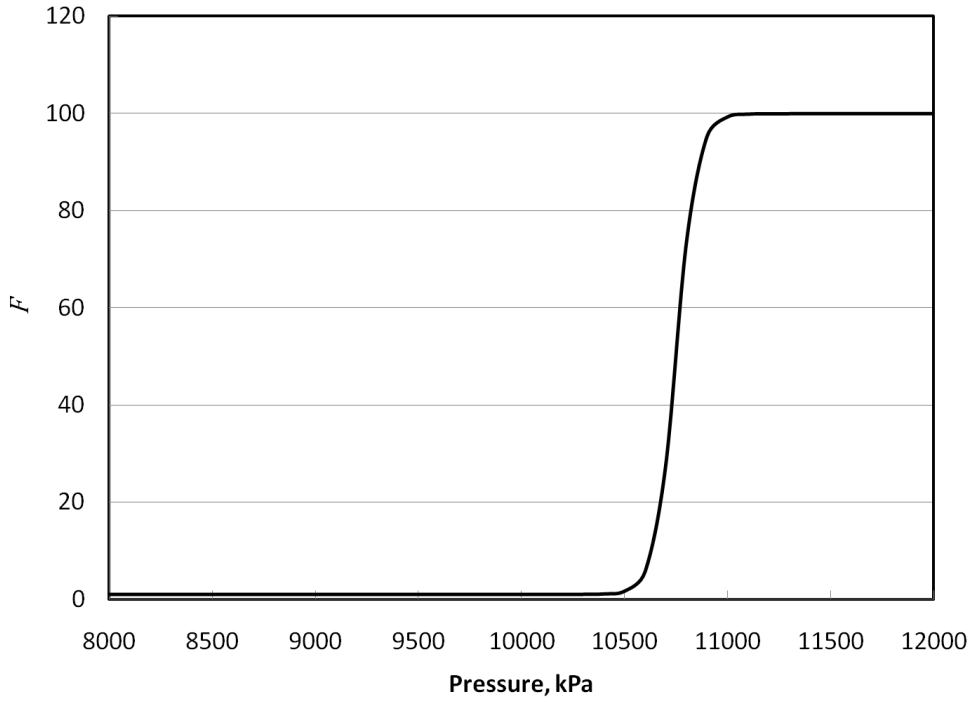

Figure 8: Transmissibility factor versus pressure (β = 100, $P_{LowerCutoff}$ = 10,500 kPa, $P_{UpperCutoff}$ = 11,000 kPa).

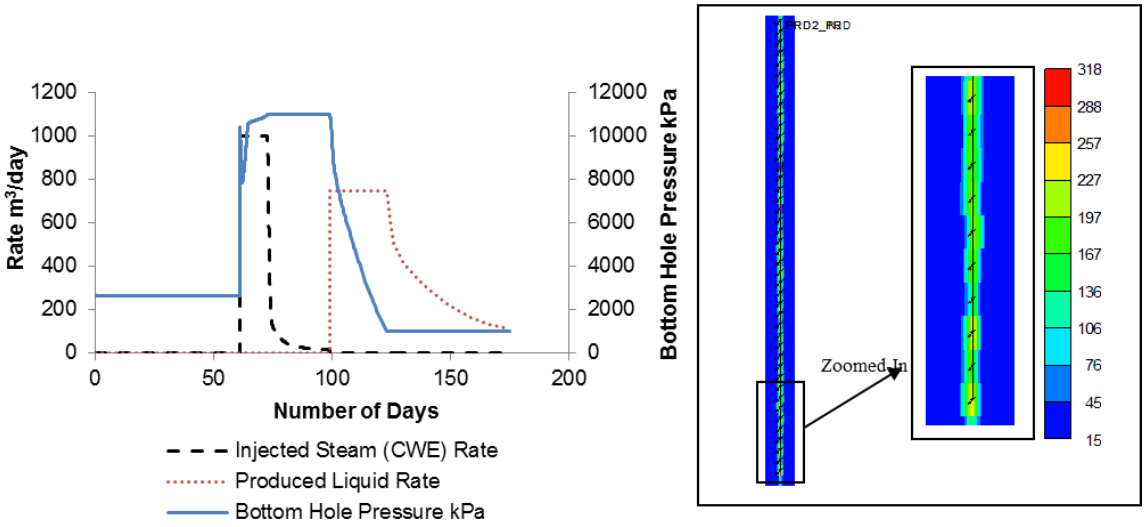

Figure 9: On left: Bottom hole pressure and injection and production rates (for injection, steam expressed as cold water equivalent volume and for production, both oil and water) for Case 3a. Steam injection starts on Day 61 and production starts on Day 99. Production continues for 76 days. On right: Temperature (in °C) profile along wellbore for Case 3a. The width of the model is 52 m.

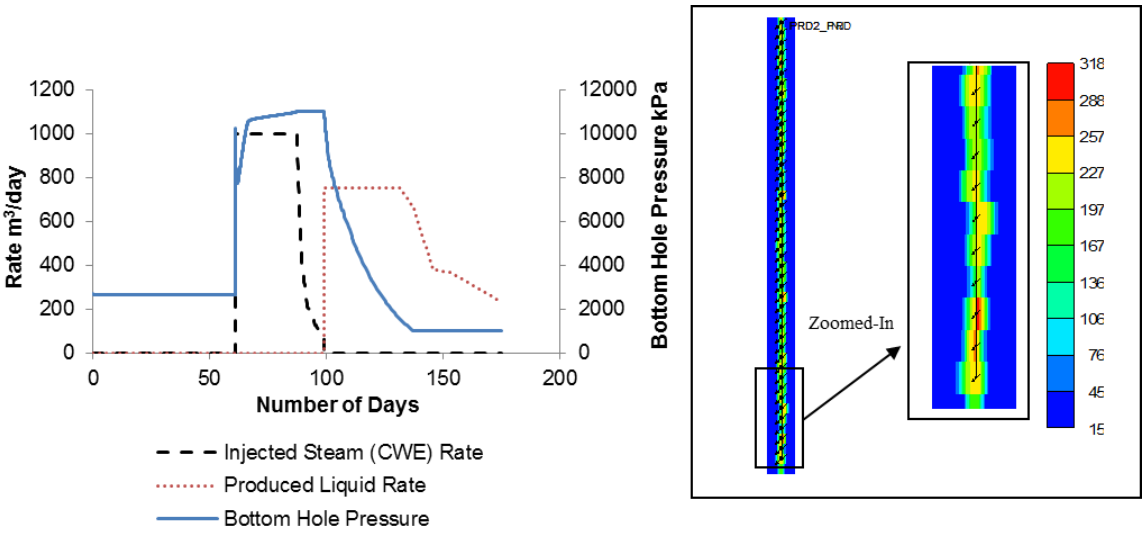

Figure 10: On left: Bottom hole pressure and injection and production rates (for injection, steam expressed as cold water equivalent volume and for production, both oil and water) for Case 3b. Steam injection starts on Day 61 and production starts on Day 99. Production continues for 76 days. On right: Temperature (in °C) profile along wellbore for Case 3b. The width of the model is 52 m.

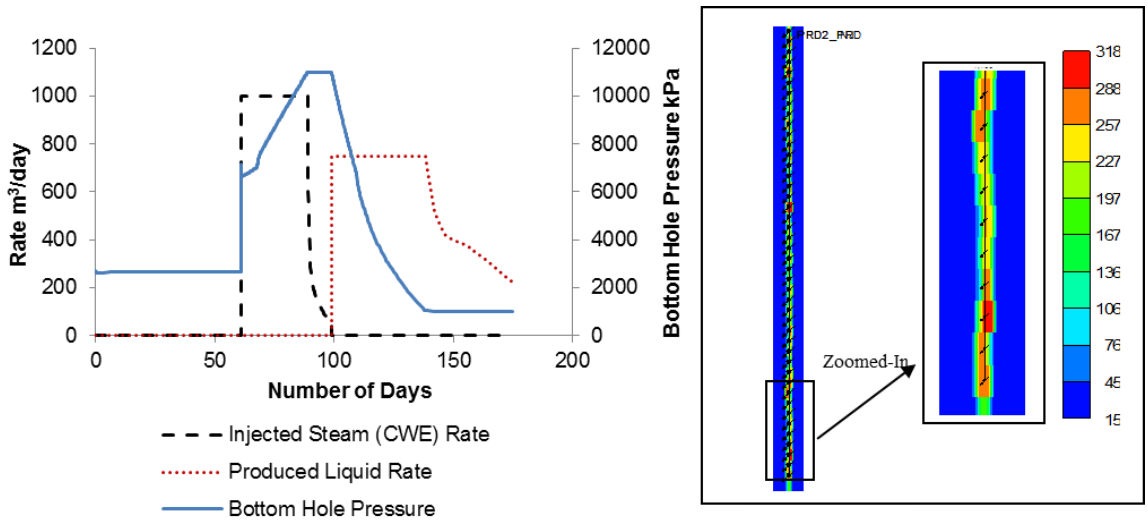

Figure 11: On left: Bottom hole pressure and injection and production rates (for injection, steam expressed as cold water equivalent volume and for production, both oil and water) for Case 3c. Steam injection starts on Day 61 and production starts on Day 99. Production continues for 76 days. On right: Temperature (in °C) profile along wellbore for Case 3c. The width of the model is 52 m.

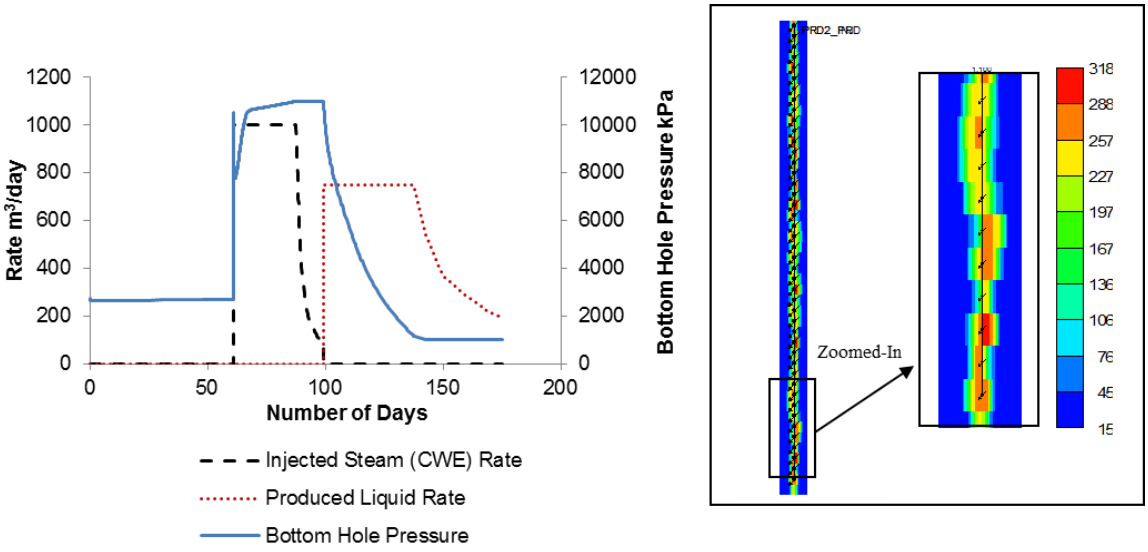

Figure 12: On left: Bottom hole pressure and injection and production rates (for injection, steam expressed as cold water equivalent volume and for production, both oil and water) for Case 3d. Steam injection starts on Day 61 and production starts on Day 99. Production continues for 76 days. On right: Temperature (in °C) profile along wellbore for Case 3d. The width of the model is 52 m.

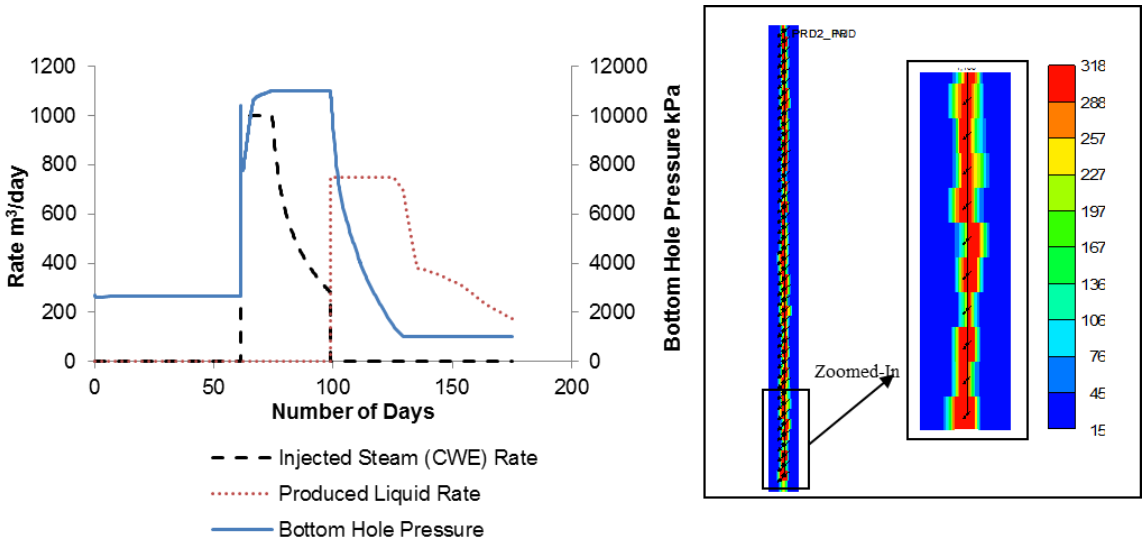

Figure 13: On left: Bottom hole pressure and injection and production rates (for injection, steam expressed as cold water equivalent volume and for production, both oil and water) for Case 3e. Steam injection starts on Day 62 and production starts on Day 100. Production continues for 76 days. On right: Temperature (in °C) profile along wellbore for Case 3e. The width of the model is 52 m.

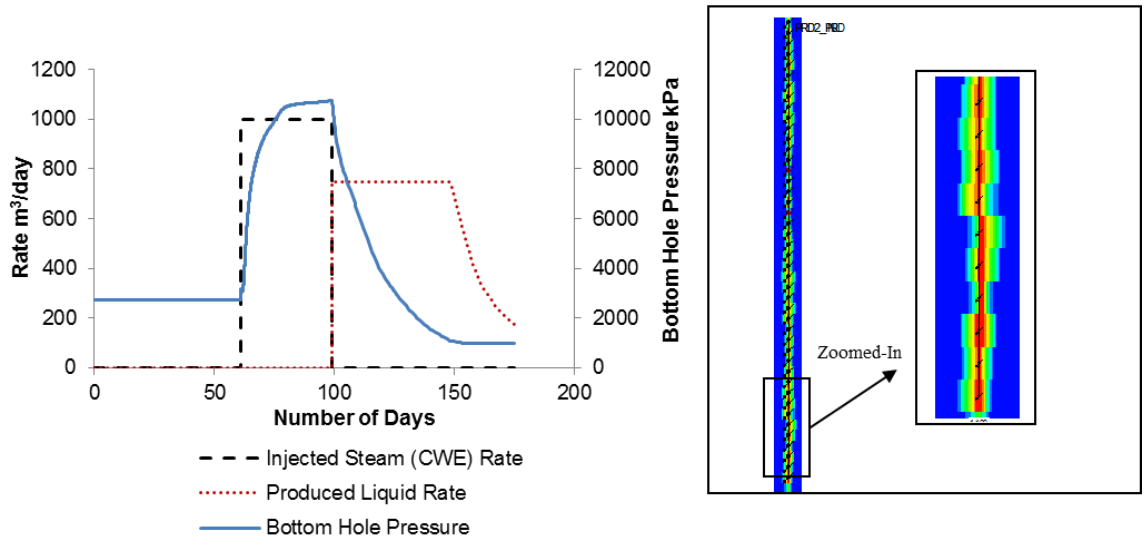

Figure 14: On left: Bottom hole pressure and injection and production rates (for injection, steam expressed as cold water equivalent volume and for production, both oil and water) for Case 4. Steam injection starts on Day 61 and production starts on Day 99. Production continues for 76 days. On right: Temperature (in °C) profile along wellbore for Case 4. The width of the model is 52 m.

Cokar, M., Kallos, M.S., Gates, I.D. (Accepted July, 2012 with revisions) A New Thermogeomechanical Theory for Gravity Drainage in SAGD. Accepted with revisions, *SPE Journal*, ID: SJ-02120028.

A New Thermogeomechanical Theory for Gravity Drainage in SAGD

Abstract

Oil sands reservoirs in Western Canada hold over 170 billion barrels of recoverable heavy oil and bitumen representing a significant source of unconventional oil. At in situ conditions, the majority of this oil has essentially no initial mobility because of its high viscosity, which is typically in the hundreds of thousands to millions of cP. In Steam Assisted Gravity Drainage (SAGD), steam injected into the formation heats oil at the edge of a depletion chamber raising the mobility, k_o/μ_o, of bitumen. Three main effects account for the increase of oil mobility. First, bitumen at steam temperature has viscosity typically less than 20 cP. Second, it is believed that shear caused by thermal expansion gradients dilate the oil sand and cause enhanced permeability. Third, dilation at the chamber edge leads to smaller residual oil saturation. Since the production rate of SAGD is directly tied to the drainage rate of mobilized oil at the chamber edge, the thermogeomechanics of the oil sand at the chamber edge is a control on the performance of SAGD. In this study, a novel SAGD drainage formula is derived that accounts for thermogeomechanical effects at the edge of the chamber. This paper couples the effects of reservoir geomechanics resulting from thermal processes into an analytical model. The results reveal that thermogeomechanics at the edge of the chamber play a significant role in enabling effective drainage of bitumen to the production well. This theory is an advancement to SAGD analytical theories because it achieves better coupling to the geomechanical effects which occur in thermal expansion processes.

Introduction

Steam-Assisted Gravity Drainage (SAGD) is the method of choice for bitumen production in the Athabasca oil sands deposit that cannot be mined. This is because the solution gas content of the oil is low and the overburden is not sufficiently competent to practice high-pressure cyclic steam stimulation. Additionally, the SAGD process is preferred over cyclical steam stimulation (CSS) even in areas where the overburden is competent because it is a more efficient process. SAGD in general works in a reservoir where there are no horizontal barriers, whereas CSS can overcome these horizontal barriers by fracturing, and thus enabling transport of steam and oil throughout the reservoir. The viscosity of Athabasca bitumen at original reservoir temperatures between 7 and 10ºC is typically greater than 1 million centipoise and thus, at original reservoir conditions, the oil is essentially immobile. However, the mobility of the oil increases by over five orders of magnitude when its temperature is raised to over 200°C. For example, Figure 1 shows the relationship between the viscosity and temperature for a typical Athabasca bitumen. At 7°C, the viscosity is approximately over 1 000 000 cP whereas at 200°C, it is under 10 cP. In a SAGD operation, there are two horizontal wells, referred to as a wellpair, located parallel to each other separated by about 5 m in the vertical direction. The top well injects steam into the reservoir whereas the bottom production well removes fluids from the reservoir. The injected steam delivers heat to the bitumen which in turn lowers its viscosity which then drains under gravity to the production well at the base of the steam chamber. As oil is produced from the reservoir, the steam chamber expands within the reservoir.

In typical practice, SAGD is analyzed by using detailed thermal reservoir simulation (Gates and Chakrabarty, 2006; Gates et al., 2008). These numerical models often use the finite volume approach to solve multiphase flow, material and energy balances, phase behavior relationships, and finite element method to determine the geomechanical behavior of the system. However, these models are complex and take hours to days to months to run depending on the fineness of the grid and transient behavior of the process. Under stochastic or response surface optimization, usually tens to hundreds to thousands of runs must be completed and as a result, rigorous optimization is not practically possible. One useful means to understand the behavior of these systems is to construct surrogate or proxy models, which provide a reasonable representation of the process but take little time, relative to the numerical model, to run. Here, we do this by constructing a simple model for SAGD that includes geomechanics based on a simple physical model of the system.

Both shear dilation and thermal dilation are known to occur in in situ thermal processes. Formation shearing within the Athabasca oil sands formation occurs and this results in the enhancement of in situ permeabilities (Collins, 2002). In this paper a modification to Butler's theory is made which includes thermal expansion effects, and thus encompasses more of the physics that occurs within the reservoir.

Thermal recovery processes such as SAGD and CSS induce a significant amount of shear dilation on the oil sands formation (Wong and Li, 2001). High temperature steam injection into the reservoir leads to thermoelastic expansion, which in turn leads to large

stress changes within the reservoir which lead to an increase in pore volume and reservoir permeability (Wong and Li, 2001; Li and Chalaturnyk, 2006). The absolute permeability of the reservoir is what enables the bitumen to flow and thus it directly affects the frontal steam advance rate and the rate of bitumen production (Wong and Li, 2001).

Modified SAGD Theory

SAGD is described by several analytical theories describing oil drainage rate at the edge of a steam chamber (Butler, 1985; Ferguson and Butler, 1988; Reis, 1992, 1993; Butler, 1997; Akin, 2005, Sharma and Gates, 2010). In these theories the reservoir is considered homogeneous, the chamber is 2D and it is symmetric around the wellpair. In the direction orthogonal to the edge of the steam chamber, heat transfer beyond the edge of the moving chamber is governed by:

$$\alpha = \frac{\partial T}{\partial \xi^2} - U\frac{\partial T}{\partial \xi} = \frac{\partial T}{\partial t} \qquad 1$$

where α is the thermal diffusivity of the reservoir, defined by $\alpha=k_{TH}/\rho Cp$, ξ is the direction normal to the steam chamber interface, and U is the steam chamber velocity in the direction normal to the interface. The steam chamber is assumed to be expanding in quasi-steady state, therefore the following temperature relationship can be derived from Equation 1, as shown by Butler (1997):

$$\frac{T - T_r}{T - T_s} = e^{-\frac{U\xi}{\alpha}} \qquad 2$$

Butler's applied Darcy's law for the case where the oil mobility depends on temperature and the temperature versus position is given by Equation (2). Butler's theory reveals the relationship between oil production rate q and other reservoir physical properties such as length of the wellpair L, initial permeability k, gravity g, thermal diffusivity of the reservoir α, change in oil saturation ΔS_o, initial porosity ϕ, height of the steam chamber h, viscosity dependence on temperature m, and kinematic viscosity of bitumen at steam temperature υ_s:

$$q = 2L\sqrt{\frac{2kg\alpha\phi\Delta S_o h}{m\upsilon_s}} \qquad 3$$

where the oil viscosity versus temperature relationship is given by:

$$\frac{\upsilon_o}{\upsilon_s} = \left(\frac{T - T_s}{T_s - T_r}\right)^m \qquad 4$$

Butler's model yields non-physical chamber shapes where the production point of the chamber translated as it expanded. Butler and Stephens (1981) altered the theory by

pinning the base of the chamber to the production well location. This model, known as the "Tandrain" model, is given by:

$$q = 2L\sqrt{\frac{1.5kg\alpha\phi\Delta S_o h}{m\upsilon_s}} \quad 5$$

Reis (1992) derived a similar theory with simplifying assumptions on the geometry of the steam chamber: he assumed that the steam chamber geometry is an inverted cone, he has also included an empirical constant a_R which was set equal to 0.4:

$$q = 2L\sqrt{\frac{kg\alpha\phi\Delta S_o h}{2a_R m\upsilon_s}} \quad 6$$

Sharma and Gates (2010) modified the theory to include relative permeability effects:

$$q = 2L\sqrt{\frac{2\alpha k k_{rocw} g\phi\Delta S_o h\Gamma(m)\Gamma(a+1)}{\upsilon_s\Gamma(m+a+1)}} \quad 7$$

where a is the Corey coefficient of the oil relative permeability curve and k_{rocw} is the oil relative permeability at connate water saturation. The results of this theory demonstrate that the most mobile oil is not at the edge of the steam chamber but rather some distance into the oil sands at the edge of the steam chamber. This is because of relative permeability effects. However, this theory did not include the effect of geomechanics.

It has been established that SAGD performance is influenced by geomechanical effects: steam injection and thermal expansion gradients yield enlarged pore pressure and shear stresses that dilate the oil sand which in turn raises its porosity which in turn increases its absolute permeability (Li and Chalaturnyk, 2006). A temperature gradient in the oil sands at the edge of the chamber leads to a thermal expansion gradient at the edge of the chamber. This means that each layer of oil sand at the chamber edge expands differently and thus there is a gradient of the dilated material at the edge of the chamber. This gradient of dilation yields a gradient of the pore pressure, which in turn impacts the porosity which in turn impacts the permeability. Thus, a temperature gradient leads to a permeability gradient in the oil sands at the edge of the chamber. Here, Sharma and Gates' theory has been modified to include dilation due to thermal expansion.

Porosity as a Function of Permeability in Oil Sands Reservoirs

As steam is injected into the reservoir at high temperatures and pressures, the reservoir dilates due to increased pore pressure and thermal expansion gradients at the edge of the chamber. As a result, the porosity and absolute permeability within the reservoir expands as steam injection occurs. As shown above in all gravity drainage theories, the higher the absolute permeability, the higher the oil rate. Figure 3 displays porosity versus permeability data originating from core data obtained from three different Athabasca oil sand reservoirs where SAGD is currently being used. The results illustrate that there is a

roughly linear dependence between the log of permeability and porosity. For the data shown in Figure 3, linear regression yields ln k(m^2) = 30.902ϕ(fraction) - 37.332 with a correlation coefficient equal to 0.7074.

Oil Mobility Profile at the Edge of Steam Chamber

The oil phase mobility as described by Butler's model is given by:

$$\lambda_o = \frac{k_{row} k}{\rho_o \upsilon_s} e^{-\frac{mU\xi}{\alpha}} \quad 8$$

The oil mobility described by the Sharma and Gates (2010) model which includes relative permeability effects, is defined as shown below:

$$\lambda_o = \frac{k_{rocw} k}{\rho_o \upsilon_s} \left(\frac{S_{io} - S_{or}}{1 - S_{wc} - S_{or}} \right) \left(1 - e^{-\frac{U\xi}{\alpha}} \right)^a \left(e^{-\frac{U\xi}{\alpha}} \right)^m \quad 9$$

In the new model developed here, the relationship between the absolute permeability and porosity is taken to be linear as described above:

$$\ln(k) = A + B\phi \quad 10$$

The porosity within the system changes as the volume of the reservoir expands due to thermal heat expansion:

$$V = V_o(1 + \beta(T - T_r)) \quad 11$$

where β is the oil sands volumetric thermal expansion coefficient. This implies that the porosity of the system depends on temperature as follows:

$$\phi = \phi_o[1 + \beta(T - T_r)] \quad 12$$

After inserting Equation 2 into Equation 12, the relationship for porosity and position becomes:

$$\phi = \phi_o \left[1 + \beta(T_s - T_r) e^{-\frac{U\xi}{\alpha}}\right] \quad 13$$

Equation 13 can now be substituted into Equation 10 to give the following relationship between the permeability, porosity, and steam and reservoir temperatures within the reservoir:

$$\ln(k) = A + B\phi_o \left[1 + \beta(T_s - T_r) e^{-\frac{U\xi}{\alpha}}\right] \quad 14$$

Thus, the oil mobility versus depth into the steam chamber can be re-written to include volumetric heat expansion as follows:

$$\lambda_o = \frac{e^{A+B\phi_o(1+\beta(T_s-T_r)e^{-\frac{U\xi}{\alpha}})}k_{rocw}}{\rho_o \upsilon_s}\left(\frac{S_{io}-S_{or}}{1-S_{wc}-S_{or}}\right)\left(1-e^{-\frac{U\xi}{\alpha}}\right)^a\left(e^{-\frac{U\xi}{\alpha}}\right)^m \quad 15$$

The location of the maximum oil mobility within the reservoir can be found by differentiating Equation 15 and setting it equal to zero. The location of the maximum oil mobility, ξ_{max}, is given by the solution of the following equation:

$$m + B\phi_o\beta(T_s-T_r)e^{-\frac{U\xi_{max}}{\alpha}} = \frac{ae^{-\frac{U\xi_{max}}{\alpha}}}{\left(1-e^{-\frac{U\xi_{max}}{\alpha}}\right)} \quad 16$$

Figure 4 compares the oil phase mobility profiles of the Butler model, Sharma and Gates' model, and Equation 15 versus distance for the case of steam chamber speed equal to 1cm/day. The results show that the new model shows a higher oil phase mobility from the steam chamber edge than that of the Sharma-Gates' model. It also shows that the Butler model in this case shows a much higher oil phase mobility than both models. The results demonstrate that relative permeability effects lower the oil phase mobility yet geomechanics raise the oil phase mobility.

Oil Flow Rate at the Edge of a Steam Chamber

Following Butler's theory and Darcy's law, the oil drainage rate in a differential element is given by the following equation:

$$d^2q = \frac{-k_o\Delta\rho g\sin\theta}{\mu_o}d\xi dz \quad 18$$

A modification of the above equation by Sharma and Gates (2010) which includes relative permeability effects is shown below:

$$d^2q = \frac{kk_{rocw}g\sin\theta}{\upsilon_s}\left(1-e^{-\frac{U\xi}{\alpha}}\right)^a\left(e^{-\frac{U\xi}{\alpha}}\right)^m d\xi dz \quad 19$$

Since the permeability within the reservoir is not constant, Equation 15 can be substituted into Equation 19 to give Equation 20 below:

$$d^2q = \frac{e^{A+B\phi_o(1+\beta(T_s-T_r)e^{-\frac{U\xi}{\alpha}})}k_{rocw}g\sin\theta}{\upsilon_s}\left(1-e^{-\frac{U\xi}{\alpha}}\right)^a\left(e^{-\frac{U\xi}{\alpha}}\right)^m d\xi dz \quad 20$$

The oil phase velocity at the edge of the steam chamber is then given by:

$$u_{oil} = \frac{d^2q}{d\xi dz} = \frac{e^{A+B\phi_o(1+\beta(T_s-T_r)e^{-\frac{U\xi}{\alpha}})}k_{rocw}\, g \sin\theta}{\upsilon_s}\left(1-e^{-\frac{U\xi}{\alpha}}\right)^a\left(e^{-\frac{U\xi}{\alpha}}\right)^m \qquad 21$$

and the oil phase velocity as given by Butler is:

$$u_{oil} = \frac{d^2q}{d\xi dz} = \frac{k_o g \sin\theta}{\upsilon_s}\left(e^{-\frac{mU\xi}{\alpha}}\right) \qquad 22$$

The oil phase velocity from the Sharma and Gates (2010) model is:

$$u_{oil} = \frac{d^2q}{d\xi dz} = \frac{kk_{rocw}\, g \sin\theta}{\upsilon_s}\left(1-e^{-\frac{U\xi}{\alpha}}\right)^a\left(e^{-\frac{U\xi}{\alpha}}\right)^m \qquad 23$$

Equations 21 to 23 are plotted in Figure 5. This represents the oil phase velocity as a function of distance from the edge of the steam chamber. The results show that the oil velocities are lower than Butler's model but higher than that obtained from the Sharma and Gates model. This is because of the permeability enhancement at the edge of the chamber due to thermal expansion. The maximum oil phase velocity obtained from the new model is about 45% higher than that of the Sharma and Gates model. The peak occurs at the same location from the edge of the chamber.

The oil velocity was then numerically integrated by using Simpson's 3/8 rule to get the oil phase flux per unit length and multiplied by two to get the flow rate from both sides of the chamber. For a 500 m length wellpair, this value is then multiplied 500 m. The results are listed in Table 1.

Results

The following section describes the results that were observed in this study. All of the values used to graph the equations are listed in Table 2. Figure 4 shows the oil phase mobility as a function of the distance from the edge of the steam chamber for Butler's model, the Sharma and Gates (2010) model, which took relative permeability effects into consideration, and the new model that has taken both the relative permeability effects and the effects of changes in permeability and porosity into consideration. The linear thermal expansion coefficient is determined using an arithmetic average in terms of the initial porosity, oil and water saturations, and the individual thermal expansion coefficients of the sand, oil and water. The interesting thing to note is that both the Sharma and Gates (2010) and the new model have maximum oil phase mobility away from the edge of the steam chamber. Also the values for the oil phase mobility for these two models are very similar, however the oil phase mobility of the new model is slightly higher than the Sharma and Gates (2010) model. This is because this new model also takes into consideration the thermal expansion effects of the oil sands reservoir when it is heated.

However, as shown in Figures 7 to 9, the oil phase mobility is very sensitive to changes in the coefficients in Equation 10 and changes to the linear thermal expansion coefficient.

The next figure that was plotted was the oil phase velocity as a function of the distance away from the edge of the steam chamber (Figure 5). Once again in the Butler model the maximum oil phase velocity occurs at the edge of the steam chamber. The oil phase velocity of the new model matches closely to the Sharma and Gates (2010) model, however, the velocity in the new model is slightly higher, and this is because of the thermal expansion due to heating that is occurring within the reservoir.

Now, to compare the volumetric flow rate of all three models, the results in Figure 5 were numerically integrated, and the results are shown in Table 1. In this table it is clear that Butler's model shows the highest rates followed by the new model and the Sharma and Gates (2010) model. These results are consistent with Figures 4 and 5 since in this new model thermogeomechanical effects are taken into consideration, and there is a clear enhancement of the permeability and the porosity within the reservoir due to heating.

Figure 6 shows the oil phase mobility as a function of the distance from the edge of the steam chamber for the new model, at different steam chamber velocities. It is clear from this model that as the steam chamber velocity decreases the maximum oil phase mobility occurs further from the edge of the steam chamber.

Figures 7 to 9 show how the oil phase mobility as a function of the distance from the steam chamber changes as the constants in Equation 10 and the linear thermal expansion coefficient are changed. From these figures it is clear that the oil phase mobility changes significantly with small changes in these variables. The values of the constants A and B are obtained from core analysis of the maximum permeability and the porosity in oil sands core samples, and depend greatly on the quality of data obtained. Also, since the results depend quite extensively on these properties, the best available and representative data should be used. Figure 9 shows the oil phase mobility as a function of the distance from the edge of the steam chamber with different values for the linear thermal expansion coefficient that is used in the new model. As mentioned above, an arithmetic average was used in conjunction with the volume of the oil, sand and water within the reservoir. As the thermal expansion coefficient is increased the oil phase mobility increases much more significantly than if this value is decreased. Therefore it is important to use representative field values to obtain the thermal expansion coefficient, because the results will vary depending on which value is used.

Conclusion

A new thermogeomechanical theory was derived for oil sands reservoirs that takes into consideration the thermal expansion that occurs at the edge of a SAGD steam chamber due to the temperature gradient there. The new theory reveals that the impact of thermal expansion on oil rates is substantial: the peak oil phase velocity is up to 45% higher than that of the Sharma and Gates model (takes only relative permeability effects into account). Thus, geomechanical effects should be included in analysis of the flow at the edge of steam chambers.

Acknowledgement
The authors would like to acknowledge the financial support from the Natural Sciences and Engineering Council of Canada (NSERC) and Alberta Innovates - Technology Futures (AI-TF).

Nomenclature

A	Constants for Equation 10
a, b	Corey coefficients (dimensionless)
a_R	Temperature coefficient by Reis (dimensionless)
c_P	Volumetric heat capacity of oil sands (J/m^3-˚C)
B	Constant for Equation 10
g	Acceleration due to gravity (m/s^2)
h	Reservoir thickness (m)
k	Absolute permeability of the reservoir (m^2)
k_{TH}	Thermal conductivity (J/s m-˚C)
k_{rocw}	Relative permeability of oil at connate water saturation (dimensionless)
k_{rw}	Relative permeability of water (dimensionless)
L	Length of the production well (m)
m	Temperature viscosity parameter (dimensionless)
q	Volumetric oil flow rate (m^3/s)
ΔS_o	Change in oil saturation from initial condition (dimensionless)
S_{wc}	Connate water saturation (dimensionless)
S_{wD}	Normalized water saturation (dimensionless)
S_o	Oil saturation (dimensionless)
S_{or}	Residual oil saturation (dimensionless)
S_{io}	Initial oil saturation (dimensionless)
T	Temperature (˚C)
T_s	Steam temperature (˚C)
T_r	Initial reservoir temperature (˚C)
U	Chamber interface velocity measured normal to the chamber edge (m/s)
u_{oil}	Volumetric oil flux at the chamber edge (m^2/s)
z	Distance measured parallel to the well direction (m)

Greek

α	Thermal diffusivity (m^2/s)
β	Linear thermal expansion coefficient (1/ºC)
ϕ	Porosity (dimensionless)
λ_o	Oil mobility (m^{3}s/kg)
μ_o	Dynamic viscosity of oil (kg/m·s)
ν_o	Kinematic viscosity of oil (m^2/s)
ν_s	Kinematic viscosity of oil at steam temperature (m^2/s)
θ	Angle between the steam chamber edge and the horizontal axis (degrees)
ρ_o	Density of oil at steam temperature (kg/m^3)
ρ_{steam}	Density of steam (kg/m^3)
ξ	Distance measured from the steam edge in the direction normal to it (m)
ξ_{max}	Distance to the location of maximum oil mobility from chamber edge (m)

Conversion Table

Property	Metric	Imperial
Length	1 m	3.28ft
Temperature	1˚C	°C x 9/5 + 32 = °F
Mass	kg	2.20 lb
Energy	Joules	0.000948 BTU

References

1. Akin, S., "Mathematical Modeling of Steam-Assisted Gravity Drainage", SPEREE, 8(5), 372-376 (2005).
2. Azad, A., and R.J. Chalaturnyk, "Geomechanical Coupling Simulation in SAGD Process; a linear geometry model," 3rd CANUS Rock Mechanics Symposium, (2009).
3. Butler, R.M., "A New Approach to the Modeling of Steam-Assisted Gravity Drainage," J. Can. Pet. Tech. 24(3), 42-51 (1985).
4. Butler, R.M., "Thermal Recovery of oil and bitumen," GravDrain Inc., Calgary, AB, ISBN 0-9682563-0-9 (1997).
5. Butler, R.M. and D. J. Stephens, "The Gravity Drainage of Steam-heated Heavy Oil to Parallel Horizontal Wells," J. Can. Pet. Tech. 20(2), 90-96 (1981).
6. Collins, P.M., "Injection Pressures for Geomechanical Enhancements of Recovery Processes in the Athabasca Oil Sands," Paper SPE79028 presented at the SPE International Thermal Operations and Heavy Oil Symposium and International Horizontal Well Technology Conference, Calgary, Alberta, 4 – 7 November (2002).
7. Ferguson, F. R. S. and R. M. Butler, "Steam Assisted Gravity Drainage Model Incorporating Energy Recovery from a cooling Steam Chamber," J. Can. Pet. Tech. 27(5), 75-83 (1988).
8. Gates, I.D., J.J., Adams, S.R. Larter, "The impact of oil viscosity heterogeneity on the production characteristics of tar sand and heavy oil reservoirs. Part II: Intelligent, geotailored recovery processes in compositionally graded reservoirs," J. Can. Pet. Tech. 47(9):40-49 (2008).
9. Gates, I.D. and Chakrabarty, N. "Optimization of Steam-Assisted Gravity Drainage (SAGD) in Ideal McMurray Reservoir," J. Can. Pet. Tech. 45(9):54-62 (2006).
10. Ito, Y., M. Ichikawa and T. Hirata, "The Growth of the Steam Chamber during the early Period of the UTF Phase B and Phase I Projects," J. Can. Pet. Tech. 40(9), 29-36 (2001a).
11. Ito, Y., T. Hirata, M. Ichikawa, "The Effect of Operating Pressure on the Growth of the Steam Chamber Detected at the Hangingstone SAGD Project," J. Can. Pet. Tech. 4(1), 47-53 (2001b).
12. Li, P., R.J. Chalaturnyk, "Permeability Variations Associated with Shearing and Isotropic Unloading during the SAGD Process," J. Can. Pet. Tech 45(1), 54-61 (2006).
13. Mehrotra, A. K. and W. Y. Svrcek, "Viscosity of compressed Athabasca bitumen," Can. J. Chem. Eng. 64(5), 844-847 (1986).

14. Reis, J.C., “A steam-assisted gravity drainage model for tar sands: linear geometry,” J. Can. Pet. Tech. 31(10), 14-20 (1992).
15. Reis, J.C., “A Steam-Assisted Gravity Drainage Model for Tar Sands: Radial Geometry,” J. Can. Pet. Tech. 32(8), 43-48 (1993).
16. Sharma, J., and Gates I.D., “Multiphase Flow at the Edge of a Steam Chamber,” Can. Journal of Chemical Engineering. (2010).
17. Wong, R.C.K., Li, Y., “A deformation Dependent Model for Permeability Changes in oil Sand due to Shear Dilation,” J. Can. Pet. Tech. 40(8), 37-44 (2001).

Table 1. Flow Rates in m3/day for all three models.

Model Type	Flow Rate (m^3/day)
Butler's Model	243
Sharma and Gates (2010)	121
New Model	162

Table 2. Typical Athabasca oil sand parameters.

Property	Value	Source
T_r, ˚C	10	(Ito, 2001)
T_s, ˚C	260	(Ito, 2001)
ρ_o, kg/m^3	998	(Ito, 2001)
h, m	30	(Ito, 2001)
L, m	500	(Ito, 2001)
ϕ	0.35	(Butler, 1997)
α, m^2/s	$7x10^{-7}$	(Ito, 2001)
k_{abs}, m^2	$3.05\ x10^{-12}$	Field Data
k_{rocw}	1	
k_{ro},	0.20	(Ito, 2001)
S_{io}	0.84	(Ito, 2001)
S_{or}	0.14	(Ito, 2001)
S_{wc}	0.16	(Ito, 2001)
υ_s, m^2/s	$4.28x10^{-6}$	(Ito, 2001)
m	3	(Ito, 2001)
Dimensionless temperature coefficient (Reis), a_R	0.4	(Ito, 2001)
Corey's parameters a b	 2 4	(Ito, 2001)
β oil sands reservoir 1/ºC	$2.128x10^{-4}$	(Calculated in this paper)
β water 1/ºC	$4.5x10^{-3}$	(Azad, 2009)
β sand 1/ºC	$5x10^{-5}$	(Azad, 2009)
β oil 1/ºC	$6.2x10^{-3}$	(Azad, 2009)

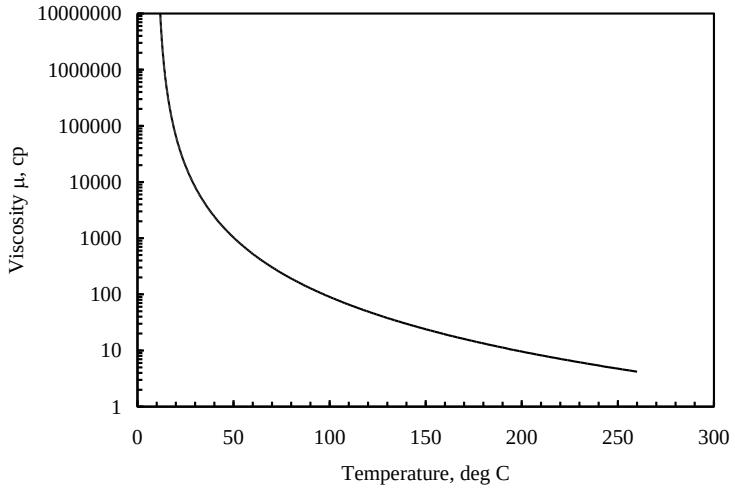

Figure 1. Athabasca bitumen viscosity as a function of temperature (Mehrotra and Svrcek, 1986).

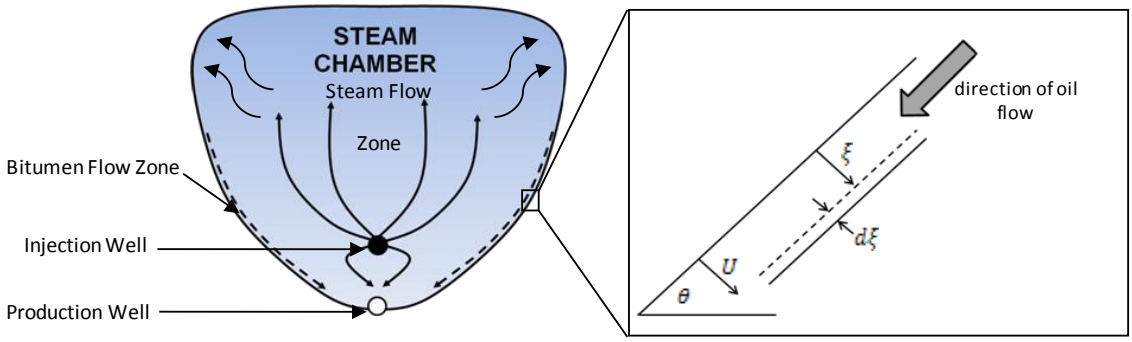

Figure 2. Cross section of steam chamber and differential element used in the derivation of the theory.

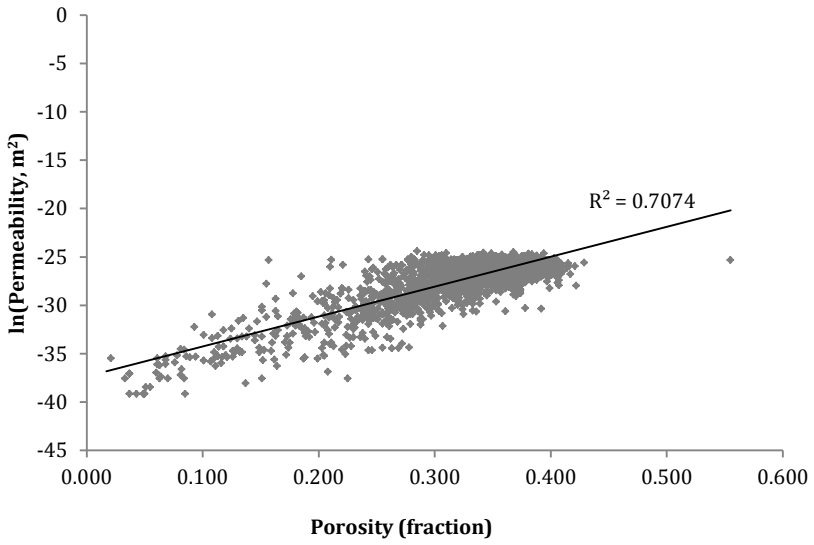

Figure 3. Typical ln(permeability) versus porosity relationship for Athabasca oil sands reservoir (available in public databases).

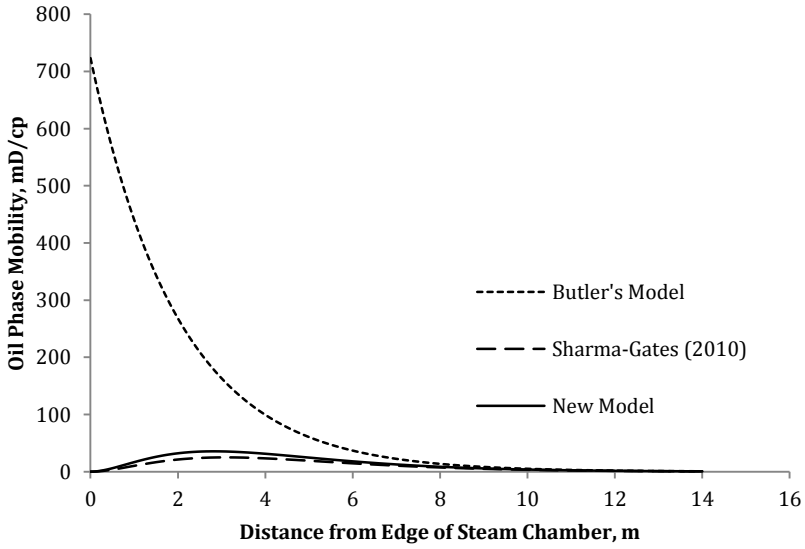

Figure 4. Comparison of oil phase mobility for Butler, Sharma and Gates (2010) and the New Model (U=1cm/day). Parameter values are listed in Table 2.

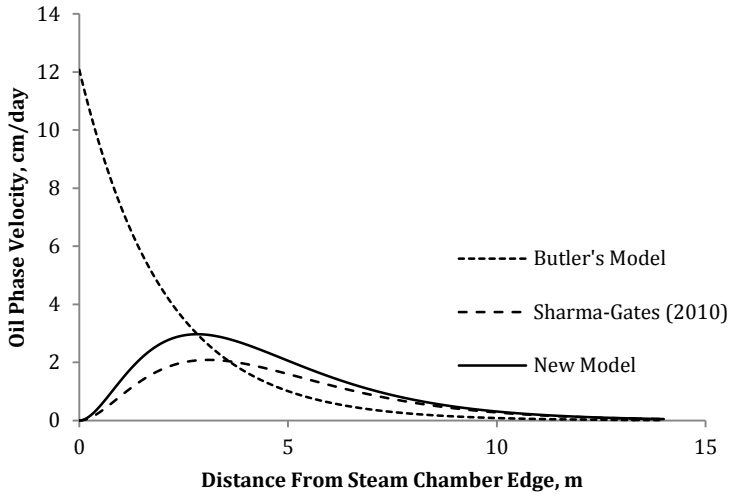

Figure 5. Comparison of oil phase velocity for all three models. Parameter values are listed in Table 2.

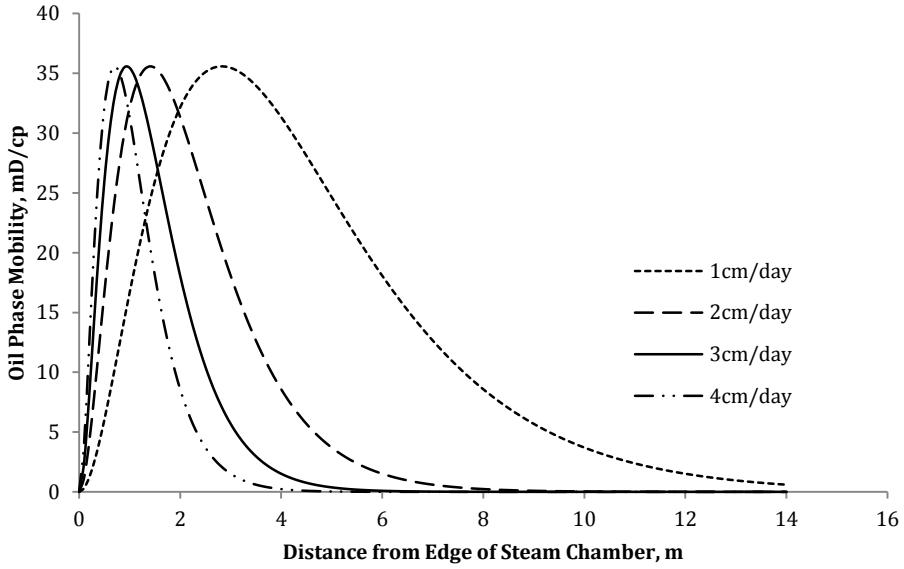

Figure 6. Oil phase mobility as a function of distance from edge of steam chamber for different steam chamber velocities, *U*. Other parameter values are listed in Table 2.

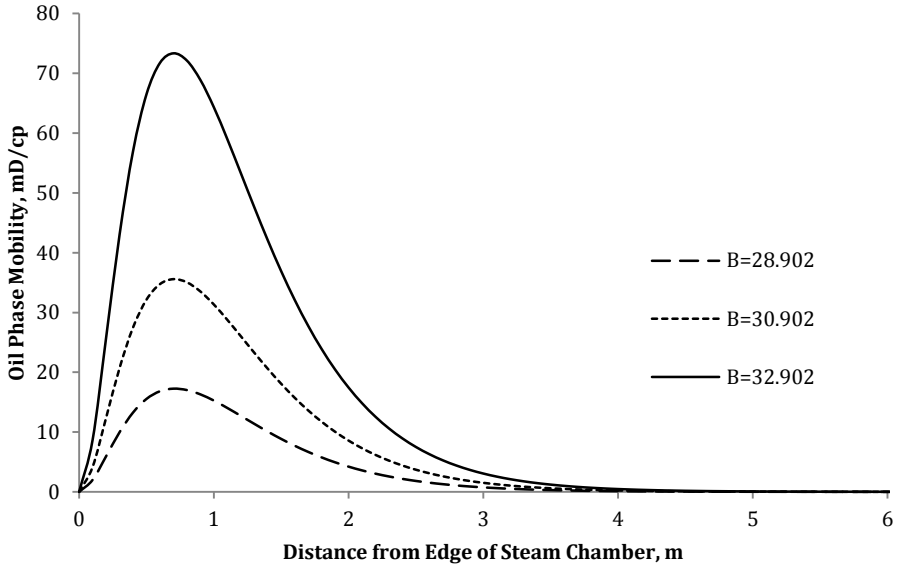

Figure 7. Oil phase mobility as a function of distance from the edge of a steam chamber: sensitivity to parameter B. Other parameter values are listed in Table 2.

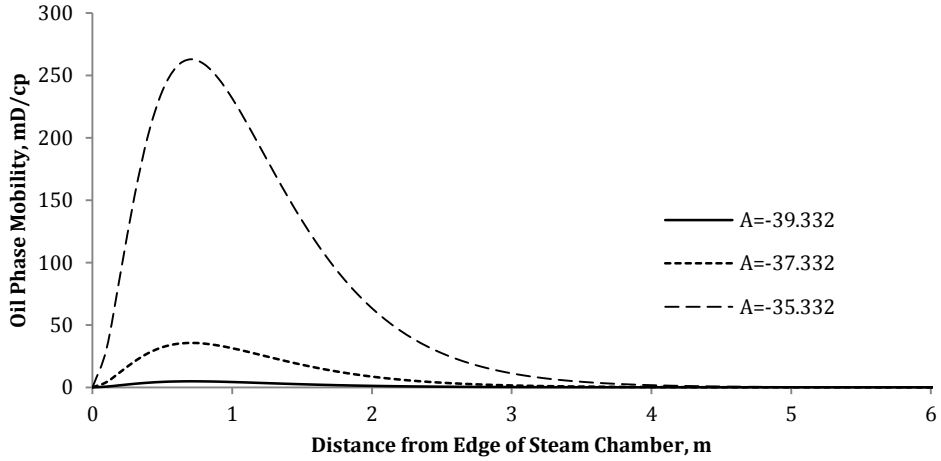

Figure 8. Oil phase mobility as a function of distance from the edge of a steam chamber: sensitivity to parameter A. Other parameter values are listed in Table 2.

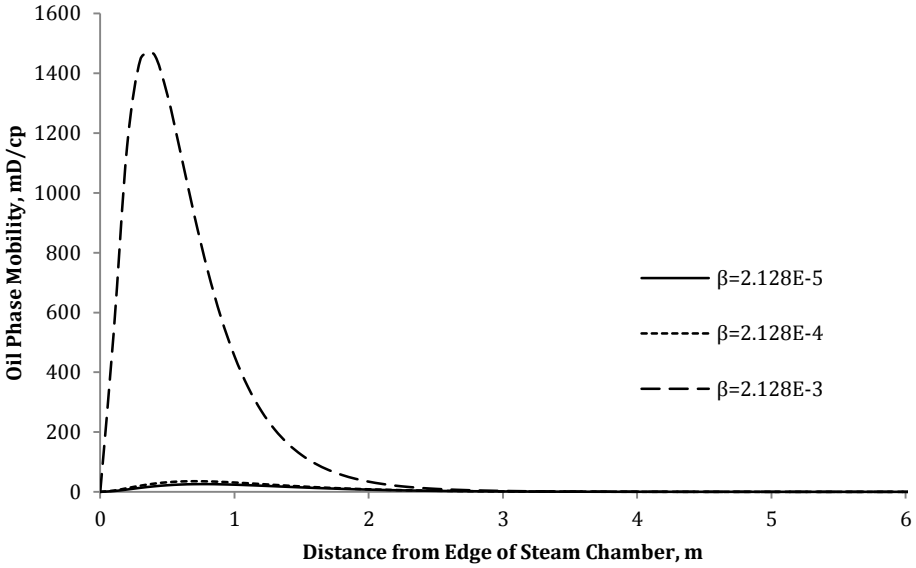

Figure 9. Oil phase mobility as a function of distance from the edge of a steam chamber: sensitivity to parameter β. Other parameter values are listed in Table 2.